An assessment of the heavy metal concentrations in the water and sediment of the uMgeni Estuary, using visible and near-infrared reflectance spectroscopy

By

Suvasha Ramcharan

Submitted in fulfilment of the academic requirements for the degree of

Master of Science in Environmental Science

in the School of Agricultural, Earth and Environmental Sciences,

University of KwaZulu-Natal, Durban.

December 2021

UNIVERSITY OF
KWAZULU-NATAL

ABSTRACT

Estuaries are one of the most productive ecosystems on earth and are essential as they provide a home to various aquatic plant and animal species. However, heavy metal contamination of estuaries associated with urbanisation and industrialisation is of particular concern as these heavy metals persist in the environment causing harmful effects in the aquatic organisms that inhabit these ecosystems. Therefore, regular assessment of heavy metal concentrations is imperative for managing the health of the estuary. Thus, this study explores remote sensing methods that facilitate the regular monitoring of heavy metal concentrations in the water and sediment of the uMgeni Estuary. Water and sediment samples were collected and analysed for aluminium, arsenic, cadmium, chromium, copper, iron, lead, magnesium, nickel, and zinc. A remote sensing analytical spectral device, FieldSpec 3 spectroradiometer, was used to record spectral measurements of the water and sediment samples in the 350-2500 nm wavelength range. Thereafter, a partial least squares regression was used to develop calibration models to predict the metal concentrations in the water and sediment from the visible and near-infrared reflectance spectra.

The results indicated that the sediment of the uMgeni Estuary contained higher concentrations of heavy metals than the water. The calibration models performed better in predicting heavy metals in the sediment than in water. The best model for predicting heavy metals in sediment was obtained for nickel with calibration and cross-validation R^2 values of 0.96 and 0.83, respectively, and RMSE values of 1.88 mg/kg and 4.34 mg/kg, respectively. The significant wavelengths of the VNIR spectrum for the detection of nickel in the sediment were 1090 nm, 1279 nm, 1398 nm, 1473 nm and 1676 nm. The best model for predicting heavy metals in water was obtained for arsenic with calibration and cross-validation R^2 values of 0.05 and 0.02, respectively, and RMSE values of 0.005 mg/L and 0.006 mg/L, respectively. The significant wavelengths of the VNIR spectrum for the detection of arsenic were 715 nm, 1137 nm, 1663 nm and 1731 nm.

It can be concluded that reflectance spectroscopy has shown potential in the prediction of heavy metals, especially from sediments; however, a limitation is a reduced accuracy in the prediction of heavy metals with a greater variability in their concentrations. Therefore, visible and near-infrared reflectance spectroscopy should not be used to replace conventional methods of analysing heavy metals in water and sediment entirely but rather to complement them.

As the candidate's supervisor I have approved this dissertation for submission.

Signed: _____ Name: _____ Date: _____

PREFACE

The experimental work described in this dissertation was carried out in the School of Agricultural, Earth and Environmental Sciences, University of KwaZulu-Natal, Durban, from March 2020 to December 2021, under the supervision of Professor Michael Gebreslasie.

This study represents the original work done by the author, Suvasha Ramcharan, and has not otherwise been submitted in any form for any degree or diploma to any tertiary institution. Where use has been made of the work of others it is duly acknowledged in the text.

DECLARATION - PLAGIARISM

I, Suvasha Ramcharan, declare that:

1. The research reported in this dissertation, except where otherwise indicated, is my original research.

2. This dissertation has not been submitted for any degree or examination at any other university.

3. This dissertation does not contain other persons' data, pictures, graphs or other information, unless specifically acknowledged as being sourced from other persons.

4. This dissertation does not contain other persons' writing, unless specifically acknowledged as being sourced from other researchers. Where other written sources have been quoted, then:
   a. Their words have been re-written but the general information attributed to them has been referenced
   b. Where their exact words have been used, then their writing has been placed in italics and inside quotation marks, and referenced.

5. This dissertation does not contain text, graphics or tables copied and pasted from the Internet, unless specifically acknowledged, and the source being detailed in the dissertation and in the References sections.

Signed: _____ Date: _____

TABLE OF CONTENTS

List of figures

List of tables

List of Abbreviations

ASD – Analytical Spectral Devices

DO – Dissolved Oxygen

DWAF – Department of Water Affairs and Forestry

EC – Electrical Conductivity

GPS – Global Positioning System

ICP-OES – Inductively Coupled Plasma Optical Emission Spectrometry

NASA – National Aeronautics and Space Administration

NIR – Near-infrared

NOAA – National Oceanic and Atmospheric Administration

PCA – Principal Components Analysis

PLS – Partial Least Squares

R^2 – Coefficient of Determination

RMSE – Root Mean Square Error

SQGs – Sediment Quality Guidelines

SWIR – Shortwave infrared

TWQR – Target Water Quality Range

UEIP – uMgeni Ecological Infrastructure Partnership

USEPA – United Stated Environmental Protection Agency

USGS – United States Geological Survey

VNIR – Visible and near-infrared

WRC – Water Research Commission

List of units

°C – Degrees Celsius

% - Percentage

km – Kilometres

m – Metres

m^3 – Cubic metres

mg/kg – Milligrams per kilogram

mg/L – Milligrams per litre

µS/cm – Micro Siemens per centimetre

mS/m – Milli Siemens per metre

nm – Nanometres

Acknowledgments

I would like to express my sincere gratitude to the following:

- God Almighty for giving me the strength, courage, knowledge and guidance to undertake this research as well as His countless blessings throughout my academic career
- My late grandmother for her unconditional love and support and for her unwavering belief in me
- My parents, Mr and Mrs Ramcharan, for all the sacrifices they have made. Thank you for your belief in me, your advice as well as your unconditional love and support through everything. I am truly grateful for you both
- My supervisor, Professor Michael Gebreslasie, for his motivation, guidance, advice, support and belief in me
- The South African National Space Agency (SANSA) for providing financial assistance
- My family and friends for their words of encouragement and support
- Miss Tessnika Sewpersad for assistance with understanding and operating the ASD spectroradiometer and for her support and advice
- Mr Xolani Gumede and Dr Fathima Ali for assistance with laboratory procedures
- Ms. Zimbini Ngcingwana from the chemistry department at the University of KwaZulu-Natal's Pietermaritzburg Campus for analysing my water samples for heavy metals
- ALS Analysis and Inspection Laboratory for analysing my sediment samples for heavy metals
- The Durban Green Corridors for assistance during field sampling

This dissertation is dedicated to the loving memory of my grandmother, the late Rajina Devi Sunputh. Thank you for always believing in me even when I didn't believe in myself. I love you forever.

CHAPTER 1: GENERAL INTRODUCTION

1.1) Introduction

According to Day (1980, p. 198), an estuary can be defined as "*a partially enclosed coastal body of water which is either permanently or periodically open to the sea and within which there is a measurable variation of salinity due to the mixture of seawater with freshwater derived from land drainage*". In other words, estuaries are bodies of water located at the interface between land and sea and form transitional zones from freshwater to saltwater environments (Cochran et al., 2019; Harris et al., 2016). In recent years, with expansions in anthropogenic activities globally, the location of estuaries has made them highly susceptible to severe anthropogenic impacts (NOAA, 2020). Furthermore, the climate change implications resulting from increased anthropogenic activities have put an additional strain on estuaries (Glamore et al., 2016). In South Africa, there are 300 functional estuaries categorised into 46 types, of which 39% are classified as critically endangered, 2% as endangered, 2% as vulnerable and 57% as at least threatened (Van Niekerk and Turpie, 2012).

Estuaries are coastal bodies of water that occur where a river meets the sea. There are different types of estuaries, each of which are classified in different ways. A common method of classifying them is according to how they formed geomorphologically (NOAA, 2020). Estuaries that exist today were formed due to the sea level rising approximately 120 m when major continental glaciers began melting 18 000 years ago (Trujillo and Thurman, 2011). According to Trujillo and Thurman (2011), based on their geomorphological origin, there are four main classes of estuaries, including coastal plain estuaries, fjord, bar-built estuaries and tectonic estuaries. The most prevalent estuary type is the coastal plain estuary, which formed due to sea-level rise, which initiated the drowning of an existing river valley (NOAA, 2020). Fjords are deep U-shaped estuaries that formed when sea-level rise during the Pleistocene Epoch caused the flooding and erosion of glaciated valleys (Trujillo and Thurman, 2011; Finlayson et al., 2018). The melting of these glaciers resulted in the formation of lower valleys, facilitating seawater inflow into river valleys, thereby forming an estuary (Finlayson et al., 2018). Bar-built estuaries are formed when the connection with the sea is occasionally restricted by a sand bar forming a shallow estuary behind the bar (Clark and O'Connor, 2019). Tectonic estuaries form when faulting, and folding occurs on land surfaces, causing a basin to form onto which freshwater or seawater flows (NOAA, 2020).

Estuarine ecosystems are influenced by seawater and freshwater derived from rivers and land runoff (Harris et al., 2016). The freshwater from rivers carries abundant supplies of nutrient-rich sediment into estuaries enabling them to support high levels of biological productivity (Geyer, 2004). Therefore, estuaries are considered as one of the most productive ecosystems on earth (Colloty et al., 2002; Forbes and Demetriades, 2008; Cloern et al., 2016). The conditions within an estuary are also highly dynamic, ranging from fresh to hypersaline, depending on the amount of fluvial and seawater inflow into the estuary (Day et al., 1990; Harris et al., 2016). For this reason, estuarine organisms need to have unique adaptations to survive and thrive in these ecosystems (Forbes and Demetriades, 2008; Sisitka, 2008).

Estuaries are essential as they provide ecosystem services that are vital to both humans and aquatic life; therefore, it is crucial that we ensure our estuaries are protected and conserved (Hu et al., 2004; Dunn et al., 2019). Ecosystem services can be defined as "*the conditions and processes through which natural ecosystems, and the species that make them up, sustain and fulfil human life*" (Daily, 1997). These services include provisioning services such as food and water, regulating services such as climate regulation and purification of air and water, and cultural services such as cultural, educational, and recreational benefits (Van Niekerk and Turpie, 2012). Some examples of the ecosystem services provided by estuaries include a nursery function, storm protection, flood regulation and carbon sequestration (Van Niekerk and Turpie, 2012). These services are critical to both humans and aquatic life alike; however, estuaries have been increasingly subject to degradation due to human activities such as estuary mouth manipulation, land-use changes and pollution (Sisitka, 2008). Therefore, it is critical to ensure measures are put in place to monitor anthropogenic activities and assess their impacts on the health of estuaries in order to prevent further deterioration.

The advancements in technology, particularly within remote sensing, have enabled the introduction of innovative ways to assess the expansions in anthropogenic activities and assess water quality (Arnous and Hassan, 2015). According to Campbell and Wynne (2011, p. 6), remote sensing is defined as "*the practice of deriving information about the earth's land and water surfaces using images acquired from an overhead perspective, using electromagnetic radiation in one or more regions of the electromagnetic spectrum, reflected or emitted from the earth's surface*." It is a science that involves acquiring and recording information about objects from a distance, such as using satellites (Gibson, 2000; Jensen, 2015). The use of remote sensing technology is particularly useful in monitoring the water and sediment quality

of various water bodies such as rivers and estuaries, as it is an inexpensive method (Melesse et al., 2007). Remote sensing is thus extremely useful as it enables us to understand the relationships and interactions between humans and the natural environment, enabling us to improve our decision-making (Jensen, 2015).

Hyperspectral remote sensing deals with reflectance spectroscopy, whereby light is studied as a function of the wavelength that is reflected or scattered from a solid, liquid or gas (Rostom et al., 2017). It refers to the science of acquiring information about the earth's surface in many narrow spectral bands (Borengasser et al., 2007). Multispectral remote sensing makes use of several broadly defined spectral regions, whereas hyperspectral remote sensing examines many narrowly defined spectral channels (Campbell and Wynne, 2011). Hyperspectral data are obtained in many extremely narrow, contiguous spectral bands enabling the detailed assessment of earth's surface materials with no gaps through which essential information may be overlooked (Govender et al., 2007; Goetz, 2009). Hyperspectral data is useful in assessing the quality of water and sediments; however, several factors can also influence the spectral reflectance of these surfaces (Lillesand et al., 2015). The factors influencing the spectral reflectance of water include the presence of suspended sediments and chlorophyll content (Lillesand et al., 2015). The factors influencing the spectral reflectance of sediments include soil moisture content, particle size, organic matter content, and the amount of iron oxide (Cierniewski and Kuśnierek, 2010).

1.2) Contextualisation of the problem and motivation of the study

As the global population rapidly increases, many land-use practices, such as agriculture, residential areas, and industries, will also have to expand to support the growing populations (Sukdeo, 2010). These expansions bring about significant threats to natural resources, as well as the quality of the environment (McGrane, 2016). Industrial and agricultural activities are critical land-use practices that form the backbone of our economy. They enable a growth in the Gross Domestic Product (GDP) of our country and job creation, which is essential to the country's development. Therefore, urban expansion is unavoidable and inevitable. However, this is not without an environmental problem, such as a deterioration in the water and sediment quality of estuaries.

Estuaries have many benefits, including ecological and socio-economic benefits (Edgar et al., 2000; Van Niekerk and Turpie, 2012). Ecologically, these ecosystems are essential as they are

home to various plant and animal species that rely on estuaries for food, with many animal species using estuaries as breeding grounds and a nursery for their young (Van Niekerk and Turpie, 2012; NOAA, 2018). Socio-economically, estuaries are essential to humans as they have an excellent aesthetic appeal, and they provide a place for recreational activities for locals and tourists (Edgar et al., 2000; Cochran et al., 2019). These activities include boating, fishing, swimming and contact sports, and sightseeing which aid in the generation of money and the creation of job opportunities for the locals (Pinto et al., 2010). Therefore, estuaries help in increasing the GDP of our economy (Van Niekerk and Turpie, 2012; Cochran et al., 2019). However, as a result of urbanisation and industrialisation, which exacerbates the effects of climate change, estuaries are increasingly subjected to degradation (Cloern et al., 2016).

Urbanisation severely affects the health of aquatic habitats as it alters the physical landscape resulting in increased impermeable surfaces such as roads and pavements (Riley, 2008). Urban runoff, due to the presence of these impermeable surfaces, causes an increase in the levels of pollutants being discharged into rivers and estuaries (Riley, 2008). Impermeable surfaces result in a significant reduction in the natural infiltration process of soils and vegetation cover, which increases runoff after heavy rains, thus decreasing the quality of aquatic ecosystems (Karakus et al., 2015). In addition, rapid industrialisation leads to excessive amounts of heavy metals being discharged into rivers and estuaries, which degrades the water and sediment quality (Ebenstein, 2012). This is consistent with a study conducted by Ebenstein (2012), where China's rapid industrialisation led to a significant increase in the number of heavy metals being discharged into rivers, which severely deteriorated the water quality of these rivers.

Furthermore, rapid urbanisation and industrialisation cause an excessive increase in carbon dioxide emissions, which exacerbates the effects of climate change (Sisitka, 2008; Whitfield et al., 2012). According to Glamore et al. (2016), climate plays a significant role in the functioning of estuarine environments. The changes in rainfall patterns resulting from climate change could alter freshwater inflows and sedimentation and erosion rates (Glamore et al., 2016). This could, in turn, lead to excess amounts of sediment and other pollutants such as heavy metals derived from land runoff flowing into the estuary.

Heavy metals are described as metals with a density higher than $5g/cm^3$ and occurs naturally in the environment (Hui, 2008). Heavy metals can be found in nearly all parts of the biotic and abiotic environment, including water, sediments, plants, animals and humans (Hui, 2008). Heavy metals enter the environment naturally through the weathering of existing rocks

containing these heavy metals and anthropogenically through the use of heavy metals in industrial and agricultural activities (Pati et al., 2013; Wuana and Okieimen, 2011). Some heavy metals, such as zinc and iron, are required by living organisms to aid growth and development (Sukdeo, 2010). However, when in excess, these can become toxic and cause health deteriorations in organisms (Hui, 2008). Pollution from land-use practices such as urbanisation and industrialisation pose significant threats to the water quality of rivers and estuaries as this can lead to an increase in heavy metal contamination (Cloern et al., 2016).

Heavy metal contamination endangers not only aquatic life within that habitat but also human life and is of particular concern as these heavy metals tend to be persistent in the environment for a long time, even after the sources of these heavy metals have been removed (Cloern et al., 2016; Javed and Usmani, 2017). The increase in industrial and agricultural activities have led to an increase in the discharge of effluents containing heavy metals into rivers and estuaries (Riley, 2008). Most heavy metals in water tend to adsorb onto the surfaces of sediments and settle to the bottom of the river or estuary (Mann et al., 2011). Industrial effluents can alter physicochemical parameters such as electrical conductivity, pH and dissolved oxygen levels of estuaries, which can cause the water to become toxic (Van Niekerk and Turpie, 2012). In addition, fluctuations in these parameters can also cause the remobilisation of the heavy metals adsorbed onto sediments, making them available for uptake by aquatic organisms (Li et al., 2013). These heavy metals tend to accumulate in aquatic organisms over time, causing damage to their organs and respiratory functions, a reduction in the rates of reproduction and even death (Verma and Dwivedi, 2013; Bisht, 2019).

It is for this reason; the heavy metal concentrations of estuaries need to be regularly assessed so that there can be adequate intervention if need be. However, conventional methods of assessing heavy metals in water and sediments can be costly, making it infeasible to monitor their concentrations regularly. Therefore, it is necessary to explore alternative ways to assess heavy metal concentrations that are more cost-effective, thus facilitating the regular monitoring of their concentrations. Remote sensing can be used to assess heavy metals in water and sediment and has been used in many international studies as an alternative to conventional methods of heavy metal assessment. According to Monaledi et al. (2019), remote sensing has become popular in water quality assessments as it offers a cost-effective way of assessing larger datasets and providing temporal and spatial coverage. A study conducted by Mouazen et al. (2021), involved the use of Landsat 7 and regression methods in the spatiotemporal prediction

and mapping of heavy metals in soil. The results of the study indicated a good link between Landsat 7 imagery and the prediction of heavy metals. The prediction models performed well in predicting heavy metal concentrations from the spectral reflectance data obtained from the Landsat 7 imagery (Mouazen et al., 2021). In recent years, the rapid advancement in hyperspectral remote sensing facilitated the use of hyperspectral data in water and sediment quality studies which yielded promising results with high accuracies (Dierssen et al., 2021). Hyperspectral remote sensing has thus been favoured by many researchers over multispectral remote sensing (Dierssen et al., 2021).

Hyperspectral data contain the detail and accuracy that enables one to examine phenomena on the earth's surface that far exceed the capabilities of traditional remote sensing (Campbell and Wynne, 2011). The capabilities of hyperspectral remote sensing enable the field of remote sensing to extend into the field of spectroscopy which is the science of obtaining accurate data on the spectral reflectance of earth's surface materials from a remote location (Milton et al., 2009). An analytical spectral device (ASD) spectroradiometer is an optical device commonly used in field spectroscopy that uses detectors to measure radiation distribution in a particular wavelength region (Rostom et al., 2017). It measures the spectral behaviour in the visible near-infrared (VNIR) and shortwave infrared (SWIR) spectra between 350 and 2500 nm with a precision of 1 nm (Janse et al., 2018). ASD makes use of a portable PC to control the scans collected by the instrument, and it also allows for the on-screen visualisation of the data collected in real-time (Danner et al., 2015). The use of hyperspectral data to assess water and sediment quality is particularly advantageous as it is inexpensive, more efficient and less time-consuming (Brando and Dekker, 2003; Rostom et al., 2017). It is for this reason; hyperspectral remote sensing will be used to analyse the heavy metal concentrations of the uMgeni Estuary.

1.3) Aim and Objectives

Aim: To assess the use of visible and near-infrared reflectance spectroscopy in the detection of heavy metals in the water and sediment of the uMgeni Estuary.

Objectives:

1. To assess heavy metal concentrations in the water and sediment of the uMgeni Estuary.
2. To assess the relationship between heavy metals and physicochemical parameters of water.

3. To assess the spectral reflectance of the water and sediment using an analytical spectral device (ASD) FieldSpec 3 spectroradiometer.

4. To develop a calibration model to predict the heavy metal concentrations from the visible and near-infrared spectral reflectance measurements.

5. To assess the relationship between the heavy metals and the visible and near-infrared spectral reflectance of the samples.

1.4) Structure of the dissertation

The introduction, contextualisation of the problem, aims and objects are discussed in chapter one, while chapter two of the dissertation covered the theoretical concepts relating to the research carried out in this study. Chapter three provides information about the study area including the location and physical characteristics, geology and soils, topography, climate, biology and the land-use occurring within the study area. Chapter four describes the methodology adopted to carry out this study and includes information on the field and laboratory data collection as well as descriptions of the data analyses performed on the acquired data. In chapter five, the results of the data analyses are presented in the form of tables and graphs. Finally, chapter six provides a detailed discussion of the results obtained in chapter five as well as provides the conclusion and recommendations for future research.

CHAPTER 2: LITERATURE REVIEW

2.1) Introduction

Water is a precious natural resource that is required for the survival of all forms of life on earth. Without water, all life on earth would cease to exist; therefore, we must ensure that all water resources are protected and that our use of aquatic ecosystems such as estuaries is sustainable. This chapter provides a review of the theoretical concepts central to this study. It begins by highlighting the general features of estuaries, their formation and classification, as well as the importance of estuaries and threats to these ecosystems. Thereafter, the review focuses on heavy metals, their impacts on estuaries, and the traditional and remote sensing methods used to extract and analyse the concentrations of these heavy metals.

2.2) Estuaries

2.2.1) General characteristics of estuaries

According to Day (1980, p. 198), an estuary can be defined as "*a partially enclosed coastal body of water which is either permanently or periodically open to the sea and within which there is a measurable variation of salinity due to the mixture of seawater with freshwater derived from land drainage*". Estuaries are found at the interface of land and sea where freshwater meets saltwater. Estuaries are, thus, influenced by the tidal inflow from the sea and the discharge of freshwater from rivers and land runoff (Whitfield, 1992; Chili, 2008; Miththapala, 2013). Estuaries are considered highly dynamic environments as the physical, chemical, and biological components of estuaries are often subjected to rapid and sometimes extreme changes (Forbes and Forbes, 2012).

Estuaries may be permanently or temporarily opened to the sea, and due to the mixture of seawater and freshwater, they have measurable variations in their salinities (Whitfield, 1992). According to Miththapala (2013), estuaries generally consist of three main zones; the first zone is where the freshwater from the river begins to meet the saltwater and contains primarily freshwater. The subsequent zone, towards the ocean, contains freshwater and saltwater of approximately equal amounts. The last zone is the point at which the water flows into the sea and contains mostly saltwater (Miththapala, 2013). In addition, according to Forbes and Demetriades (2008), a reduction in fluvial input could cause an estuary to become a lagoon,

leading to fresh or hypersaline conditions. The increase in the fluvial input, on the other hand, could cause an estuary to become a river mouth with very little to no saline input (Forbes and Demetriades, 2008).

The geographic location of estuaries enables them to host a variety of unique habitats from the sea to the land, thus enabling them to support a high level of biodiversity (Harrison, 2004; Moyle, 2020). Estuaries serve many functions, including a nursery to many fish and invertebrates, a place of recreation, and a source of food and income (Cisneros, 2013). Therefore, estuaries are critical ecosystems, and they need to be protected to maintain their functioning. However, these estuaries are increasingly adversely affected by human activities (Harris et al. 2016). As a result of these activities, many South African estuaries have become functionally degraded. According to Turpie et al. (2002), this is often accompanied by a loss of species or a decline in populations. It is, therefore, crucial that the health status of estuaries be continuously monitored to ensure the conservation of these precious ecosystems.

2.2.2) Classification of estuaries

There are many different types of estuaries, each of which can be classified in different ways. One method is the geomorphological classification, proposed by Harrison et al. (2000), classifying estuaries according to their geomorphological origin. According to Turpie (2004), this classification includes six types of estuaries based on the mouth status, whether it is opened or closed, the size of the estuary, and the presence of a sand bar. Estuaries that exist today were formed due to the sea level rising approximately 120 m when major continental glaciers began melting 18 000 years ago (Trujillo and Thurman, 2011). According to Trujillo and Thurman (2011), based on their geomorphological origin, there are four main classes of estuaries, including coastal plain estuaries, fjord, bar-built estuaries and tectonic estuaries. The most common type of estuary is the coastal plain estuary formed due to sea-level rise, which initiated the drowning of an existing river valley (NOAA, 2020). Fjords are deep U-shaped estuaries formed when sea-level rise during the Pleistocene Epoch caused the flooding and erosion of glaciated valleys (Trujillo and Thurman, 2011; Finlayson et al., 2018). Presently, these glaciers have melted, resulting in lower valleys that facilitate seawater inflow into river valleys, thereby forming an estuary (Finlayson et al., 2018). Bar-built estuaries also referred to as lagoon-type estuaries, are formed when the connection with the sea is occasionally restricted by a sand bar, forming a shallow estuary behind the bar (Clark and O'Connor, 2019). This sand bar is formed when sediments are continuously deposited parallel to the coast due to wave action (Trujillo

and Thurman, 2011; Clark and O'Connor, 2019). Tectonic estuaries form when faulting, and folding occurs on land surfaces, causing a depression or a basin to form onto which freshwater or seawater flows (NOAA, 2020). The mixing of seawater and freshwater thus forms a tectonic estuary.

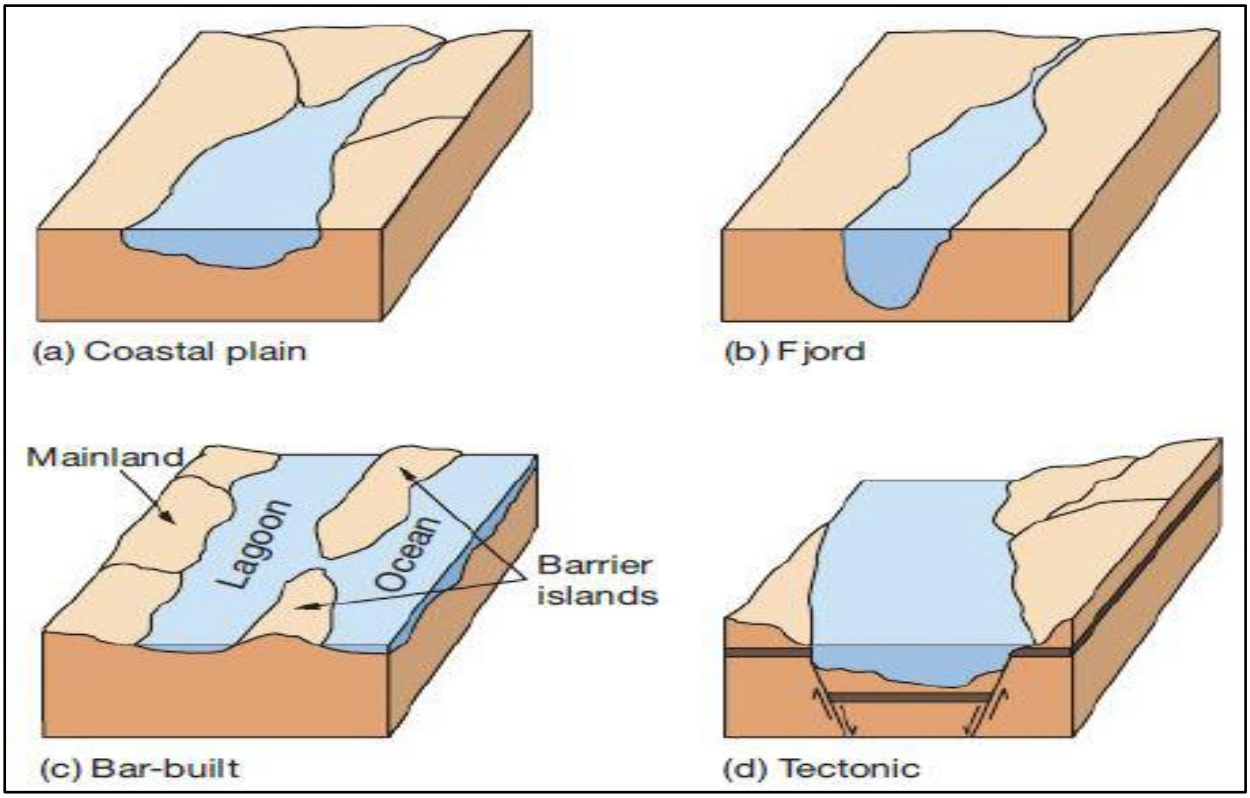

Figure 2.1: Diagram illustrating the classification of estuaries by geomorphological origin (Source: Trujillo and Thurman, 2011).

Another method of estuarine classification is based on water circulation and how the river and tidal flows interact within an estuary (Finlayson et al., 2018). Freshwater is less dense and flows across the upper layer of the estuary towards the sea, whereas the denser saltwater flows in a layer just below toward the head of the estuary (Trujillo and Thurman, 2011). However, tidal movement within an estuary can cause the freshwater and saltwater to become mixed despite having varying densities (Finlayson et al., 2018). This, in turn, results in a more significant variation in physicochemical parameters within an estuary. According to Trujillo and Thurman (2011), four types of estuaries can be classified based on water circulation and the physical characteristics of the estuary. These include vertically mixed estuaries, slightly stratified estuaries, highly stratified estuaries, and salt wedge estuaries. A vertically mixed estuary is a shallow, low-volume estuary and occurs when the tidal flows are more prevalent

(Finlayson et al., 2018). Freshwater mixes uniformly with seawater, resulting in salinity levels being evenly distributed from the surface to the bottom of the estuary (Trujillo and Thurman, 2011). Across the estuary, salinity levels increase from the head to the mouth; therefore, salinities are lowest at the head due to freshwater inflow and highest at the mouth due to seawater inflow (Webb, 2019). A slightly stratified or partially mixed estuary is usually a deeper estuary and occurs when the river and tidal flows are equal (Finlayson et al., 2018). Waves and currents mix surface waters; however, mixing may not extend to the lower layers resulting in, the lower layers of the estuary having higher salinity levels than the surface layers. (Webb, 2019). Salinity levels are highest near the mouth and decrease as one move upstream (NOAA, 2020). A highly stratified estuary is a deep estuary, and as a result of the deeper depths, freshwater and saltwater only mix close to the surface (Webb, 2019). The upper layer salinity levels increase from the head to the mouth, reaching levels near to that of the open sea (Trujillo and Thurman, 2011; Webb, 2019). The lower layer salinity levels, on the other hand, are uniform at any depth throughout the estuary (Trujillo and Thurman, 2011). Mixing occurring at the interface of the upper and lower waters forms a net movement of water from the bottom to the surface, with the surface waters becoming more saline as the deep waters mix with it (Trujillo and Thurman, 2011). This results in the formation of strong haloclines at the interface of the upper and lower waters. A salt wedge estuary occurs when the river flows dominate tidal flows (Finlayson et al., 2018) and results from a wedge of saltwater intruding the estuary beneath the freshwater (Trujillo and Thurman, 2011). The freshwater is less dense and flows out along the surface, and saltwater flows in at depth, creating a wedge of saltwater flowing at the bottom (Webb, 2019). The freshwater flows over the denser saltwater leading to a sharp horizontal salinity gradient or pycnocline at depth and a pronounced vertical salinity gradient or halocline at any point throughout the estuary (Trujillo and Thurman, 2011; Finlayson et al., 2018).

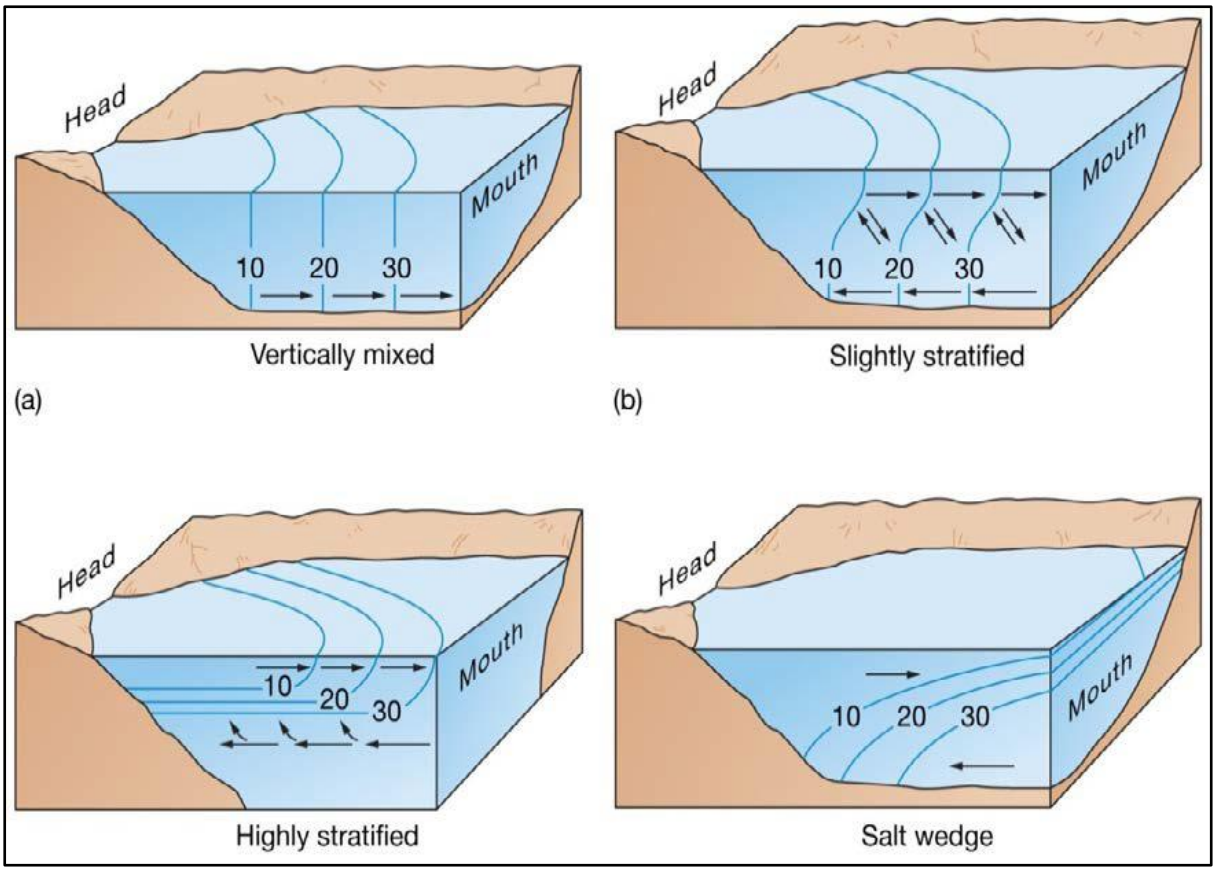

Figure 2.2: Diagram illustrating the classification of estuaries by water circulation (Source: Trujillo and Thurman, 2011).

The Whitfield classification is another method that is widely used to classify estuaries in southern Africa. It classifies estuaries into five main types: permanently open estuaries, estuarine bays, river mouths, temporarily open/closed estuaries and estuarine lakes (Sisitka, 2008). These five types can be characterised by the tidal prism size, which is the amount of tidal water exchange, mixing process, as well as their average salinity levels (Turpie, 2004). Permanently open estuaries, estuarine bays and river mouths tend to be permanently open to the sea, whereas all temporarily open/closed estuaries (TOCEs) and many estuarine lakes close periodically (Turpie, 2004). Permanently open estuaries are typically large systems with the river catchments of the estuaries having a perennial flow in their natural condition and a moderate tidal exchange with the sea (Whitfield, 1992; Sisitka, 2008). They have a moderate tidal prism (1-10 x 10^6 m^3), a tidal or riverine mixing process, and a mean salinity ranging between 10 - >35 ppt (Turpie, 2004). Wetlands or salt marshes can be found within permanently open estuaries, and the fauna is primarily marine and estuarine (Whitfield, 1992; Turpie, 2004). Estuarine bays have wide mouths with a strong tidal exchange with the sea,

leading to a permanently open mouth (Sisitka, 2008). They have a large tidal prism (>10 x 10^6 m^3), resulting in the regular replacement of estuarine water in the lower and middle reaches (Whitfield, 1992; Sisitka, 2008), tidal mixing process, and mean salinity ranging between 20-35 ppt (Turpie, 2004). Estuarine bays are usually associated with extensive wetland and mangrove swamps, and marine and estuarine species dominate these estuaries without freshwater species in the lower and middle reaches (Whitfield, 1992; Turpie, 2004). River mouths have large river catchments, with the river typically dominating the physical processes within the estuary (Whitfield, 1992). These estuaries are associated with strong riverine outflow, which inhibits marine inflow. They have a small tidal prism (<1 x 10^6 m^3), riverine mixing process, and mean salinity of <10 ppt (Turpie, 2004). Freshwater species dominate these estuaries, with marine and estuarine species generally confined to the lower reaches (Whitfield, 1992). Temporarily open/closed estuaries or TOCEs generally have small river catchments and are often closed for many months of the year and sometimes for many years at a time (Sisitka, 2008). The formation of sand bars at the mouth, which inhibits the connection with the sea, is characteristic of these estuaries (Turpie, 2004). This occurs due to low river flow conditions and longshore sand movement on the adjacent coast (Whitfield, 1992). They have a small tidal prism (<1 x 10^6 m^3); however, the prism is absent when the sand bar is fully developed (Whitfield, 1992). The mixing process is driven by wind and the mean salinity levels range between 1 - > 35 ppt (Turpie, 2004). TOCEs are dominated by marine and estuarine species; however, during oligohaline conditions, the abundance of some freshwater species increases (Whitfield, 1992). Estuarine lakes occur where a coastal lake is connected to the sea by a channel of variable length and width (Sisitka, 2008). Most estuarine lakes in southern Africa formed due to a drowned river valley that was primarily infilled by reworked sediments and is now separated from the ocean by vegetated dunes (Whitfield, 1992). These dunes can completely divide the lake and the sea leading to a loss of estuarine characteristics, forming a system known as a coastal lake. They have a small tidal prism (<0.1 x 10^6 m^3), a mixing process that is wind-driven and mean salinity levels ranging between 1 - > 35 ppt (Turpie, 2004). Depending on the salinity conditions, marine, estuarine and freshwater species can all be found within these estuaries (Turpie, 2004).

2.2.3) Importance of estuaries

Estuaries are essential as they provide a home to various plant and animal species and provide various ecosystem services (Barbier et al., 2011). The concept of ecosystem services was

established to illustrate how the goods and services provided by natural ecosystems benefit society and create awareness for biodiversity conservation (Birkhofer et al., 2015). These services can be divided into three primary categories: provisioning services, regulating services, and cultural services (Van Niekerk and Turpie, 2012).

Provisioning services refer to the products derived from ecosystems for basic human needs and include food, raw materials, and medicines (Thrush et al., 2013; Daborn and Redden, 2016; Trettin et al., 2019). Estuaries are home to a variety of fish and shellfish that can be harvested by recreational and commercial fishers (Thrush et al., 2013). The raw materials derived from estuaries include sand and aggregate for construction, salt, and hydrocarbons, including oil and gas (Daborn and Redden, 2016). In terms of medicine, the biological and chemical compounds from estuarine plants and animals have been researched for their potential pharmaceutical and nutritional benefits (Thrush et al., 2013; Daborn and Redden, 2016).

Regulating services refer to the ecosystem functions that provide value and include regulation of waste and carbon sequestration (Van Niekerk and Turpie, 2012; Trettin et al., 2019). These services are essential to humans as it aids in producing the air we breathe and mitigating anthropogenic impacts (Thrush et al., 2013). Estuarine organisms aid in removing harmful pollutants discharged into the water from human activities, thus aiding in water purification (De Groot et al., 2002). Bacteria found in bottom estuarine sediments are capable of detoxifying heavy metals, and some species of shellfish are capable of sequestering heavy metals, thus reducing the risk of toxicity to other aquatic species (Thrush et al., 2013). According to Igiri et al. (2018), microbes such as bacteria use up heavy metals and metalloids present in the water for generating energy, thus reducing their concentrations in the water. In addition, microbes are also capable of converting heavy metal ions from one oxidation state to another, thus minimising their harmfulness (Igiri et al., 2018).

Carbon sequestration refers to the process of capturing and storing carbon dioxide to reduce the amount available in the atmosphere, thus contributing to climate regulation (Heckbert et al., 2011; Perera and Amarasinghe, 2019). Estuarine ecosystems can sequester carbon dioxide within biomass and soil (Van Niekerk and Turpie, 2012; Perera and Amarasinghe, 2019). All primary producers use carbon dioxide for photosynthesis; however, large estuarine vegetation such as mangroves and seagrasses can store carbon dioxide over a more extended period (Thrush et al., 2013). According to Schmidt et al. (2011), the carbon found in soil organic matter accounts for more than three times the carbon found in the atmosphere or terrestrial

vegetation. The ability of estuaries to store significant amounts of carbon in sediment and biomass aids in reducing the effects of climate change and global warming due to increased carbon dioxide emissions (Nellemann et al., 2009).

Cultural services refer to the value obtained from the existence of an ecosystem such as an estuary (Cochran et al., 2019). Cultural services include aesthetic experiences, ecotourism, and recreational and educational benefits (Trettin et al., 2019). Culturally, estuaries are essential to humans as they contribute to human well-being and overall quality of life (Edgar et al., 2000). Estuaries have an excellent aesthetic appeal, act as tourist attractions as they provide a place for people to enjoy leisure-time as well as partake in numerous recreational activities, including fishing, swimming, boating, canoeing, sight-seeing as well as picnics (De Groot et al., 2002; Pinto et al., 2010). In addition, estuarine ecosystems allow for educational opportunities such as academic research and environmental programmes (Hutcheson et al., 2018). This provides people with the opportunity to study them and information on their importance, thus aiding in their conservation (Hutcheson et al., 2018).

Estuaries also have ecological and socio-economic benefits. Ecologically, estuaries are among the most productive ecosystems in the world. This productivity can be attributed to the interaction between marine and riverine environments (NOAA, 2019). They receive nutrients and sediments from these environments enabling them to support a wider variety of life (NOAA, 2019). According to Van Niekerk and Tupie (2012), ecological benefits provided by estuaries include nursery function, filtration, flood regulation and storm protection.

Estuaries are commonly referred to as "nurseries of the sea" as they provide nesting and breeding grounds for several animal species (NOAA, 2019). Daily tidal fluctuations result in changes to the water depth and chemistry of estuaries, creating a wide range of habitats within the estuary (NOAA, 2020). Seagrass beds present in estuaries create a safe ground for juvenile fish and invertebrates to feed and avoid predation until they grow big enough to survive in the open sea (Hughes et al., 2014). Estuaries also serve as a major stopover for migratory animal species, including waterfowl and salmon (NOAA, 2020). Wetland and salt marsh habitats that fringe estuaries aid in filtering out sediment and pollutants derived from land runoff (Nelson and Zavaleta, 2012). This results in cleaner and more transparent water entering the estuaries, which benefit aquatic life. Estuarine plants such as mangroves, reeds and seagrasses also act as a natural buffer against floods and storms (Barbier et al., 2011). They absorb and provide a barrier against floodwaters from land and storm surges from the sea.

Economically, estuaries are extremely valuable to communities and businesses along the coast. They provide many benefits and opportunities and make significant contributions to the local and national economy (Van Niekerk and Turpie, 2012). Estuaries bring in substantial revenue for local governments as they increase the value of the property developed along the estuaries (Van Niekerk and Turpie, 2012). Estuaries also provide a host of recreational activities and act as tourist attractions, enabling them to create job opportunities for the locals as well as generate significant income for the local economy (Pinto et al., 2010).

2.2.4) Threats to estuaries

There has been an increasing concern for the health status of South African estuaries since the 1970s, when it was discovered that only a few estuaries remain in their natural state. According to Turpie (2004), most of the estuaries in South Africa have been altered and impacted by human activities. In addition, climate change exacerbated by increased anthropogenic activities has severely impacted estuarine ecosystems. The present ecological state refers to a set of categories (A – F) that describe the ecological condition of estuaries and was developed by the department of water and sanitation (Van Niekerk et al., 2019). Category A refers to estuaries in their natural state, category B refers to estuaries with a few changes and are largely natural. Categories C and D refer to moderately modified and largely modified estuaries, respectively and categories E and F refer to highly degraded and extremely degraded estuaries, respectively (Van Niekerk et al., 2013). According to Van Niekerk et al. (2019), the uMgeni Estuary is in a poor condition and the present ecological state of the uMgeni Estuary is highly degraded.

The increase in the global population of the world has resulted in a significant increase in human activities. This, in turn, has resulted in the negligent use of water resources, and the outcome of this is water pollution (Pillay, 2002). Pollution can be described as the addition of substances into the environment at a faster rate than it can be recycled, decomposed or stored in a harmless form (Nathanson, 2010). Therefore, pollution is most likely to cause negative impacts on the environment and the organisms that inhabit it (Nathanson, 2010).

Pollutants can be in the form of gases or organic and inorganic compounds, and according to Sukdeo (2010), these can be either natural or synthetic compounds. As a result of human activities, the amount of these compounds increases. This can lead to the environment becoming toxic, which has detrimental effects on the organisms that inhabit the environment (Pillay, 2002). Pollution can be emitted from either a point source or a non-point source

(Nathanson, 2010). Point source pollution is the pollution emitted from a single, known source and is usually easier to control as it only has one source (Pillay, 2002). Non-point source pollution, on the other hand, refers to the pollution that is emitted from various sources, and this type of pollution is more difficult to pinpoint and control as it has many sources (Sukdeo, 2010). Therefore, non-point source pollution has a higher level of pollutants than point source pollution (Nathanson, 2010).

According to Showalter et al. (2000), non-point source pollution occurs from either the atmosphere, such as acid rain entering a watercourse or when surface water is drained into a river. Non-point pollution can occur due to expansions in activities such as urban, residential and agricultural land-use practices. According to Pillay (2002), this makes it difficult to control and manage non-point source pollution. In point source pollution, the concentrations of pollutants in the environment decrease with distance from the source (Pillay, 2002). However, for non-point source pollution, the impact on the environment is more severe (Sukdeo, 2010).

According to Sukdeo (2010), the water quality of rivers and estuaries of a country has a strong link to the uses of water and the levels of economic development. The economic sectors which have the most impacts on estuaries in South Africa include the following:

2.2.4.1) Urban sector

The rapidly increasing world population has resulted in rapid urbanisation. The significant expansion in urban areas has, in turn, led to an increase in the demand for infrastructure such as roads to allow for easy accessibility in and around the area (Azevedo et al., 2016). The clearing of land to make way for this new infrastructure puts a strain on aquatic ecosystems.

Urbanisation has resulted in an increase in non-permeable surfaces associated with development, which has resulted in a decrease in the amount of rain that can penetrate the surface to contribute to groundwater supplies (Riley, 2008). These non-permeable surfaces have increased urban runoff, consisting of a mixture of petrol, hydrocarbons, and organic compounds such as heavy metals and other nutrients (Wuana and Okieimen, 2011). These substances can enter a river system and be transported into estuaries can accumulate, causing highly toxic conditions within the estuary (Sukdeo, 2010). There have not been many studies done on the impacts of urban runoff on aquatic life. However, according to Nunkumar (2002), the effects of urban runoff being discharged into river systems and eventually estuaries is approximately equal to the effects of secondarily treated domestic sewage.

Urbanisation can also be linked to a significant increase in the amount of waste and sewage production (Pires et al., 2015). If there are no proper disposal and treatment procedures in place or if there are any faults with the structures put in place to treat the sewage, it can be discharged into rivers (Sukdeo, 2010). The waste can, in turn, be transported into estuaries resulting in contamination and eutrophication of the water (Anderson et al., 2002).

2.2.4.2) Commercial agriculture

Commercial agriculture, such as sugarcane farming in and around river catchments and estuaries, is one of the main threats to estuaries (Forbes and Forbes, 2012). Chemicals such as fertilisers, pesticides, and herbicides commonly used in agriculture may make their way into rivers through surface runoff (Jeppesen et al., 2015). In order to grow and complete their lifecycles, plants require both macronutrients (mainly nitrogen, phosphorous and potassium) and micronutrients (heavy metals such as iron, chromium and zinc). However, some soils are deficient in heavy metals; therefore, fertilisers have been introduced to these soils to aid in plant growth (Wuana and Okieimen, 2011). As a result of increased commercial agricultural activities, large quantities of fertilisers are continuously applied to croplands leading to significant increases in heavy metals in soils (Wuana and Okieimen, 2011).

Furthermore, pesticides and herbicides also contain heavy metals, and the increased use of these chemicals in agriculture also results in heavy metal accumulation in soils. This is consistent with a study conducted by Tariq et al. (2016), where soil samples from cotton fields treated with pesticides were tested for heavy metals. The results indicated an increase in heavy metals such as copper, nickel and cadmium with an increase in the use of certain pesticides (Tariq et al., 2016). Surface runoff causes large amounts of sediments and soils to be washed into rivers, and when these chemicals get into the water, they can cause nutrient and heavy metal levels to increase (Forbes and Forbes, 2012). Increases in nutrients and heavy metals can, in turn, alter the functioning of the ecosystem and cause a decline in aquatic biodiversity (Forbes and Forbes, 2012).

The conversion of land for agricultural purposes has led to severe impacts on the water quality of rivers and estuaries. A riparian buffer zone is a portion of land with vegetation and is found along the boundaries of a waterway (Mackenzie, 2015). Riparian vegetation provides a barrier between the water and the land. This type of vegetation is essential as when contaminants from runoff flow towards the river, they become trapped in the roots of the vegetation, enabling the

contaminated water to infiltrate the soil (Mackenzie, 2015). When natural vegetation is cleared for commercial farming, it results in high levels of erosion, as the soil becomes less stable and is exposed to the effects of wind and water erosion (Sukdeo, 2010). These types of erosion can lead to high levels of sediment being discharged into rivers and estuaries, resulting in siltation and sedimentation (Hubbard et al., 2004; Sukdeo, 2010).

Siltation occurs when fine sediment particles transported into rivers and estuaries remain in suspension and causes the water to become murky (Bell et al., 2000). On the other hand, sedimentation occurs when these suspended particles settle at the bottom of the river or estuary (Bell et al., 2000). Siltation is especially common in areas where riparian vegetation has been replaced by agricultural practices (Hubbard et al., 2004). Siltation can cause the turbidity of the water to increase due to the excess sediments, which has further implications. Some of these implications include reduced visibility in fish and a reduction in the depth at which light can penetrate the estuary (Mackenzie, 2015). Siltation can also be caused by an increase in built-up areas and activities such as sand mining and dredging in and around river banks and estuaries (Azevedo et al., 2016). Sand mining is particularly detrimental to the river and estuarine systems as this cause a widening of the floodplain, which reduces the stability of the river and its natural functioning (Sukdeo, 2010). Dredging refers to the process by which silt, sediments and other debris are removed from the bottom of water bodies (NOAA, 2020). However, sediment spills often occur during the dredging process, which causes an increase in suspended sediment particles resulting in siltation (Smith et al., 2019). Furthermore, the clearing of land for development exposes the soil to wind and water erosion, elevating the rates of sedimentation and siltation of rivers and estuaries (Pillay, 2002).

Additionally, the abstraction of water from river systems to be used in the irrigation of agricultural land can lead to a significant reduction in the flow rates of a river and freshwater inflow into estuaries (Du Preez and Hosking, 2010; Jeppesen et al., 2015). This can severely impact the functioning of estuaries. Habitat loss for a variety of fish, bird and vegetation species, and a reduction in the area available for boating activities are some of the consequences of a reduction in freshwater inflow into estuaries (Du Preez and Hosking, 2010).

2.2.4.3) Industrial sector

The industrial sector is regarded as a critical component as it aids in developing the economy of a country. Industries are associated with generating large amounts of money through the sale

of manufactured goods and providing job opportunities and skills, thus contributing to economic growth (Sukdeo, 2010). However, the industrialisation of a country is not without environmental impacts. Industrial activities often result in the pollution of the environment and water resources, leading to the subsequent degradation of the environment.

According to Adekunle and Eniola (2008), rivers are usually seen as a means to dispose of wastewater and effluents, especially from industries found close to rivers. The effluents from industries usually contain large amounts of chemicals containing heavy metals which significantly increases the level of pollution within a water body (Hsu et al., 2016). They can cause changes to the physical, biological and chemical properties of the water (Adekunle and Eniola, 2008). According to Sukdeo (2010), industrial effluents are currently among the most common sources of water pollution, and the amounts of these effluents constantly increase as countries are becoming more and more industrialised.

Industrial effluents initially alter a water body's physical and chemical properties, and these alterations lead to the biological deterioration of that water body (Sukdeo, 2010). These effluents are toxic to aquatic life as they tend to accumulate in fish leading to adverse health impacts including poisoning, diseases and death (Zeitoun and Mehana, 2014). This is consistent with a study conducted by Fatima and Usmani (2013) where the ecological impacts of heavy metal accumulation in fish tissue were investigated. The results indicated that fish living in waters containing excessive levels of chromium, nickel and lead from industrial effluents had severe liver and kidney damage due to the bioaccumulation of these heavy metals (Fatima and Usmani, 2013). As a result of the rapid industrialisation of countries, it is becoming increasingly difficult to reduce the negative impacts of these effluents and protect aquatic ecosystems such as estuaries.

Table 2.1: Estuary pressure assessment for the uMgeni Estuary (Sourced from: Van Niekerk et al., 2018).

Key estuarine pressures	**Levels**
Flow modification	Very high
Pollution	Very high
Habitat loss	Very high
Fishing effort	Very high
Artificial breaching	Low
Invasive aliens: Plants	Medium
Invasive aliens: Fish	Very high

2.3) Sediment processes

Sediment refers to the fragmented material produced by the physical or chemical weathering of rocks and includes deposits such as gravel, sand, mud, minerals and shells (Colby, 1963). Sediments typically consist of loose fragments of rocks or minerals broken of bedrock, mineral crystals precipitated out of the water, and shells (Marshak, 2008). Sediment can be categorised into three broad groups based on their grain size, namely gravel, sand and mud (Colby 1963; Marshak, 2008). A commonly used scale to determine grain size is the Wentworth scale that was first proposed by Wentworth (1922). Based on this scale, gravel has grains larger than 2 mm in diameter, sand has grains that fall between 2 mm and 0.0625 mm, and mud has grains smaller than 0.0625 mm in diameter (Wentworth, 1922; Sukdeo, 2010). Mud can be further divided into silt with grains ranging from 0.0625 mm to 0.0039 mm in diameter and clay with grains smaller than 0.0039 mm in diameter (Sukdeo, 2010).

Gravel is a loose aggregate of rock fragments ranging from granule to boulder-sized fragments (Marshak, 2008). Sand is a loose granular material comprising finely divided rock and mineral fragments (Valentine, 2019). Sand is formed by the weathering of rocks and is composed of finer particles than gravel but coarser than silt (Marshak, 2008; Valentine, 2019). Silt comprises

particles that range between very fine sand and clay (McNally and Mehta, 2004). Silt particles are similar in appearance to sand; however, silt particles are smaller, have a larger surface area per unit mass and are frequently coated with clay (Ural, 2018). Therefore, they may display some physio-chemical properties of clay (Pather, 2014). Clay is a plate-like, very fine-grained material composed of clay minerals (Marshak, 2008). Clay minerals are formed by the disintegration of primary rock-forming minerals and are also known as secondary silicates (Ural, 2018). The combination of silts and clays is referred to as mud and tend to dominate the bed and banks of most estuaries (Pather, 2014).

While rainfall and surface runoff are the forces that drive soil erosion, highly turbulent fluvial streams are the driving force of stream erosion, which is the primary transport agent of sediments (Ouillon, 2018). In the aquatic environment, sediments can either be transported as suspended load, where they remain in the water column, wash load where they remain in suspension even when the water is not flowing or bedload where they settle to the bottom of the water body (Abed, 2009; Fondriest Environmental, 2014). Sediment transport depends on the size of particles and the velocity and turbulence of the system (Sukdeo, 2010). Generally, finer particles are transported as suspended load, with larger particles transported as bed load (Sukdeo, 2010). Sediments in water also undergo many periods of resuspension, transport and deposition as they move from the source of rivers to the river mouth or estuary (Ouillon, 2018). In addition, the decreasing slope of the watercourse from the source to the mouth introduces grain sorting leading to finer particles being transported into estuaries (Ouillon, 2018). In studies related to pollution, sediment is often referred to as the fine fraction, consisting of particles smaller than 63 µm and is the fraction to which pollutants adsorb (Villars and Delvigne, 2001). Estuarine sediments, thus, have a great potential to fix and accumulate most heavy metals from the river and estuarine water (He et al., 2019).

Estuaries provide a route for sediments to be transported from land to coastal and marine ecosystems (Pather, 2014). In addition to the sediments originating in the estuary itself, sediments are constantly transported into and out of estuaries via fluvial and marine systems (Sukdeo, 2010). The sediments found within estuaries are derived from either fluvial or marine ecosystems (Abed, 2009). Sediments in these environments are essential as they provide habitats for benthic organisms and suitable spawning grounds. In addition, sediments provide nutrients to aquatic plants and vegetation in nearshore ecosystems such as marshes (Fondriest Environmental, 2014). The transport and deposition of sediments are thus critical as they

provide many benefits to aquatic ecosystems. However, the transport and deposition of excessive amounts of sediment can negatively impact aquatic life. For example, excessive levels of suspended sediment can hinder the amount of light from reaching submerged aquatic plants and clog fish gills (Fondriest Environmental, 2014).

2.4) Sediment transport

To adequately understand surface water quality issues, it is crucial to understand the transport of particulate material and pollutants in rivers, lakes, and oceans. Grain size plays an essential role in transporting sediments within the water from the fluvial environment to the estuarine environment (McNally and Mehta, 2004). Coarse sediment, including gravel and sand, are transported as bed load within a river system. According to Pather (2014), the amount of bed load carried by a river influences its channel geometry and ability to recover from natural or human interferences, including floods and upstream impoundments. Finer sediments, including silts and clays, are less dense, thus remain in suspension within the water column (Bell et al., 2000). These sediments are thus transported as suspended load within rivers (Villars and Delvigne, 2001). Suspended load is important for depositional processes as it carries the required sediment to develop and maintain deltaic and estuarine environments (Pather, 2014).

Cohesive sediment transport processes are introduced when fine sediment particles enter an estuary (Villars and Delvigne, 2001). Cohesive sediment is a mixture of silts, clays, organic materials, and colloidal particles transported from fluvial and marine environments to depositional environments (Bruens et al., 2002). Fine-grained sediments are primarily responsible for transporting chemicals within aquatic ecosystems due to their high surface-to-mass ratios (Bruens et al., 2002). In addition, fine-grained sediments become more chemically and biologically active due to their surface electrical charges, which better facilitate the adsorption of pollutants onto these sediments (Bisht, 2019). These sediments can facilitate the transportation of contaminants and impact the optical properties of the water column (Keen and Furukawa, 2007).

When river sediment is transported into estuaries and comes into contact with saline water, a process known as flocculation occurs (Villars and Delvign, 2001). Flocculation is the process by which particle aggregates are formed from individual particles, usually fine-grained particles, for example, clay particles (Villars and Delvigne, 2001). As a result of their size, shape, and electrical charge distribution, clay mineral particles introduce cohesion. Clay tends

to coagulate into aggregates due to Van der Waal's forces (Ural, 2018). When this process occurs, the collision between two particles results in the formation of an aggregate, and this process continues until an equilibrium is reached (Ural, 2018). According to Pather (2014), all clay particles suspended in the water column become cohesive when salinities exceed 2-3 ppt. However, salinities greater than 10 ppt result in inter-particle cohesion, affecting the structure of the aggregates formed. Flocculation is influenced by both physical hydrodynamic forces and biological activities (Wang et al., 2013). In addition, flocculation influences the settling velocity of suspended particles and the rate of deposition within an estuary (Wang et al., 2013; Pather, 2014).

2.5) Deposition of sediments

Stream velocity refers to the speed of the water within a stream, and settling velocity can be described as the rate of settling in still water (Nelson, 2015). Sediment particles have a tendency to settle with respect to the velocity of the water. At a low velocity, streams display laminar flow where the water flows in parallel paths (Salles, 2020). At a high velocity, streams display turbulent flow where the water flows haphazardly (Salles, 2020). In aquatic systems with turbulent flow, fine sediments will remain in suspension, whereas in aquatic systems with laminar flow, suspended particles will slowly settle to the bed (Nelson, 2015). This process is referred to as deposition. When the flow of water slows down or becomes still, coarse fluvial sediments that are heavier cannot be supported by the river turbulence; therefore, they become deposited on the river and stream beds (Bell et al., 2000).

Sediment deposition is primarily regulated by hydrodynamic processes that circulate and mix estuarine waters (Tinmouth, 2010). The mixing of seawater and freshwater creates a brackish environment within estuaries, enhancing deposition (Bell et al., 2000). Sediment deposition is, thus, greatest near the head of an estuary where seawater enters the estuary and flocculation occurs (Bell et al., 2000). The rise and fall of the water levels resulting from tides and the occurrence of turbidity maxima during slack tides or low-energy phases also enhance particle settling (Chapman and Wang, 2001). The larger settling velocities of flocs enhance deposition during slack tides, resulting in the formation of prominent mud reaches in the central portion of estuaries (Chapman and Wang, 2001; Flemming, 2011). Fine sediments such as muds are thus, deposited on the fringes of the central part of an estuary by river processes, tides and waves (Bell et al., 2000). This occurs due to enhanced flocculation, coagulation and aggregation of suspended particles due to the mixing of freshwater and saltwater (Flemming,

2011). In addition, deposition can also be enhanced by vegetation such as marshes. According to Loaiza and Findlay (2008), the plant stems on a marsh surface can trap sediment particles by reducing the velocity of the water and providing a surface for sediment to adhere to.

Periods of high velocities, such as after flood events, subsequently cause erosion of the estuarine bed. When the turbulent waters flow over the deposited sediments, it can cause some sediment particles to be removed from the bed and become suspended once again (McNally and Mehta, 2004). According to Whitfield and Bate (2007), a single large-scale flood event can result in the scouring out of sediments that were deposited over decades. Flood events result in sediments being flushed out of estuaries and into the ocean thus, facilitating the removal of pollutants trapped in the sediment (Whitfield and Bate, 2007). However, these events also transport large volumes of sediment from the river system, deposited when the flow velocity decreases.

2.6) Water quality and sediment quality guidelines

Rivers and estuaries play a significant role in linking the land to the sea. They can be described as a transport system, as they provide pathways that carry sediments and pollutants from inland to the coast (Pillay, 2002). They also support a wide range of activities, including the supply of water for agricultural use, industrial use, and recreational use (Pillay, 2002). As a result of rapid urbanisation and industrialisation, it has led to the increase in the discharge of effluents carrying heavy metals and metals into rivers and estuaries (Sukdeo, 2010). The significant increase in pollution has led to the increased need for thorough and continuous evaluation of the water and sediment quality of rivers and estuaries (Pillay, 2002). Regular water and sediment quality assessments are required to monitor the health of aquatic ecosystems and protect them from further degradation.

To evaluate whether the water and sediment quality of an aquatic ecosystem is acceptable or unacceptable, there has to be a set of guidelines to check against (DWAF 1996). The South African water quality guidelines are expressed as a range of values known as the target water quality range (TWQR). Water quality parameters that remain within this TWQR will pose little to no adverse effects on the health of the aquatic life, thus ensuring their protection (DWAF, 1996).

South Africa does not have its own set of sediment quality guidelines (SQG) for its aquatic ecosystems as these are still being developed (Gordon and Muller, 2010). As a result,

international guidelines are used to assess the sediment quality of aquatic ecosystems in South Africa. SQGs are a crucial tool in evaluating the degree of contamination in estuarine and marine sediments (Hübner et al., 2009). The National Oceanic and Atmospheric Administration (NOAA) undertakes numerous studies on the chemical concentrations of marine and estuarine sediments annually, and their scientists developed a set of numerical SQGs (Hartwell et al., 2018). Long and Morgan (1990) developed a set of SQGs for NOAA based on the responses of biological organisms to chemical concentrations in their aquatic environments. They developed two threshold ranges, including effects range low (ERL) and effects range median (ERM) values. According to Long et al. (1995), ERL refers to the concentration below which toxic effects are scarcely observed, and ERM refers to the concentrations above which adverse effects frequently occur. The DWAF (1996) TWQR for aquatic ecosystems, and the NOAA (1999) SQGs were used in this study.

2.7) Heavy metals

Heavy metals are metallic chemical elements naturally found in the earth's crust (Jaishankar et al., 2014). They are referred to as heavy metals as they have a high atomic weight and a density that is greater than 5 g/cm^3 (Hui, 2008; Tchounwou et al., 2012). Heavy metals can be found in nearly all parts of the biotic and abiotic environment, including water, sediments, plants, animals and humans (Hui, 2008). These heavy metals are naturally occurring in the environment, and some heavy metals such as iron and zinc are essential for various biochemical and physiological functions of living organisms (Sukdeo, 2010; Jaishankar et al., 2014). However, when their concentrations exceed naturally occurring levels, it can be potentially harmful to both humans and aquatic life (Moodley et al., 2014).

Heavy metals are present in aquatic systems in various chemical species (de Souza Machado et al., 2016). Total heavy metals refer to the concentration of heavy metals measurable in water or sediment after acid digestion and include heavy metal precipitates, heavy metals within mineral lattices, heavy metals adsorbed onto sediment and organic matter, as well as dissolved heavy metals (de Souza Machado et al., 2016). Dissolved heavy metals can be defined as the portion of total heavy metals that pass through a 0.45 µm filter, such as colloids (Guéguen and Dominik, 2003). Particulate heavy metals can be defined as the portion of nonfilterable heavy metals that are mobile to the dissolved phase and can be recorded in water after acid extraction (de Souza Machado et al., 2016). It includes heavy metals in inorganic precipitated or co-precipitated forms such as carbonates and hydrous Fe- Mn oxides and adsorbed onto sediment

and organic matter particles (Namieśnik, and Rabajczyk, 2010). Bioaccumulated heavy metals describe the portion of heavy metals ingested by organisms. Bioavailable heavy metals, on the other hand, include heavy metal species that are bioaccessible and can be distributed, metabolised, eliminated, and bioaccumulated by an organism (Drexler et al., 2003). Heavy metals are of particular concern due to their environmental persistence, toxicity, and ability to be integrated into food chains (Pati et al., 2013). Heavy metals are not biodegradable and can persist in the environment for an extended period of time, even after the sources of these heavy metals have been removed (Javed and Usmani, 2017).

2.7.1) Sources of heavy metals

According to Pati et al. (2013), heavy metals have a geogenic origin, such as from the leaching or weathering of rocks and an anthropogenic origin, such as mining and other industrial activities. In aquatic ecosystems, these heavy metals are transported in dissolved or particulate form, where sediment and other suspended particles are crucial in heavy metal adsorption, desorption and sedimentation processes (de Souza Machado et al., 2016). Heavy metals present in estuaries are typically derived from riverine particulate and dissolved heavy metals, point sources such as harbour activities, land runoff, sewage, and industrial effluents (de Souza Machado et al., 2016).

2.7.1.1) Natural sources

The natural sources of heavy metals include volcanic eruptions and the disintegration of metal-bearing rocks (Ali et al., 2019). Heavy metals naturally occur within the earth's crust (Tchounwou et al., 2012). The earth's crust comprises three primary rocks, namely, igneous, sedimentary and metamorphic rocks. Magma refers to molten rock that originates from the earth's mantle and consists of various chemical elements such as heavy metals (Bradl, 2005). When magma rises to the earth's surface as a result of volcanic eruptions or plate tectonics and cools, it solidifies to form igneous rocks (Marshak, 2008). As magma rises and cools, it causes chemical reactions to occur, producing various minerals in a process referred to as magmatic differentiation (Nelson, 2012). Heavy metals are integrated as trace elements into the crystal lattice of these minerals that form when the magma cools (Bradl, 2005). During the final stages of magmatic differentiation, magmatic-hydrothermal fluids are produced, containing many heavy metals and other elements (Sharma and Srivastava, 2014). As these hot fluids intrude

into the surrounding rock, chemical reactions occur that cause minerals to precipitate as ores comprising a high concentration of heavy metals and other elements (Bradl, 2005).

The physical weathering of pre-existing rocks, such as igneous rocks, results in the formation of fine-grained sediment particles that undergo transportation and deposition (Marshak, 2008). The continued deposition of these particles over time causes them to become compacted and cemented, resulting in the formation of sedimentary rocks (Marshak, 2008). Hydrothermal fluids may also be produced during sedimentary processes. According to Sharma and Srivastava (2014), pore fluids may become heated in the sedimentary sequence, which may also lead to hydrothermal fluid circulation occurring within basins. When a sill which is a sheet-like intrusion of igneous rock, intrudes sedimentary rocks, heat can be transferred either through conduction or convection of fluids (Haile et al., 2019). The porous and permeable nature of sedimentary rocks enables them to hold and transport fluids such as water, gasses and oils (Bradl, 2005). According to Haile et al. (2019), igneous sills that have intruded highly porous sedimentary rocks have led to the mobility of hydrothermal fluids. As a result, sedimentary rocks may also contain ore deposits of many heavy metals if they were infiltrated with these hydrothermal fluids (Bradl, 2005). Metamorphic rocks are formed when igneous, sedimentary or other metamorphic rocks are exposed to increased temperature and pressure conditions deep within the earth's crust (Marshak, 2008). These primary rocks contain various amounts of different heavy metals, and the physical weathering of these rocks at the earth's surface can naturally introduce heavy metals and other elements into the environment (Ali et al., 2019).

2.7.1.2) Anthropogenic sources

The most common anthropogenic sources of heavy metals include industrial activities, urban areas and agriculture. Industrial activities such as mining of heavy metal ores, steel processing, manufacturing of paints and dyes, smelting, combustion emissions, and petrochemical plants either use or produce heavy metals (Wuana and Okieimen, 2011). These heavy metals are often directly discharged into rivers and eventually estuaries through industrial effluents and can cause adverse effects on aquatic organisms inhabiting rivers and estuaries (Wuana and Okieimen, 2011). In addition, heavy metals can be emitted into the atmosphere from industrial emissions. These heavy metals are subsequently deposited onto soils as the metal-bearing dust falls (Chen et al., 2005). These heavy metals can also accumulate in soils and be washed into

rivers and estuaries through surface runoff (Nadal et al., 2004). Industries broadly use heavy metals, making them a primary anthropogenic source of heavy metals (Nadal et al., 2004).

Urban areas are another primary anthropogenic source of heavy metals (Chen et al., 2005). Traffic emissions are a significant contributor to heavy metal pollution on urban surfaces, which can eventually be transported into aquatic environments through surface runoff (Ferreira et al., 2016). The traffic pollutants are emitted from the engines of vehicles via internal combustion, by tyre, brake and road wear, as well as fuel evaporation (Ferreira et al., 2016). Residential areas are another source of heavy metal pollution in urban areas through the release of heavy metal-containing household wastes and sewage (Huang et al., 2020). The concrete surfaces of urban areas result in a decrease in permeability and an increase in surface runoff (Riley, 2008). This facilitates the transportation of different pollutants, including heavy metals, into stormwater drains which are subsequently discharged into rivers and estuaries (McGrane, 2016). An additional potential source of heavy metals to rivers and estuaries from urban areas are landfills. Municipal waste can consist of cleaning products, batteries, pesticides, and oils and paints, which can all consist of various amounts of heavy metals and other metals (Brand et al., 2018). The contaminated leachate of landfills can thus, release heavy metals into groundwater which can be subsequently discharged into surface waters leading into estuaries (Brand et al., 2018). According to a study conducted by Yang et al. (2011) that assessed the heavy metal contamination of topsoil in urban areas in China, it was found that areas concentrated with industrial areas, residential areas, and roads had highly elevated levels of heavy metals. These areas account for the most elevated concentrations of heavy metals being released into the natural environment (Nadal et al., 2004; Yang et al., 2011).

Agricultural activities are another source of heavy metals as they involve the use of fertilisers and pesticides in order to improve crop yields and productivity (Wuana and Okieimen, 2011). These fertilisers and pesticides often contain various heavy metals such as arsenic, zinc and copper, and their excessive use can introduce elevated levels of these heavy metals into the natural environment (Wuana and Okieimen, 2011). These heavy metals can accumulate in soils and be washed into rivers and estuaries through surface runoff after heavy rains and cause adverse effects on the organisms inhabiting these ecosystems.

2.7.2) Factors affecting the accumulation of heavy metals in sediment

Sediments have a strong affinity for heavy metals, and within the natural environment, sediments typically contain the majority of heavy metals through the process of adsorption (Hsu et al., 2016). Adsorption refers to the accumulation of ions at the interface between a solid phase and an aqueous phase (McLean and Bledsoe, 1992). Heavy metals have a tendency to adsorb more onto sediment particles as compared to water and become temporarily trapped (Hsu et al., 2016; Huang et al., 2020). Once bound to sediment and soils, heavy metals become persistent as elemental contaminants are not biodegradable (Mann et al., 2011). The ability of heavy metals to bind to sediment particles depends on several factors, including grain size, organic matter content and cation exchange capacity (Parker, 1983; Lin and Chen, 1998). These factors aid in removing heavy metals from the water column which inhibits their mobility; however, this is temporary and can be reversible (Mann et al., 2011).

2.7.2.1) Grain size

Grain size plays a significant role in sediment entrainment, transport and deposition (Maslennikova et al., 2012). Fine-grained sediments are known to contain more heavy metals than coarse-grained sediments, as finer sediments have a larger surface-to-volume ratio (Maslennikova et al., 2012). In addition, fine sediment particles such as silts and clays are negatively charged, which facilitates the adsorption of heavy metals onto their surface (Huang et al., 2020). Therefore, fine-grained sediments act as sinks for heavy metals and with estuaries being a sink for fine-grained sediments, the level of heavy metal contamination in estuaries is typically high (Abed, 2009).

2.7.2.2) Organic matter

Organic matter refers to materials initially produced by living plants and animals that return to the soil and undergo the process of decomposition (Bot and Benites, 2005). It consists of residues of plants and animals as well as living and dead microorganisms such as bacteria, fungi and algae (Magdof and Van Es, 2021). Estuarine ecosystems are significant zones for organic matter processing and provide a ground for the mixing of land- and marine-derived organic matter (Canuel and Hardison, 2016). Estuaries acquire organic matter from terrestrial materials bearing organic matter which enter rivers leading into estuaries, and marine materials containing organic matter which are carried into estuaries through the action of tides (Remeikaite-Nikiene et al., 2016). In addition, mangroves also play a role in supplying organic

matter to estuaries as these environments contain a large number of decaying leaves and other plant material (Canuel and Hardison, 2016). According to Lin and Chen (1998), organic matter present in the water column act as scavengers for heavy metals and these heavy metals can be subsequently adsorbed onto bottom sediments. Organic matter consists of a net negative charge and will attract positively charged particles such as heavy metal cations (Brady and Weil, 2007). These heavy metals adsorb onto the surface of the organic matter, thus inhibiting the mobility and bioavailability of the heavy metals (Brady and Weil, 2007).

2.7.2.3) Cation exchange capacity

Cations that are adsorbed onto clay and organic matter can be replaced by other cations. The ability of soil colloids, including clay and organic matter particles, to adsorb and exchange cations refers to cation exchange capacity (Meetei et al., 2020). The cation exchange of heavy metals is influenced by the amount of negative charge on the surface of sediment particles (Rieuwerts et al., 1998). The higher the cation exchange capacity of sediment, the higher the negative charge, and the more cations can be adsorbed (Lin and Chen, 1998). The cation exchange capacity thus influences the mobility of heavy metals in sediments as increases in cation exchange capacity facilitates their adsorption onto sediments which subsequently inhibits the mobility of heavy metals in sediments (de Matos et al., 2001).

2.7.3) Factors affecting the remobilisation of heavy metals

The adsorption of heavy metals onto sediments is a temporary process as these heavy metals are removed from the water column only and not the estuarine environment (Mann et al., 2011). According to Mann et al. (2011), heavy metals bound to sediments can undergo various reversible changes depending on the chemistry of the aquatic environment, such as changes in pH. Heavy metals can be released back into the water column as a result of resuspension or desorption (Sojka et al., 2019).

Heavy metals stored in sediments can be remobilised and resuspended into the water column due to changes in chemical and physical conditions (Sojka et al., 2019). Chemical processes such as the oxidation of organic matter in the upper sediments by bacteria can cause trace metals to dissolve into pore waters (Superville et al., 2014). This can, in turn, lead to the partial mobilisation of these heavy metals, which can be subsequently released into the overlying water column (Superville et al., 2014). Physical processes such as flooding, human disturbances, and bioturbation caused by benthic organisms can cause sediment to be disturbed

and resuspended into the water column (Zhang et al., 2014). According to Zhang et al. (2014), the release of heavy metals into the water column is enhanced by these disturbances to the sediment. For example, bioturbation can cause heavy metals from pore water and iron and manganese hydroxides to be released into the overlying water column (Atkinson et al., 2007). This, in turn, increases the bioavailability of these heavy metals to aquatic life.

Desorption of heavy metals refers to the process by which heavy metals are released from their binding site. Heavy metals tend to desorb more rapidly when sediments become resuspended in the water column (Superville et al., 2014). Desorption can be caused by competition with other cations for adsorption sites which can cause certain heavy metals to be released into the overlying water column (Riba et al., 2003). Complexation reactions play a vital role in heavy metal speciation in water which also impacts the desorption of heavy metals (Noegrohati, 2005). Heavy metals that can form strong complexes or ligands in water have an affinity to form the same complexes on sediment particles (Noegrohati, 2005). Organic and inorganic ligands can interact with the surfaces of heavy metal cations and form stable negatively charged complexes with these cations. These subsequently block adsorption sites which inhibit heavy metal retention in sediments and soils, thus resulting in their release into the overlying water column (Caporale and Violante, 2016).

The processes of adsorption and desorption of heavy metals between sediment and the water column significantly impact their bioavailability to aquatic organisms and their toxicity (Gao et al., 2003). In addition, any changes to the physical and chemical conditions can influence the mobility of heavy metals and facilitate the release of heavy metals stored in sediments to the overlying water column (Gao et al., 2003). The physicochemical parameters used in this study include conductivity, pH and dissolved oxygen. Each of these parameters and how they influence heavy metals is discussed in the sections below.

2.7.3.1) Electrical conductivity

The electrical conductivity of water refers to the ability of water to conduct heat or electricity and is generally measured in Siemens per metre (S/m) or micro-Siemens per centimetre (µS/cm). The conductivity of water is dependent on the current number of ions found in the water (Alam et al., 2007). The source of these conductive ions is dissolved salts and inorganic substances, including chlorides, sulphides and carbonates (DWAF, 1996; Alam et al., 2007).

An increase in the number of ions in the water will cause the conductivity of the water to increase.

The electrical conductivity of water is an essential indicator of water quality as it is an early indicator of changes in the water column. It estimates the presence of ionic substances in water and is often used as a substitute measure of total dissolved solids present in the water (Pal et al., 2015). Events including flooding, evaporation or pollution from anthropogenic activities can cause significant changes to the conductivity of water (Pal et al., 2015). The conductivity can increase drastically by pollution from human activities such as agricultural runoff and sewage contamination, which leads to an increase in chloride, phosphate and nitrate ions in the water (Fashae et al., 2019). The addition of organic compounds into rivers can cause a decrease in conductivity as these compounds do not disintegrate into ions (Hacısalihoğlu and Karaer, 2016). Both cases will lead to an increase in dissolved solids in the water, which severely impacts the water quality (Pal et al., 2015). The electrical conductivity of water impacts the levels of heavy metals as high electrical conductivity levels result in a decrease in the adsorption of heavy metals onto sediment (Hacısalihoğlu and Karaer, 2016). This, in turn, increases the mobility of heavy metals. The electrical conductivity can also be used to estimate the total dissolved solids (TDS) and salinity levels of water. In South Africa, only water quality guidelines for the TDS levels in aquatic ecosystems have been developed and there are no guidelines specific for electrical conductivity or specific to each salt ion (Griffin et al., 2014). According to the USEPA (2012), the normal background levels of electrical conductivity for most rivers in the United States range from 50-1500 µS/cm and waters with high levels of electrical conductivity have levels ranging from 1000 – 10000 µS/cm and these levels indicate saline conditions. Industrial waters can have electrical conductivities of up to 10000 µS/cm (USEPA, 2012).

2.7.3.2) pH

pH is a common index of the water quality of an aquatic ecosystem and is a measure of the hydrogen ion activity in a water body (Brijlal, 2005). It is a measure of how acidic or alkaline the water is. When the number of hydrogen ions in the water increases, the pH will decline, making the water more acidic (Naidoo, 2005). Alternatively, when the hydrogen ions in the water decrease, this will cause the pH levels to increase, which causes the water to be more basic (Naidoo, 2005). The pH scale ranges from 0-14, where 7 is a neutral pH, a pH of 0-7 indicates acidic conditions, and a pH of 7-14 indicates basic conditions (Sukdeo, 2010).

According to DWAF (1996), the pH of most freshwater systems in South Africa ranges between 6 and 8. The pH of estuarine ecosystems ranges from 7.0 to 7.5 in the freshwater portion of estuaries near the head, whereas the more saline portion of estuaries near the mouth has a pH range between 8.0 and 8.6 (USEPA, 2006).

The photosynthetic activities of plants alter the carbon dioxide concentrations in the water at different times of the day (Pedersen et al., 2013). During the day, photosynthesis occurs where carbon dioxide is taken up, and oxygen is released. However, at night respiration occurs where oxygen is taken up, and carbon dioxide is expelled by aquatic plants and animals (Mack, 2003). Carbon dioxide dissolves in water forming carbonic acid, which breaks up to form bicarbonate and hydrogen ions. Therefore, this process will increase hydrogen ion concentrations in the water, thus causing a decrease in pH (DWAF, 1996; Pedersen et al., 2013). The changes in pH levels at different times of the day will have direct and indirect effects on aquatic life and bacterial processes. Human activities such as agriculture have led to excessive amounts of nutrients being discharged into aquatic environments, leading to algal blooms. This, in turn, can cause drastic fluctuations in pH over a short period of time which causes stress in the aquatic organisms (USEPA, 2006). Extremely high and extremely low pH levels can cause damage to the gills, skin, and eyes of fish species and make them more vulnerable to diseases, such as red spot disease (NOAA, 2021).

Low pH levels may also corrode the heavy metals present in the water, leading to toxic and highly acidic waters (NOAA, 2021). Low pH levels can encourage the solubility of heavy metals (Zhang et al., 2018). pH is also important in terms of mobility as the availability of heavy metals is relatively low when the pH range is between 6.5 to 7 (Hacısalihoğlu and Karaer, 2016). According to Li et al. (2013), low pH levels in the range of 4-7 cause an increase in the competition between hydrogen ions and dissolved heavy metals for ligands. Subsequently, the adsorption capabilities and bio-availabilities of the heavy metals decrease, increasing the mobility of heavy metals. In addition, soluble and carbon-bound heavy metals precipitate more easily under low pH conditions (Li et al., 2013). According to Hacısalihoğlu and Karaer (2016), trace metals that have been adsorbed onto sediments can be resuspended into the overlying water column under low pH conditions. Low pH levels weaken the strength of heavy metal association, which inhibits sediment from retaining heavy metals (Hacısalihoğlu and Karaer, 2016).

2.7.3.3) Dissolved oxygen

Dissolved oxygen forms one of the most critical water quality parameters because all forms of aquatic life require sufficient dissolved oxygen levels to survive. The level of dissolved oxygen in aquatic environments is thus the main factor that determines the type and abundance of organisms that inhabit them (Dean, 2018). All forms of aquatic life can thrive in water within a specific range of dissolved oxygen. Dissolved oxygen levels outside the normal ranges that organisms can tolerate results in physiological and behavioural stress which can be devastating to aquatic life (Sukdeo, 2010). Dissolved oxygen refers to the free oxygen molecule (O_2) found in the water and is not chemically bonded to the water (Mack, 2003). Dissolved oxygen moves freely into and out of the water at constant concentrations. The concentration of dissolved oxygen is dependent on oxygen sources, oxygen sinks and oxygen solubility (Mack, 2003). There are two primary sources of dissolved oxygen in water, including internal and external sources. The internal source of dissolved oxygen is through the photosynthetic activity of aquatic plants (Dean, 2018). When algae and aquatic plants undergo photosynthesis during the day, they release pure oxygen gas directly into the water (Mack, 2003). The external source of dissolved oxygen is oxygen diffusion from the atmosphere (Dean, 2018). Water has the ability to absorb different types of gasses at different rates. The mixing of surface waters by wind and waves increases the surface area to volume, which increases the rate at which oxygen can be dissolved in water (Mack, 2003).

The oxygen sinks include the aquatic organisms that consume dissolved oxygen. The levels of dissolved oxygen are steadily used up by respiring aquatic organisms such as fish, algae, aquatic plants and microorganisms (Mack, 2003). In addition, decomposers, including bacteria and fungi, require oxygen to break down organic matter, reducing dissolved oxygen levels. Oxygen solubility refers to the ease with which oxygen can dissolve in water and is dependent on atmospheric pressure, water temperature and salinity (Dean, 2018). The solubility of oxygen increases with increasing atmospheric pressure. The higher atmospheric pressure will result in a force being exerted on the surface of the water, which will inhibit dissolved oxygen from escaping (Dean, 2018). Lower elevations have higher atmospheric pressure than higher elevations; therefore, water at low elevations contain more dissolved oxygen than water at higher elevations (Mesner and Geiger, 2010). The solubility of oxygen increases as temperature decreases; therefore, colder water will contain more dissolved oxygen than warmer water

(Mack, 2003). The solubility of oxygen increases as salinity decreases; therefore, freshwater contains more dissolved oxygen than saltwater (Mack, 2003; Mesner and Geiger, 2010).

The levels of dissolved oxygen in water fluctuate daily due to changes in tides, temperature and the photosynthetic activity of plants. Excessively high levels of dissolved oxygen in estuaries can cause deleterious effects in fish as it can cause the capillaries in the gills of fish to rupture (Dean, 2018). However, low levels of oxygen, also known as hypoxia, is of more significant concern. Hypoxic conditions in estuarine environments resulting from increased nutrient enrichment from anthropogenic activities cause many species of fish and aquatic plants to die (Dean, 2018). Furthermore, the amount of dissolved oxygen also plays a role in the release of heavy metals from sediments. A study conducted by Kang et al. (2019) that assessed the effects of dissolved oxygen on the concentrations of heavy metals in river sediments, indicated that certain heavy metals are released from river sediments into the overlying water column under anoxic conditions (low oxygen levels). However, increased dissolved oxygen levels caused heavy metals to adsorbed onto sediment from the overlying water column (Kang et al., 2019). Dissolved oxygen levels below 3 mg/L are considered low and a cause for concern (Dean, 2018).

2.7.4) Toxicity of heavy metals

Heavy metals are naturally occurring substances in the environment; however, the rapid increase in human activities has resulted in these heavy metals exceeding their natural levels, which has severe implications on living organisms (Cheung et al., 2003). Heavy metals are a threat to living organisms as they are persistent in the environment and tend to accumulate in living organisms over time (Verma and Dwivedi, 2013). Trace elements refer to elements that naturally occur in low concentrations and range from parts per billion (ppb) to less than 10 parts per million (ppm) in various environments (Tchounwou et al., 2012). Trace elements are vital for life functions, and plants and animals have various methods of accumulating adequate amounts of trace elements from their environment (Mann et al., 2011). Heavy metals can be found in trace amounts; however, they are still toxic even at low concentrations (Sukdeo, 2010). This is because they tend to bioaccumulate in biological organisms over some time (Verma and Dwivedi, 2013). As a result of their ability to be transported by various environmental mediums, heavy metals can bioaccumulate and biomagnify in aquatic organisms and food webs (Sukdeo, 2010).

According to Verma and Dwivedi (2013), bioaccumulation refers to the build-up of elements in biological organisms over time resulting in higher concentrations found within the organism in comparison to the element's concentration in the environment. These elements accumulate in living organisms through ingestion from their environment and are stored quicker than they are broken down or excreted (Verma and Dwivedi, 2013). Bioaccumulation of elements depends on the chemical availability of the elements within the environment and the organism's ability to ingest and excrete them (Mann et al., 2011). Biomagnification refers to the process whereby pollutants are transferred to organisms from the food they ingest, resulting in higher concentrations in comparison to the source (Mann et al., 2011). Biomagnification occurs along food chains. The levels of these pollutants are amplified as they move up different trophic levels (Sukdeo, 2010). This is because successive trophic levels consume large amounts of food to sustain metabolic functioning, and if the food is contaminated, that contaminant will be ingested in significant quantities by the consumer (Mann et al., 2011). Therefore, higher-order consumers will receive a higher level of that pollutant (Sukdeo, 2010).

The following describes the sources of the heavy metals that were assessed in this study and their implications on the health of aquatic organisms as a result of their elevated concentrations.

2.7.4.1) Aluminium (Al)

Aluminium naturally occurs in the air, water and soil and is the third most abundant element present within the earth's crust (Ingerman et al., 2008; Gupta et al., 2013). Aluminium enters the environment naturally through the physical weathering of rocks. Anthropogenic sources of aluminium include solid waste linked to industrial activities such as paper, metal construction, textile, leather industries and other aluminium processing industries (DWAF, 1996). Aluminium is considered a non-essential metal as aquatic organisms do not require this metal to function (Jaishankar et al., 2014). The pH of water and organic matter content significantly influences aluminium toxicity, with low pH levels increasing aluminium's toxicity. The mobilisation of toxic aluminium ions due to changes in pH leads to plant poisoning, crop decline or failure, and the death of aquatic life (Jaishankar et al., 2014). Aluminium that accumulates in plants can impede root growth, cause cellular modifications in leaves, and yellowing and death of leaves (Gupta et al., 2013). Excessive levels of aluminium can have deleterious effects on aquatic biota. This includes impacting the ability of certain fish to regulate ions and accumulating on the gills of fish, subsequently impeding respiratory functions and causing them to die (Jaishankar et al., 2014). High levels of aluminium also affect birds

and other animals that consume fish contaminated with aluminium, such as the thinning of eggshells and low birth weights in young (DWAF, 1996). The target water quality range (TWQR) for aluminium should be ≤ 5 µg/L when pH is below 6.5, and TWQR should be ≤ 10 µg/L when pH is greater than 6.5 (DWAF, 1996).

2.7.4.2) Arsenic (As)

Arsenic is a naturally occurring metalloid element and is the twentieth most abundant element on earth. Arsenic occurs in both inorganic and organic forms; however, the inorganic forms are considered more toxic to the environment and living organisms (Jaishankar et al., 2014). The natural sources of arsenic include volcanic eruptions and soil erosion. The anthropogenic sources include the industrial manufacturing of agricultural products such as insecticides, herbicides and fungicides (Tchounwou et al., 2012). Other anthropogenic sources include dye and detergent manufacturers, mining industries, metal processing industries, and manufacturers of glass and ceramics (DWAF, 1996). Arsenic occurs in many oxidation states, including III, IV and V depending on the pH and redox potential of water, with arsenic (III) and arsenic (V) being the most common forms (DWAF, 1996; Abbas et al., 2018). The carcinogenic nature of arsenic makes it toxic to animal and plant life even at low concentrations. However, arsenic's effects on living organisms depend on its chemical state, the nature of the environment, and the organism's biological sensitivity (Pather, 2014). Arsenic exposure has a variety of adverse effects on vertebrates and invertebrates. These effects include a decline in the growth and reproduction of fish and invertebrate species and a reduced migration in fish (Pather, 2014). In terms of the toxic effects of arsenic on plants, arsenic (V) is more toxic to plants than arsenic (III) (DWAF, 1996). It inhibits plant growth and nutrient absorption and decreases the ability of cells to produce adenosine triphosphate (ATP) and carry out metabolic processes (Finnegan and Chen, 2012; Abbas et al., 2018). According to the SQGs proposed by NOAA (1999), the ERL for arsenic is 8.2 mg/kg and the ERM for arsenic is 70 mg/kg. According to DWAF (1996), TWQR for arsenic should be ≤ 10 µg/L.

2.7.4.3) Cadmium (Cd)

Cadmium is a heavy metal present in the earth's crust at an average concentration of 0.2 mg/kg (DWAF, 1996). According to the ATSDR (2012) ranking, cadmium is regarded as the seventh most toxic heavy metal. Cadmium enters the environment naturally through the weathering of rocks containing cadmium (DWAF, 1996). The anthropogenic sources of cadmium include

wastes produced by industries involved in the manufacturing of alloys, paints, batteries and plastics, and mining activities (Tchounwou et al., 2012). In addition, another anthropogenic source of this heavy metal includes the use of fertilisers and pesticides containing cadmium in agricultural activities, which can be discharged into rivers and estuaries through surface runoff (DWAF, 1996). Cadmium readily adsorbs onto clay minerals and organic matter, and once cadmium enters the natural environment, it can remain in soils and sediments for several decades (Estifanos, 2006; Jaishankar et al., 2014). Cadmium at low concentrations is toxic to all forms of life (Levit, 2010). Plants gradually take up cadmium which can accumulate in them and be transferred across the food chain (Jaishankar et al., 2014). According to DWAF (1996), cadmium is chemically similar to zinc and can easily replace zinc in some enzymes. The replacement of zinc by cadmium can adversely impact enzyme activity, leading to physiological effects in plants and animals (Jaishankar et al., 2014). In aquatic ecosystems, cadmium can bioaccumulate in macrophytes, phytoplankton, zooplankton, invertebrates and fish (DWAF, 1996). When exposed to cadmium, it can accumulate in the gills, liver and kidneys of fish, leading to toxic effects (Levit, 2010). Cadmium accumulation in aquatic animals has also been found to cause iron deficiency, liver disease, and nerve or brain damage (Levit, 2010). The toxicity of cadmium is dependent on its chemical speciation and hardness. The chemical speciation of cadmium is influenced by the pH and temperature of the water and the ligands and metal cations present in the water (DWAF, 1996). Hardness can be described as the sum of calcium and magnesium concentrations which are both expressed as calcium carbonate in mg/L (DWAF, 1996). According to the SQGs proposed by NOAA (1999), the ERL for cadmium is 1.2 mg/kg and the ERM for cadmium is 9.6 mg/kg.

Table 2.2: The TWQR for cadmium at different water hardness in aquatic ecosystems (Adapted from DWAF, 1996).

Hardness (mg $CaCO_3$/L)	< 60 (soft)	60-119 (medium)	120-180 (hard)	> 180 (very hard)
TWQR - Cadmium concentration (µg/L)	0.15	0.25	0.35	0.40

2.7.4.4) Chromium (Cr)

Chromium is a relatively scarce metal, and its presence in aquatic ecosystems is generally very low (DWAF, 1996). Chromium occurs in several oxidation states ranging from chromium (II) to chromium (VI), with the most common forms being chromium (III) and chromium (VI) (Tchounwou et al., 2012). However, chromium (VI), the hexavalent form, is a highly oxidised state and highly soluble at all pH levels, which is more toxic than the other reduced chromium forms (DWAF, 1996; Jaishankar et al., 2014). The equilibrium between chromium (III) and chromium (VI) in natural waters is influenced by pH and redox potential, and their toxicity is influenced by hardness and pH (DWAF, 1996). Chromium enters aquatic ecosystems in minimal amounts naturally through the physical degradation of rocks bearing chromium. However, elevated levels of chromium in aquatic ecosystems can be attributed to anthropogenic activities such as industries (Tchounwou et al., 2012). Industries contributing to these elevated levels of chromium include metal processing factories, pulp and paper production, steel welding, chromate manufacturing, and the production of ferrochrome and chrome pigments (Jaishankar et al., 2014). Chromium released into the environment from anthropogenic sources is usually in the hexavalent form, which has become an increasing concern as it is highly toxic and is considered a carcinogen (Tchounwou et al., 2012). The use of chromium in agriculture has led to soil contamination which impacts plants by reducing root growth and inhibiting the germination of seeds (Jaishankar et al., 2014). Fish are more resistant to chromium concentrations; however, in young fish, low concentrations of chromium have been known to cause a reduction in the growth phase (DWAF, 1996). In addition, invertebrates and algae show the least resistance to chromium concentrations. According to the SQGs proposed by NOAA (1999), the ERL for chromium is 81 mg/kg and the ERM for chromium is 370 mg/kg. According to DWAF (1996), for dissolved chromium (VI), the TWQR should be ≤ 7 µg/L, and for dissolved chromium (III), TWQR should be ≤ 12 µg/L.

2.7.4.5) Copper (Cu)

Copper is a common metallic element found in the rocks and minerals of the earth's crust and is one of the world's most extensively used heavy metal (DWAF, 1996). The natural sources of copper include the weathering of rocks or the dissolution of copper minerals and native copper. The anthropogenic sources of copper include effluents from sewage treatment plants, the corrosion of copper pipes, the agricultural use of copper in fungicides and pesticides, and atmospheric fallout from mining, refining, coal-burning and iron- and steel-manufacturing

industries (DWAF, 1996). Copper is regarded as an essential trace metal as it plays a role in enhancing the biochemical and physiological functioning of plants and animals (Tchounwou et al., 2012). In vertebrates such as fish, copper forms an essential constituent of several key enzymes and is important for nervous system function and haemoglobin synthesis (Woody and O'Neal, 2012). However, elevated levels of copper are toxic to plants and animals and are one of the most toxic elements to aquatic organisms (Woody and O'Neal, 2012). Copper occurs in four oxidation states, including 0, I, II and III, with copper (II) being the most toxic to aquatic life (DWAF, 1996). The toxicity of copper is dependent on water quality parameters. It increases with a decrease in water hardness, a decrease in dissolved oxygen and when it occurs in combination with other heavy metals (DWAF, 1996). According to Woody and O'Neal (2012), excessive levels of copper in water cause a reduced ability to resist diseases, alter migration, impede respiration, and impede brain functions in fish. In addition, copper, even at low concentrations, reduces nitrogen-fixation by blue-green algae (DWAF, 1996). According to the SQGs proposed by NOAA (1999), the ERL for copper is 34 mg/kg and the ERM for copper is 270 mg/kg.

Table 2.3: The TWQR for copper at different water hardness in aquatic ecosystems (Adapted from DWAF, 1996).

Hardness (mg $CaCO_3$/L)	< 60 (soft)	60-119 (medium)	120-180 (hard)	> 180 (very hard)
TWQR – Copper concentration (µg/L)	0.3	0.8	1.2	1.4

2.7.4.6) Iron (Fe)

Iron is the fourth most abundant element in the earth's crust; however, its concentration in water is usually low due to low solubility (Xing and Liu, 2011). Iron naturally enters the environment through the degradation of sulphide ores such as pyrite and igneous, metamorphic and sedimentary rocks (DWAF, 1996). The anthropogenic sources of iron include acid mine drainage, corrosion of iron and steel, processing of minerals, landfill leachates, and sewage (DWAF, 1996; Javed and Usmani, 2017). Iron is the most vital element for the growth and survival of all life forms (Jaishankar et al., 2014). Iron is essential for chlorophyll and protein biosynthesis in plants, and in iron-deficient conditions, photosynthesis productivity may be

reduced (Rout and Sahoo, 2015). In animals, iron is a vital component of respiratory pigments such as haemoglobin and several enzymes (DWAF, 1996). However, elevated levels of iron can become toxic to both plants and animals. Iron occurs in two primary forms in water, including the ferrous (Fe^{2+}) state and the ferric (Fe^{3+}) state, with the ferric state being the most common form found in surface waters (Javed and Usmani, 2017). In addition, the toxicity of iron is dependent on whether it is in the ferrous or ferric state (Xing and Liu, 2011). Elevated iron levels are known to impair the growth and healthy functioning of plant cells (Rout and Sahoo, 2015). In aquatic animals, high levels of iron are known to cause clogging of the gills of fish and cause damage to the eggs of many fish species (Vuori, 1995). The TWQR for iron should not vary by more than 10% of the background dissolved iron concentration for a particular site at a specific time (DWAF, 1996).

2.7.4.7) Lead (Pb)

Lead can be described as a bluish-grey metal that naturally occurs in the earth's crust in negligible amounts (Tchounwou et al., 2012). Lead naturally enters the environment through the degradation of sulphide ores (DWAF, 1996). Anthropogenic activities such as mining, milling and smelting of lead, burning of fossil fuels, manufacturing of batteries and paint, as well as industrial and municipal discharge of wastewater all contribute to elevated levels of lead in the natural environment (DWAF, 1996; Lee et al., 2019). Lead occurs in organic and inorganic forms that are toxic to the environment; however, the organic forms of lead are more toxic to aquatic life (Kumar et al., 2020). The organic forms of lead are primarily found in dust, soil and old paint, whereas the inorganic form occurs in leaded gasoline (Kumar et al., 2020). Lead also occurs in several oxidation states, including 0, I, II and IV, with lead (II) thought to be the state in which most lead is bioaccumulated in aquatic organisms (DWAF, 1996). Low pH levels in water cause an increase in the bioavailability of lead accumulated by aquatic life. Elevated levels have adverse impacts on aquatic plant and animal life. Lead toxicity in plants inhibits root growth and photosynthesis and impedes seed germination (Nas and Ali, 2018). Lead toxicity also affects membrane permeability and causes a histological change in leaves (Nas and Ali, 2018). As a result of bioaccumulation, exposure to lead even at low concentrations can be lethal to aquatic animals (Lee et al., 2019). Lead accumulation in the various tissues of fish is toxic to target organs and triggers oxidative stress, which causes synaptic damage and neurotransmitter malfunction (Lee et al., 2019). In addition, low concentrations of lead impact fish species by inducing the formation of a film of coagulated

mucus over the gills and entire body. This causes suffocation leading to higher fish mortalities (DWAF, 1996). Lead uptake by aquatic organisms is dependent on the amount of calcium present; therefore, water hardness influences the toxicity of lead in aquatic ecosystems (DWAF, 1996). According to the SQGs proposed by NOAA (1999), the ERL for lead is 46.7 mg/kg and the ERM for lead is 218 mg/kg.

Table 2.4: The TWQR for lead at different water hardness in aquatic ecosystems (Adapted from DWAF, 1996).

Hardness (mg $CaCO_3$/L)	< 60 (soft)	60-119 (medium)	120-180 (hard)	> 180 (very hard)
TWQR – Lead concentration (µg/L)	0.2	0.5	1.0	1.2

2.7.4.8) Magnesium (Mg)

Magnesium is the eighth-most abundant element in the earth's crust and is an essential macronutrient to all life forms (Gregersen and Hanusa, 2012). Magnesium enters the environment naturally through the physical weathering of rocks bearing magnesium ions. The anthropogenic sources of magnesium include industrial processes involving the addition of magnesium to plastics and other materials, fertilisers containing magnesium as well as organic compounds discharged from wastewater treatment plants (Potasznik and Szymczyk, 2015). Magnesium is an essential element in animals as it plays a significant role in protein synthesis, enzyme activation, energy transfer and cellular homeostasis in animals (Van Dam et al., 2010). Magnesium is also essential to plants as it is a central atom of the chlorophyll molecule; therefore, it plays a vital role in primary production (Van Dam et al., 2010). Magnesium deficiency in plants affects photosynthesis and inhibits plant growth (Jezek et al., 2015). Magnesium deficiency in aquatic organisms such as fish adversely affects growth and development (Luo et al., 2016). However, elevated levels of magnesium are also known to be detrimental to aquatic animals. Water hardness refers to the sum of calcium and magnesium concentrations in water, and an imbalance between these ions due to an increase in magnesium ions is toxic to aquatic species (DWAF, 1996). According to Luo et al. (2016), increased water hardness and high magnesium levels can lead to low fertilisation rates in some species of fish.

In addition, an increase in water hardness results in an increase in the toxicity of other heavy metals such as lead and cadmium (Luo et al., 2016).

2.7.4.9) Nickel (Ni)

Nickel is a transition metal present in the environment only in small amounts (Wuana and Okieimen, 2011). Nickel exists in several oxidation states, including II, III and IV, with nickel (II) being the most stable form and is dominant in natural waters with a pH range of 5-7 (Javed and Usmani, 2017). Nickel occurs naturally in plants, soils and water, with the most significant accessible natural source of nickel being the ocean (Ahmad and Ashraf, 2012). Anthropogenic sources of nickel include nickel mining and electroplating, metal plating industries, burning of fossil fuels, and air emissions from power plants (Wuana and Okieimen, 2011). Nickel is essential in small doses. In plants such as legumes, nickel forms part of the vital component of some enzymes involved in nitrogen assimilation (Ahmad and Ashraf, 2012). However, elevated levels of nickel can cause adverse effects on plants and animals. Nickel toxicity on plants causes a reduction in the growth of shoots and roots, poor development of branches, reduced biomass production, and the impairment of germination processes (Ahmad and Ashraf, 2012). Nickel toxicity is also known to cause various cancers in the bodies of animals and a growth decline in microorganisms (Wuana and Okieimen, 2011). According to the SQGs proposed by NOAA (1999), the ERL for nickel is 20.9 mg/kg and the ERM for nickel is 51.6 mg/kg.

2.7.4.10) Zinc (Zn)

Zinc is a metallic element that naturally occurs on earth. This element occurs in two oxidation states in aquatic ecosystems, including zinc metal and zinc (II) (DWAF, 1996). Zinc naturally occurs in crustal rocks and ores and enters the environment naturally through the weathering of these rocks (Wuana and Okieimen, 2011). Anthropogenic sources of zinc include its use in industrial activities such as mining, combustion of coal and waste, steel processing, and fertiliser and insecticides used in agriculture (Wuana and Okieimen, 2011). Zinc is an essential micronutrient for all life forms; however, elevated levels can harm both plants and animals. In plants, zinc plays a vital role in photosynthesis, growth, and plant resistance against diseases (Rudani et al., 2018). According to Rudani et al. (2018), a deficiency in zinc severely impedes the growth and yield of plants. However, zinc toxicity has been found to inhibit metabolic activity and root growth in plants (Rout and Das, 2009) and inhibit photosynthesis in algae and

other aquatic plants (DWAF, 1996). In animals, zinc is a central component in many biochemical processes that support life, including cellular respiration, protein and lipid metabolism, and the maintenance of cell membrane integrity (Akram et al., 2019). A zinc deficiency can lead to reduced growth rate, increases in mortality, low body weight, cataracts, and erosion of the fin and skin of fish (Akram et al., 2019). However, elevated levels of zinc are known to be toxic to fish and other aquatic organisms even at low concentrations (DWAF, 1996). Zinc can accumulate in the bodies of fish and can biomagnify up the food chain and affect other organisms that consume the fish (Wuana and Okieimen, 2011). In addition, zinc can induce the formation of insoluble compounds in the mucus covering the gills of fish which can be lethal (DWAF, 1996). The sub-lethal effects of zinc toxicity in aquatic organisms include a decline in the rates of shell growth, oxygen uptake, and larval development (DWAF, 1996). According to the SQGs proposed by NOAA (1999), the ERL for zinc is 150 mg/kg and the ERM for zinc is 410 mg/kg.

2.8) Remote sensing

All objects on the surface of the earth emit electromagnetic radiation, and they also reflect radiation emitted from other objects (Campbell and Wynne, 2011). Remote sensing analysts can better understand the characteristics of vegetation, soils or water bodies on the earth's surface by recording emitted and reflected radiation and analysing the behaviour and interactions it has with objects (Campbell and Wynne, 2011). It is, therefore, imperative to have a good understanding of the electromagnetic spectrum, to be able to interpret remote sensing data. The electromagnetic spectrum comprises a range of different wavelengths of light energy ranging from gamma rays with the highest frequency and shortest wavelength to radio waves that have the lowest frequency and longest wavelength and include visible light (Ashraf et al., 2011). Remote sensing instruments collect light energy within specific regions of the electromagnetic spectrum to derive information (Richards and Jia, 2006). The main regions used in remote sensing are visible light, reflected and emitted infrared, and microwave regions, and this radiation is measured in spectral bands (Ashraf et al., 2011). Remote sensing, therefore, involves developing a relationship between the amount of electromagnetic energy reflected or emitted in specific bands and the chemical, biological and physical characteristics of the phenomena investigated (Jensen, 2015).

Remote sensing has three primary forms depending on the wavelengths of energy detected and the purpose of the study. According to Campbell and Wynne (2011), the first is to record the

reflection of solar radiation from the earth's surface. Here, energy in the visible and near-infrared portions of the electromagnetic spectrum are used. The second form of remote sensing involves recording radiation emitted from the earth's surface (Campbell and Wynne, 2011). Emitted energy from the earth's surface mainly originates from shortwave energy from the sun that was absorbed, then emitted back into the atmosphere at longer wavelengths (NASA, 2010). The emitted energy is strongest in the far-infrared spectrum; therefore, this type of remote sensing needs special instruments to record these wavelengths (Campbell and Wynne, 2011). This type of remote sensing is known as passive remote sensing as it involves the use of an instrument to sense the energy emitted by the earth instead of the energy produced by the sensor (Richards and Jia, 2006). The third form of remote sensing involves using instruments that generate their own energy before recording the reflection of that energy from the earth's surface (Campbell and Wynne, 2011). This type of remote sensing is referred to as active remote sensing as the sensors provide their own energy, making them independent of solar and terrestrial radiation (Richards and Jia, 2006). The remote sensing instruments measure the electromagnetic radiation reflected or emitted from the earth's surface, which can help us determine information about the surface features (Ashraf et al., 2011). The patterns of reflectance and absorption over different wavelengths for soil, water and vegetation are very distinctive from each other (Goetz, 2009). The spectral reflectance from one feature varies over the range of wavelengths in the electromagnetic spectrum, and this can be referred to as the spectral signature of that feature (Goetz, 2009; Ashraf et al., 2011).

2.8.1) Hyperspectral remote sensing

According to Goetz (2009, p. S5), hyperspectral remote sensing or imaging spectrometry can be defined as *"the acquisition of images in hundreds of contiguous, registered, spectral bands such that for each pixel a radiance spectrum can be derived."*. Multispectral remote sensing makes use of several broadly defined spectral regions. Hyperspectral remote sensing imagers, on the other hand, examines many narrowly defined spectral channels (Campbell and Wynne, 2011). Hyperspectral imaging is advantageous over multispectral imaging. The narrower and contiguous bands of hyperspectral data enable the detailed assessment of earth's surface materials with no gaps through which important information may be overlooked (Govender et al., 2007; Goetz, 2009; Campbell and Wynne, 2011).

Hyperspectral data contain the detail and accuracy that enables one to examine phenomena on the earth's surface that far exceed the capabilities of traditional remote sensing (Campbell and

Wynne, 2011). These capabilities of hyperspectral remote sensing enable the field of remote sensing to extend into the field of spectroscopy, which is the science of examining very accurate spectral data at a laboratory or field scale. Reflectance spectroscopy refers to the study of light as a function of the wavelength reflected from materials on the earth's surface (Aggarwal, 2004). The solar energy that is incident on earth's surface features can be absorbed or reflected and features absorb and reflect differently at different wavelengths of the electromagnetic spectrum (Ashraf et al., 2011). Wavelength-dependent absorptions distinguish different features on earth, and these images of reflected solar radiation are referred to as spectral signatures (Govender et al., 2007). According to Aggarwal (2004, p. 32), spectral reflectance can be described as *"a ratio of reflected energy to incident energy as a function of wavelength and is used to quantify these spectral signatures."* The spectral signatures of hyperspectral data are contiguous, which facilitates the in-depth analysis of surface materials and biological and chemical processes (Govender et al., 2007).

Spectroradiometers are useful tools in the analysis of the spectral reflectance of materials (Goetz, 2009). An analytical spectral device (ASD) spectroradiometer is an optical remote sensing device that uses detectors to record the distribution of radiation in a particular wavelength region (Rostom et al., 2017). It measures the spectral behaviour in the visible near-infrared (VNIR) and shortwave infrared (SWIR) spectra between 350 and 2500 nm with a precision of 1 nm. ASD is a full-range spectroradiometer and is computer-controlled (Danner et al., 2015). A portable PC is used to control the scans collected by the instrument, and it also allows for the on-screen visualisation of the data collected in real-time (Danner et al., 2015). The ASD spectroradiometer needs to be warmed up for at least 90 minutes prior to its use. This is necessary as the three arrays of the spectroradiometer warm up at different rates, thus when given ample time to warm up, they will reach an equivalent internal instrument temperature (ASD, 2000). ASD obtains all wavelength and radiometric calibrations after a 90-minute warm-up; therefore, adhering to the appropriate warm-up period will increase the quality of your data significantly as well as minimise errors (ASD, 2000). Hyperspectral data acquired from ASD spectroradiometers will first need to be pre-processed to exclude the effect of atmospheric components, which may change the observed spectral reflectance patterns (Rostom et al., 2017).

The signals obtained from analytical devices such as ASD are subject to spectral noise, which may be caused by physical and chemical factors as well as inaccuracies in the experimental

procedures (Xu et al., 2008). These noises in the spectra can cause low signal-to-noise ratios and low spectral resolutions (Xu et al., 2008). Another factor that can also degrade the spectra is baselines or background signals which influence the peak area and height of the spectra, leading to inaccuracies (Gholizadeh et al., 2016). Therefore, pre-processing is necessary to maintain the precision and accuracy of the spectral reflectance data acquired from spectroradiometers.

The spectral reflectance of a feature as a function of wavelength can be graphically displayed and is referred to as the spectral reflectance curve (Lillesand et al., 2015). These spectral reflectance curves provide us with more information on the spectral characteristics of the object of interest (Lillesand et al., 2015). The spectral reflectance curves of earth's surface features are useful in analysing transparent water bodies as well as sediments or soils. However, certain factors may influence the spectral reflectance of water and sediments.

2.8.1.1) Factors affecting the spectral reflectance of water

The most distinctive trait of water is the absorption in the NIR region and beyond. Most of the radiation is absorbed by water in the NIR and mid-infrared regions (Navalgund, 2001). These wavelengths comprise complex interactions between energy and matter that depend on several factors (Lillesand et al., 2015). The reflectance in the visible portion of the spectrum depends on the reflectance of the surface water and the bottom and suspended material within the water column (Navalgund, 2001). According to Lillesand et al. (2015), clear water displays the greatest reflectance at 600 nm. In addition, the presence of organic and inorganic material has a significant effect on the transmittance of the water, which in turn affects the reflectance (Karabulut and Ceylan, 2005). For example, a water body consisting of high amounts of suspended sediments resulting from soil erosion will have higher visible reflectance than other 'clear' water within the same area (Lillesand et al., 2015). Furthermore, when looking at the chlorophyll content of a water body, an increase in chlorophyll will cause a decrease in the reflectance in the blue wavelengths and increase the green wavelengths (Navalgund, 2001). This is particularly useful in detecting algae using remote sensing (Lillesand et al., 2015).

2.8.1.2) Factors affecting the spectral reflectance of sediments

Several factors influence the spectral reflectance of sediments and soils, including soil moisture content, particle size, organic matter content, and the amount of iron oxide. The higher the moisture content of the soil, the lower the spectral reflectance will be as water is a stronger

absorber of light as compared to soil (Bogrekci and Lee, 2004). Water surrounds soil particles and easily fills the air spaces between them, which causes a decrease in reflectance as water is a strong absorber (Cierniewski and Kuśnierek, 2010). The size of soil particles influences their reflectance as light is scattered differently by coarse-grained particles compared to fine-grained particles (Kaleita et al., 2005). The larger the soil particles, the lower the spectral reflectance will be. This is because coarse particles have irregular shapes with many gaps in between, enabling incident light to be trapped (Cierniewski and Kuśnierek, 2010). The higher the soil organic matter content, the lower the spectral reflectance will be. Soil organic matter influences the colour of soils with darker soils comprising of higher organic matter content, which lowers the reflectance of the soil (Galvao and Vitorello, 1998; He et al., 2009).

Similarly, iron oxides present in soils also influence the soil colour; however, this depends on the type of iron oxide present (Sahwan et al., 2020). For example, soil rich in hematite displays darker colours, such as deep red, whereas soil rich in goethite displays lighter colours ranging from yellow to light brown (Sahwan et al., 2020). According to Pereira et al. (2019), goethite has higher spectral reflectance in comparison to hematite, with hematite displaying higher absorption of light energy in the spectral region between 300 nm and 800 nm. Therefore, soils rich in the iron oxide goethite will cause an increase in the spectral reflectance of the soil, whereas soils rich in hematite will cause a decrease in the soil spectral reflectance (Pereira et al., 2019).

2.8.2) Remote sensing for the prediction of heavy metals in water and sediment

A study conducted by Monaledi (2019), involved the use of an ASD spectroradiometer to record the spectral reflectance of 78 water samples collected from the Mooi River in Carletonville, South Africa. In the study, water samples were poured into petri dishes and placed on a black surface to avoid background reflectance. Thereafter, the spectral reflectance of the water samples was recorded under clear sky conditions. The spectral noisy regions were removed and a support vector machine regression model was used to estimate the concentrations of the water quality parameters from the spectral reflectance data. It was found that the model performed well in the prediction of magnesium concentrations with R^2 and RMSE values of 0.98 and 2%, respectively. However, the model performed poorly in the prediction of iron concentrations with R^2 and RMSE values of 0.51 and 102%, respectively (Monaledi, 2019).

Another study conducted by Rostom et al. (2017) involved the use of hyperspectral remote sensing to evaluate the water quality of the Mariut Lake, Egypt. In the study, 22 water samples were collected from the Mariut Lake and the heavy metal concentrations of the water samples were determined using chemical analyses in a laboratory. In addition, an ASD FieldSpec 3 spectroradiometer was used to measure the spectral reflectance patterns of the lake water. Statistical tools were used to develop prediction models to determine the relationship between the laboratory-measured heavy metal concentrations and the estimated heavy metal concentrations using the spectroradiometer. It was found that the correlation coefficient R^2 values for the prediction of chromium, nickel, copper, cadmium, lead, iron and zinc were 0.86, 0.82, 0.97, 0.27, 0.88, 0.87 and 0.27, respectively. It was also found that the significant wavelengths for the prediction of heavy metals were 945 nm, 989 nm and 990 nm for chromium, 989 nm and 1013 nm for nickel, 704 nm for copper, 887 nm, 952 nm and 1001 nm for cadmium, 989 nm and 990 nm for lead, 366 nm for iron and 977 nm, 996 nm and 1001 nm for zinc (Rostom et al., 2017).

In another study conducted by Seifi et al. (2019) that investigated the visible-infrared spectroscopy and chemical properties of water near the Darrehzar porphyry copper mine in the Kerman Province, Iran. Sampling was done in winter and summer from different parts of the mine with eight water samples collected in winter and two water samples collected in summer. Two samples were collected from each sample point and one was used to test for pH, electrical conductivity and spectroscopy analysis and the other was used for the assessment of elements. The spectral measurements of the samples were recorded using an ASD FieldSpec 3 spectroradiometer. The spectral noise was removed from the spectra using ViewSpec Pro and Spectral Analysis and Management System (SAMS) software. The relationship between pH, EC and heavy metals were determined through regression coefficient (R). It was found that there were three absorption features at 650 nm, 975 nm and 1165 nm and two reflectance peaks at 804 nm and 1070 nm. The absorption features of the spectra were analysed, and it was found that the absorption features related to pH and electrical conductivity were found in the wavelength regions close to 975 nm. The total element concentrations displayed a negative correlation with the absorption feature at 650 nm and a positive correlation with the absorption features at 975 nm and 1165 nm. Significant correlations were found between the absorption feature at 975 nm and cobalt, manganese, nickel, lead and sulphur. This was attributed to electronic processes that occur in transition metals which occur around 800 nm. In addition, the regions between the absorption features at 650 nm and 975 nm were attributed to the

indicator spectral regions for zinc and the regions between the absorption features at 975 nm and 1165 nm were attributed to the indicator spectral regions for manganese. Iron showed a significant correlation with the absorption feature at 1165 nm and this was attributed to crystal field transitions of ferrous iron which occurs in the 900-1100 nm region (Seifi et al., 2019).

In a study conducted by Yang et al. (2021), multispectral satellite imagery was used to estimate heavy metal concentrations including arsenic, copper and lead in the topsoil of the Daxigou mining area in the Shaanxi Province, China. 44 soil samples were collected and the samples were sieved and dried before chemical analyses. 24 Landsat 8 images were downloaded from the USGS Earth Explorer website and were corrected for atmospheric effects using ENVI software. The Landsat 8 images were characterised by strong absorption between the 400 nm and 500 nm wavelength regions. The spectral reflectance increased between 500 nm and 780 nm and decreased between 780 nm and 900 nm. The reflectance of the images associated with contaminated soils displayed an increasing spectral reflectance between 1200 nm and 2500 nm indicating these four spectral ranges were suitable in distinguishing between heavy metal-contaminated soil and uncontaminated soil. In addition, the reflectance of bands B2-B7 showed strong correlations with the lead concentrations and the reflectance of bands B2-B4 showed strong correlations with the copper and arsenic concentrations and the spectral values of bands B2-B7 from the Landsat 8 images were selected. A linear model, a rule-based M5 model tree and a genetic algorithm-back propagation (GA-BP) model were developed to estimate the heavy metal concentrations from the Landsat 8 images. It was found that the GA-BP model improved the accuracy of estimating arsenic, copper and lead concentrations in the soil as the RMSE for the GA-BP model was lower than that of the linear model and the M5 model tree (Yang et al., 2021).

Another study conducted by Mouazen et al. (2021) involved the use of regression methods and Landsat 7 for spatiotemporal prediction and mapping of heavy metals between Ghent and Antwerp, Belgium. 435 soil sampling stations were selected and the corresponding heavy metal concentrations were extracted from the Land-Use/Cover Area Frame Survey (LUCAS) database. Four Landsat 7 images dated 2009, 2013, 2016 and 2020 were downloaded from USGS Earth Explorer and the digital number (DN) value of pixels corresponding to the soil sampling locations in each band was converted to spectral reflectance, using ArcMap. Partial least squares regression (PLSR), random forest (RF) and support vector machine (SVM) regression models were used to predict the 10 soil heavy metal concentrations (antimony, lead,

nickel, manganese, mercury, copper, chromium, cobalt, cadmium and arsenic) from the spectral features of the Landsat 7 images. It was found that the RF machine learning algorithm performed better in the prediction of the 10 heavy metals than the PLSR and SVM models for 2009. The R^2 of prediction and the residual prediction deviation (RPD) of prediction values were used to assess the accuracy of the models and the R^2 of prediction and the residual prediction deviation (RPD) of prediction values obtained for the prediction of the 10 heavy metals using the RF algorithm ranged from 0.62 to 0.92 and 1.23 to 2.79, respectively.

In another study conducted by Todorova et al. (2014), the near-infrared spectroscopy was used to estimate heavy metal concentrations in 124 soil samples collected from crop fields in the Stara Zagora Region, Bulgaria. The soil samples were air-dried, crushed and sieved using a 2 mm sieve and the samples were divided into two sets where one set was used for chemical analyses and the other set was used to record spectral measurements. A Spectrum One NTS, FT-NIR Spectrometer (Perkin Elmer, Waltham, MA, USA) was used to record spectral reflectance measurements in the near-infrared spectral regions. 300 scans were recorded and averaged to obtain the final reflectance spectrum for each soil sample. The noisy spectral regions were removed and the spectra were pre-processed before a PLS regression model was used to predict the heavy metals from the reflectance spectra. The samples were divided into calibration and prediction sets and the prediction set was used to test the accuracy of the model. It was found that the best model was obtained for the prediction of copper and the predictions of zinc, lead and nickel were found to be less accurate. In addition, it was found that the important wavelengths for the prediction of copper were 1500 nm, 2184 nm and 2244 nm. The important wavelengths for the prediction of zinc were 1500 nm, 2217 nm, 2295 nm and 2354 nm. The important wavelengths for the prediction of lead were 1894 nm, 2295 nm and 2142 nm and the important wavelengths for the prediction of nickel were 1904 nm, 2168 nm and 2245 nm.

In another study conducted by Choe et al. (2008), field spectroscopy and hyperspectral remote sensing were used to map the heavy metal pollution in the stream sediments of the Rodalquilar mining area, Spain. 49 dry sediment samples were collected from stream channels in the Rodalquilar area and were analysed for heavy metals. The spectral measurements of the sediment samples were recorded using an ASD FieldSpec Pro spectroradiometer in a dark room to avoid interference from stray light. Each sediment sample was poured into a 60 x 15 mm dish with a sample depth of 8 mm and the spectral measurements were recorded using a contact

probe. Continuum removal and normalisation was performed on the spectra obtained to enhance the absorption features and the relationships between the spectral absorption features and heavy metal concentrations were assessed using the Pearson correlation coefficient. The relationship between the spectral parameter values and metal levels were assessed using two types of multiple linear regression (MLR) including stepwise and enter. Three parameters including spectral ratios, continuum removal and band-depth analysis were derived from the spectral variations associated with heavy metals in the sediment. It was found that band ratios between 500 nm and 610 nm and between 778 nm and 1344 nm was caused by spectral variations associated with iron oxide. It was also found that the absorption depth near 500 nm increased with high concentrations of heavy metals. In addition, the absorption depth and area values around 2200 nm, associated with lattice OH minerals, decreased with high heavy metal concentrations. It was found that the enter MLR performed better than the stepwise MLR. R^2 and RPD values were used to assess the accuracy of the MLR prediction models. The R^2 values obtained for lead, zinc and arsenic were 0.615, 0.596 and 0.876, respectively and the RPD values obtained for lead, zinc and arsenic were 1.39, 1.387 and 2.562, respectively.

Another study conducted by Kemper and Sommer (2002) used reflectance spectroscopy to estimate the heavy metal contamination in soils after a mining accident in the west of Seville, Spain. A total of 214 soil samples were collected and chemically analysed for heavy metals. The soil samples were air-dried and sieved using a 2 mm sieve before the spectral reflectance of the samples were measured using an ASD FieldSpec 2 spectroradiometer. The spectra were pre-processed using a Gaussian model which resulted in a resampled spectra with a reduction in the wavelengths (from 2151 to 108), producing smooth spectra with less over-fitting. The data was then transformed to absorption (log 1/R) to account for scattering effects before first- and second-order derivatives were applied using the Savitzky-Golay method. The samples were divided into calibration and validation sets with 119 samples in the calibration set and 118 samples in the validation set. The prediction models to predict the laboratory-measured heavy metal concentrations from the spectral reflectance measurements were built using stepwise MLR and an artificial neural network (ANN). R^2 and RPD values were used to assess the accuracy of the MLR and ANN prediction models. It was found that for the MLR, the R^2 values for arsenic, cadmium, copper, iron, mercury, lead, sulphur, antimony and zinc were 0.837, 0.51, 0.54, 0.721, 0.957, 0.944, 0.839, 0.929 and 0.234, respectively and the RPD values were 3.83, 1.23, 1.23, 1.92, 5.77, 5.30, 2.38, 4.66 and 0.59, respectively. It was found that for the ANN, the R^2 values for arsenic, cadmium, copper, iron, mercury, lead, sulphur, antimony

and zinc were 0.858, 0.494, 0.446, 0.714, 0.929, 0.940, 0.845, 0.927, 0.220, respectively and the RPD values were 3.28, 0.96, 0.84, 1.98, 4.30, 5.89, 2.66, 4.55 and 0.51, respectively. In addition, a correlogram was developed to analyse the correlation between the heavy metals and spectral reflectance information. It was found that there was a high positive correlation (or peak) at around 550 nm which was caused by the charge transfer band in the ultraviolet region of the spectrum. The area with the highest negative correlations (or absorption features) between 700-1400 nm was linked to the strong absorption of the ferrous ion at around 1000 nm. Three peaks were observed between 1400 nm and 2200 nm which was attributed to strong molecular water bands at 1400 nm and 1900 nm in combination with hydroxyl absorptions centred at 1400 nm and 2200 nm. An absorption feature was also observed at 2350 nm which was caused by carbonate absorption and similar to the features associated to OH-bearing secondary minerals, its depth was negatively correlated with heavy metal concentrations (Kemper and Sommer, 2002).

CHAPTER 3: DESCRIPTION OF THE STUDY AREA

3.1) Introduction

The uMgeni River and Estuary is the chosen study area for this research. The uMgeni River catchment is an extensive system (Cooper, 1993); therefore, the study was focused only on the lower uMgeni system near the coast as seen in Figure 3.2. This chapter aims at introducing the selected study area. It entails a detailed description of the study area, including location and physical characteristics, geology and soils, topography, climate, biology, as well as information about the land-use and land cover in and around the area.

3.2) Location and physical characteristics

The eThekwini Municipality is located in the province of KwaZulu-Natal, along the east coast of South Africa (Figure 3.1). This municipality covers an area of 2291 km^2 and includes the city of Durban, which is the third-largest city in South Africa (Pather, 2014). The eThekwini Municipality consists of 16 estuaries, of which the uMgeni Estuary falls and is the chosen study area for this study.

The uMgeni Estuary is located at 29°48'36"S 31°02'08"E and is situated 5 km north of the centre of Durban (Forbes and Demetriades, 2008). The uMgeni Estuary is regarded as a permanently open estuary and is the only estuary of this type that falls within the eThekwini municipal boundary (Forbes and Demetriades, 2008). The uMgeni Estuary is a coastal system with a river length of 230 km long and a catchment area of approximately 5000 km^2 (Glennie, 2001; Olaniran et al., 2014). This makes uMgeni the largest catchment in KwaZulu-Natal. The uMgeni Estuary is a river-dominated estuary extending from the Indian Ocean into the uMgeni River catchment (Glennie, 2001). The main urban centres of Durban and Pietermaritzburg are located within the uMgeni catchment, and over 3.5 million people from Howick towards the coast receive their water from this catchment (WRC, 2002; Umgeni Water, 2017).

The uMgeni River originates in the foothills of the Drakensberg area in KwaZulu-Natal at an elevation of 1889 m and flows eastwards towards the Indian Ocean at the mouth (Chili, 2008; Tinmouth, 2010; Banda and Kumarasamy, 2020). The river flows from the Valley of a Thousand Hills with a gentle gradient for 24 km before it enters the Indian Ocean through the northern suburbs of Durban (Olaniran et al., 2014). According to the UEIP (2016), 42% of

KwaZulu-Natal's population depends on the uMgeni River catchment for their water supply. The river flow is regulated by four dams built upstream and downstream of the catchment, namely, Midmar, Albert Falls, Nagle and Inanda dams (Namugize, 2017). These dams supply water for agricultural purposes and to the residential areas and informal settlements of both Pietermaritzburg and Durban (Namugize, 2017). The land cover found within the uMgeni catchment is regarded as heterogeneous, comprising urban areas, forests, subsistence and commercial agriculture, and the Port of Durban (Banda and Kumarasamy, 2020). There are five bridges constructed across the uMgeni Estuary. These bridges include the Ellis Brown viaduct located at the mouth, the Athlone bridge about 1.4 km from the mouth, the Connaught Interchange about 2.5 km from the mouth, a railway bridge a further 150 m upstream and lastly, the bridge on the N2 freeway (Forbes and Demetriades, 2008). The uMgeni catchment is also boarded by Beachwood mangroves that extend to the mouth (Glennie, 2001).

The uMgeni Estuary is funnel-shaped with the mouth positioned towards the south as a result of a sandbar that expands southward (Tinmouth, 2010). An artificial groyne was established on the southern bank of the uMgeni Estuary to minimise scour due to tides and the northerly movement of sediment due to longshore drift (Njoya, 2002). In addition, the salinity levels of the estuary fluctuate, depending on the tides and the volume of freshwater inflow (Tinmouth, 2010). During high tides, the estuary is dominated by saltwater, and during low tides, a salt wedge forms in the zone between the estuary's head and Athlone Bridge (Tinmouth, 2010).

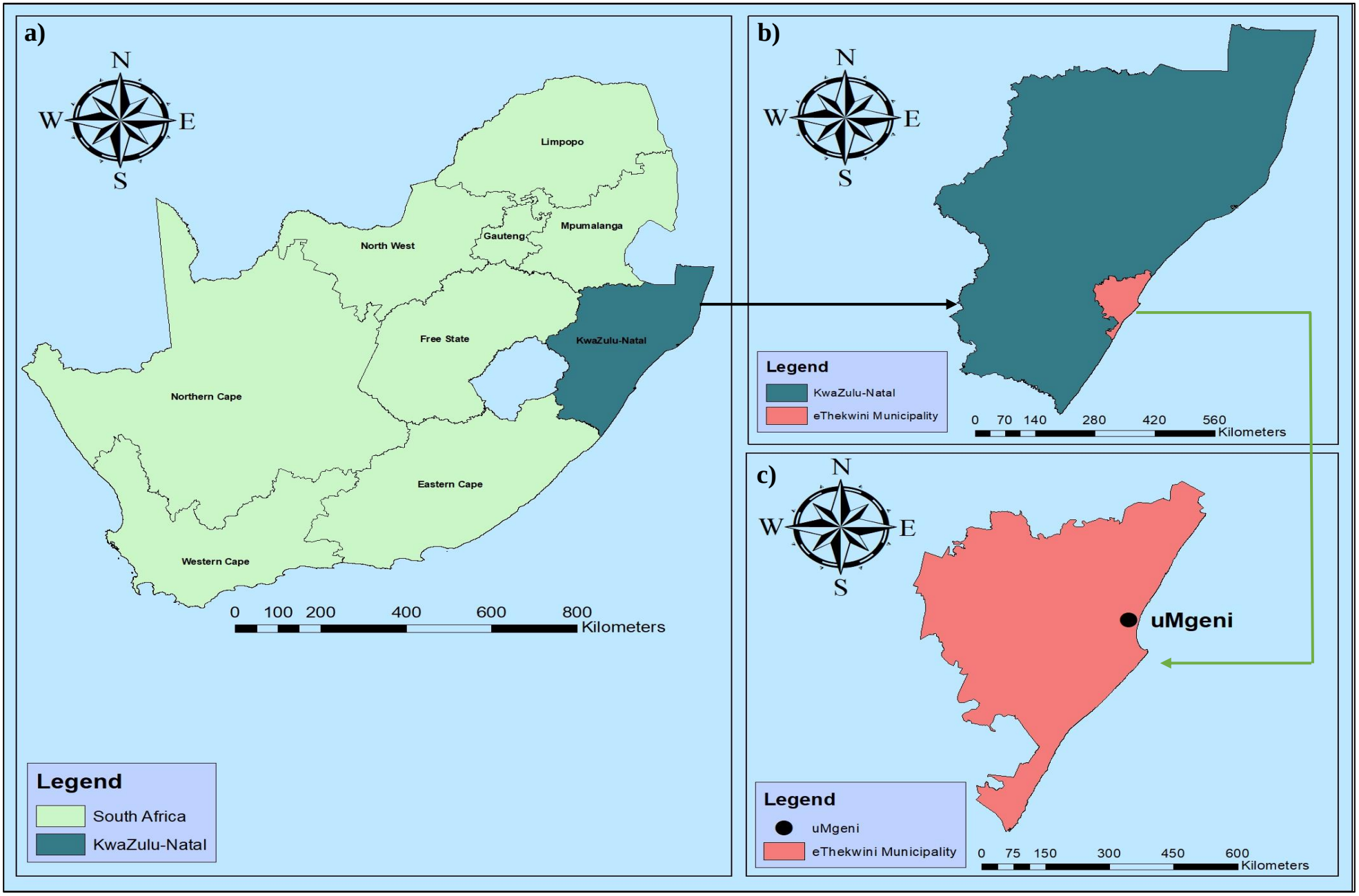

Figure 3.1: Locality map of uMgeni: a) South Africa; b) KwaZulu-Natal, and c) the eThekwini Municipality.

Figure 3.2: Satellite image illustrating the study area (Source: Google Earth, date accessed: March 2021).

3.3) Geology and Soils

Hinterland geology and the soils developed on it are important as they influence the nature and volume of sediment available for transport by rivers to the coasts (Cooper, 1991). The coast of KwaZulu-Natal has a variety of geological formations. According to Marshall and von Brunn (1999), the dominant geology found along the KwaZulu-Natal coastal belt includes the Natal Group Sandstone, Ecca Shale and Dwyka Tillite beds with intrusions of basic igneous rock dolerite as well as igneous outcrops of granite. The Archaean and Proterozoic basements in KwaZulu-Natal consist of granites and greenstones (Schlüter, 2008). These are superimposed by the Natal Group, which are Phanerozoic sedimentary rocks consisting of conglomerates, sandstones, siltstones and mudrocks (Marshall and von Brunn, 1999; Hicks, 2009). The Natal Group is overlain by the Karoo Supergroup, namely the basal Dwyka Group covered by the Ecca Group (Schlüter, 2008). The Dwyka Group predominantly comprises diamictites, conglomerates, sandstones and mudrocks, whereas the Ecca Group primarily consists of mudrocks, sandstones, siltstones and mudstones (Hicks, 2009). Figure 3.3 illustrates KwaZulu-Natal's geology and depicts the geology that falls within the eThekwini Municipality.

The uMgeni catchment comprises a wide variety of rock types. The upper reaches of the catchment comprise Ecca and Beaufort Group lithologies comprising fine-grained lacustrine

and fluvial sedimentary rocks (Cooper, 1993). These lithologies are intruded by Late Jurassic Karoo Dolerite, which is underlain by Dwyka tillite (Cooper, 1991). Archaean granite is found in the middle of the catchment. According to Begg (1978), this is the source of most sands found within the catchment and the pink sands found within the estuary. Downstream of the catchment near the Connaught Interchange, the river flows over Ecca and Dwyka rocks (Abed, 2009). The alluvium is found near the coast on the Springfield Flats, with Tertiary and Pleistocene coastal deposits exposed on the sides of the valley (Cooper, 1991).

The uMgeni Estuary is underlain by shale that is fractured towards the surface and comprises dolerite intrusions (Pather, 2014). According to Begg (1978), in 1972, the head of the estuary consisted of fine sands, and sand and gravel were characteristic of the middle reaches. The lower reaches were primarily made up of black anaerobic silt beneath deposits of sand, with the Beachwood mangroves comprising sand of uniform composition, and the mouth of the estuary predominantly consisted of sand (Begg, 1978). According to the results of the sediment analyses undertaken between 2007 and 2008 by Forbes and Demetriades (2008), the estuary's mouth primarily consisted of fine to medium sands, the middle reaches comprised uniform medium sands, and the upper reaches consisted of very fine sands.

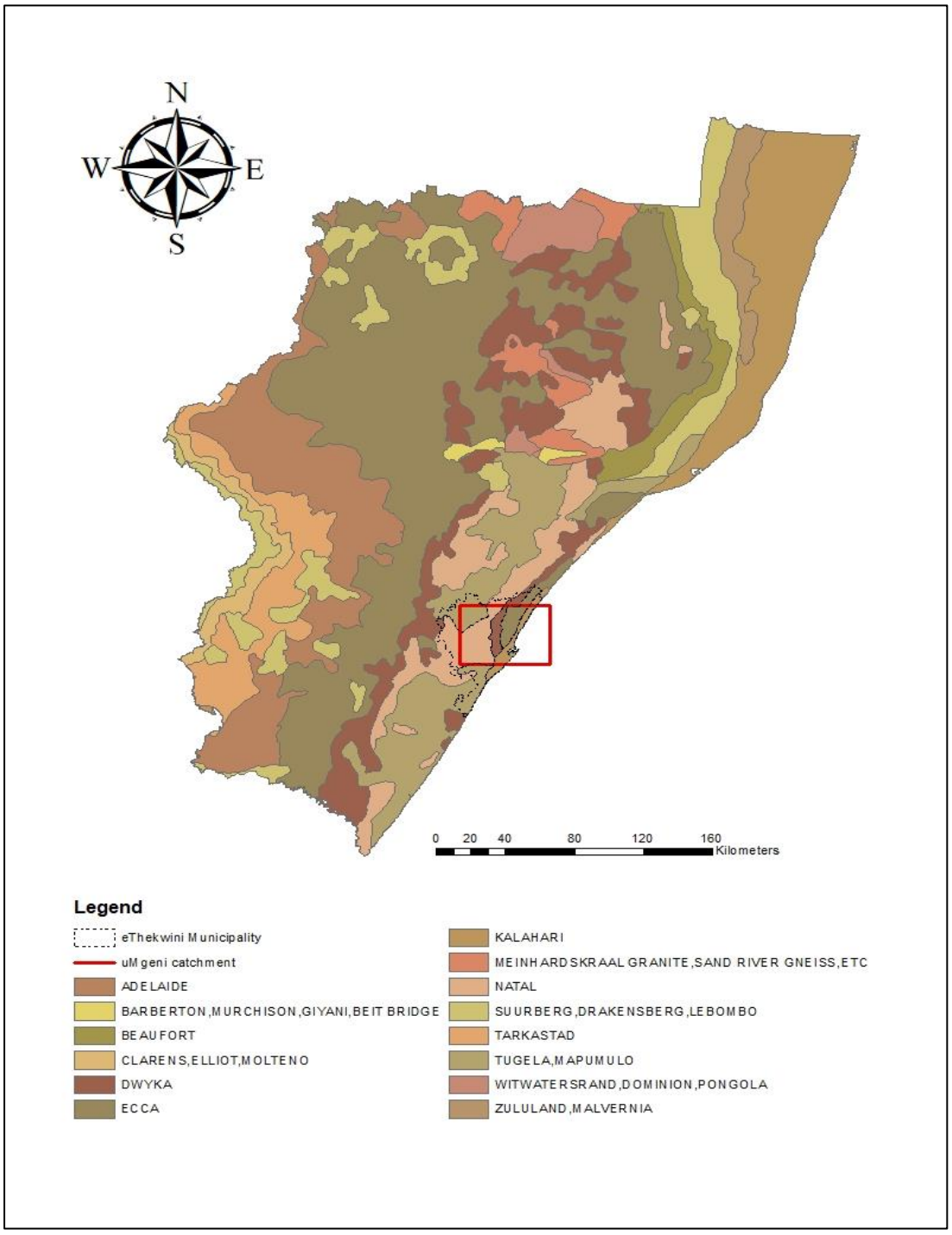

Figure 3.3: Map depicting the geology of the study area within the eThekwini Municipality in KwaZulu-Natal (map created with data sourced from www.gis.durban.co.za and accessed on 18/02/2021).

3.4) Topography

According to Cooper (1993), the topography of KwaZulu-Natal province can be characterised by steep hinterland and a lack of coastal plains in the southern parts of the province. Coastal plains dominate the northern areas of the province near Zululand and beyond the border towards Mozambique (Cooper, 1993). According to Abed (2009), the Drakensberg Mountain range forms a large watershed from which the main perennial rivers flow towards the Indian Ocean. There are approximately 74 rivers, including 9 major perennial rivers, 55 minor perennial rivers and 10 secondary rivers, flowing towards the Indian Ocean (Cooper, 1990).

The topography and climate of KwaZulu-Natal result in high sediment yields and erosion, being experienced near the coast (Abed, 2009). In addition, the KwaZulu-Natal coastline is dominated by sandy beaches due to the high fluvial sediment loads that maintain beaches and barrier environments that develop across the inlets of estuaries (Abed, 2009; Pather, 2014).

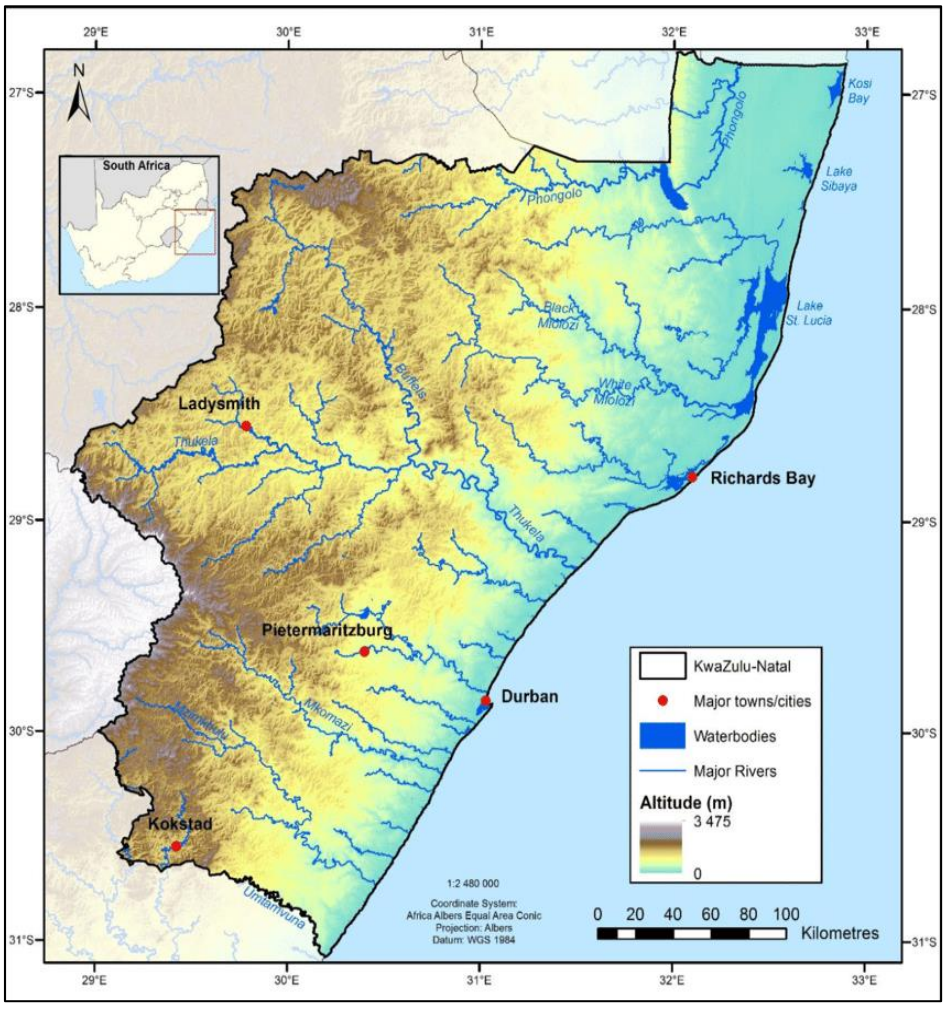

Figure 3.4: Map of the topography of KwaZulu-Natal (Source: Turpie et al., 2020).

3.5) Climate

The coast of KwaZulu-Natal experiences a subtropical climate with warm and rainy summers and cool and dry winters (Njoya, 2002). The influence of the warm Aghulus current promotes annual average temperatures ranging from warm to hot in summer and mild in winter (Glennie, 2001; Pather, 2014). The temperatures experienced in KwaZulu-Natal Durban in summer range from 23 ºC to 33 ºC, with winter temperatures ranging from 16 ºC to 25 ºC (SA-Venues, 2021). The average annual temperatures experienced within the uMgeni catchment range between 14 ºC and 22 ºC (Umgeni Water, 2017).

The uMgeni River catchment is subjected to increased variability and extreme weather events, including more flood and drought events (Hay, 2017). Increased temperatures resulting from global warming and climate change lead to heat stress on people, livestock and wildlife (Hay, 2017). The higher temperatures have also resulted in an increase in evaporation which reduces the efficacy of dams as water storage facilities (Umgeni Water, 2013). In addition, the rise in temperatures has also impacted the distribution of fauna and flora and facilitated the spread of alien invasive plants. According to Hay (2017), alien invasive wattle trees found within the uMgeni catchment consume approximately 7.2 million cubic metres of water which is well over the amounts consumed by indigenous vegetation. This is particularly problematic during periods of drought as this amount consumed by the alien species is equivalent to the annual water requirements of 100 000 people (Hay, 2017).

The rainfall experienced by the uMgeni catchment is seasonal, with a higher amount of rainfall experienced in the summer months (October to March). According to Cooper (1993), 80% of annual rainfall in KwaZulu-Natal is experienced during the summer months. Winter rainfall is substantially lower and usually occurs as a result of the northward-moving coastal low-pressure systems (Pather, 2014). The amount of rainfall across the uMgeni catchment is highly variable, increasing from the western to the eastern part of the catchment (Banda and Kumarasamy, 2020). The coastal portion of the catchment experiences rainfall ranging between 1000 mm to 1500 mm annually, whilst the more inland areas of the catchment experience rainfall ranging between 800 mm to 1000 mm annually (Warburton et al., 2012).

Occasionally, KwaZulu-Natal experiences periods of intense rainfall leading to extensive flooding throughout the province (Cooper, 1993). These flood events alter sediment patterns

and lead to the erosion and transportation of high sediment loads from rivers into estuaries (Njoya, 2002).

3.6) Biology

Biologically, the type and abundance of species found within estuaries are strongly influenced by the mouth state (Van Niekerk and Turpie, 2012). The permanently open mouth state of the uMgeni Estuary enables it to be easily accessible to marine species that use estuaries for reproduction and nurseries (Van Niekerk and Turpie, 2012). According to Forbes and Demetriades (2008), the open mouth state and strong salinities enable the uMgeni Estuary to support a wide variety of fish species. The uMgeni Estuary is also home to 24 taxa of benthic invertebrates, and bird communities were also found to be in high abundance and reasonably diverse (Forbes and Demetriades, 2008). In addition, the uMgeni Estuary is surrounded by Beachwood mangroves which are also home to a wide variety of plant and animal species (WRC, 2002). These include red data fish, reptiles, birds, invertebrates, and three species of mangroves, including the white, black and red mangroves (Beachwood Mangroves Nature Reserve, 2013).

3.7) Land-use

Land-use can be described as the human activities that occur on the earth's surface and include agriculture, forestry, and urban development (Kercival, 2015). Land-use change can be defined as the process through which anthropogenic activities change the natural environment, such as deforestation (Liang et al., 2012). According to Jewitt et al. (2015), between the years 2005-2011, the KwaZulu-Natal province has lost 7.6% of its natural landscape due to anthropogenic transformations such as agriculture, timber plantations, the built environment and the establishment of dams and mines. The uMgeni River catchment comprises a wide variety of land-uses. The uMgeni River is responsible for approximately 65% of the total economic production in KwaZulu-Natal (WRC, 2002). However, according to Olaniran et al. (2014), the uMgeni River near the mouth has been significantly modified over the years with alterations in riparian vegetation and flow direction to make way for anthropogenic activities. The increase in anthropogenic activities and the subsequent alterations in land-use and land cover have significantly reduced the water quality of the river and estuary (Olaniran et al., 2014).

Abed (2009) states that the predominant land-use in the uMgeni catchment is intensive farming of tropical fruits, sugar, crops, and dairy farming. A golf course, yacht club, restaurants, and

other recreational facilities have also been established on the southern bank of the uMgeni Estuary. Residential and commercial areas have been developed on the northern bank of the estuary (Begg, 1978). Figure 3.5 below depicts the land-use and land cover found along the uMgeni catchment between 2013 and 2014. As seen in Figure 3.5, the lower uMgeni catchment near the mouth, a majority of the land-use is occupied by urban township, urban village and urban built-up areas. The land cover includes natural vegetation such as dense trees, open trees, low vegetation and grass, and bare land, which facilitates expansions in urban development in the future. The Beachwood Mangroves Nature Reserve is also found at the mouth of the uMgeni Estuary and is a 76-hectare protected area (Beachwood Mangroves Nature Reserve, 2013).

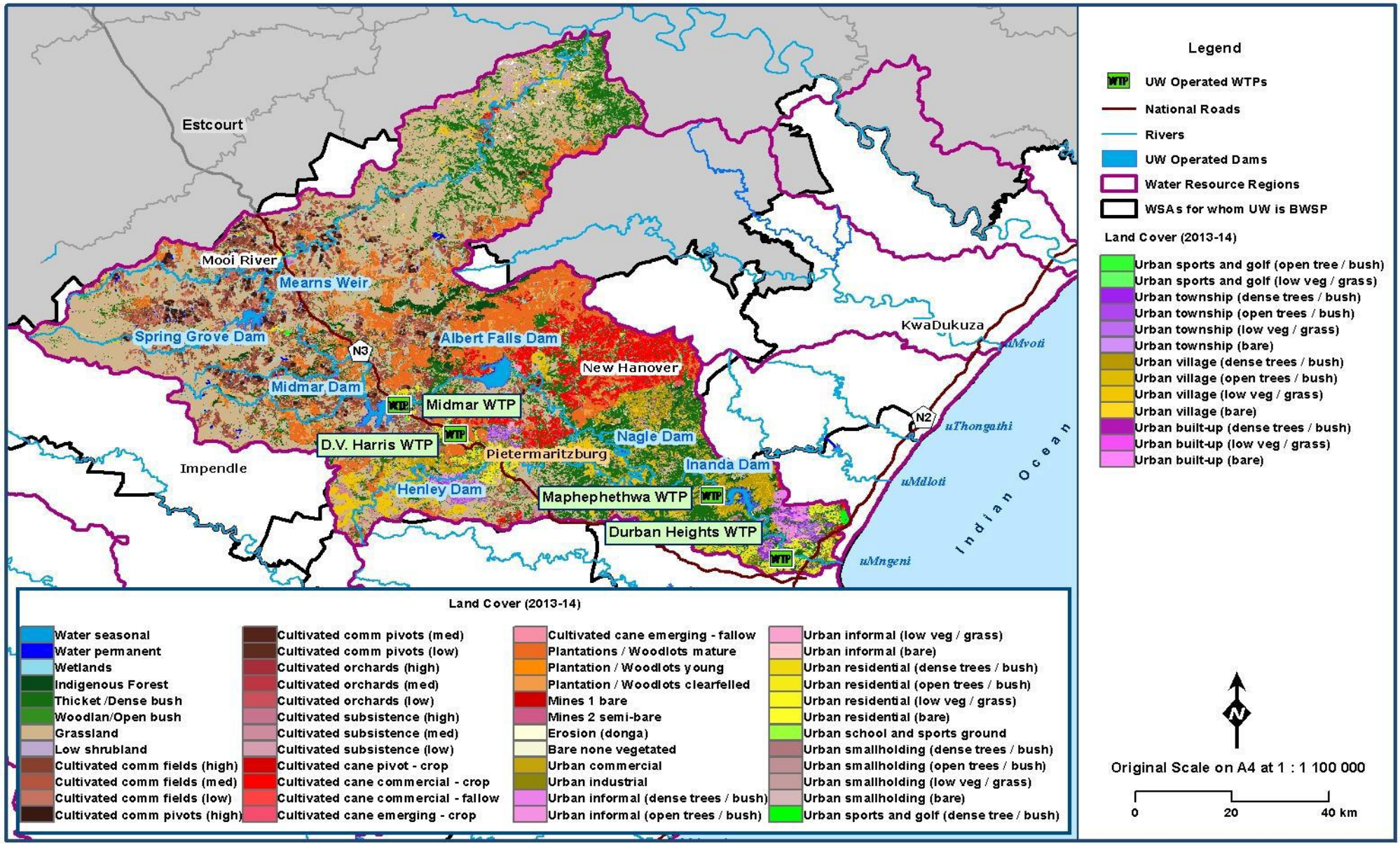

Figure 3.5: Land-use and land cover map of the uMgeni catchment between the years 2013-2014 (Source: Umgeni Water, 2017).

CHAPTER 4: METHODOLOGY

4.1) Introduction

This chapter provides details on the materials and methods used in this study in order to achieve the aim and objectives of the study. It includes information on how data collection of the water and sediment samples in the field and laboratory were carried out. The types of statistical techniques employed on the water and sediment data obtained and the accuracy assessments are also discussed. The results obtained following the methodology employed in this chapter are presented in the results chapter of the dissertation.

4.2) Data collection

4.2.1) Field sampling

Field data collection involved the collection of water and sediment samples from the uMgeni Estuary. The field sampling was undertaken on the 8th April 2021, during the wet season. The weather was calm with partly cloudy conditions experienced in the morning and sunny conditions at noon. Sampling was conducted between 9:30 am and 12:30 pm during low tide.

The water samples were collected in a systematic pattern along a line transect from three designated sampling locations A, B and C as seen in Figure 4.1. Systematic sampling involves selecting a random starting point and each sample is collected at regularly spaced intervals in a particular pattern (Bellhouse, 2005). The sampling locations were randomly selected and at each location, five samples were collected along transect lines approximately 10 m apart across the estuary, collecting a total of 15 water samples. The systematic technique is a widely used sampling technique and was selected as it is simple, efficient and less time-consuming (Bellhouse, 2005). 500 ml plastic bottles were used to collect the water samples to be analysed for their heavy metal content as heavy metals can adsorb irreversibly on other surfaces, such as glass (Kaflé, 2019). Samples were taken from just below the water's surface. The sampling bottles were rinsed three times with the sample water before the final sample was taken. Upon collecting the final sample, the bottles were allowed to fill whilst completely submerged in the water and capped underwater to avoid contamination (Wilde and Radtke, 1998; Bartram and Ballance, 2020). This process was repeated at each sampling point. The water samples were immediately placed in a cooler box and away from the sun.

The sediment samples were collected along the banks of the estuary. Five samples were collected from each sampling location A, B and C collecting a total of 15 sediment samples. The sediment samples were collected from top horizon sediments, at 0-2 cm depth. These samples were collected using a spade and were collected at a specified distance of approximately 10 m a part and stored in plastic zip lock bags. The samples were immediately placed in a cooler box and away from the sun to preserve the samples (Kianpoor Kalkhajeh et al., 2019). The GPS locations of each sampling point was also recorded. The samples were then transported on ice to the laboratory for analysis; the water samples were stored in a cold room at 4°C prior to analysis.

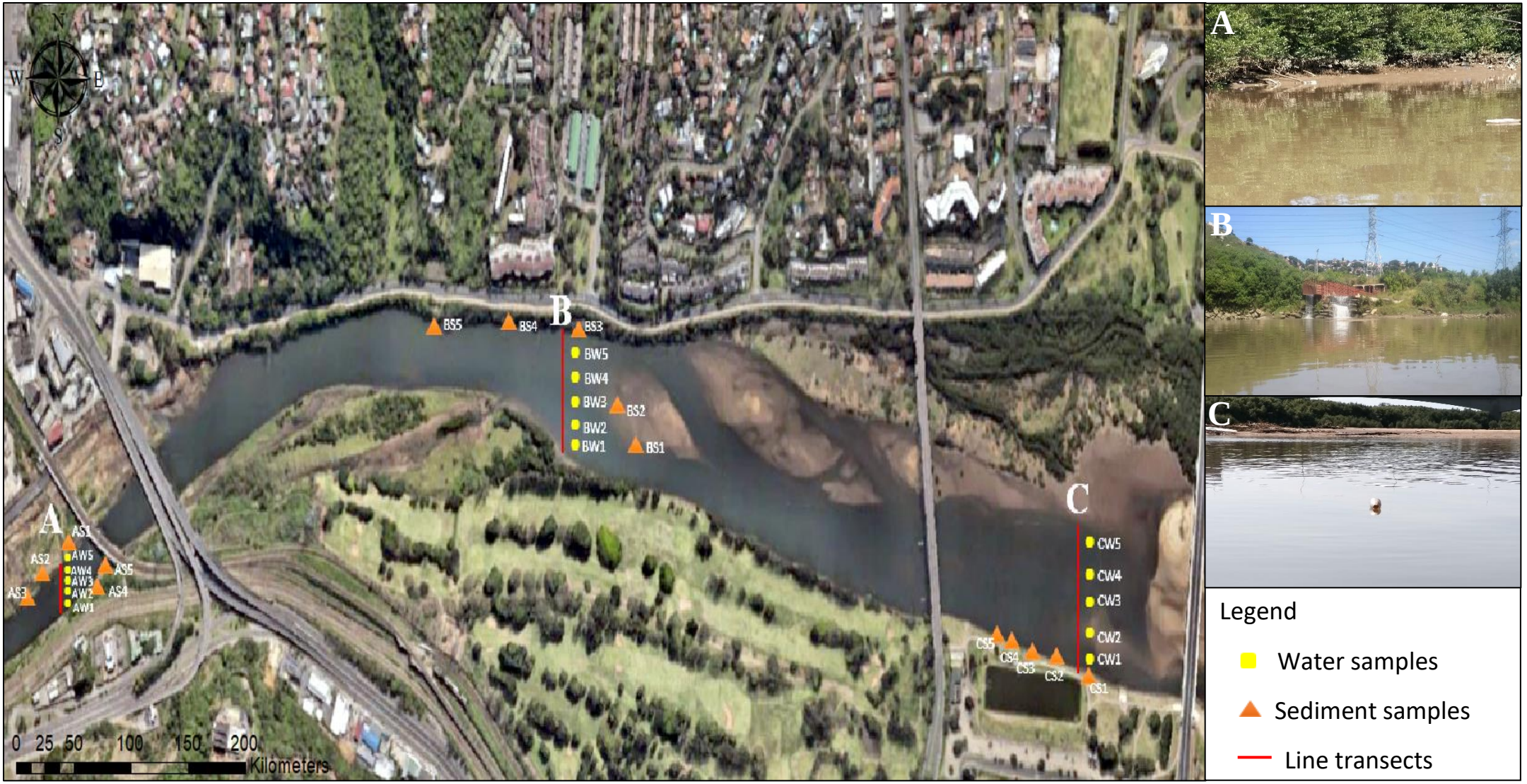

Figure 4.1: Map of the sampling points of the uMgeni estuary with images depicting the areas close to the three main sampling sites A, B and C.

4.2.2) Laboratory data collection

At the laboratory the samples were tested for pH, dissolved oxygen and electrical conductivity using a multi-parameter device as seen in Figure 4.2. The pH meter was first calibrated with pH 4, pH 7 and pH 9 buffer solutions before any readings were taken. The pH electrode was rinsed with distilled water before using each buffer solution. Thereafter, water samples were poured into 60 ml beakers and placed on a magnetic stirrer with a stir bar set at a steady pace to ensure homogenisation of the water samples. The pH, dissolved oxygen and electrical conductivity electrodes were then dipped into each sample and the readings were recorded three times and averaged. All electrodes were rinsed with distilled water before each reading was recorded. This procedure was repeated for the 15 water samples.

pH is important in terms of mobility as the availability of heavy metals is relatively low when the pH range is between 6.5 to 7 (Hacısalihoğlu and Karaer, 2016). Low pH levels can encourage the solubility of heavy metals (Zhang et al., 2018). According to Li et al. (2013), low pH levels cause an increase in the competition between hydrogen ions and dissolved heavy metals for ligands. Subsequently, the adsorption capabilities and bio-availabilities of the heavy metals decrease resulting in an increase in the mobility of heavy metals. In addition, soluble and carbon-bound heavy metals precipitate more easily under low pH conditions (Li et al., 2013). Electrical conductivity (EC) gives an estimate of the presence of ionic substances in water. It is often used as a surrogate measure of total dissolved solids present in the water. An increase in the EC results in a decrease in the adsorption of heavy metals on sediment (Hacısalihoğlu and Karaer, 2016). The amount of dissolved oxygen also plays a role in the release of heavy metals. A study conducted by Kang et al. (2019), indicated that certain heavy metals are released from river sediments into the overlying water column in anoxic conditions (low oxygen levels) and adsorbed by sediment from the overlying water column in aerobic conditions. The samples were stored in a cold room in the laboratory at 4 °C until further analysis.

Figure 4.2: Multi-parameter device apparatus used to record pH, dissolved oxygen and electrical conductivity measurements of the water samples.

The water samples were centrifuged with a centrifuge machine at a rotation speed of 5000 rpm for 10 minutes in order to separate the solid and liquid phases. Thereafter, the samples were carefully filtered into 50 mL ICP tubes using a 0.45 µm syringe filter. A multi-element standard solution was included with the samples and transported to the chemistry department on the Pietermaritzburg Campus to be analysed for the heavy metals of interest using inductively coupled plasma optical emission spectroscopy (ICP-OES). ICP-OES is a traditional analytical method used to determine the number and concentration of elements that are present in a particular sample (Boss and Fredeen, 1997). ICP-OES is based on the principle that when plasma energy is introduced to a sample from the outside, the elements or atoms move from the ground state to an excited state (Ghosh et al., 2013). When these excited atoms revert to a low energy position, emission rays are discharged, and the emission rays that correspond to the photon wavelength are recorded (Ghosh et al., 2013). The type of element is determined based on the position of the photon rays. The concentration of each element detected is subsequently determined based on the intensity of the rays (Kiran and Raja, 2017). The samples were

analysed for the following ten heavy metals, aluminium (Al), arsenic (As), cadmium (Cd), chromium (Cr), copper (Cu), iron (Fe), lead (Pb), magnesium (Mg), nickel (Ni) and zinc (Zn). These heavy metals were chosen as they are commonly found in effluent discharge and are a cause of concern even if they are found in trace amounts (Akpor et al., 2014).

For solid samples such as sediments, the samples first need to be converted into an aqueous phase in a process known as acid digestion in order to be analysed spectroscopically (Güven and Akinci, 2011). In the laboratory, the sediment samples were first air-dried at room temperature for three weeks before being crushed with a pestle and mortar in order to obtain fine particles. Fine sediment particles act as metal sinks owing to their net negative charge and involvement in sorption and cation exchange processes (Adeogun et al., 2012; Arnous and Hassan, 2015). Thereafter, the sediment samples were placed into clean plastic zip lock bags and transported in a cooler box, away from the sun, to the ALS Analysis and Inspection Laboratory in Durban for acid digestion and heavy metal analysis. The acid digestion involved the use of a combination of hydrochloric acid and nitric acid and the samples were digested by heating them on a hotplate. The digested samples were then analysed for the heavy metals of interest using ICP-OES.

4.2.3) Remote sensing data collection

The remote sensing data collection involved the collection of spectral characteristics of the water and sediment samples using an analytical spectral device (ASD) FieldSpec 3 spectroradiometer. An analytical spectral device (ASD) spectroradiometer is an optical device that uses detectors to measure the distribution of radiation in a particular wavelength region (Rostom et al., 2017). It measures the spectral behavior in the visible near-infrared (VNIR) and shortwave infrared (SWIR) spectra between 350 and 2500 nm in a precision of 1 nm. ASD is a full-range spectroradiometer and is computer-controlled (Danner et al., 2015). A portable PC is used to control the scans collected by the instrument and it also allows for the on-screen visualisation of the data collected in real-time. All analyses were done in a dark room to eliminate interference by stray light and diffusion radiation (Choe et al., 2008).

The ASD spectroradiometer was first allowed to warm up for at least 90 minutes before use. The dark current and radical was first collected and then optimisation was done before any data was collected. This process ensures the appropriate light settings are set for the source of light that is used to record the spectra (Salisbury, 1998). If the light source does not change

significantly, then re-optimisation is not necessary. However, if the measurements recorded reaches saturation, to decrease the saturation level of the detectors, optimisation is necessary (Janse et al., 2018). In order to acquire radiometric data in reflectance, a Spectralon plate or white reference panel was used as a standard reference (white reference) of the reflectance (Eitelwein et al., 2015), and these white reference measurements were recorded. The white reference is a calibration panel which gives a 100 % reflectance of incident illumination to calibrate the target reflectance (Hatchell, 1999; Eitelwein et al., 2015). When spectral measurements are recorded, it is recommended to take white reference readings every 10-15 minutes for better reflectance spectra (Janse et al., 2018). White reference measurements were recorded every 15 minutes to obtain spectral information.

Field of View (FOV) refers to the solid angle through which light incident on the target material enters the spectroradiometer (Mac Arthur et al., 2012). When collecting spectral measurements, it is important to set the FOV and other factors such as height, distance and angle from the target material (Mac Arthur et al., 2012; Janse et al., 2018). In most cases, however, the spectral signatures are captured using the nadir position. Spectral scanning involved the use of a 1.5 nm or 25° field of view bare fibre optic placed at a specific height from the sample. This was done to ensure that spectra outside the petri dish was not captured by the sensor (Monaledi, 2019). The FOV was calculated using the following formulae:

$$r = \tan\left(\frac{\alpha}{2}\right) \times H \qquad (1)$$

Where, r = radius of circular FOV with area A.

H = height of spectrometer held above the object surface.

α = angular FOV for spectrometer.

$$A = \pi r^2 \qquad (2)$$

Where, A = sampled area.

Spectral measurements were then recorded using ASD which records reflectance in the spectral range of 350-2500 nm (Kemper and Sommer, 2002). The spectral resolution of the ASD spectroradiometer is 3 nm @ 700 nm and 10 nm @ 1400/2100 nm with spectral intervals 1.4 nm @ 350-1050 nm and 2 nm @ 1000-2500 nm (ASD., 2000). The electrons inside the ASD generates an amount of electrical current that is always added to the incoming photons of light, this signal then generates false data known as dark current (DC) (Agrawal and Deshmukh,

2018). DC refers to the amount of electrical current inherent in the electrical components of the spectroradiometer (Janse et al., 2018). It is the systematic noise from the electronics and detectors of the instrument (Hatchell, 1999). DC reflects variations due to changes in temperature as well as time variations and is automatically collected during every optimisation (Janse et al., 2018). It is stored and applied for every spectral measurement, however, in order to acquire accurate data, the DC at each channel should be subtracted from the total DC for that channel (Janse et al., 2018). The ASD FieldSpec spectroradiometer software automatically recorded and subtracted the DC from the spectral measurements which ensured accurate data was recorded (Hatchell, 1999).

The reflectance measurements can be affected by atmospheric factors such as scattering of atmospheric gases and particles (Salisbury, 1998; Janse et al., 2018). Light energy gets refracted by these small particles and if any of these conditions are present during spectral measurements, they should be recorded in the spectral metadata (Janse et al., 2018). This is done so that any loss in the signal identified during post-processing can be attributed to these factors and the measurement can be excluded. All reflectance values were plotted graphically and the noisy spectral regions were excluded.

In the laboratory, the sediment samples were first air-dried and sieved using a 2 mm mesh sieve to obtain fine particles. Thereafter, each water and sediment sample were poured into a circular petri dish with a diameter of 9 cm and placed on a black surface to avoid background interference in the reflectance. The Field of view (FOV) for the water and sediment samples were calculated as follows:

$r = \tan(\frac{\alpha}{2}) \times H$

$4.5 = \tan(\frac{25}{2}) \times H$

$H = \frac{4.5}{\tan(\frac{25}{2})}$

$= 20.3$ cm

$A = \pi r^2$

$= \pi(4.5)^2$

$= 63.62$ cm^2

The ASD spectroradiometer was warmed up for 90 minutes before use and a quartz-halogen lamp was warmed up for 30 minutes before use. Thereafter, once the instrument was warmed up, DC and radical measurements were recorded and then optimisation was done before a bare fibre optic cable was used to record the spectral reflectance of each sample. The bare optical fibre cable was placed 20.3 cm from the sample and a quartz-halogen lamp was used as a source of illumination. The lamp was placed on a tripod at a 50 cm height from the surface to reduce interference fringes at a zenith angle of 45 degrees from the surface and at a horizontal distance of 50 cm. The position of the tripod was fixed to ensure a constant illumination distance and angle orientation so that the flux density was the same. Ten measurements were taken for each sample and averaged.

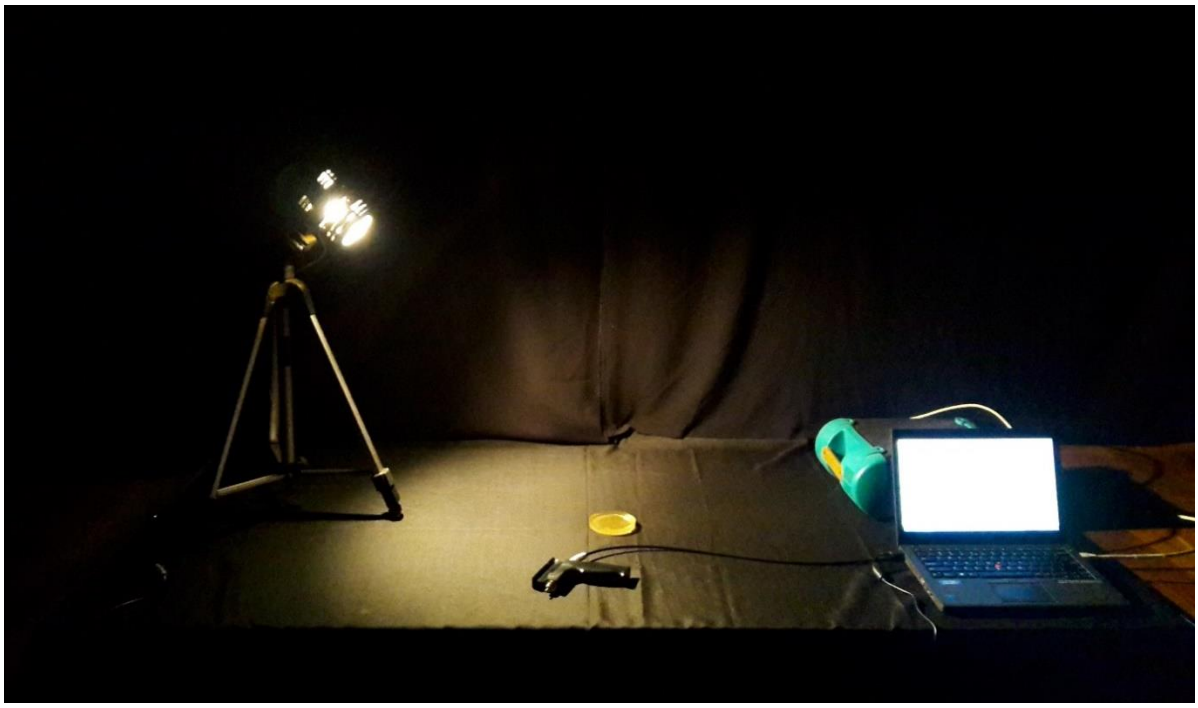

Figure 4.3: ASD laboratory set up for the collection of spectral measurements of the water samples.

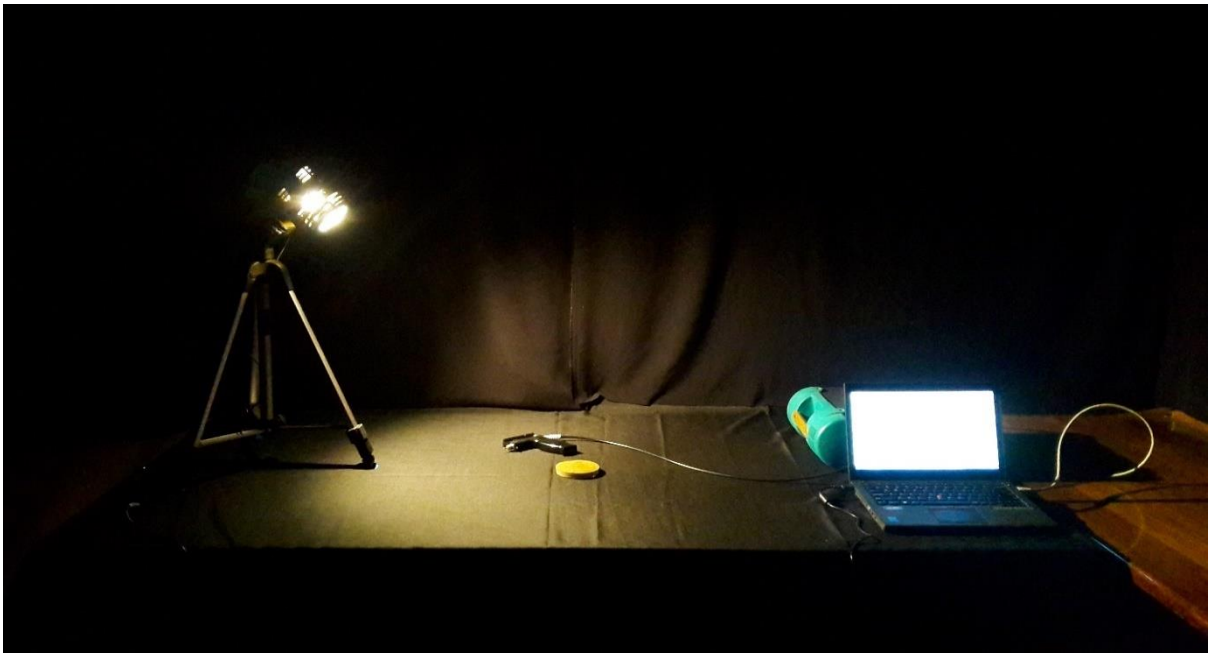

Figure 4.4: ASD laboratory set up for the collection of spectral measurements of the sediment samples.

4.3) Data analysis

Data analysis of the water and sediment data involved the pre-processing of the spectral reflectance data of the water and sediment samples obtained from the ASD spectroradiometer, descriptive statistics of the laboratory measured water and sediment data to describe the characteristics of the data and statistical analyses of the water and sediment data performed to identify outliers, build calibration models and assess the prediction accuracies of the models using cross-validation.

4.3.1) Data pre-processing

4.3.1.1) Water data

The spectral reflectance data and the laboratory measured data of the 15 water samples were imported into the Unscrambler®X 10.4 software. The spectral reflectance data were first plotted graphically to identify noisy spectral regions. The 350-549 nm, 951-1129 nm and beyond 1800 nm spectral regions were removed prior to further analyses as these regions were noisy and could cause a deterioration in the quality of the results. In data pre-processing, when the spectral plots are recorded a slope in the spectra may occur and to reduce these effects Savitzky-Golay first and second derivative transformations can be performed (ASD., 2000).

The Savitzky-Golay technique of derivative transformations rely on a least-squares fit of a polynomial through the data points (Mark and Workman, 2010).

According to Aggarwal (2004), the spectral reflectance of surface features is equivalent to the proportion of reflected energy to incident energy as a function of wavelength. If we let the spectral reflectance x_i be a function of wavelength λ, the spectral reflectance can be given by:

$$X_i(\lambda) = [E_R(\lambda) / E_I(\lambda)] \times 100 \quad (3)$$

Where,

$X_i(\lambda)$ = Spectral reflectance at a specific wavelength

$E_R(\lambda)$ = Energy of wavelength reflected from object

$E_I(\lambda)$ = Energy of wavelength incident on the object

The derivative of the function can be given by:

Zero order:

$$x_i = f(\lambda) \quad (4)$$

First order:

$$\frac{d(xi)}{d\lambda} = f'(\lambda) \quad (5)$$

Second order:

$$\frac{d^2(xi)}{d\lambda^2} = f''(\lambda) \quad (6)$$

According to Hatchell (1999), depending on the data, more noise can be introduced to the spectra with each derivative transformation done. The use of the Savitzky-Golay second derivative resulted in more noise being added to the data; therefore, the Savitzky-Golay first derivative using a 1st order polynomial with 43 smoothing points was used. A first order derivative is equivalent to the rate of change of reflectance with respect to wavelength (Owen, 1995). The first derivative is effective in smoothing the data, enhancing spectral features and

removing baseline effects from the scattering of light (do Nascimento et al., 2017; González-Fernández et al., 2019).

4.3.1.2) Sediment data

The concentrations of laboratory measured sediment data were provided in mg/kg for most heavy metals, however, the concentrations of aluminium, iron and magnesium were provided in percentage mass (%m/m). In order to work with uniform units and to facilitate the comparability between the heavy metals, the mass percentages of aluminium, iron and magnesium were converted into mg/kg. According to Strawn et al. (2015), one percent by mass is equal to 10000 mg/kg and can be given by:

$$1\%\ x\ \frac{10000\ mg/kg}{\%} = 10000\ mg/kg \qquad (7)$$

The spectral reflectance data and the laboratory measured data of the 15 sediment samples were imported into the Unscrambler®X 10.4 software. The spectral reflectance data were first plotted graphically to identify noisy spectral regions. The 350-599 nm, 861-1069 nm and beyond 1760 nm spectral regions were removed prior to further analyses as these regions were extremely noisy. Thereafter, the Savitzky-Golay smoothing pre-processing treatment with 25 smoothing points and a zero-order polynomial was used. The Savitzky-Golay smoothing filter is also known as the least squares digital polynomial smoothing filter and is the most commonly used smoothing filter in spectroscopy (Bromba and Ziegler, 1981). Savitzky and Golay demonstrated in their research that least squares smoothing filters are efficient in reducing spectral noise while preserving the shape and height of spectral peaks (Schafer, 2011). According to Press and Teukolsky (1990), these filters make spectral lines in noisy spectral data smooth and more visible without a loss of resolution. The Savitzky-Golay smoothing filter is thus a useful pre-processing technique that can be used in spectroscopic analyses as it minimises noise and smooths out the spectra without altering the shape of the spectra (Člupek et al., 2007).

According to Schafer (2011), in the Savitzky-Golay smoothing filter technique, if we let a window of N = 2M + 1 samples be centred at n = 0, where M denotes the half width of the calculation interval, the polynomial coefficients can be given by:

$$p(n) = \sum_{k=0}^{N} a_k n^k \qquad (8)$$

To reduce the mean-squared calculation error for 2M + 1 samples centred at n = 0:

$$\varepsilon_N = \sum_{n=-M}^{M}(p(n) - x[n])^2 = \sum_{n=-M}^{M}(\sum_{k=0}^{N} a_k n^k - x[n])^2 \quad (9)$$

According to Krishnan and Seelamantula (2012), once the polynomial is fitted, the smoothed output value, y [0], can be computed at the central index 0, resulting in the zeroth polynomial coefficient:

$$y[0] = p(0) = a_0 \quad (10)$$

The output value at the next sample is calculated by shifting the interval to the right by one sample so that the origin becomes the middle sample of the new set of 2M + 1 samples (Schafer, 2011). This process is known as data centring as the polynomial fitting is repeated at the central location and this can be done for each input sample resulting in a new polynomial and a new output sequence, y[n]. (Schafer, 2011).

According to Savitzky and Golay (1964), the new output value at each position is equivalent to a linear combination of the set of input samples. To determine if the least squares polynomial smoothing for all shifts of the 2M + 1 sample interval is equal to filtering with a finite impulse response, the optimal coefficients of equation (8) must be calculated by differentiating equation (9) with respect to each of the N + 1 unknown coefficients and equating the derivative to zero (Krishnan and Seelamantula, 2012).

For i = 0, 1,…, N,

$$\frac{d\,\varepsilon_N}{d\,a_i} = \sum_{n=-M}^{M} 2n^i(\sum_{k=0}^{N} a_k n^k - x[n]) = 0 \quad (11)$$

According to Schafer (2011), the set of N + 1 equations in N + 1 unknowns can be obtained by interchanging the order of (10) and can be given by:

$$\sum_{k=0}^{N}(\sum_{n=-M}^{M} n^{i+k})a_k = \sum_{n=-M}^{M} n^i x[n] \quad i = 0,1,\dots,N. \quad (12)$$

In order to obtain optimal smoothing results, it is important to ensure that N ≤ 2M, that is, there needs to be as many data samples as there are coefficients in the polynomial calculation.

4.3.2) Descriptive statistics of the water and sediment data

The laboratory measured water and sediment data were analysed for descriptive statistics in Microsoft Excel to summarise the data and describe the characteristics of the data. The minimum and maximum variables, mean and standard deviations were assessed for both the water and sediment data.

4.3.3) Statistical analyses of the water and sediment data

4.3.3.1) Correlation analyses of the water data

The laboratory measured water quality data were imported into IBM SPSS 27 software and analysed for correlation analyses. Prior to running the correlation analysis, the data was first checked to ensure it did not violate the assumptions of the correlation statistical test. For example, if the data are normally distributed a Pearson correlation may be used as this correlation analysis assumes normality in the data (Schober et al., 2018). However, one of the assumptions of the Pearson correlation is violated in the case of datasets that do not follow a normal distribution (Schober et al., 2018). Therefore, the Pearson correlation cannot be used to determine correlations between these variables and to resolve this, a transformation can be done on the dataset to make the data follow a normal distribution. However, if the transformation still does not result in a normal distribution, a nonparametric test that does not assume normality in the datasets should be used. The one-sample Kolmogorov-Smirnov test is generally used to determine if a given set of data follows a particular distribution such as a normal distribution (Singh et al., 2013).

A one-sample Kolmogorov-Smirnov test was first conducted to test for normality in the datasets. The laboratory measured water quality data did not follow a normal distribution; therefore, a log transformation was performed in SPSS to try and make the data follow a normal distribution. However, the transformation still resulted in a non-normal distribution; therefore, a nonparametric test was used. A Spearman rank correlation also known as Spearman's Rho analysis was undertaken to assess the relationships between each heavy metal detected in the water and pH, electrical conductivity and dissolved oxygen. The Spearman rank correlation is the nonparametric statistic alternative to the Pearson correlation and it does not assume normality in the data (Schober et al., 2018). This type of correlation analysis uses the ranked values of the variables instead of the raw data itself and assumes monotonic relationships which can be robust against outliers (Schober et al., 2018). A monotonic relationship is one where

either one variable increases and the other variable also increases or one variable increases and the other variable decreases (Ramzai, 2020). This is similar to the Pearson correlation, however, in monotonic relationships the rates of increase or decrease are not always constant as in the case of linear relationships (Ramzai, 2020).

In order to run the Spearman rank correlation, the original data for the 15 samples were first converted into ordered ranks where 1 represented the lowest concentration and 15 represented the highest concentration. This process was done in SPSS using the rank cases function. The Spearman correlation coefficient ($r_{s)}$ values range from -1 to +1, where positive values indicate positive monotonic correlations, negative values indicate negative monotonic correlations and a value of zero indicates no monotonic correlation. According to Evans (1996), the strength of the correlation between two variables can be described by the following ranges, absolute r values between 0.00-0.19 are regarded as very weak, 0.20-0.39 as weak, 0.40-0.59 as moderate, 0.60-0.79 as strong and absolute r values between 0.80-1.00 are regarded as very strong.

4.3.3.2) Principal components analysis

Outliers occur as a result of spectral measurement errors as well as instrument errors and if these are present in the data they should be removed (Hatchell, 1999). A principal components analysis (PCA) was performed on the first derivative pre-processed spectra of the water data and the Savitzky-Golay smoothing pre-processed spectra of the sediment data using the Unscrambler®X software in order to identify outliers in the dataset. PCA refers to the statistical technique that is used to minimise the dimensionality of large datasets. It reduces the number of variables of a large dataset of correlated variables, while retaining most of the important information (Jolliffe and Cadima, 2016). The PCA produces principal components which are new uncorrelated variables that contain most of the variation from the initial variables retained in the first few components (Jolliffe and Cadima, 2016). The new variables are generated as weighted averages of the initial variables. The PCA equation in matrix notation is given by:

$$Y = W'X \qquad (13)$$

Where W is a matrix of coefficients generated by the PCA.

The first principal component (PC1) is computed so that it accounts for the largest variance possible in the data. Let principal components = Y and variables = X, PC1 (Y_1) is given by the linear combination of variables X_1, $X_{2,..}$,X_p and is mathematically expressed as:

$$Y_1 = a_{11} X_1 + a_{12} X_2 + \ldots a_{1p} X_p \quad (14)$$

The second principal component (PC2) is similarly computed, it is uncorrelated with PC1 and it accounts for the second highest variance in the data. The mathematic equation for PC2 is given by:

$$Y_2 = a_{21} X_1 + a_{22} X_2 + a_{2p} X_p \quad (15)$$

This procedure continues until p principal components are calculated, where the number of PCs equals the initial number of variables. The data is initially mean-centred to ensure that the data is centred around the origin of the principal components (Dunn, 2021). The data points that are positioned close to the origin of the PCA scores plot indicate the data points that are closer to the mean and those found further away are potential outliers (Dunn, 2021). PCA is thus, effective in detecting outliers in the data and any outliers detected by the PCA was removed prior to further analyses.

4.3.3.3) Partial least squares regression analysis

Building a calibration model is one of the most important steps in the prediction of analytes of interest from reflectance spectra and involves calculating a regression equation based on the spectra recorded and the known analyte information, such as heavy metals (ASD., 2000). This model can then be used to predict future unknown parameters. The partial least squares (PLS) regression method was used to build a calibration model to predict heavy metal concentrations in the water and sediment from visible near-infrared (VNIR) spectra using laboratory measured concentrations as a reference. The PLS regression for the water data was built using 14 samples as the outlier sample detected by the PCA was removed. The PLS regression for the sediment data was built using all 15 samples as the PCA did not detect any outliers in the sediment data. PLS regression is a multivariate regression technique and works efficiently in regression cases where there are multiple correlated predictor variables and a small sample size (Abdi, 2003; Mevik and Wehrens, 2020).

The aim of a PLS regression is to model a linear relationship between predictor (X) and response (Y) variables and to predict Y from X (Abdi, 2003). PLS regression operates by creating uncorrelated latent variables using the present correlations between predictor and response variables while retaining most of the variance of the predictor variables (Rosipal and Trejo, 2001). These latent variables are linear combinations of the initial predictor variables and the weights used to calculate these linear combinations are equivalent to the covariance

among predictor and response variables (Rosipal and Trejo, 2001). Thereafter, a least squares regression is calculated on the subset of the extracted latent variables.

According to Pirouz (2006), simplified mathematical equations underlying a PLSR can be given by:

$$N = W'Y \quad (16)$$

$$Y = PN + E \quad (17)$$

$$\text{Substituting } Y = PW'Y + E = PW'Y + (I-PW')\,Y \quad (18)$$

Where, N represents a PC, Y represents the observed scores, W represents the composing weights, P represents the PC loadings and E represents the residual variance.

The matrix is based on singular value decomposition (SVD) which is the factorisation of a complex matrix that does not necessitate matrix inversions and is given by:

$$R = W'DP \quad (19)$$

Where, W represents an orthogonal matrix with left singular vectors, W′ represents I which is the identity matrix, P represents an orthogonal matrix with right singular vectors, and D represents a diagonal matrix of singular vectors. An eigenvalue represents how much variance there is in the data in a particular direction. If D represents a diagonal of eigenvalues, then the rows in the P matrix represents the PC loadings and the columns in the W′D matrix represents the PC scores (Pirouz, 2006).

4.3.3.4) Accuracy assessment

Once the calibration model is built, the validity of the model should be tested. The leave-one-out (LOO) cross-validation method also known as a full cross-validation was used to test the validity of the calibration models for both the water and sediment data as the sample size for both datasets were small and the LOO cross-validation method is suitable for small datasets (Hatchell, 1999). This cross-validation method uses the same dataset for both calibration and validation (Estifanos, 2006). In the LOO cross-validation method, one sample is left out and the rest of the samples are used to build the calibration model (Campbell and Wynne, 2011). This PLS regression model can then be used to predict the one sample that was left out, which is advantageous as it allows for the model to be tested independently (Hatchell, 1999). This procedure continues by leaving out other samples and predicting them and is repeated until

every sample is excluded once and then included in the next round (Estifanos, 2006). The accuracies of the models were evaluated using the coefficient of determination (R^2) and the root mean square error (RMSE) for both the calibration and cross-validation.

According to Renaud and Victoria-Feser (2010), R^2 represents the percentage of variance of the dependent variable that is explained by its linear relationship with the independent variable and is given by:

$$R^2 = \frac{ESS}{TSS} = 1 - \frac{RSS}{TSS} \tag{20}$$

Where, ESS represents the explained sum of squares, TSS represents the total sum of squares and RSS represents the residual sum of squares.

The RMSE is a standard system of measurement that is often used to evaluate how well a regression model performs (Chai and Draxler, 2014). It measures the error of a regression model in predicting the response variables and assumes unbiased and normally distributed errors (Chai and Draxler, 2014). Mathematically, the RMSE is given by:

$$RMSE = \sqrt{\sum_{i=1}^{n} \frac{(\hat{y}_i - y_i)^2}{n}} \tag{21}$$

Where, $\hat{y}_i$ represents the predicted values, y_i represents the measured values and n represents the number of observations.

According to Todorova et al. (2014), an accurate PLS regression model is one that has high R^2 values and low RMSE values and would indicate that the model performed well in predicting the response variables. According to Henseler et al. (2009), R^2 values less than 0.19 for a prediction model is considered as very low accuracies, R^2 values between 0.19 and 0.33 are considered low accuracies, R^2 values between 0.33 and 0.67 are considered as moderate accuracies and R^2 values greater than 0.67 are considered as high predictive accuracies. In addition, according to Veerasamy et al. (2011), the difference between the calibration and cross-validation R^2 values should not be more than 0.3 as differences greater than 0.3 would indicate a poor predictive model, leading to less reliable results.

CHAPTER 5: RESULTS

5.1) Introduction

This chapter provides the results obtained from the data analyses undertaken in this study. It includes the descriptive statistics of the laboratory-measured water and sediment data. It also includes the statistical analyses performed on the laboratory-measured water and sediment data and spectral reflectance measurements of the water and sediment data including correlation analyses, principal components analyses and partial least squares regression analyses. The results are presented in the form of tables and graphs.

5.2) Descriptive statistics

5.2.1) Water data

5.2.1.1) Sample statistics of the laboratory-measured water quality parameters

In table 5.1, it can be seen that the levels of pH, electrical conductivity, dissolved oxygen, arsenic, cadmium, iron and magnesium ranged from 7.36-7.86, 4.1960-1744.34 µS/cm, 5.22-7.53 mg/L, 0-0.0193 mg/L, 0-0.0017 mg/L, 0-0.0186 mg/L and 28.9-167 mg/L, respectively. Cadmium recorded the lowest concentration in the water column in comparison to the other heavy metals with a mean concentration of 0.0007 mg/L. Magnesium recorded the highest concentrations within the water column with a mean concentration of 53.01 mg/L compared to arsenic, cadmium and iron. The pH concentrations recorded for the uMgeni Estuary was slightly alkaline with a mean concentration of 7.57. Electrical conductivity recorded the highest maximum concentration with a concentration of 1744.34 µS/cm. Electrical conductivity also displayed the highest mean concentration of 661.61 µS/cm. The coefficient of variation (CV) results indicated the variation in the data were relatively low for pH, electrical conductivity, dissolved oxygen, and arsenic with CV values <1. Therefore, indicating the data does not deviate much from the mean. However, the CV values were high for cadmium, iron and magnesium with CV values closer to 1, indicating greater variation in the data in comparison to the other water quality parameters.

Table 5.1: Descriptive statistics of the laboratory-measured water quality parameters.

Parameters	N	Minimum	Maximum	Mean	Standard Deviation	CV
pH	15	7.36	7.86	7.57	0.16	0.02
Electrical conductivity (µS/cm)	15	4.1960	1744.34	661.61	398.51	0.6
Dissolved oxygen (mg/L)	15	5.22	7.53	6.7	0.54	0.08
Arsenic (mg/L)	15	0	0.0193	0.0092	0.0055	0.6
Cadmium (mg/L)	15	0	0.0017	0.0007	0.0007	1
Iron (mg/L)	15	0	0.0186	0.005	0.0049	1
Magnesium (mg/L)	15	28.9	167	53.01	47.22	0.9

5.2.1.2) Mean pH concentrations

The pH levels for site A, B and C of the study area were all within the neutral range of pH. In Figure 5.1, it can be seen that there was a decline in the mean pH levels from site A which is located more upstream of the river, to site C which is located at the mouth. Site A recorded higher levels of pH overall in comparison to sites B and C. The mean pH levels for sites A, B and C were ~7.78, ~7.47 and ~7.46, respectively.

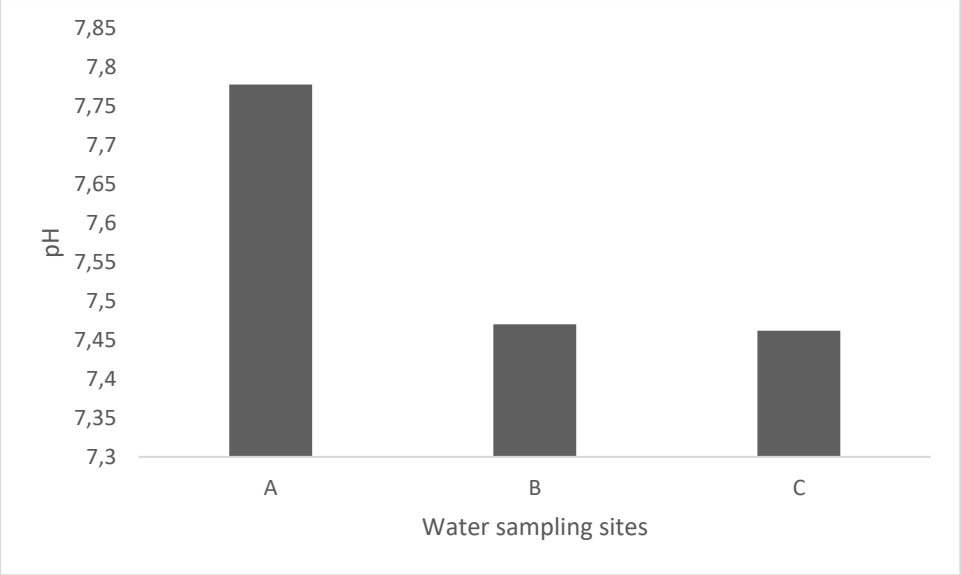

Figure 5.1: Showing the mean pH levels at each water sampling site of the uMgeni Estuary.

5.2.1.3) Mean electrical conductivity concentrations

In Figure 5.2, it can be seen that the electrical conductivity levels for the uMgeni Estuary generally increased from sites A to C. Site C recorded higher electrical conductivity levels overall in comparison to sites A and B. The mean electrical conductivity levels for site A, B and C were ~603.10 µS/cm, ~674.01 µS/cm and ~707.72 µS/cm, respectively.

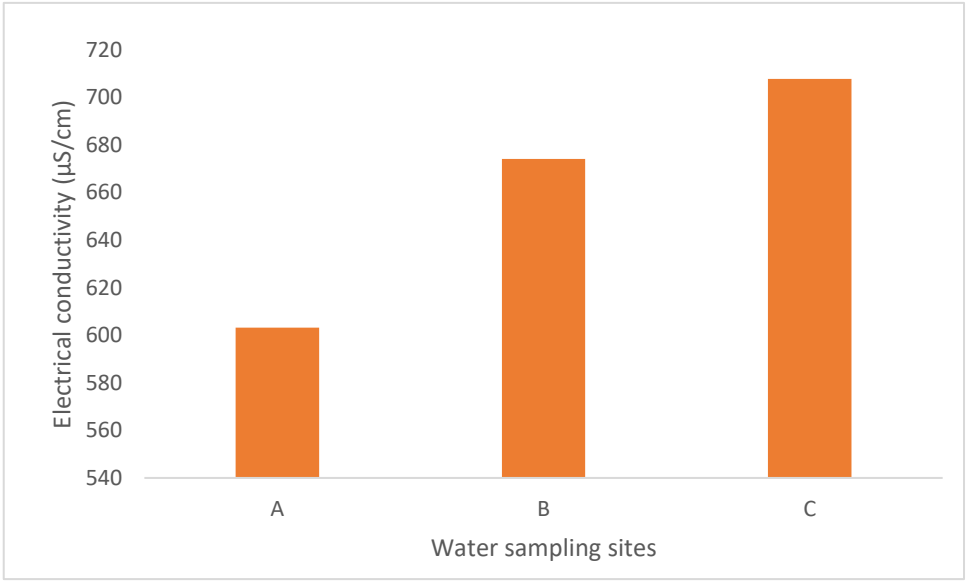

Figure 5.2: Showing the mean electrical conductivity levels (µS/cm) at each water sampling site of the uMgeni Estuary.

5.2.1.4) Mean dissolved oxygen concentrations

In Figure 5.3 below, it can be seen that site C recorded the lowest overall dissolved oxygen levels in comparison to sites A and B. The dissolved oxygen levels for sites A and B were similar with site B recording slightly higher dissolved oxygen levels overall in comparison to site A. The mean dissolved oxygen levels for sites A, B and C were ~6.87 mg/L, ~6.9 mg/L and ~6.34 mg/L, respectively.

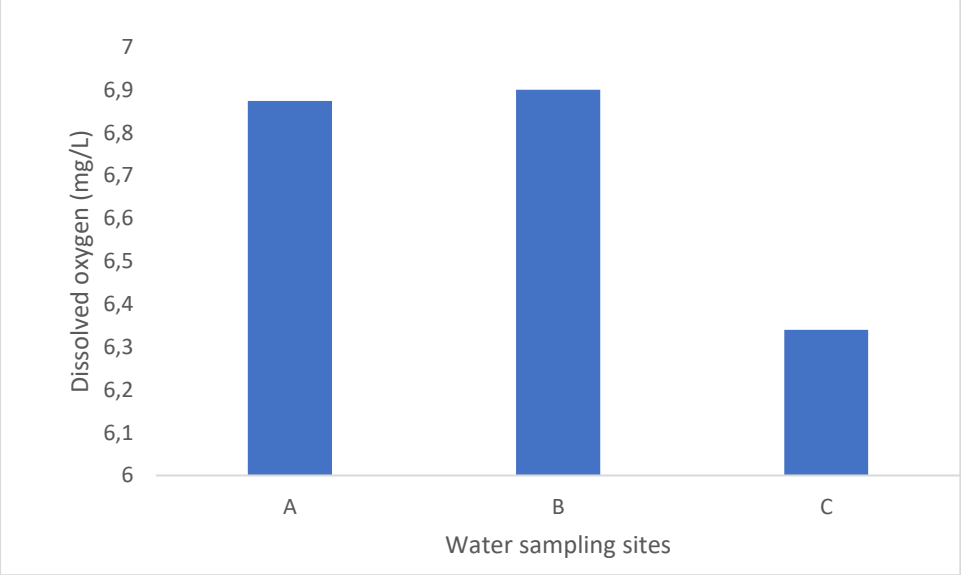

Figure 5.3: Showing the mean dissolved oxygen levels (mg/L) at each water sampling site of the uMgeni Estuary.

5.2.1.5) Mean arsenic concentrations

In Figure 5.4, it can be seen that the arsenic concentrations in the water column of the uMgeni Estuary fluctuated from site A to site C. Site B recorded lower arsenic concentrations in comparison to sites A and C with site C recording higher arsenic concentrations overall. The mean arsenic concentrations for sites A, B and C were ~0.00903 mg/L, ~0.00661 mg/L and ~0.01185 mg/L, respectively.

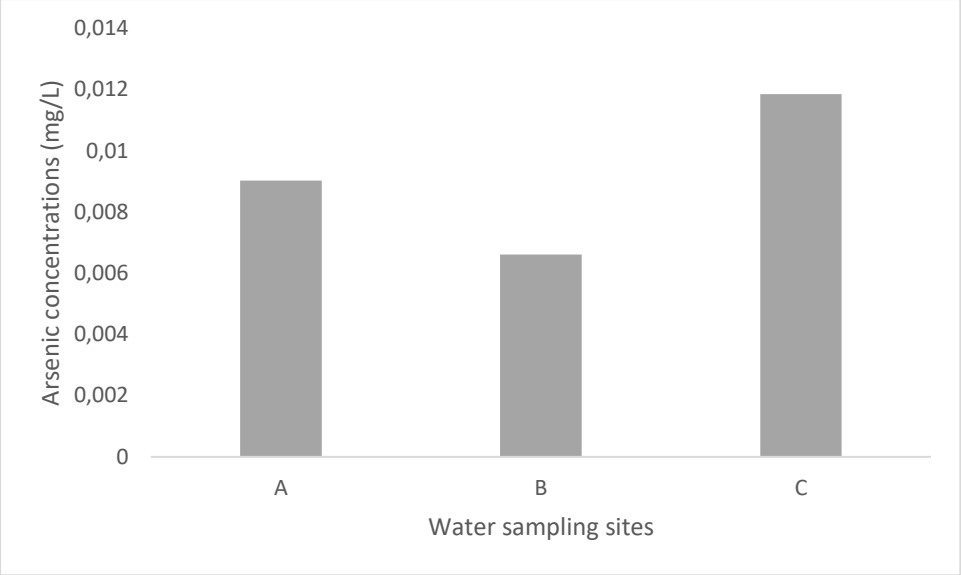

Figure 5.4: Showing the mean concentrations of arsenic (mg/L) at each water sampling site of the uMgeni Estuary.

5.2.1.6) Mean cadmium concentrations

In Figure 5.5, it can be seen that site B recorded higher cadmium concentrations overall in comparison to sites A and C. Sites A and C recorded similar cadmium concentrations with site C recording slightly lower cadmium concentrations than site A. The mean cadmium concentrations for sites A, B and C were ~0.00064 mg/L, ~0.00093 mg/L and ~0.00063 mg/L, respectively.

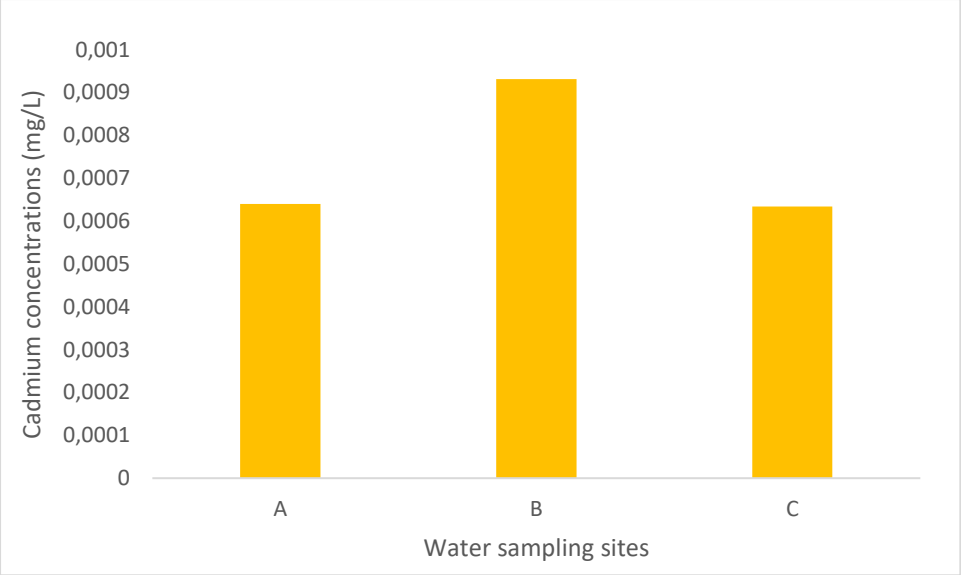

Figure 5.5: Showing the mean concentrations of cadmium (mg/L) at each water sampling site of the uMgeni Estuary.

5.2.1.7) Mean iron concentrations

In Figure 5.6, it can be seen that site B recorded higher iron concentrations overall in comparison to sites A and C. Sites A and C recorded similar iron concentrations with site C recording higher iron concentrations than site A. The mean iron concentrations for sites A, B and C were ~0.0042 mg/L, ~0.0059 mg/L and ~0.0049 mg/L, respectively.

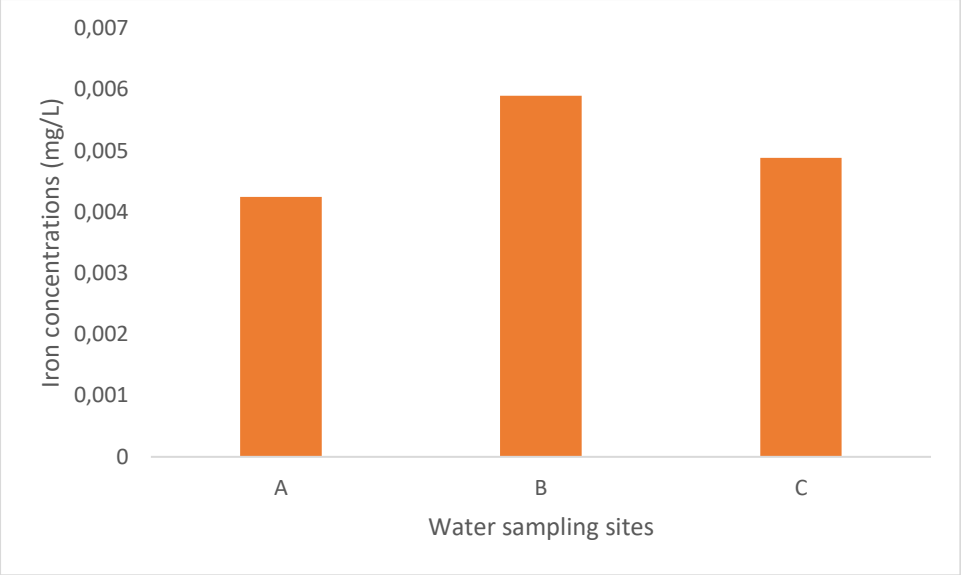

Figure 5.6: Showing the mean concentrations of iron (mg/L) at each water sampling site of the uMgeni Estuary.

5.2.1.8) Mean magnesium concentrations

In Figure 5.7, it can be seen that the magnesium concentrations for the uMgeni Estuary generally increased from sites A to C. Site C recorded higher magnesium concentrations overall in comparison to sites A and B. The magnesium concentrations were similar for sites A and B with site B recording higher magnesium concentrations than site A. The mean magnesium concentrations for sites A, B and C were ~30.02 mg/L, ~32.48 mg/L and ~96.52 mg/L, respectively.

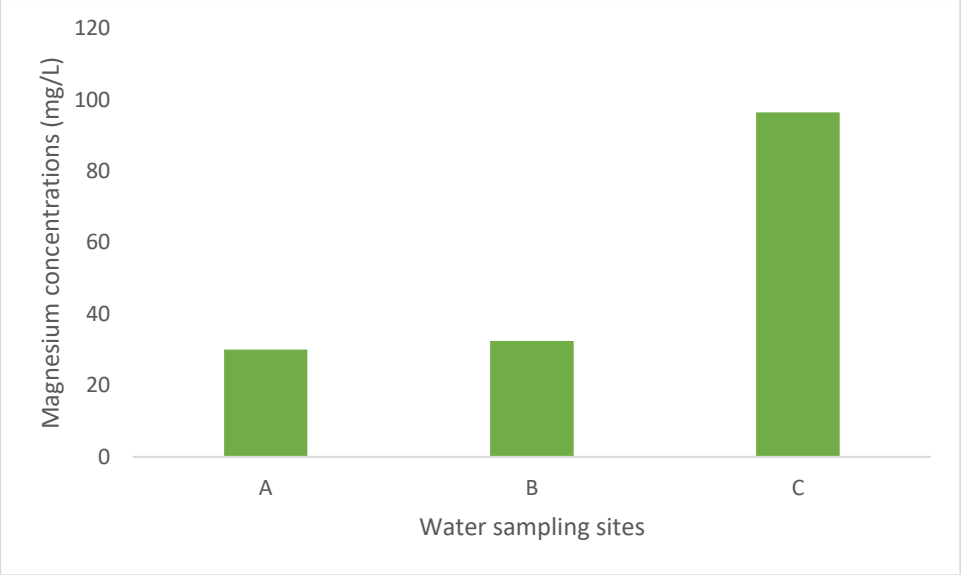

Figure 5.7: Showing the mean concentrations of magnesium (mg/L) at each water sampling site of the uMgeni Estuary.

5.2.2) Sediment data

5.2.2.1) Sample statistics of the laboratory-measured heavy metal concentrations in the sediment

In table 5.2, it can be seen that the heavy metal concentrations in the sediments ranged from 0-3.4 mg/kg, 1600-28600 mg/kg, 400-3400 mg/kg, 200-2700 mg/kg, 6.5-65 mg/kg, 2.1-53 mg/kg, 2.2-40 mg/kg, 1.8-32 mg/kg and 29-232 mg/kg for arsenic, iron, magnesium, aluminium, chromium, copper, lead, nickel and zinc, respectively. The highest metal concentrations in the sediments were recorded for iron with a mean concentration of 17853.33 mg/kg followed by magnesium and aluminium with mean concentrations of 2306.67 mg/kg and 1740 mg/kg, respectively. The lowest metal concentrations in the sediments were recorded for arsenic with a mean concentration of 1.87 mg/kg. Cadmium concentrations in the sediment samples were the lowest overall as they were found to be below the detection limit and was excluded from the analyses. The CV values were low for all the heavy metals with values <1 indicating the data does not deviate much from the mean.

Table 5.2: Descriptive statistics of the laboratory-measured heavy metal concentrations in the sediment.

Heavy metal	N	Minimum	Maximum	Mean	Standard deviation	CV
Arsenic (mg/kg)	15	0	3.4	1.87	1.12	0.6
Iron (mg/kg)	15	1600	28600	17853.33	8571.20	0.5
Magnesium (mg/kg)	15	400	3400	2306.67	1021.53	0.4
Aluminium (mg/kg)	15	200	2700	1740	710.94	0.4
Chromium (mg/kg)	15	6.5	65	42.03	19.36	0.5
Copper (mg/kg)	15	2.1	53	34.23	17.23	0.5
Lead (mg/kg)	15	2.2	40	24.12	11.72	0.5
Nickel (mg/kg)	15	1.8	32	20.31	10.12	0.5
Zinc (mg/kg)	15	29	232	153	65.57	0.4

5.2.2.2) Mean arsenic concentrations

Arsenic had the lowest concentrations overall in the sediments of the uMgeni Estuary in comparison to the other heavy metals. In figure 5.8, it can be seen that the arsenic concentrations fluctuated from sites A to C with site C recording higher arsenic concentrations in comparison to sites A and B. The mean arsenic concentrations for sites A, B and C were ~1.64 mg/kg, ~1.1 mg/kg and ~2.88 mg/kg, respectively.

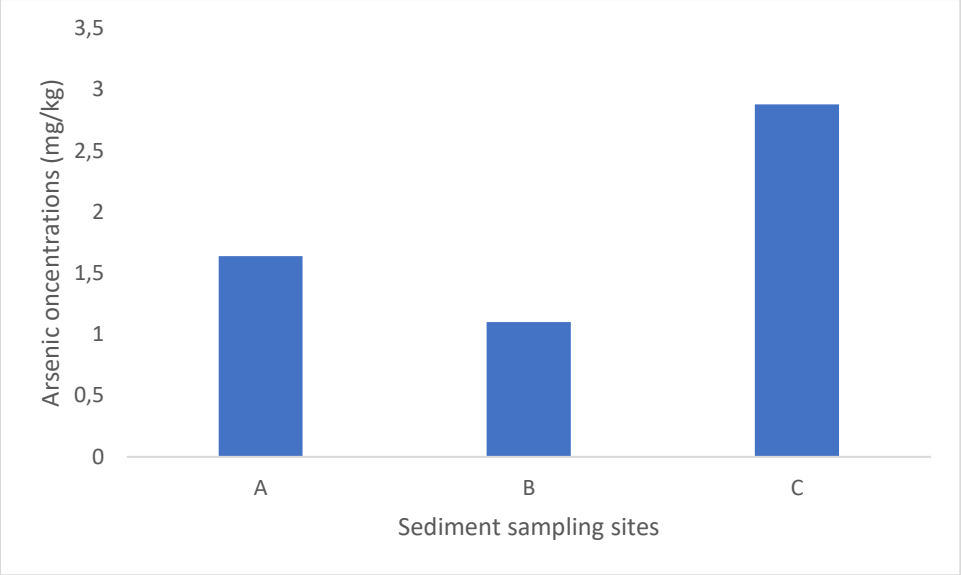

Figure 5.8: Showing the mean concentrations of arsenic (mg/kg) at each sediment sampling site of the uMgeni Estuary.

5.2.2.3) Mean iron concentrations

In figure 5.9, it can be seen that the iron concentrations in the sediments of the uMgeni Estuary were the highest in comparison to the other heavy metals. Site B recorded lower concentrations in comparison to sites A and C. Sites A and C had similar iron concentrations with site C recording higher iron concentrations than site A. The mean iron concentrations recorded at sites A, B and C were ~20700 mg/kg, ~11420 mg/kg and ~21440 mg/kg, respectively.

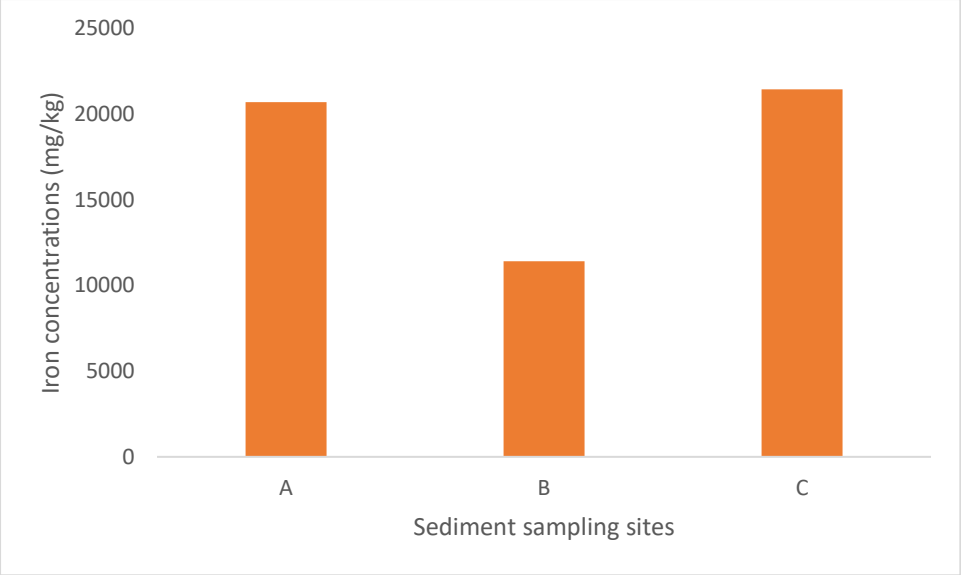

Figure 5.9: Showing the mean concentrations of iron (mg/kg) at each sediment sampling site of the uMgeni Estuary.

5.2.2.4) Mean magnesium concentrations

In figure 5.10, it can be seen that the magnesium concentrations were also relatively high in the sediments of the uMgeni Estuary in comparison to the other heavy metals. The magnesium concentrations fluctuated from sites A to C with site C recording higher magnesium concentrations in comparison to sites A and B. The mean magnesium concentrations recorded at sites A, B and C were ~2260 mg/kg, ~1480 mg/kg and ~3180 mg/kg, respectively.

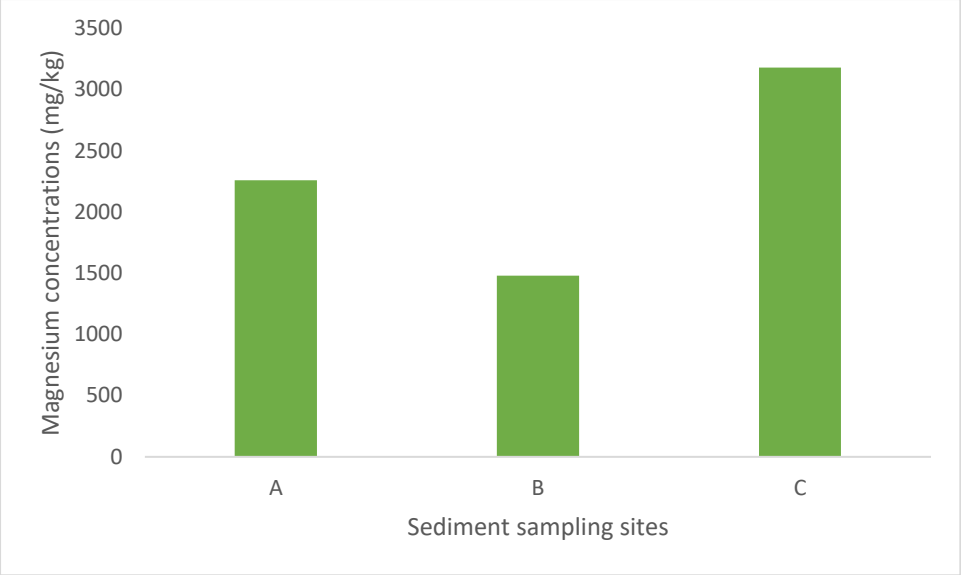

Figure 5.10: Showing the mean concentrations of magnesium (mg/kg) at each sediment sampling site of the uMgeni Estuary.

5.2.2.5) Mean aluminium concentrations

In figure 5.11, it can be seen that aluminium concentrations were relatively high for the uMgeni Estuary with site C recording higher aluminium concentrations in comparison to sites A and B. The mean aluminium concentrations for sites A, B and C were ~1680 mg/kg, ~1400 mg/kg and ~2140 mg/kg, respectively.

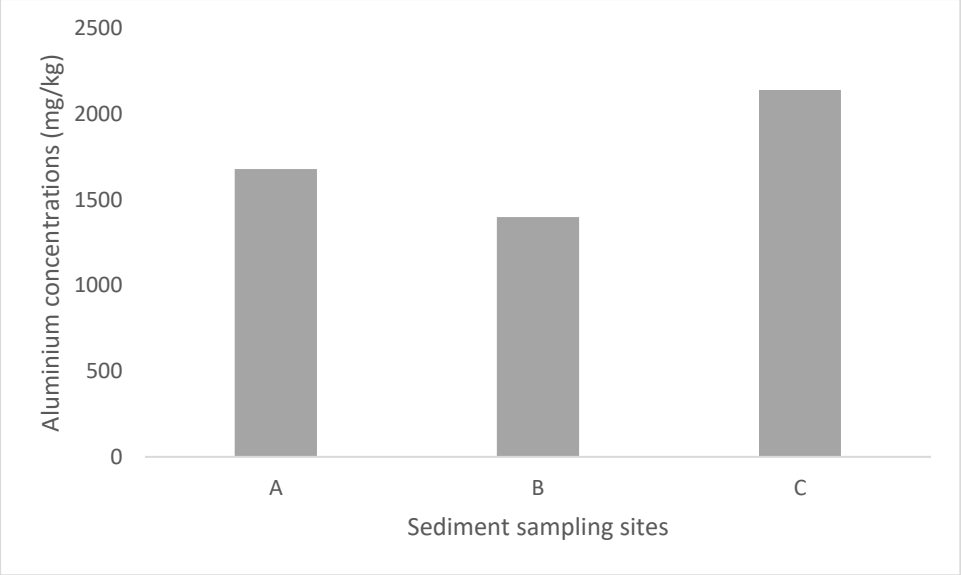

Figure 5.11: Showing the mean concentrations of aluminium (mg/kg) at each sediment sampling site of the uMgeni Estuary.

5.2.2.6) Mean chromium concentrations

In figure 5.12, it can be seen that the chromium concentrations fluctuated from sites A to C with site C recording higher chromium concentration overall in comparison to sites A and B. The mean chromium concentrations for sites A, B and C were ~43.2 mg/kg, ~27.5 mg/kg and ~55.4 mg/kg, respectively.

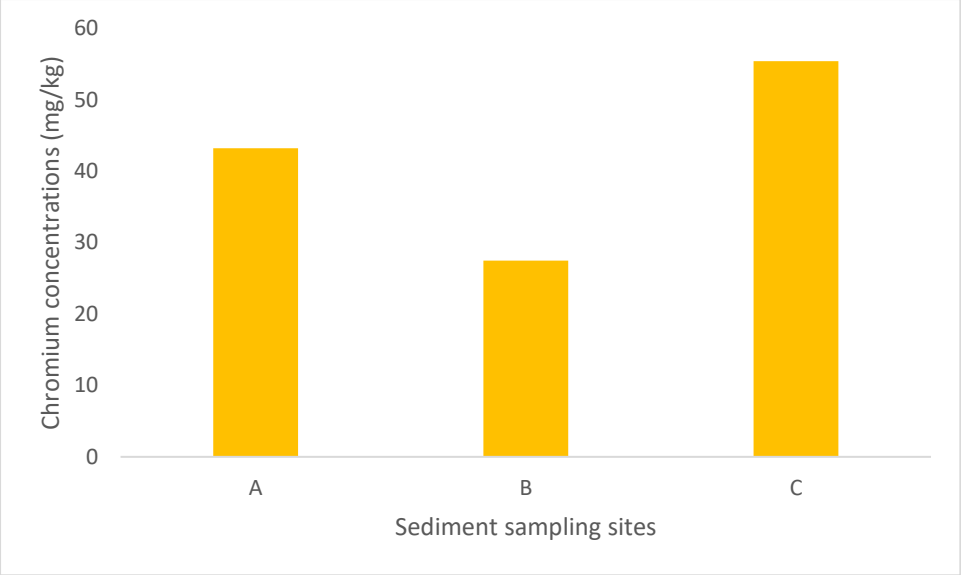

Figure 5.12: Showing the mean concentrations of chromium (mg/kg) at each sediment sampling site of the uMgeni Estuary.

5.2.2.7) Mean copper concentrations

In figure 5.13, it can be seen that the copper concentrations fluctuated from sites A to C with site C recording higher copper concentrations overall in comparison to sites A and B. The mean copper concentrations recorded at sites A, B and C were ~38 mg/kg, ~22.7 mg/kg and ~42 mg/kg, respectively.

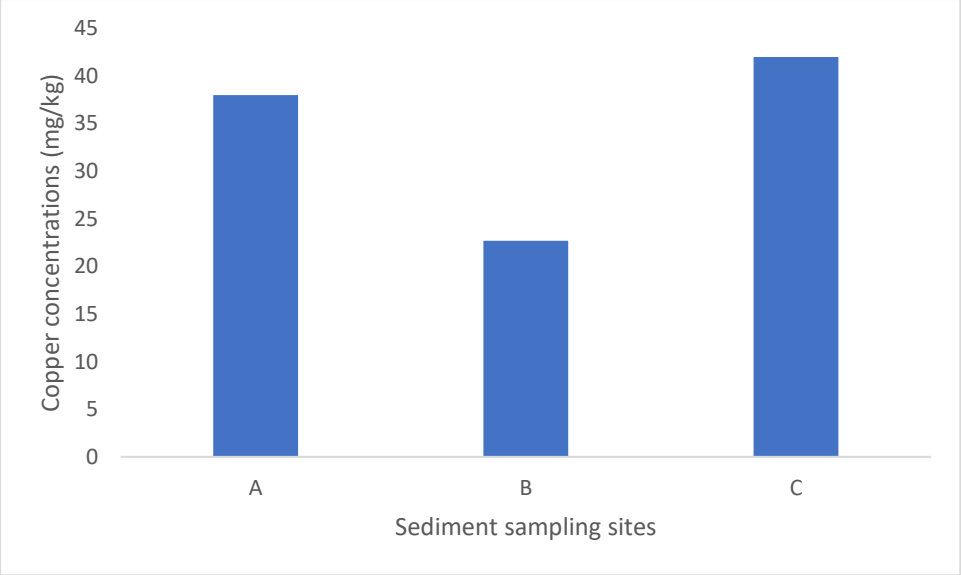

Figure 5.13: Showing the mean concentrations of copper (mg/kg) at each sediment sampling site of the uMgeni Estuary.

5.2.2.8) Mean lead concentrations

In figure 5.14 it can be seen that the lead concentrations fluctuated from sites A to C with site C recording higher copper concentrations overall in comparison to sites A and B. The mean lead concentrations recorded at sites A, B and C were ~25.4 mg/kg, ~14.76 mg/kg and ~32.2 mg/kg, respectively.

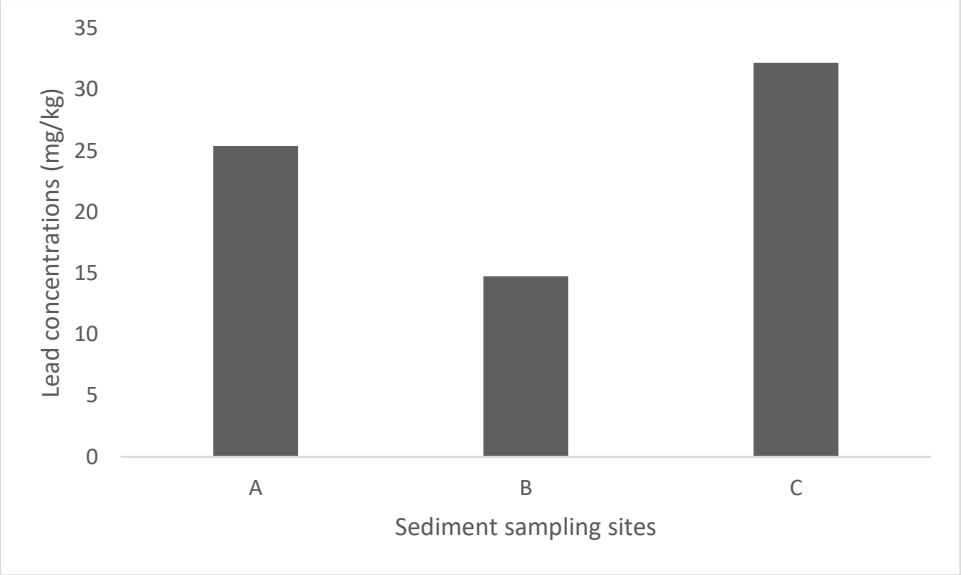

Figure 5.14: Showing the mean concentrations of lead (mg/kg) at each sediment sampling site of the uMgeni Estuary.

5.2.2.9) Mean nickel concentrations

In figure 5.15, it can be seen that the nickel concentrations fluctuated from sites A to C with site C recording higher nickel concentrations overall for the estuary in comparison to sites A and B. The mean nickel concentrations recorded at sites A, B and C were ~21.94 mg/kg, ~12.2 mg/kg and ~26.8 mg/kg, respectively.

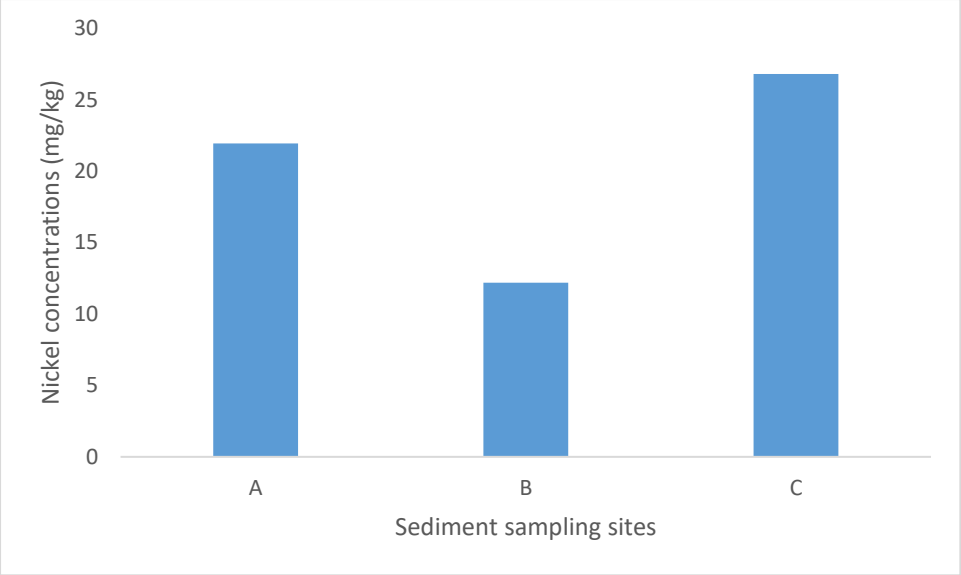

Figure 5.15: Showing the mean concentrations of nickel (mg/kg) at each sediment sampling site of the uMgeni Estuary.

5.2.2.10) Mean zinc concentrations

In figure 5.16, it can be seen that the zinc concentrations fluctuated from sites A to C with site C recording higher zinc concentrations in comparison to sites A and B. The mean zinc concentrations recorded at sites A, B and C were ~160.2 mg/kg, ~104.2 mg/kg and ~194.6 mg/kg, respectively.

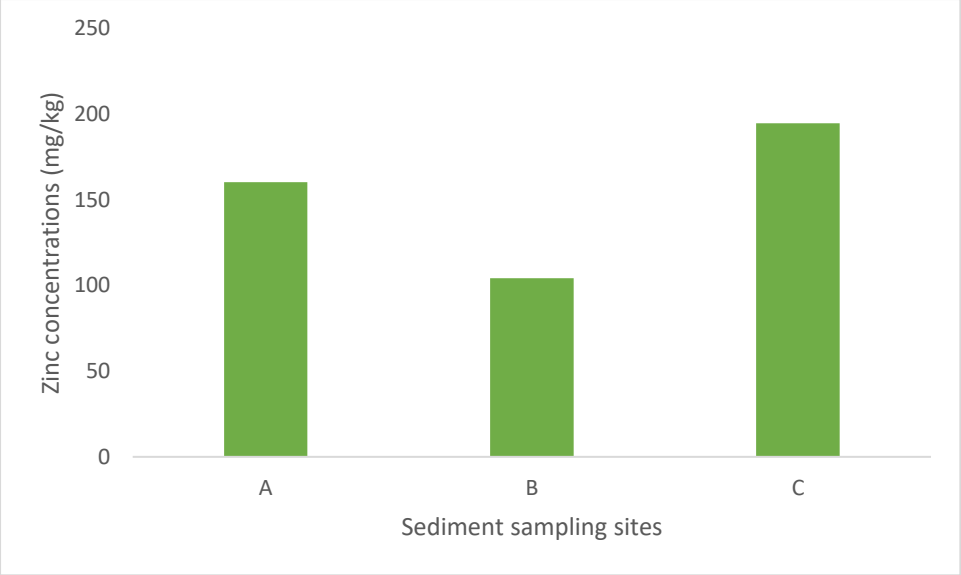

Figure 5.16: Showing the mean concentrations of zinc (mg/kg) at each sediment sampling site of the uMgeni Estuary.

5.2.3) Comparison between heavy metal concentrations in water and sediment

The descriptive statistic results observed in tables 5.1 and 5.2 indicate that more heavy metals were found in the sediment samples than the water samples. In addition, it can be seen from figures 5.4-5.16 that the metal concentrations in the water and sediment of the uMgeni Estuary were higher at site C near the river mouth compared to the sites further upstream, with the exception of iron concentrations in the water which displayed higher concentrations at site B. Furthermore, from figures 5.4-5.10 it can also be seen that the sediment samples contained significantly higher concentrations of arsenic, iron and magnesium heavy metals than the water samples.

5.3) Statistical analyses

5.3.1) Water data

5.3.1.1) Correlations between heavy metals and physicochemical parameters

The results of the one-sample Kolmogorov-Smirnov test indicated the data were not normally distributed, violating one of the Pearson correlation analysis assumptions. Therefore, Spearman rank correlation analyses were undertaken to determine the relationships between the concentrations of each metal and pH, electrical conductivity and dissolved oxygen

concentrations. Figures 5.17, 5.18, 5.19, and 5.20 depict scatterplots with cubic regression lines, which provided a better fit for the data than the linear function.

The Spearman rank correlation coefficient (r_s) values between arsenic concentrations and pH, electrical conductivity and dissolved oxygen were 0.100, 0.129 and -0.179, respectively with *p* values 0.723, 0.648 and 0.524, respectively. These results indicate weak positive correlations between arsenic concentrations and pH and electrical conductivity and a weak negative relationship between arsenic concentrations and dissolved oxygen. As pH and electrical conductivity increased, arsenic concentrations in the water slightly increased and as dissolved oxygen levels increased, arsenic concentrations in the water decreased. The *p* values for the correlation between arsenic concentrations and pH, electrical conductivity and dissolved oxygen were all greater than 0.05 indicating the results were not statistically significant. Figure 5.17 depicts the scatterplots with cubic regression lines of arsenic and pH, electrical conductivity and dissolved oxygen. The cubic R^2 values were 0.126, 0.028 and 0.211, respectively. These results indicate weak relationships between the concentrations of arsenic and the water quality parameters. The variations in pH, electrical conductivity and dissolved oxygen explains very little of the variation in arsenic concentrations. The variations in pH, electrical conductivity and dissolved oxygen only explained 12.6%, 2.8% and 21.1% of the variation in arsenic concentrations, respectively.

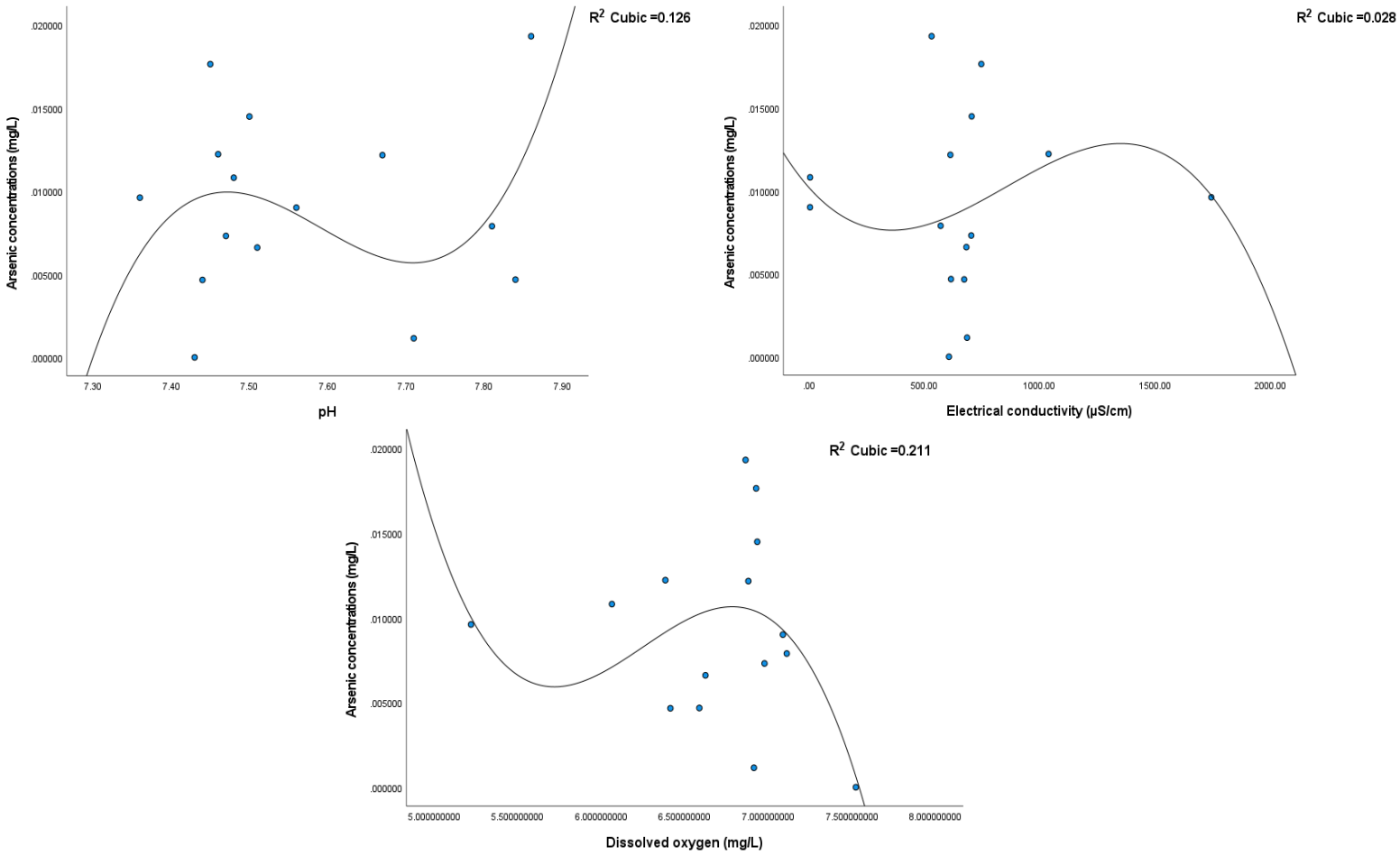

Figure 5.17: Scatterplots with cubic regression lines depicting the relationship between arsenic concentrations (mg/L) and pH, electrical conductivity (µS/cm) and dissolved oxygen (mg/L).

The Spearman rank correlation coefficient (r_s) values between cadmium concentrations and pH, electrical conductivity and dissolved oxygen were -0.117, -0.584 and 0.318, respectively and *p* values 0.678, 0.022 and 0.248, respectively. The results indicate a weak negative correlation between cadmium concentrations and pH, a moderate negative correlation between cadmium concentrations and electrical conductivity and a weak positive relationship between cadmium concentrations and dissolved oxygen. As pH and electrical conductivity increased, cadmium concentrations in the water decreased and as dissolved oxygen levels increased, cadmium concentrations in the water also increased. The *p* value was greater than 0.05 for the correlation between cadmium concentrations and pH and dissolved oxygen indicating the results were not statistically significant. However, the *p* value for the correlation between

cadmium concentrations and electrical conductivity was less than 0.05 indicating that this result was statistically significant. Figure 5.18 depicts the scatterplots with cubic regression lines of cadmium and pH, electrical conductivity and dissolved oxygen. The cubic R^2 values were 0.102, 0.326 and 0.270, respectively. These results indicate weak relationships between the concentrations of cadmium and the water quality parameters. The variations in pH, electrical conductivity and dissolved oxygen explains very little of the variation in cadmium concentrations. The variations in pH, electrical conductivity and dissolved oxygen explains 10.2%, 32.6% and 27% of the variation in cadmium concentrations, respectively.

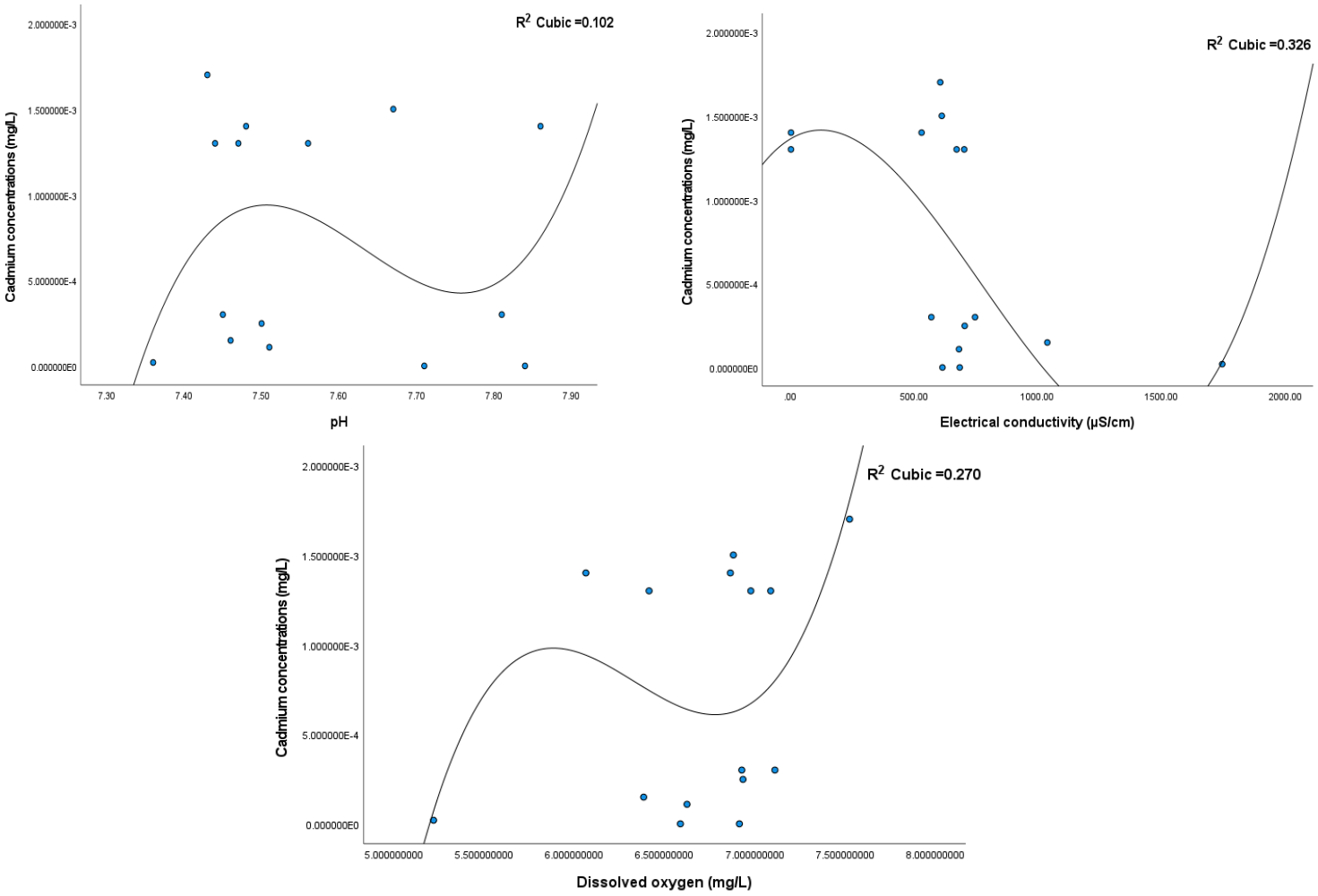

Figure 5.18: Scatterplots with cubic regression lines depicting the relationship between cadmium concentrations (mg/L) and pH, electrical conductivity (µS/cm) and dissolved oxygen (mg/L).

The Spearman rank correlation coefficient (r_s) values between iron concentrations and pH, electrical conductivity and dissolved oxygen were -0.061, 0.339 and 0.197, respectively and *p*

values 0.829, 0.216 and 0.480, respectively. The results indicate a very weak negative correlation between iron concentrations and pH, and weak positive correlations between iron concentrations and electrical conductivity and dissolved oxygen. As pH increased, iron concentrations in the water decreased and as electrical conductivity and dissolved oxygen levels increased, iron concentrations in the water increased. The *p* values for the correlation between iron concentrations and pH, electrical conductivity and dissolved oxygen were all greater than 0.05 indicating the results were not statistically significant. Figure 5.19 displays the scatterplots of iron concentrations and pH, electrical conductivity and dissolved oxygen. The cubic R^2 values were 0.134, 0.316 and 0.192, respectively. These results indicate weak relationships between the concentrations of iron and the water quality parameters. The variations in pH, electrical conductivity and dissolved oxygen explains very little of the variation in iron concentrations. The variations in pH, electrical conductivity and dissolved oxygen explains 13.4%, 31.6% and 19.2% of the variation in iron concentrations, respectively.

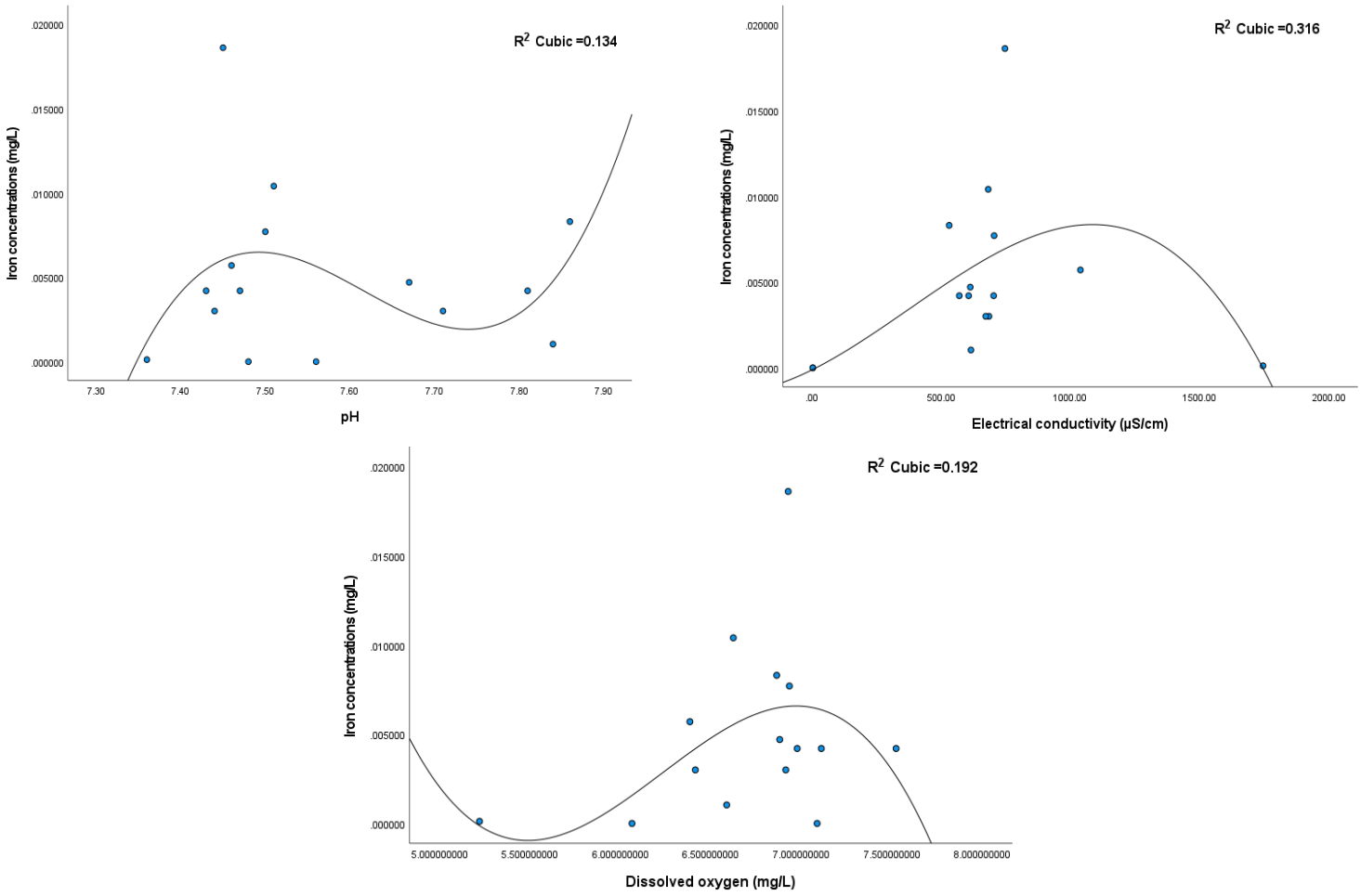

Figure 5.19: Scatterplots with cubic regression lines depicting the relationship between iron concentrations (mg/L) and pH, electrical conductivity (µS/cm) and dissolved oxygen (mg/L).

The Spearman rank correlation coefficient (r_s) values between magnesium concentrations and pH, electrical conductivity and dissolved oxygen were -0.446, -0.254 and -0.339, respectively and *p* values 0.095, 0.362, 0.216, respectively. The results indicate a moderate negative correlation between magnesium concentrations and pH and weak negative correlations between magnesium concentrations and electrical conductivity and dissolved oxygen. As pH, electrical conductivity and dissolved oxygen levels increased, magnesium concentrations in the water decreased. The *p* values were greater than 0.05 for the correlations between magnesium concentrations and pH, electrical conductivity and dissolved oxygen indicating the results were not statistically significant. Figure 5.20 displays the scatterplots of magnesium concentrations and pH, electrical conductivity and dissolved oxygen. The cubic R^2 values were 0.103, 0.996 and 0.136, respectively. These results indicate weak relationships between the concentrations of magnesium and pH and dissolved but a strong relationship between magnesium concentrations and electrical conductivity. The variations in pH and dissolved oxygen explains

very little of the variation in magnesium concentrations and the variations in electrical conductivity explains much of the variation in magnesium concentrations. The variations in pH, electrical conductivity and dissolved oxygen explains 10.3%, 99.6% and 13.6% of the variation in magnesium concentrations, respectively.

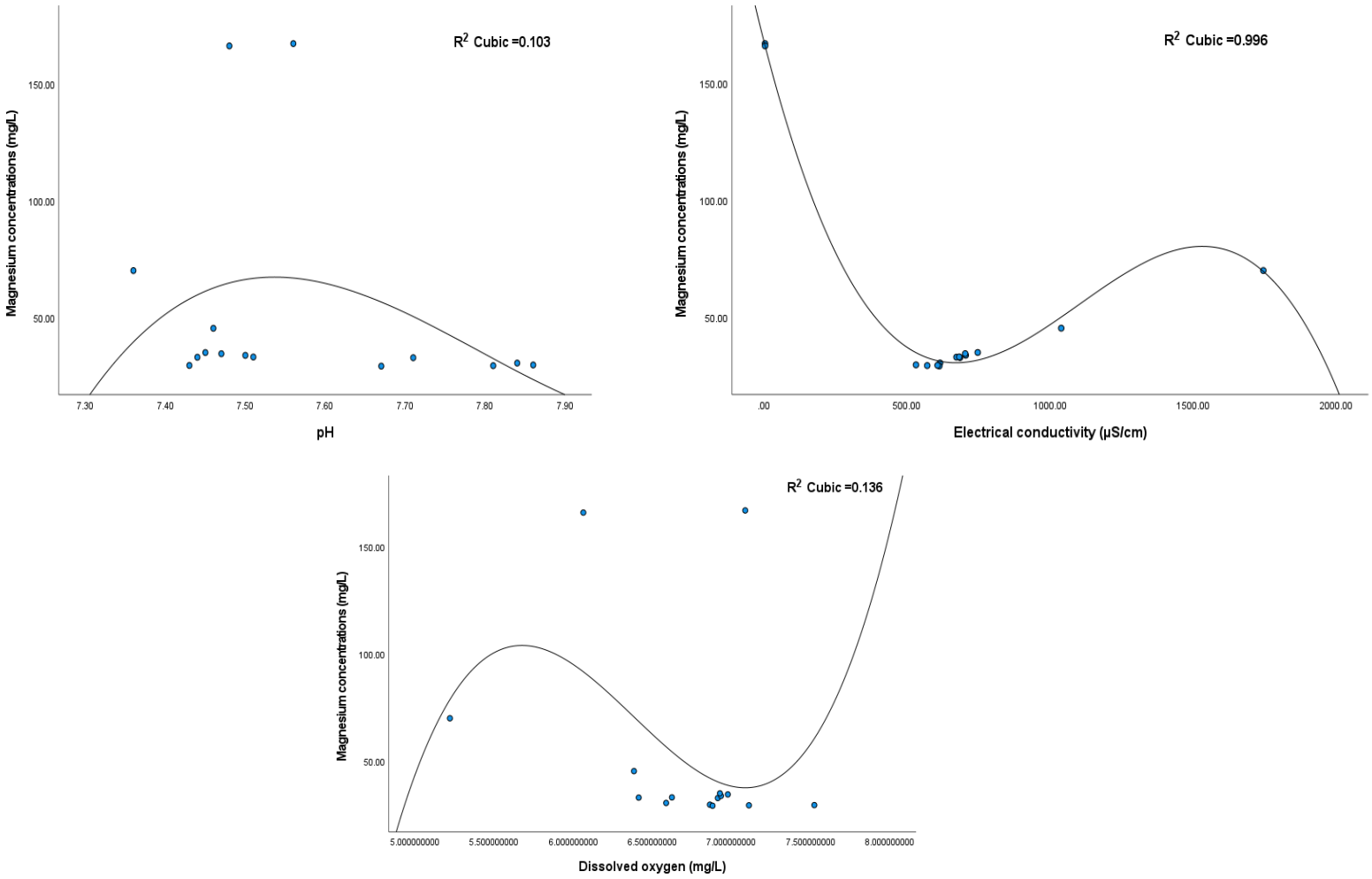

Figure 5.20: Scatterplots with cubic regression lines depicting the relationship between magnesium concentrations (mg/L) and pH, electrical conductivity (µS/cm) and dissolved oxygen (mg/L).

5.3.1.2) Spectral reflectance curves of heavy metals from water samples

Figure 5.21 depicts the spectral reflectance curve of the raw spectral data obtained from the ASD spectroradiometer scanning of the water samples across the visible and near-infrared spectrum (VNIR). From figure 5.21 it can be observed that there is a baseline offset and the spectra is noisy which needs to be accounted for before subsequent analyses.

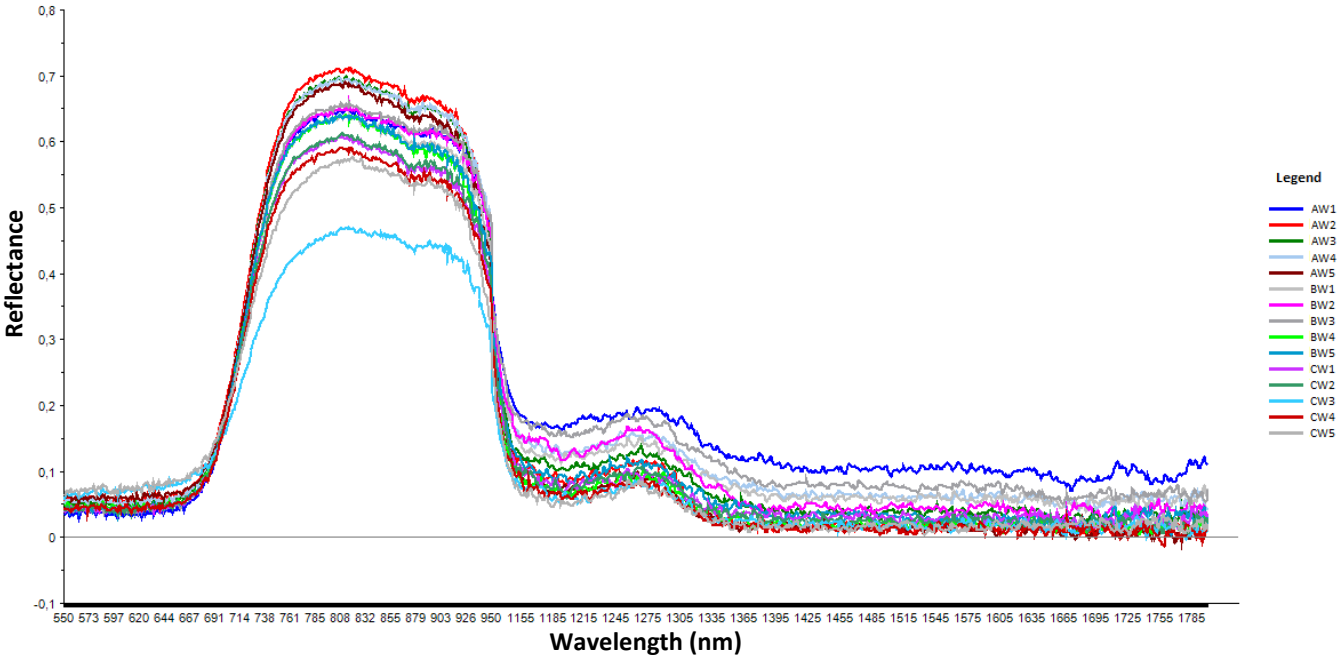

Figure 5.21: Raw spectral reflectance curve of the water samples.

Figure 5.22 below, illustrates the spectral reflectance curve of the first-derivative pre-processed spectral reflectance data obtained for the water samples. It can be seen that this pre-treatment resulted in a significant reduction in noisy spectra as well as removed baseline offsets and smoothed the data well. The derivative transformations are also useful as they indicate the reflectance peaks and absorption features in the spectra more clearly. Absorption features can be observed near 900 nm, 1131 nm, and 1309 nm with a reflectance peak occurring near 720 nm.

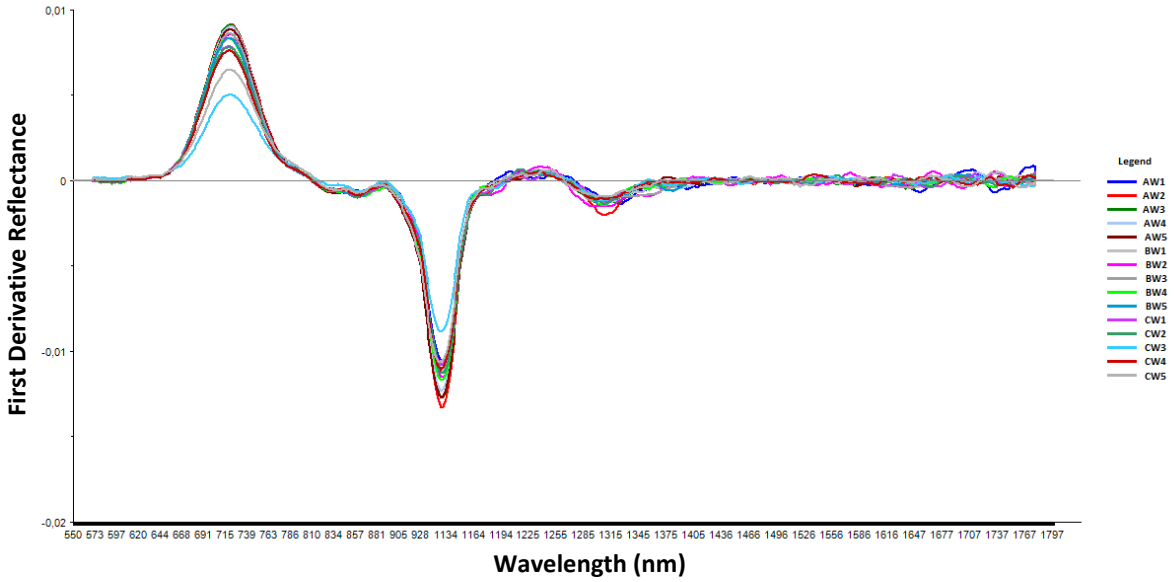

Figure 5.22: First derivative pre-processed spectral reflectance curve of the water samples.

5.3.1.3) Principal components analysis

A principal components analysis (PCA) was carried out on the first derivative pre-processed reflectance spectra for the 15 water samples in order to identify sample outliers in the data prior to further analyses. The scores plot results identified one sample outlier which is indicated in green as seen in figure 5.23 below and this sample was excluded from the partial least squares regression model. The closer the sample points are to the origin of the scores plot, the closer these sample points are to the mean. In addition, the results of the PCA scores plot also indicated that principal component 1 (PC-1) explained 73% of the variance in the data whilst principal component 2 (PC-2) explained only 12% of the variance in the data.

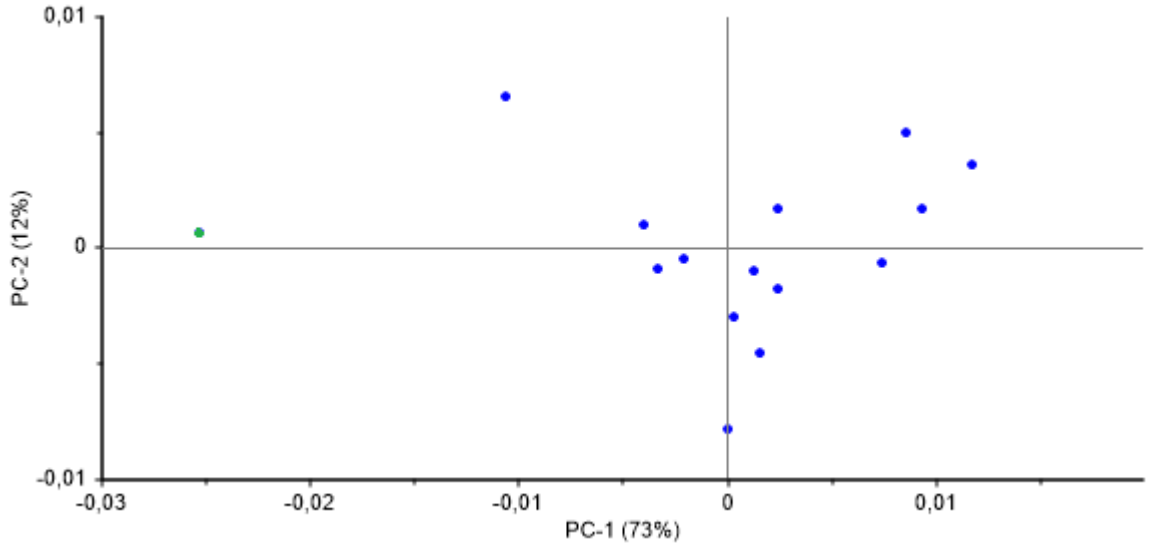

Figure 5.23: Principal components analysis (PCA) of the first derivative pre-processed VNIR reflectance spectra of all water samples (n=15) with the outlier sample indicated in green.

5.3.1.4) Partial least squares regression analysis

Figure 5.24 shows the scatterplots of the different water quality parameters measured in the laboratory against the values predicted by the partial least squares (PLS hereafter) regression model. Table 5.3 summarises the coefficient of determination (R^2 hereafter) and root mean square error (RMSE hereafter) values for both the calibration and cross-validation data produced by the PLS regression model. From table 5.3, it can be seen that the PLS regression model developed to predict heavy metals, pH and electrical conductivity parameters from VNIR reflectance spectra produced predictive accuracy results ranging from very low to high. The calibration and cross-validation R^2 and RMSE results were analysed and the best result was obtained for pH. The model predicted pH concentrations from VNIR reflectance spectra with moderate predictive accuracies for both the calibration and cross-validation data with calibration and cross-validation R^2 values of 0.33 and 0.35, respectively. The calibration and cross-validation RMSE values for pH were 0.126 and 0.134, respectively. The best result obtained for the prediction of heavy metals in the water was obtained for the prediction of arsenic (As). The model predicted arsenic concentrations from VNIR reflectance spectra with low predictive accuracies for both the calibration and cross-validation data with calibration and cross-validation R^2 values of 0.05 and 0.02 respectively. The calibration and cross-validation RMSE values for arsenic were 0.005 mg/L and 0.006 mg/L, respectively. The worst result was obtained for the prediction of iron (Fe) concentrations. The model predicted iron concentrations

from VNIR reflectance spectra with a very low prediction accuracy for the calibration data and a moderate accuracy for the cross-validation data with calibration and cross-validation R^2 values of 0.01 and 0.33, respectively. The calibration and cross-validation RMSE values for iron were 0.0046 mg/L and 0.0052 mg/L, respectively. The model predicted magnesium concentrations from VNIR reflectance spectra with moderate accuracies for both the calibration and cross-validation data with calibration and cross-validation R^2 values of 0.67 and 0.56, respectively. However, the calibration and cross-validation RMSE values for magnesium were high with calibration and cross-validation RMSE values of 26.93 mg/L and 33.51 mg/L, respectively. The model predicted electrical conductivity (EC) concentrations from VNIR reflectance spectra with low accuracies for both the calibration and cross-validation data with calibration and cross-validation R^2 values of 0.31 and 0.19, respectively. Furthermore, the calibration and cross-validation RMSE values for electrical conductivity were high with calibration and cross-validation RMSE values of 217.78 µS/cm and 255.29 µS/cm, respectively. The model predicted cadmium (Cd) concentrations from VNIR reflectance spectra with very low accuracies for both the calibration and cross-validation data with calibration and cross-validation R^2 values of 0.13 and 0.06, respectively. The calibration and cross-validation RMSE values for cadmium were 0.00060 mg/L and 0.00067 mg/L, respectively. The differences in calibration R^2 and cross-validation R^2 for pH, electrical conductivity, arsenic, cadmium, iron and magnesium were 0.02, 0.12, 0.03, 0.07, 0.32 and 0.11, respectively.

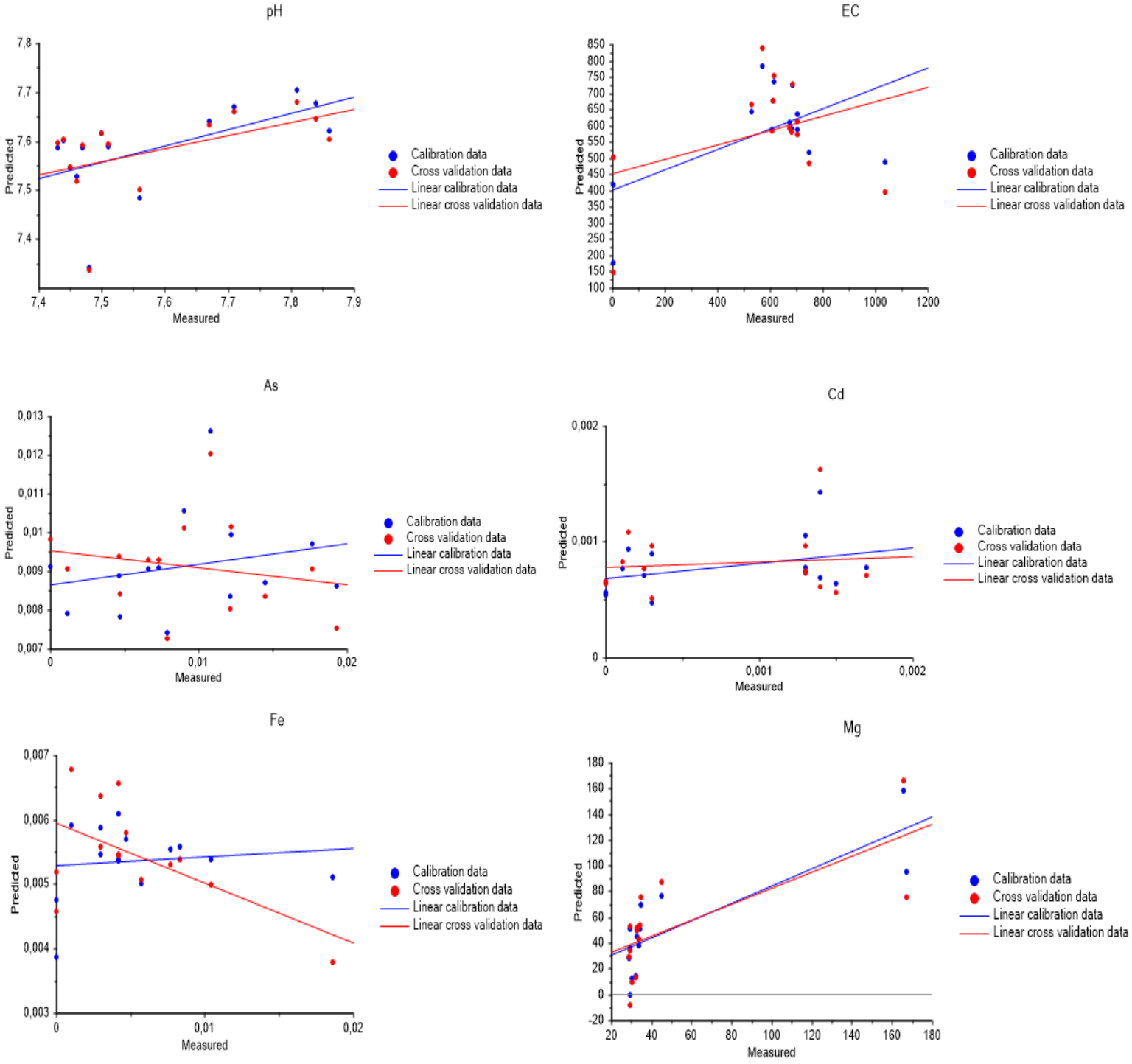

Figure 5.24: Scatterplots depicting the concentrations of pH, electrical conductivity (EC), arsenic (As), cadmium (Cd), iron (Fe) and (Mg) of the water samples measured in the laboratory against the concentrations predicted using ASD and PLS regression.

Table 5.3: R^2 and RMSE values for the calibration and cross-validation data produced by the PLS regression model of the water data.

Parameter	N	Calibration R^2	Cross-validation R^2	Calibration RMSE	Cross-validation RMSE
pH	14	0.33	0.35	0.126	0.134
EC	14	0.31	0.19	217.78	255.29
As	14	0.05	0.02	0.005	0.006
Cd	14	0.13	0.06	0.00060	0.00067
Fe	14	0.01	0.33	0.0046	0.0052
Mg	14	0.67	0.56	26.93	33.51

Figure 5.25 displays the graphs of the regression coefficients of the heavy metals and water quality parameters produced by the PLS regression model. The regression coefficients are used to determine the response value from the predictor measurements and can be used to identify which independent variables have a significant impact on the dependent variables. It provides an idea for which wavelengths are important for the modelling of the concentrations of the heavy metals and water quality parameters. From figure 5.25, it can be seen that for pH, the significant regions of the VNIR spectrum are 725 nm, 929 nm, 1136 nm and 1708 nm. The significant regions of the VNIR spectrum for electrical conductivity are 719 nm, 929 nm, 1134 nm and 1707 nm. The significant regions of the VNIR spectrum for arsenic are 715 nm, 1137 nm, 1663 nm and 1731 nm. The significant regions of the VNIR spectrum for cadmium are 718 nm, 1136 nm, 1666 nm and 1731 nm. The significant regions of the VNIR spectrum for iron are 717 nm, 929 nm, 1135 nm and 1709 nm and the significant regions of the VNIR spectrum for magnesium are 715 nm, 1137 nm, 1667 nm and 1730 nm.

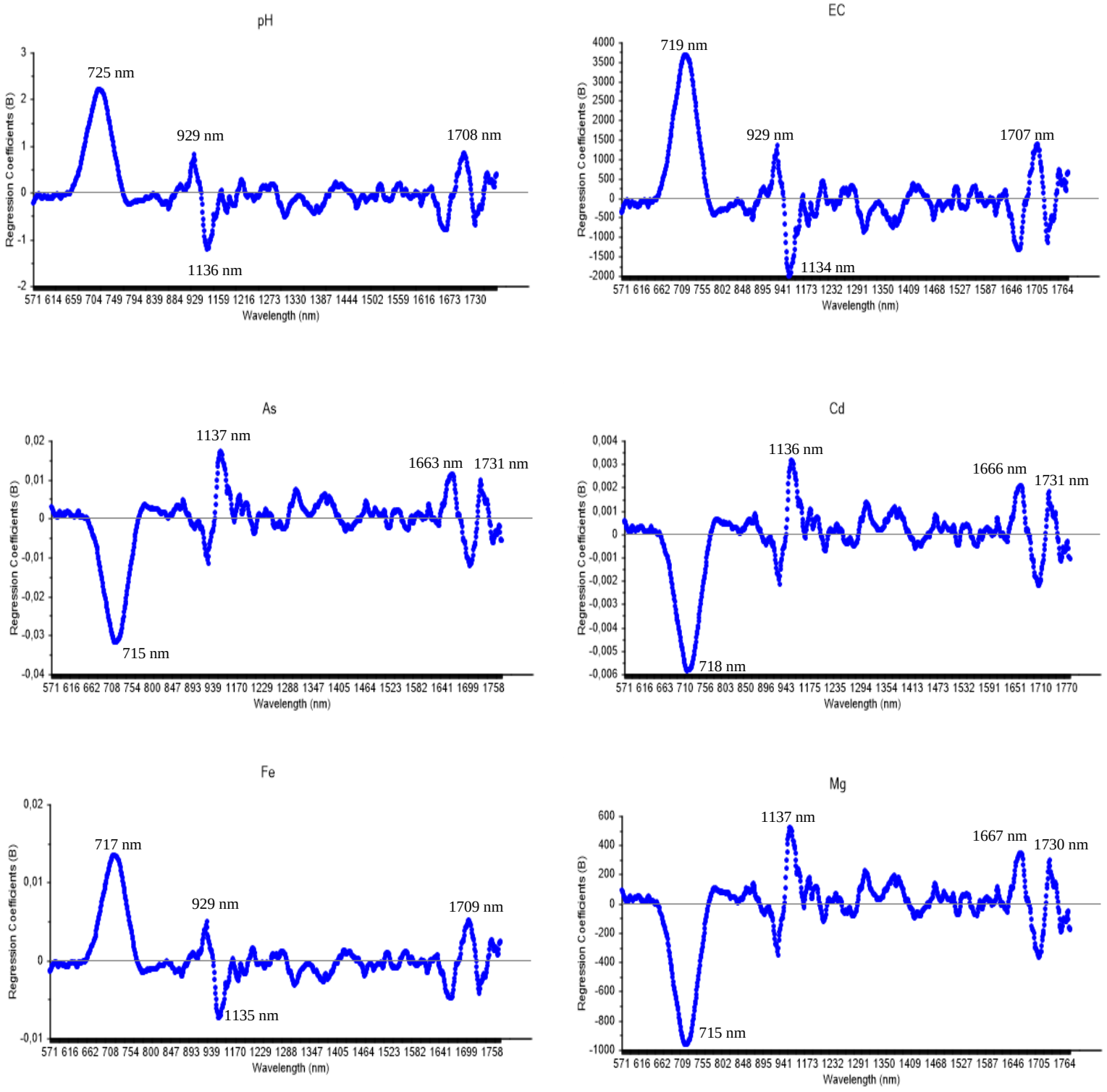

Figure 5.25: Regression coefficients for pH, electrical conductivity (EC), arsenic (As), cadmium (Cd), iron (Fe), and magnesium (Mg) concentrations acquired from the PLS regression analysis.

5.3.2) Sediment data

5.3.2.1) Spectral reflectance curves of heavy metals from sediment samples

Figure 5.26 shows the spectral reflectance curve of the raw spectral data obtained from the ASD spectroradiometer scanning of the sediment samples across the VNIR spectrum. From figure 5.26, it can be observed that the spectra of the sediment samples were noisy and the spectral noise needed to be minimised before further analyses.

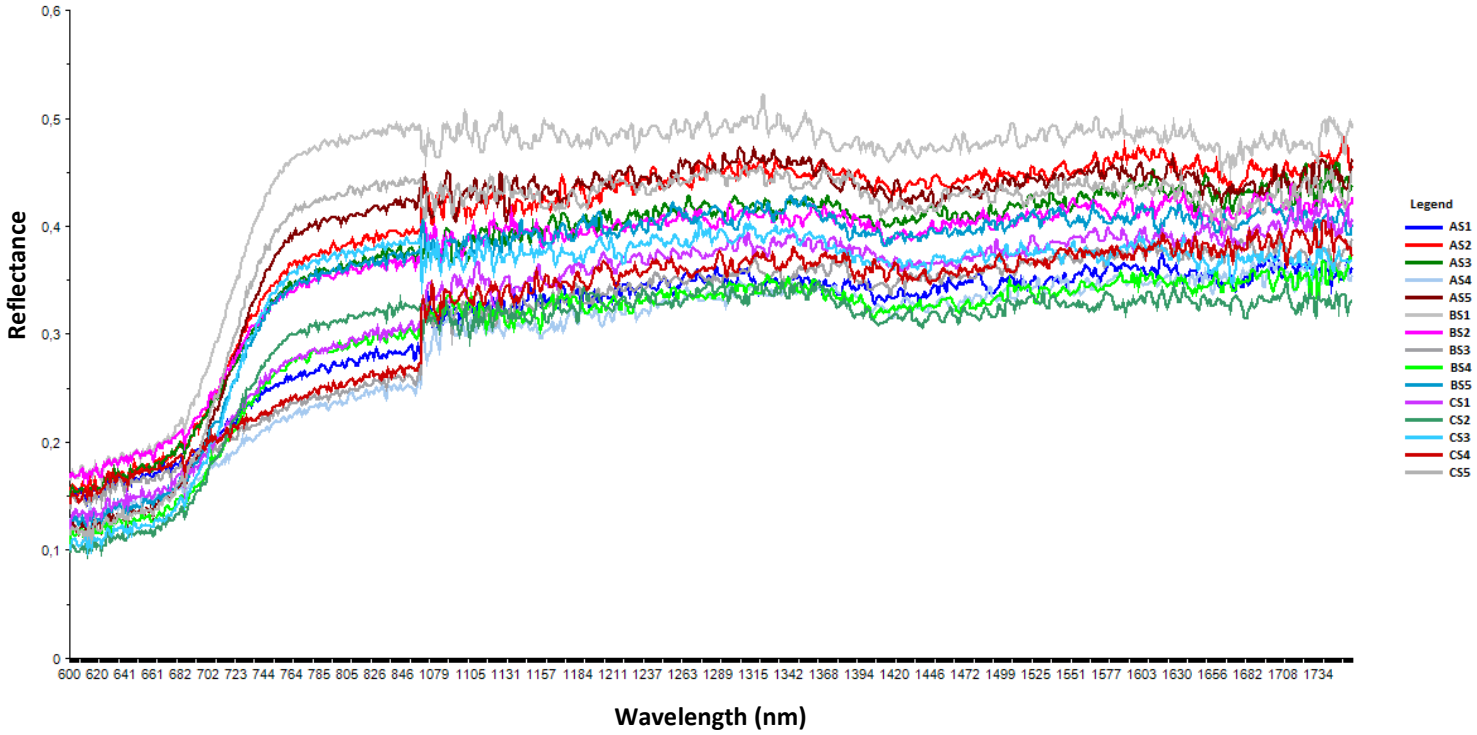

Figure 5.26: Raw spectral reflectance curve of the sediment samples.

Figure 5.27 below shows the spectral reflectance curve of the Savitzky-Golay smoothing pre-processed spectral reflectance data obtained for the sediment samples. It can be seen that this pre-treatment significantly reduced the spectral noise and smoothed the data well making the spectral lines clear and more visible. Absorption features can be observed around 1090 nm, 1420 nm and 1670 nm.

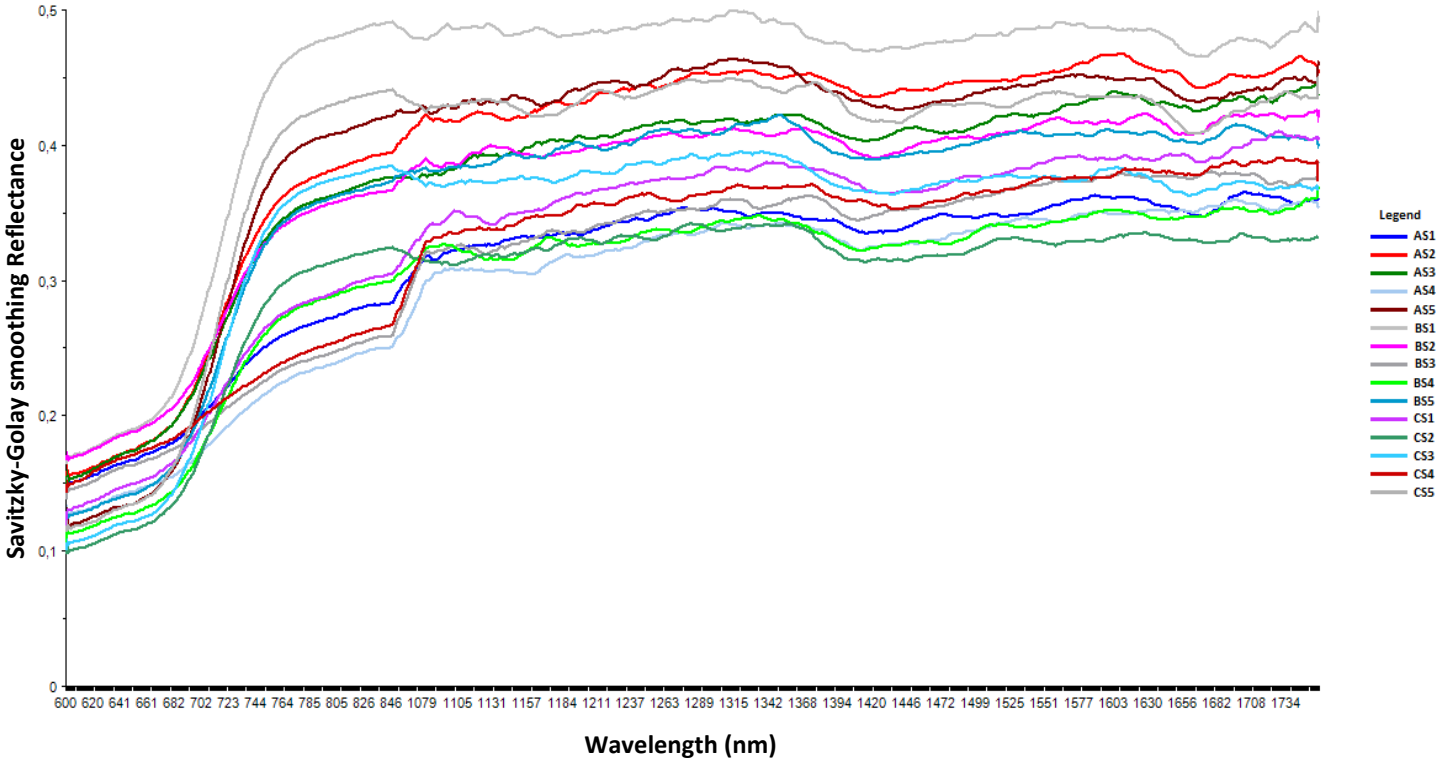

Figure 5.27: Savitzky-Golay smoothing pre-processed spectral reflectance curve of the sediment samples.

5.3.2.2) Principal components analysis

A PCA was undertaken on the Savitzky-Golay smoothing pre-processed spectra of the sediment samples in order to determine if there were any sample outliers that needed to be removed prior to subsequent analyses. The results of the scores plot seen in Figure 5.28 did not indicate any outlier samples; therefore, all 15 sediment samples were used in the PLS regression analysis. The sample points that were found closer to the origin of the scores plot indicated that these sample points were closer to the mean. In addition, the results of the PCA scores plot also indicated that principal component 1 (PC-1) explained 93% of the variance in the data whilst principal component 2 (PC-2) only explained 6% of the variance in the data.

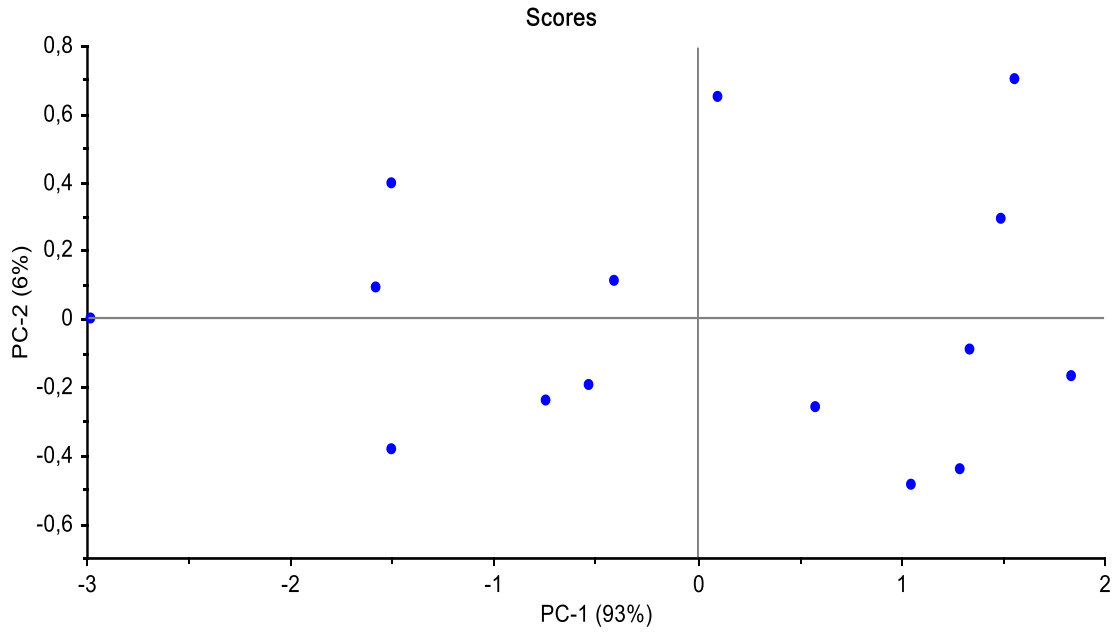

Figure 5.28: Principal components analysis (PCA) of the Savitzky-Golay smoothing pre-processed VNIR reflectance spectra of all sediment samples (n=15).

5.3.2.3) Partial least squares regression analysis

Figure 5.29 illustrates the scatterplots of the different heavy metal concentrations measured in the laboratory against the values predicted by the PLS regression model. Table 5.4 summarises the R^2 and RMSE values for both the calibration and cross-validation data produced by the PLS regression model. From table 5.4, it can be seen that the PLS regression model developed to predict the metal concentrations from VNIR reflectance spectra produced predictive accuracy results ranging from low to high. The calibration and cross-validation R^2 and RMSE results were analysed and the best result was obtained for Nickel (Ni) concentrations. The model predicted nickel concentrations from VNIR reflectance spectra with a high predictive accuracy for both the calibration and cross-validation data and low RMSE values with calibration and cross-validation R^2 values of 0.96 and 0.83, respectively. The calibration and cross-validation RMSE values for nickel were 1.88 mg/kg and 4.34 mg/kg, respectively. The worst result was obtained for the prediction of aluminium (Al) concentrations. The model predicted aluminium concentrations from VNIR reflectance spectra with a moderate prediction accuracy for the calibration data and a low prediction accuracy for the cross-validation data with calibration and cross-validation R^2 values of 0.67 and 0.19, respectively. In addition, the RMSE values obtained for aluminium were high with calibration and cross-validation RMSE values 395.77 mg/kg and 662.19 mg/kg, respectively. The model predicted arsenic (As)

concentrations from VNIR reflectance spectra with a high predictive accuracy for the calibration data and a moderate predictive accuracy for the cross-validation data with calibration and cross-validation R^2 values of 0.86 and 0.61, respectively. The calibration and cross-validation RMSE values for arsenic were 0.41 mg/kg and 0.72 mg/kg, respectively. The model predicted chromium (Cr) concentrations from VNIR reflectance spectra with high accuracies for both the calibration and cross-validation data with calibration and cross-validation R^2 values of 0.94 and 0.77, respectively. The calibration and cross-validation RMSE values for chromium were 4.41 mg/kg and 9.61 mg/kg, respectively. The model predicted copper (Cu) concentrations from VNIR reflectance spectra with high accuracies for both the calibration and cross-validation data with calibration and cross-validation R^2 values of 0.86 and 0.68, respectively. The calibration and cross-validation RMSE values for copper were 6.16 mg/kg and 10.06 mg/kg, respectively. The model predicted iron (Fe) concentrations from VNIR reflectance spectra with a high predictive accuracy for the calibration data and a moderate predictive accuracy for the cross-validation data with calibration and cross-validation R^2 values of 0.96 and 0.67, respectively. However, the RMSE values obtained for iron were high with calibration and cross-validation RMSE values 1678.67 mg/kg and 5079.12 mg/kg, respectively. The model predicted lead (Pb) concentrations from VNIR reflectance spectra with high accuracies for both the calibration and cross-validation data with calibration and cross-validation R^2 values of 0.94 and 0.72, respectively. The calibration and cross-validation RMSE values for lead were 2.87 mg/kg and 6.43 mg/kg, respectively. The model predicted magnesium (Mg) concentrations from VNIR reflectance spectra with a high predictive accuracy for the calibration data and a moderate predictive accuracy for the cross-validation data with calibration and cross-validation R^2 values of 0.88 and 0.66, respectively. However, the RMSE values obtained for magnesium were high with calibration and cross-validation RMSE values 346.42 mg/kg and 613.57 mg/kg, respectively. The model predicted zinc (Zn) concentrations from VNIR reflectance spectra with high accuracies for both the calibration and cross-validation data with calibration and cross-validation R^2 values of 0.92 and 0.70, respectively. The calibration and cross-validation RMSE values for zinc were 17.46 mg/kg and 37.43 mg/kg, respectively. The differences in calibration R^2 and cross-validation R^2 for aluminium, arsenic, chromium, copper, iron, lead, magnesium, nickel and zinc were 0.48, 0.25, 0.17, 0.18, 0.29, 0.22, 0.22, 0.13 and 0.22, respectively.

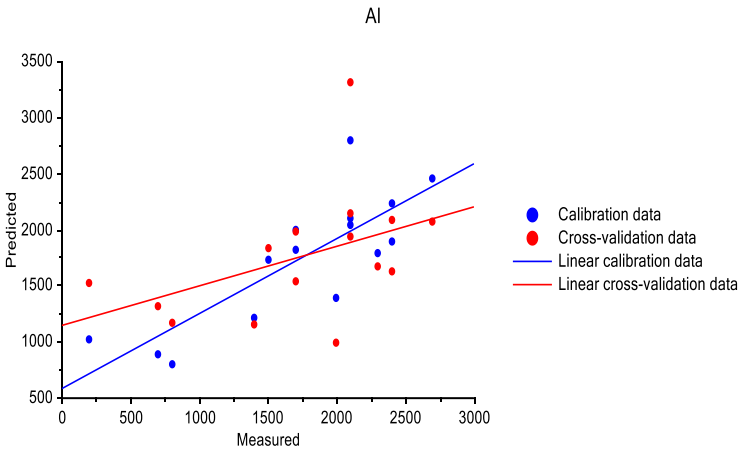
Al
Predicted
Measured
Calibration data
Cross-validation data
Linear calibration data
Linear cross-validation data

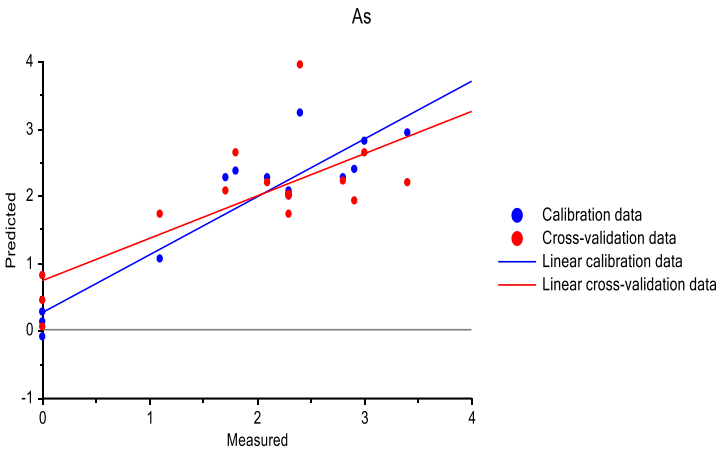
As
Predicted
Measured
Calibration data
Cross-validation data
Linear calibration data
Linear cross-validation data

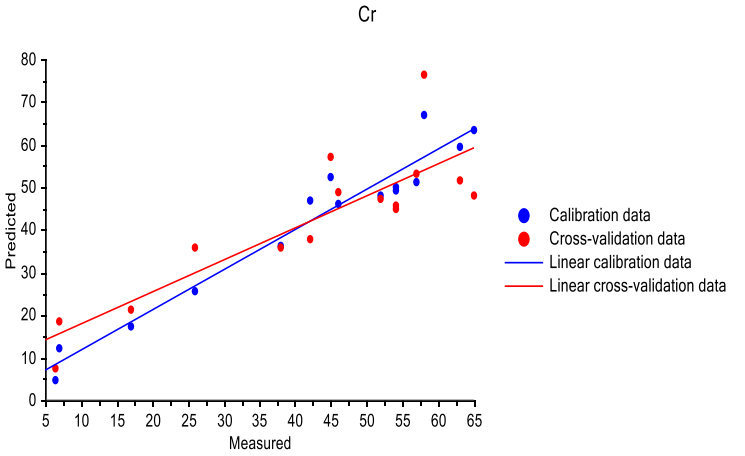
Cr
Predicted
Measured
Calibration data
Cross-validation data
Linear calibration data
Linear cross-validation data

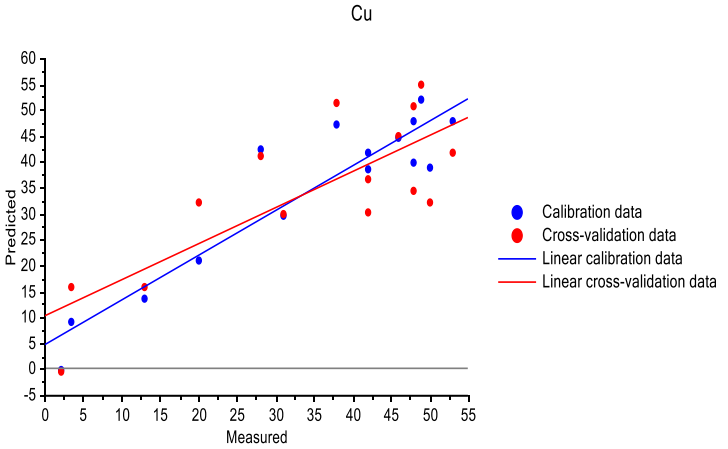
Cu
Predicted
Measured
Calibration data
Cross-validation data
Linear calibration data
Linear cross-validation data

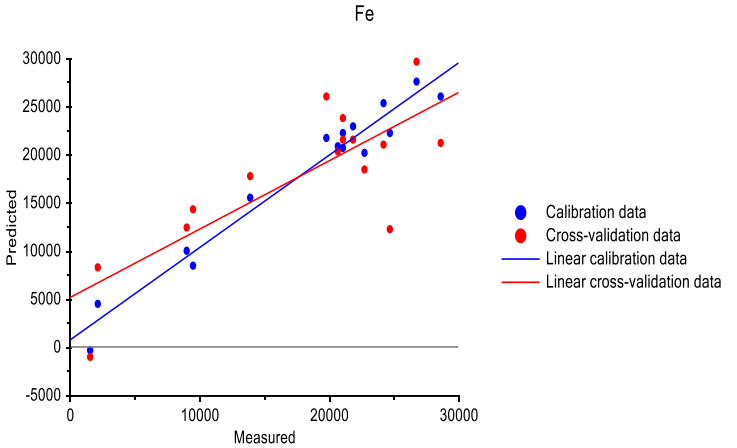
Fe
Predicted
Measured
Calibration data
Cross-validation data
Linear calibration data
Linear cross-validation data

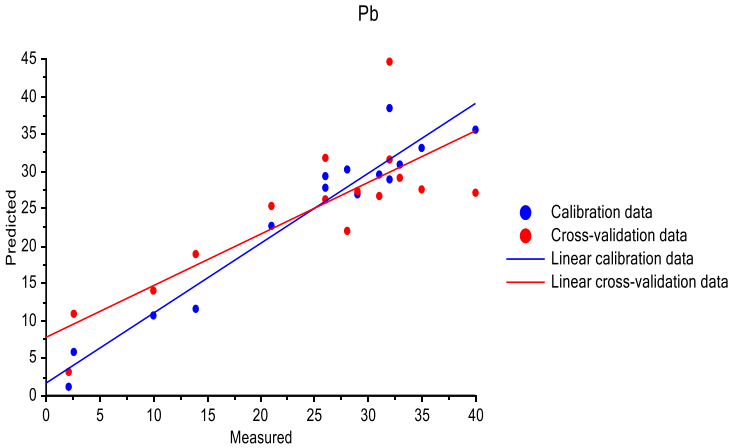
Pb
Predicted
Measured
Calibration data
Cross-validation data
Linear calibration data
Linear cross-validation data

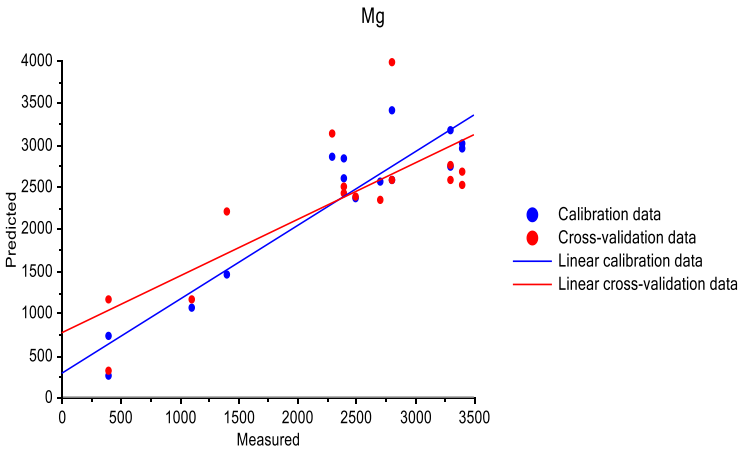
Mg
Predicted
Measured
Calibration data
Cross-validation data
Linear calibration data
Linear cross-validation data

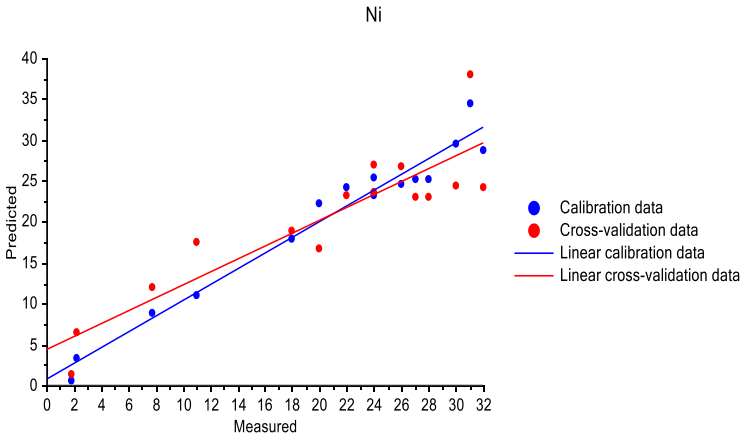
Ni
Predicted
Measured
Calibration data
Cross-validation data
Linear calibration data
Linear cross-validation data

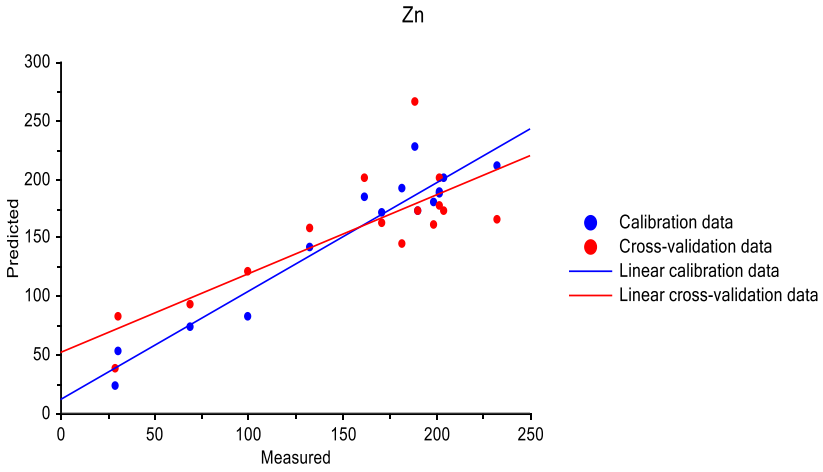

Figure 5.29: Scatterplots depicting the concentrations of aluminium (Al), arsenic (As), chromium (Cr), copper (Cu), iron (Fe), lead (Pb), magnesium (Mg), nickel (Ni) and zinc (Zn) of the sediment samples measured in the laboratory against the concentrations predicted using ASD and PLS regression.

Table 5.4: R^2 and RMSE values for the calibration and cross-validation data produced by the PLS regression model of the sediment data.

Metal	N	R^2 calibration	R^2 cross-validation	RMSE calibration	RMSE cross-validation
Aluminium	15	0.67	0.19	395.77	662.19
Arsenic	15	0.86	0.61	0.41	0.72
Chromium	15	0.94	0.77	4.41	9.61
Copper	15	0.86	0.68	6.16	10.06
Iron	15	0.96	0.67	1678.67	5079.12
Lead	15	0.94	0.72	2.87	6.43
Magnesium	15	0.88	0.66	346.42	613.57
Nickel	15	0.96	0.83	1.88	4.34
Zinc	15	0.92	0.70	17.46	37.43

Figure 5.30 below displays the graphs of the regression coefficients of the heavy metals produced by the PLS regression model. From Figure 5.30, it can be seen that the important regions of the VNIR spectrum for the detection of aluminium are 1284 nm, 1396 nm, 1474 nm and 1677 nm. The important regions of the VNIR spectrum for the detection of arsenic are 1090 nm, 1278 nm, 1398 nm, 1471 nm and 1678 nm. The important regions of the VNIR spectrum for the detection of chromium are 1279 nm, 1397 nm, 1473 nm and 1676 nm. The important regions of the VNIR spectrum for the detection of copper are 1091 nm, 1280 nm, 1395 nm, 1474 nm and 1677 nm. The important regions of the VNIR spectrum for the detection of iron are 1090 nm, 1283 nm, 1395 nm, 1476 nm and 1676 nm. The important regions of the VNIR spectrum for the detection of lead are 1091 nm, 1278 nm, 1392 nm, 1472 nm and 1676 nm. The important regions of the VNIR spectrum for the detection of magnesium are 1090 nm, 1281 nm, 1397 nm, 1474 nm and 1675 nm. The important regions of the VNIR spectrum for the detection of nickel are 1090 nm, 1279 nm, 1389 nm, 1473 nm and 1676 nm. The important regions of the VNIR spectrum for the detection of zinc are 1090 nm, 1278 nm, 1395 nm, 1479 nm and 1677 nm.

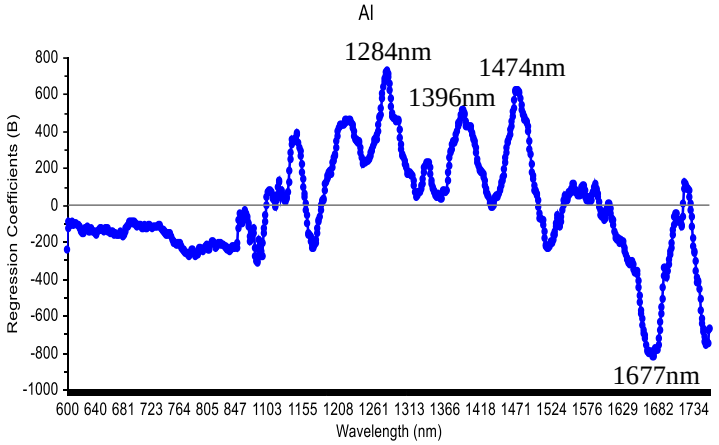
Al
1284nm
1474nm
1396nm
1677nm
Regression Coefficients (B)
Wavelength (nm)

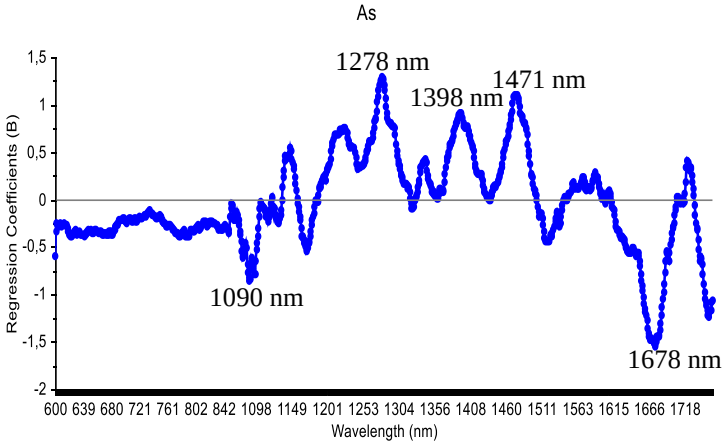
As
1278 nm
1471 nm
1398 nm
1090 nm
1678 nm
Regression Coefficients (B)
Wavelength (nm)

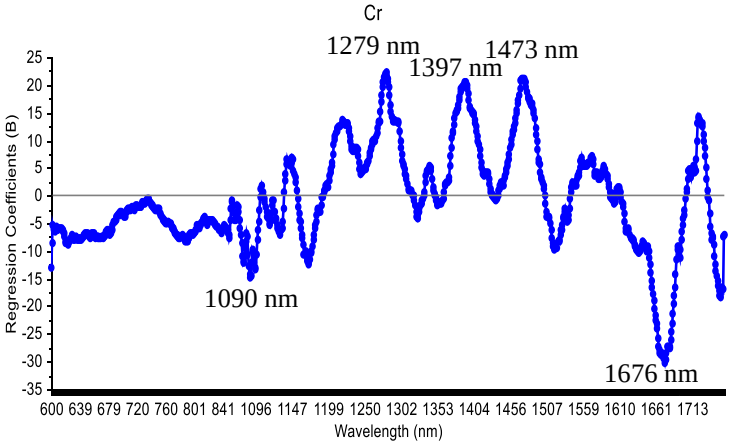
Cr
1279 nm
1473 nm
1397 nm
1090 nm
1676 nm
Regression Coefficients (B)
Wavelength (nm)

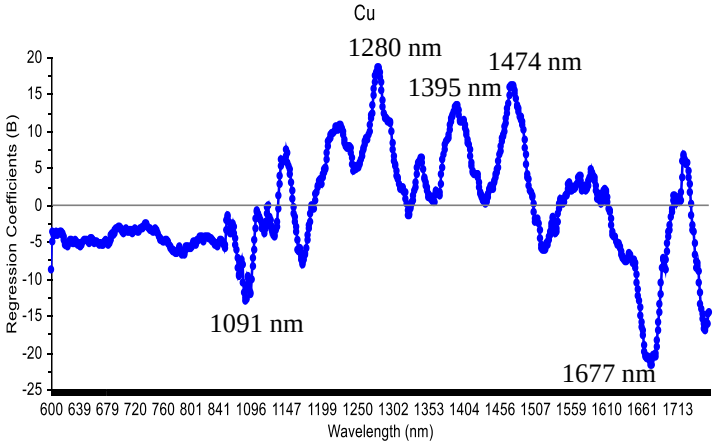
Cu
1280 nm
1474 nm
1395 nm
1091 nm
1677 nm
Regression Coefficients (B)
Wavelength (nm)

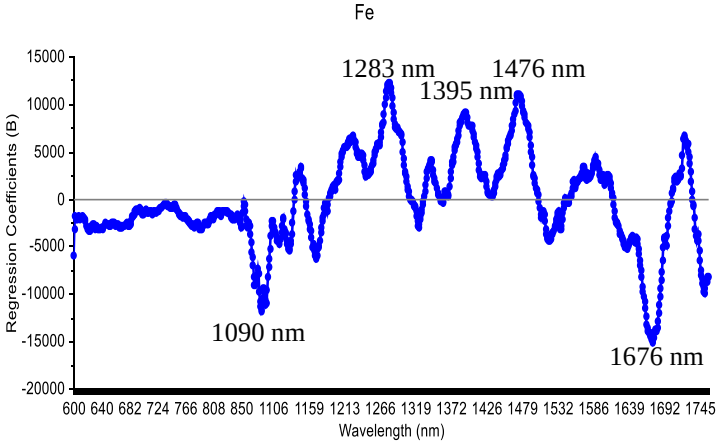
Fe
1283 nm
1476 nm
1395 nm
1090 nm
1676 nm
Regression Coefficients (B)
Wavelength (nm)

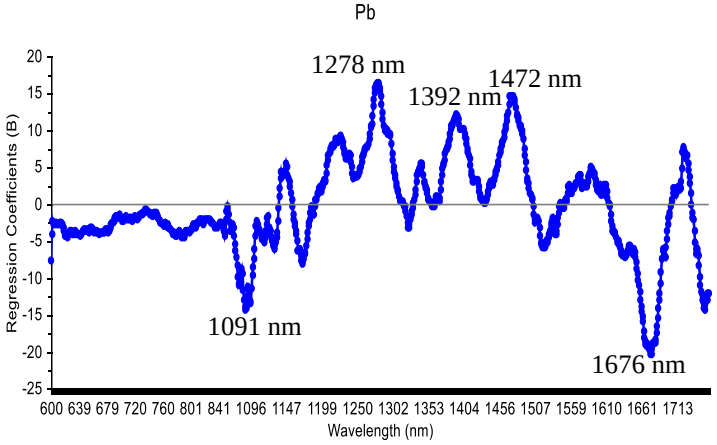
Pb
1278 nm
1472 nm
1392 nm
1091 nm
1676 nm
Regression Coefficients (B)
Wavelength (nm)

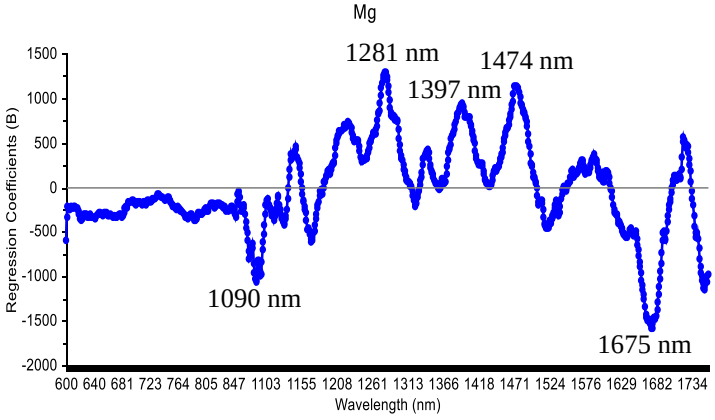
Mg
1281 nm
1474 nm
1397 nm
1090 nm
1675 nm
Regression Coefficients (B)
Wavelength (nm)

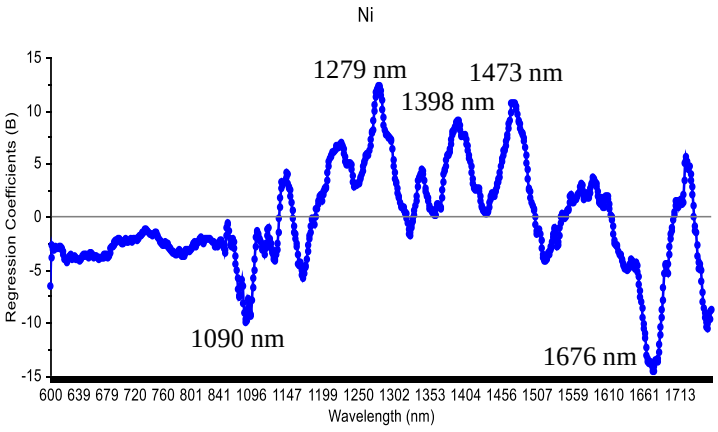
Ni
1279 nm
1473 nm
1398 nm
1090 nm
1676 nm
Regression Coefficients (B)
Wavelength (nm)

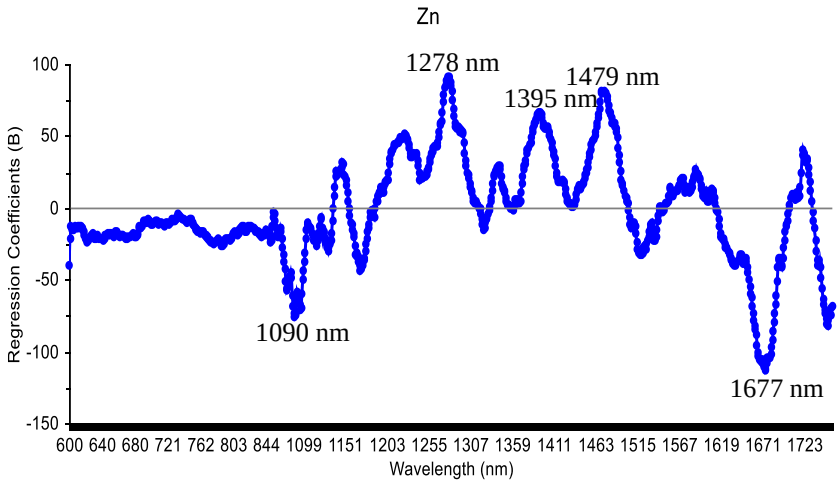

Figure 5.30: Regression coefficients for aluminium (Al), arsenic (As), chromium (Cr), copper (Cu), iron (Fe), lead (Pb), magnesium (Mg), nickel (Ni) and zinc (Zn) concentrations acquired from the PLS regression analysis.

CHAPTER 6: DISCUSSION AND CONCLUSION

6.1) Introduction

This chapter involves a critical discussion of the results obtained in this study in order to make inferences on the use of visible near-infrared reflectance spectra in the prediction of heavy metals in water and sediments. The results are discussed in conjunction with the results attained from previous literature. Thereafter, the limitations of this study will be discussed along with the conclusion of the study and possible recommendations for future research.

6.2) Discussion

6.2.1) Factors influencing the concentrations of physicochemical parameters and heavy metals in the water of estuaries

The water quality parameters of a river and estuary vary spatially. According to Walling and Webb (1975), several factors contribute to spatial variations in physicochemical parameters and heavy metal concentrations, including natural factors such as chemical weathering and anthropogenic factors such as land-use changes. However, one of the main reasons for the observed variation in these concentrations in recent years is the significant increase in the land-use practices associated with aquatic ecosystems (Kaushal et al., 2013).

The pH levels were alkaline at all sampling sites of the uMgeni Estuary and fell within the permissible levels for aquatic ecosystems of 6 - 8 as proposed by DWAF (1996). This is consistent with the results obtained in a previous study conducted by Singh (2013), where a portion of the study focused on the analysis of the physicochemical parameters of water samples collected from the uMgeni River and Estuary. However, it was noticeable that the pH levels were more alkaline further upstream at site A from the estuary in comparison to the mouth at site C. A reason for the alkaline pH could be the photosynthetic activity of the plants in and around the estuary. The pH of water becomes alkaline when the hydroxide ions exceed the hydrogen ions in the water (Barker and Ridgwell, 2012). When the process of photosynthesis occurs, carbon dioxide is taken up from the water, which causes an increase in pH (Grzywna and Bronowicka-Mielniczuk, 2020). Carbon dioxide dissociates in water to produce carbonic acid, which partially dissolves to produce hydrogen, bicarbonate and carbonate ions (Barker and Ridgwell, 2012). According to Boyd (2015), when carbon dioxide is removed from the water during photosynthesis, the bicarbonate ions dissolve and form more

carbon dioxide and carbonate ions. The hydrolysis of carbonate ions will, in turn, cause the pH to increase, leading to more alkaline or basic waters (Boyd, 2015). Another reason for this could be an increase in alkaline substances released from industrial effluents, and agricultural and urban runoff discharged into the river further upstream (Munjal and Singh, 2020). Ionic compounds or salts such as sodium hydroxide consist of alkali metals that produce hydroxide ions when they dissolve in water (Munjal and Singh, 2020). Therefore, an increase in industrial effluents consisting of these ionic compounds discharged into rivers can cause an increase in the pH levels of the water. Agricultural runoff from practices such as the use of lime or calcium carbonate and bicarbonate in increasing the soil pH required for specific crops can increase the alkalinity of rivers. This is consistent with a study conducted by Raymond et al. (2008) that assessed the human impacts on water and carbon fluxes for the Mississippi River in the United States. The results of the study concluded that an increase in agricultural practices increases river discharge; therefore, agricultural practices that make use of high calcium carbonate and bicarbonate concentrations can cause more alkaline waters (Raymond et al., 2008). Urban infrastructure consisting of cement and calcium can lead to the alkalinisation of rivers (Davies et al., 2010). The impermeable surfaces present in urban areas leads to urban runoff into rivers and estuaries containing these substances, which raises the pH of rivers (Kaushal et al., 2013). This is consistent with a study conducted by Davies et al. (2010) that assessed the impact of two drainage materials, concrete and PVC pipes on, urban water chemistry. Water samples were collected from an underdeveloped catchment and an urban catchment and were compared, and then the water samples were passed through a concrete and PVC pipe. The results indicated bicarbonate and carbonate concentrations were significantly higher in the urban river samples and had slightly alkaline conditions compared to the slightly acidic natural river samples. The water exposed to a concrete pipe also displayed increased bicarbonate concentrations and slightly alkaline conditions.

The electrical conductivity measures the ability of water to conduct an electric current and is a proxy for the concentrations of ions dissolved in the water (Elkhorn Slough Reserve, 2017). Ions such as calcium, sodium, magnesium and chloride dissolved in water are in a charged state and conduct electric currents (Elkhorn Slough Reserve, 2017). Electrical conductivity can also provide information on the salinity of an aquatic ecosystem, which measures the total salts dissolved in the water (Ratnayake et al., 2017). The electrical conductivity levels obtained from sampling sites A, B and C for the uMgeni Estuary were within the normal background levels for rivers as proposed by USEPA (2012). The results from the study showed an increasing

trend of conductivity levels from upstream at site A of the uMgeni Estuary towards site C at the mouth, with higher conductivity levels recorded near the mouth. This is consistent with the results obtained in a previous study conducted by Singh (2013), where the electrical conductivity levels of the uMgeni River were analysed and the levels ranged from 21.6-5150 mS/m with the maximum electrical conductivity level recorded near the mouth. A reason for this is that the levels of electrical conductivity are generally highest near the mouth of a river, where there is a more significant influence from saltwater. Seawater has high salinity levels and thus, contains high amounts of dissolved salts such as sodium and chloride, leading to higher electrical conductivity levels (Griffin et al., 2014; Nthunya et al., 2018). This is consistent with a study conducted by Ratnayake et al. (2017), where the sediment and physicochemical characteristics of the Madu-Ganga Estuary in Sri Lanka were investigated. It was found that the electrical conductivity of the water decreased from the mouth of the estuary to more upstream as a result of the dilution of seawater by freshwater (Ratnayake et al., 2017). The electrical conductivity levels were also slightly elevated at site B near the middle reaches of the uMgeni Estuary. A reason for these elevated conductivity levels can be attributed to the industrial and residential areas located along the estuary. According to Kinuthia et al. (2020), industrial and domestic effluents discharged into rivers causes an increase in the electrical conductivity of the water. This is in line with the results obtained from a study conducted by Kinuthia et al. (2020) that investigated the heavy metal concentrations in the wastewater of open drainage channels in Nairobi, Kenya. The results indicated higher levels of electrical conductivity at the sampling sites located near residential and industrial areas. This is also consistent with another study conducted by Moroşanu et al. (2017) that investigated different methodologies to identify the leading factors of the electrical conductivity of the Jiu catchment in Romania. The results indicated a strong positive correlation between electrical conductivity and human activities such as mining, urbanisation and industrialisation. Land-uses such as urbanisation, and industrial activities can cause an increase in ionisable substances such as pollutants to be discharged into rivers (Moroşanu et al., 2017).

Dissolved oxygen levels are crucial for the survival of all aquatic organisms, and most organisms have a specific range of dissolved oxygen levels that are tolerable; however, dissolved oxygen levels outside this range can lead to physiological and behavioural stress (Pearce and Schumann, 2003; Wenner et al., 2004). The dissolved oxygen levels at sampling sites A, B and C of the uMgeni Estuary fell within the permissible limits of not below 5 mg/L 99% of the time, as proposed by DWAF (1996). However, it was noticeable that the highest

levels of dissolved oxygen were recorded at site B, with a mean of 6.9mg/L, and the lowest levels were recorded at site C near the mouth, with a mean of 6.34 mg/L. A reason for this could be that the mouth contains higher salinity levels and dissolved salts than the upper reaches of the estuary, and according to Sherwood et al. (1991), waters that consist of high amounts of dissolved salts contain lower dissolved oxygen levels. This is consistent with a study undertaken by O'Boyle et al. (2009) that investigated dissolved oxygen levels in the estuarine and coastal waters of Ireland. It was found that the lowest levels of dissolved oxygen were recorded in the lower reaches of the estuaries investigated in their study. The ions from salts tend to attract water molecules to hydrate the ions, which lowers the affinity of nonpolar oxygen molecules to water (Brini et al., 2017). The dissolved oxygen gets displaced from the water with the addition of salts which is a process known as salting out; therefore, increases in ionic salts leads to a decrease in the solubility of gases such as dissolved oxygen (Brini et al., 2017). Another factor that impacts dissolved oxygen levels is land-use activities occurring along estuaries (Wenner et al., 2004). This is consistent with a study conducted by Lerberg et al. (2000) that investigated the effects of watershed development on tidal creek microbenthic organisms of the Charleston Harbour in the United States. In this study, water samples were also analysed for dissolved oxygen, and it was found that estuaries impacted by industrialisation and urbanisation had lower dissolved oxygen levels. Nutrients such as nitrogen and phosphorous used in anthropogenic activities are often washed into rivers and estuaries from surface runoff. These nutrients drive excessive growth in phytoplankton which lowers dissolved oxygen levels due to the respiration and decomposition processes of these organisms (O'Boyle et al., 2009).

The water samples were analysed for aluminium, arsenic, cadmium, chromium, copper, iron, lead, magnesium, nickel and zinc; however, the levels of aluminium, chromium, copper, lead, nickel and zinc were all found to be below the detection limit. A reason for this could be that arsenic, cadmium, iron and magnesium are more mobile heavy metals than the others and were easily displaced from sediments they were adsorbed to under certain environmental conditions (Smedley and Kinniburgh, 2001). The concentrations of all heavy metals at sites A, B and C were within the permissible levels as proposed by DWAF (1996) for aquatic ecosystems. In addition, the concentrations of arsenic, cadmium and iron were very low at all sampling sites, and a reason for this could be the dilution of the heavy metals in the water due to a recent rainfall event (Perveen et al., 2017). A noticeable trend in the data was that the concentrations of arsenic, cadmium and magnesium showed a general increase from site A to C except for

iron which had slightly higher levels recorded at site B. A reason for the increases in these levels towards site C at the mouth of the estuary could be due to the land-use activities occurring along the estuary. The land-use along the uMgeni Estuary includes industrial activities and residential and commercial areas, which are the primary sources of heavy metals (Masindi and Muedi, 2018). The major stormwater drainage system leading into the estuary is located near site B, facilitating the easy transport of these heavy metals and other substances from these land-uses into the river system. This is consistent with a study conducted by Perveen et al. (2017) that assessed the levels of heavy metals in the water near an industrial area in Islamabad, Pakistan. The results showed that water samples collected near the industrial site had higher heavy metal concentrations than the water samples collected from other sampling sites. This is also in line with another study conducted by Kinuthia et al. (2020), where the levels of heavy metals in the wastewater were investigated in open drainage channels in Nairobi, Kenya. It was found that the wastewater near an industrial area in Nairobi had higher mercury and lead concentrations than other sampling areas, and this was attributed to the intense land-use activities occurring near the river catchment (Kinuthia et al., 2020). In addition, the cadmium results obtained for the uMgeni Estuary in this study is consistent with the cadmium results obtained in a previous study conducted by Olaniran et al. (2014) that assessed the physicochemical qualities and heavy metal concentrations of the uMgeni River. The water samples were collected seasonally from five sampling sites along the uMgeni River from the mouth to the Inanda dam. The results indicated that cadmium levels in the water of the uMgeni River ranged from 0.073 mg/L to 0.416 mg/L with the maximum cadmium concentration recorded at the mouth (Olaniran et al., 2014).

6.2.2) The effects of physicochemical parameters on the concentrations of heavy metals in water

With time, heavy metals that enter rivers and estuaries adsorb onto sediment particles and settle to the river bed. However, changes to the chemical environment of the river can result in these heavy metals being released into the overlying water column leading to deteriorations in the water quality (Zhang et al., 2018). The levels of pH of water have a significant impact on the mobility of heavy metals. According to Appel and Ma (2002), pH levels significantly influence the adsorption of heavy metals and control the solubility of hydroxides, carbonates and phosphates of heavy metals. High amounts of hydrogen ions due to lower pH levels encourage the cations of many heavy metals to be released into the overlying water column.

In contrast, alkaline pH conditions will favour the adsorption of the heavy metals onto sediments reducing the heavy metal concentrations in the water column (Edmunds et al., 2015). The correlation analyses between pH and each of the heavy metals indicated that an increase in pH was accompanied by decreases in the concentrations of cadmium, iron and magnesium in the water column. This is consistent with the results obtained in a previous study conducted by Olaniran et al. (2014) that assessed the physicochemical parameters and heavy metal concentrations of the uMgeni River. The results obtained for the cadmium and pH concentrations indicated generally lower cadmium concentrations at sites with higher pH levels in comparison to sites that had lower pH levels (Olaniran et al., 2014). This is also consistent with the results obtained in a study conducted by Zhang et al. (2018) that analysed the effects of pH on the release of heavy metals from contaminated sediment. Leaching tests were performed using river water as leachate, and it was found that the release of heavy metals from the contaminated sediment decreased with an increase in pH (Zhang et al., 2018). However, the positive correlation between pH and arsenic indicated that an increase in pH leads to increased arsenic concentrations. A reason for this could be that arsenic is an oxyanion-forming metalloid and the ability of oxyanions to adsorb onto sediments tend to weaken as the pH increases (Smedley and Kinniburgh, 2001). This can lead to an increase in the mobility of arsenic and thus its persistence in the water column even in neutral to slightly alkaline conditions (Smedley and Kinniburgh, 2001; Edmunds et al., 2015). This is consistent with a study conducted by Lerda and Prosperi (1996) that investigated the water quality of a river in Cordoba, Argentina. It was found that arsenic concentrations were relatively high at sampling sites that recorded high pH levels. This is also in line with the findings of another study conducted by Antelo et al. (2005) that assessed the effects of pH on the adsorption of arsenate, a chemical form of arsenic, at the goethite-water interface. The results also showed a decrease in the adsorption of arsenic onto sediments with an increase in pH levels. In addition, the results of the correlation analyses between the levels of pH and each of the heavy metals were not statistically significant. A reason for this could be insufficient evidence to explain the changes in the metal concentrations with respect to the pH levels (Lane et al., 2013). Therefore, the null hypothesis of pH has no effect on the concentrations of arsenic, cadmium, iron and magnesium in the water is not rejected. However, the null hypothesis is not accepted either as there is also no evidence to support the hypothesis that pH has no effect on these heavy metal concentrations (Lane et al., 2013).

Electrical conductivity measures the ability of water to conduct electric currents and is dependent on the concentrations of salts dissolved in the water as salts are ionic and are capable of conductive electric currents (USEPA, 2021). Therefore, electrical conductivity gives a good indication of the salinity levels, which indicates the concentrations of salts in the water. The higher the electrical conductivity levels of an aquatic environment, the higher the number of dissolved salts and thus the higher salinity levels (Du Laing et al., 2008; USEPA, 2021). The salinity levels of aquatic ecosystems can cause the solubility and bioavailability of heavy metals to either increase or decrease depending on the composition of the solution (Usman, 2015). According to Hacısalihoğlu and Karaer (2016), an increase in electrical conductivity causes a decrease in the adsorption of heavy metals onto sediment. High conductivity levels indicate high amounts of salts in the water, and these salts are cations that can be exchanged with heavy metals stored in sediment in a process known as cation exchange (Keniston, 2015). This, in turn, releases the heavy metals into the overlying water column; thus, higher electrical conductivity levels lead to an increase in the desorption of heavy metals from sediments (Keniston, 2015). The correlation analyses between electrical conductivity and each of the heavy metals indicated that as electrical conductivity increased, arsenic and iron concentrations in the water column of the uMgeni Estuary increased. This is consistent with a study conducted by Hacısalihoğlu and Karaer (2016) that assessed the relationships between heavy metals in sediment and water in Lake Uluabat, Turkey. The results of the study also indicated positive correlations between heavy metals and electrical conductivity. However, the opposite was observed for cadmium and magnesium, where an increase in electrical conductivity caused a decrease in cadmium and magnesium concentrations in the water column.

A reason for this could be high levels of organic matter discharged into the estuary from land-use activities (Johansson, 2014). The organic matter causes heavy metals to readily adsorb onto their surface, reducing the heavy metals' mobility and bioavailability (Brady and Weil, 2007; Kumar et al., 2015). According to Karaca (2004), organic matter has a high cation exchange capacity, which facilitates the formation of chelating complexes with heavy metals such as cadmium, which immobilises the heavy metals. According to Johansson (2014), cadmium adsorbs onto the organic matter in aerobic conditions, forming hydroxide complexes, reducing the number of free cadmium ions in the water column. The adsorption of heavy metals under high organic matter conditions is enhanced provided the organic ligands form a strong complex with the heavy metal ion and has a strong affinity with the surface (Narwal and Singh, 1998). These results were in line with the findings obtained in a study conducted by Kumar et al.

(2015) that assessed the relationship between the concentrations of heavy metals and salinity gradients and the accumulation of heavy metals in mussels. It was found that the concentrations of heavy metals, including cadmium, were lower in sampling sites with high salinity levels. The sampling sites with high salinities also had high electrical conductivity; therefore, heavy metal concentrations also decreased with increasing electrical conductivity. In addition, the results of the correlation analyses between the levels of electrical conductivity and arsenic, iron and magnesium were not statistically significant. A reason for this could be inadequate evidence to explain the changes in the heavy metal concentrations with respect to the electrical conductivity levels (Lane et al., 2013). Therefore, the null hypothesis of the electrical conductivity has no effect on the arsenic, iron and magnesium concentrations in the water is not rejected. However, the null hypothesis is not accepted either as there is no evidence to support the null hypothesis that electrical conductivity has no effect on these heavy metal concentrations (Lane et al., 2013). However, the results were statistically significant for the correlation between cadmium concentrations in the water and electrical conductivity.

The desorption of heavy metals from sediments and into the overlying water column occurs in aerobic conditions, and anaerobic or anoxic conditions typically favour adsorption of the heavy metals onto sediments (Li et al., 2013). The correlation analyses between dissolved oxygen and each of the heavy metals indicated that as dissolved oxygen levels increased, cadmium and iron concentrations in the water increased. This is in line with the results obtained from a study conducted by Li et al. (2013) that investigated the effects of dissolved oxygen on the release of heavy metals from storm sewer sediments. It was found that the release of zinc, chromium, copper and lead heavy metals from sediments and into the overlying water column increased in sampling sites with high dissolved oxygen levels in comparison to hypoxic sites. However, the opposite was observed for arsenic and magnesium, where the arsenic and magnesium concentrations in the water decreased with increasing dissolved oxygen levels. A reason for this could be the formation of ionic bonds by reducible heavy metals and iron and manganese hydroxides which facilitate the adsorption of heavy metals onto sediments (Atkinson et al., 2007). According to Huang et al. (2017), the oxidation of iron and manganese ions is more rapid under high dissolved oxygen conditions, facilitating the formation of hydroxides that adsorb dissolved heavy metals, subsequently decreasing desorption. This can explain the trend of a decrease in heavy metal concentrations in the water column with increasing dissolved oxygen levels (Huang et al., 2017). This is consistent with a study conducted by Atkinson et al. (2007) that assessed the effects of dissolved oxygen in the overlying water on metal release

from marine sediments polluted with heavy metals. The results indicated lower heavy metal concentrations in the water column in sites that contained high dissolved oxygen levels. In addition, the results of the correlation analyses between the levels of dissolved oxygen and arsenic, cadmium, iron and magnesium were not statistically significant. A reason for this could be insufficient evidence to explain the changes in the heavy metal concentrations with respect to the dissolved oxygen levels (Lane et al., 2013). Therefore, the null hypothesis that dissolved oxygen has no effect on the arsenic, cadmium, iron and magnesium concentrations in the water is not rejected. However, the null hypothesis is not accepted either as there is no evidence to support the null hypothesis that dissolved oxygen has no effect on these heavy metal concentrations (Lane et al., 2013).

6.2.3) The effects of certain constituents on the spectral reflectance of water

When a ray of light incident on a non-opaque surface is redirected, a process known as reflection occurs (Aggarwal, 2004). The spectral reflectance of an object on the earth's surface is the ratio of reflected energy to incident energy as a function of wavelength (Navalgund, 2001). With respect to the spectral reflectance of water, the majority of the energy striking the water's surface is either absorbed or transmitted, and very little of this energy is reflected (Aggarwal, 2004). However, according to Aggarwal (2004), some factors may influence the reflection characteristics of a water body, including the depth of the water body, roughness of the water's surface and the chemical and physical constituents present in the water column. According to Navalgund (2001), constituents such as dissolved gases and most inorganic salts do not influence the spectral reflectance of water. In contrast, constituents such as turbidity and organic and inorganic material cause an increase in the spectral reflectance of water, and the reflectance peaks occur along longer wavelengths.

The raw spectral reflectance curve obtained for the water samples in this study displays high spectral reflectance peaks occurring over longer wavelengths, indicating that some constituents present in the water are responsible for the higher reflectance. The constituents that could be responsible for the observed higher reflectance include suspended sediment particles as well as organic and inorganic matter (Navalgund, 2001). This is consistent with the results obtained by a study conducted by Lodhi et al. (1998), where water spectral reflectance containing different suspended sediment concentrations was analysed. The results indicated that water samples containing high levels of suspended sediments displayed higher reflectance across all wavelengths, with clear water displaying the lowest reflectance across all wavelengths. It was

also observed that the reflectance peaks of samples with higher suspended sediment concentrations occurred over longer wavelengths than the reflectance peaks for clear water (Lodhi et al., 1998). The results are also in line with the results obtained in a study conducted by Karabulut and Ceylan (2005), where a portion of the study focused on the spectral reflectance of water with varying levels of organic matter. In the experiments, the sediment samples were analysed for organic matter and were added to different tanks filled with water, each with sediments of different organic matter content. The water was then mixed to allow the sediments to remain in suspension, and the spectral reflectance was recorded to observe the differences in the reflectance of the water with respect to varying organic matter levels. The results indicated that water containing suspended sediment with higher organic matter content displayed higher reflectance than the water containing suspended sediment with lower organic matter content (Karabulut and Ceylan, 2005).

6.2.4) Effects of outliers on the results of calibration models

The results of the PCA scores plot identified an outlier sample that was scattered further away from the rest of the samples on the PCA plot. This outlier sample was removed prior to the development of the calibration model in order to improve the prediction results. The resulting model without the outlier sample increased the R^2 and decreased the RMSE values leading to better prediction results. This is consistent with the results obtained in a study conducted by Todorova et al. (2014) that analysed the potential of near-infrared spectroscopy for estimating heavy metals in soil. The results of the PCA scores plot identified six outlier samples, and calibration models were developed on all the samples as well as on the remaining samples after the outliers were removed. It was found that the model produced better results on the exclusion of the outlier samples (Todorova et al., 2014). These results were also consistent with the results obtained in a study conducted by Siebielec et al. (2004) that assessed the use of near- and mid-infrared reflectance spectroscopy in estimating the metal concentrations of soil. It was found that removing sample outliers improved the prediction results for the remaining samples in the dataset. According to Siebielec et al. (2004), removing sample outliers improves the predictions as the calibration model is not impacted by less useful information.

6.2.5) Prediction of the concentrations of heavy metals and water quality parameters in the water samples using visible and near-infrared spectroscopy

The fourth objective of this study was to develop calibration models for the prediction of heavy metals from spectral reflectance measurements. The calibration and cross-validation R^2 and RMSE values were evaluated to determine the predictive accuracies of the models. The calibration R^2 indicates how well the model performs in predicting the calibration data, and the cross-validation R^2 indicates how well the model performs in predicting new data (Bevilacqua and Bro, 2020). The prediction results for the parameters in water from the most accurate to the least accurate in terms of R^2 calibration were magnesium, pH, electrical conductivity, cadmium, arsenic and iron. The prediction results for the parameters in water from the most accurate to the least accurate in terms of R^2 cross-validation were magnesium, pH, iron, electrical conductivity, cadmium and arsenic.

However, according to Scott (2019) and Bevilacqua and Bro (2020), a good Q^2 value, which is the R^2 of the prediction data or the R^2 of the cross-validation data in this study, is a value that is close to the R^2 of the calibration data. This indicates that the model works independently of the data used in the calibration (Scott, 2019). In addition, according to Veerasamy et al. (2011), the difference between R^2 calibration and R^2 cross-validation should not be large and should not be more than 0.3. The larger the difference between R^2 calibration and R^2 cross-validation, the more inaccurate and less reliable the results are (Bevilacqua and Bro, 2020). The R^2 calibration and R^2 cross-validation results obtained for the predictions of this study's heavy metals and water quality parameters were close to each other. The differences between the R^2 calibration and R^2 cross-validation were <0.3 for all parameters except iron which had a difference of 0.32. Therefore, the least accurate prediction overall was obtained for iron. There is very limited research done on the use of spectroradiometers in water quality assessments; therefore, the comparison of all the water quality parameters observed in this study with the results of previous studies was difficult. The results obtained for iron is consistent with a study conducted by Monaledi (2019), where remote sensing was used to assess the water quality of the Mooi River in Carletonville, South Africa. In the study, an ASD spectroradiometer was also used to assess the spectral reflectance of the water samples, and a support vector machine regression model was used to estimate the concentrations of the water quality parameters from the spectral reflectance data. The model also produced poor prediction accuracies for iron, where the model overestimated the laboratory-measured low iron

concentrations, and the laboratory-measured high iron concentrations were underestimated by the model (Monaledi, 2019).

The prediction results for arsenic, cadmium, iron, and electrical conductivity obtained in this study ranged between very low and low accuracies with R^2 calibration and R^2 cross-validation ranging from below 0.19 to between 0.19 and 0.32. A reason for the very low and low accuracies achieved for arsenic, cadmium, and iron could be the low concentrations of these heavy metals observed in the water column. This is consistent with a study conducted by Hively et al. (2011) that assessed the use of airborne hyperspectral imagery in mapping soil parameters of tilled agriculture soil on the Eastern Shore of Chesapeake Bay, United States. In this study, reflectance spectra were extracted from hyperspectral imagery of the study area, and soil samples were collected and analysed for carbon content and specific elements. A PLS regression was then performed to predict the concentrations of the soil parameters from the reflectance spectra. It was found that the model predicted soil parameters with low concentrations poorly in comparison with the results of the other parameters (Hively et al., 2011). Therefore, the low predictive accuracies obtained for these heavy metals were likely associated with the low concentrations of these heavy metals in the water.

The low predictive accuracy obtained for electrical conductivity could be associated with greater variability in the data and the small sampling size used in this study (Todorova et al., 2014). According to Kuang and Mouazen (2013), for parameters with high variability in their datasets, a higher number of samples is required in order to account for the variability. This is consistent with a study conducted by Todorova et al. (2014), where near-infrared spectroscopy was used to estimate heavy metal concentrations in soils. The study also evaluated the effect of sample size on the PLS regression model results, and it was found that an increase in the sample size led to an improvement in the prediction accuracies (Todorova et al., 2014). The prediction results for pH and magnesium, on the other hand, achieved moderate accuracies. A reason for this could be the smaller variability in the data for pH and the higher concentrations of magnesium in the water compared to the other parameters (Kuang and Mouazen, 2013). This is also in line with the results of the study conducted by Monaledi (2019), where the model also produced good results for magnesium and pH as both parameters were predicted with high accuracies.

In addition to evaluating the calibration and cross-validation R^2 values, it is also essential to note the RMSE values of the models. A model with low RMSE values is generally desired as

this would indicate a good quality model as the RMSE represents the concentrations of the heavy metals that may not be described by the model (Estifanos, 2006). If these values are high, despite having relatively good calibration and cross-validation R^2 results, it could lead to wrongful assumptions of the heavy metal contamination in the area under study (Estifanos, 2006). The RMSE values were low for pH, arsenic, cadmium and iron, indicating that these model results are reliable. However, the RMSE values for electrical conductivity and magnesium were higher and indicate that these model results are less accurate and reliable. A reason for the higher RMSE values for electrical conductivity and magnesium could be the greater variability in the data for these parameters and the small sample size; thus, a larger sample size would be required to improve the accuracies of these results (Kuang and Mouazen, 2013). The best model for the prediction of water quality parameters was achieved for the prediction of pH levels as the calibration and cross-validation R^2 values achieved were moderate with low RMSE values. In terms of the prediction of heavy metals in water from the VNIR spectrum, the best model was obtained for arsenic. Although the model for arsenic produced very low calibration and cross-validation R^2 values, the difference between the calibration and cross-validation R^2 values was the lowest compared to the other heavy metals and it also had low calibration and cross-validation RMSE values.

6.2.6) Important wavelengths for the prediction of heavy metals and water quality parameters in water

The fifth objective of this study was to assess the relationship between the heavy metals and the VNIR reflectance spectra. When a particular wavelength region in a spectral reflectance curve displays high amounts of reflectance, it forms a peak in the curve (Srivastava, 2021). When there is low reflectance at a particular wavelength region, this causes a trough or valley in the curve; thus, the peaks represent a strong reflection of incident energy, and the troughs represent the predominant absorption of energy (Srivastava, 2021). Therefore, a decrease in reflectance at a particular wavelength region will form absorption features.

In statistics, the regression coefficient is the slope of the regression of the response variable on the predictor variable and provides information on the change in the response variable per change in the predictor variable (Mark and Workman, 2018). The regression coefficients plot displays the positive and negative peaks of the predictor variable; that is, the VNIR spectra and the heights of these peaks represent the significance of those wavelengths in the prediction model (Estifanos, 2006). The positive peaks indicate a positive correlation between the heavy

metal or water quality parameter and the VNIR spectra, while the negative peaks indicate a negative correlation between the heavy metal or water quality parameter and the VNIR spectra (Mark and Workman, 2018). The positive peaks can thus indicate reflectance peaks, and the negative peaks can indicate absorption features. Therefore, the regression coefficients plots from the PLS regression model can be used to identify the significant wavelengths in the VNIR spectra for the prediction of heavy metals and water quality parameters (Todorova et al., 2014).

According to Gómez (2014), absorption and backscattering coefficients are impacted by the optical properties of pure water and the dissolved substances in the water column. Therefore, absorption and backscattering of water and the particles dissolved in the water essentially make up reflectance spectra (Gómez, 2014). Absorption features present in the VNIR and SWIR spectral regions occur due to electronic and vibrational processes (Fang et al., 2018). Electronic processes occur in isolated ions where absorption of photons at certain wavelength regions occurs, causing the ion's energy state to move to a higher state (Fang et al., 2018). In contrast, the reduction of the energy state to a lower energy state leads to a photon being emitted (Estifanos, 2006). Crystal field transitions in mineral spectra are responsible for electronic transitions as a result of vacant electron shells (Estifanos, 2006). In the case of transition metals, ions located in a crystal field have split orbital energies compared to isolated ions, resulting in the absorption of a photon that moves an electron from a lower to a higher energy state (Fang et al., 2018). The splitting of orbital energies differs from mineral to mineral, causing an ion to display different absorption features. In addition, the energy levels of an electron are influenced by the valence state of an element, the type of ligands, and the distance between the heavy metal and ligand (Fang et al., 2018). In vibrational processes, a molecule is subject to vibrations depending on the strength of the bonds between the molecule and the molar mass of the elements in the molecule (Estifanos, 2006). The vibrational processes of water and hydroxides lead to overtone absorptions (Sakudo et al., 2006). In addition, certain minerals display absorption features in the VNIR spectral region due to overtones and vibrational processes associated with the stretching and bending of molecular bonds, including O-H, C-H, C-C and N-H (Fang et al., 2018). For example, according to Crowley et al. (2003), photons close to 1400 nm are absorbed by water molecules for O-H stretching.

Water displays absorption features in the 400-2500 nm spectral range, which occurs due to three vibrational modes of the water molecule, including symmetrical stretching, bending and asymmetrical stretching (Davies and Calvin, 2016). Pure heavy metals display no absorption

in the NIR spectral region, and reflectance peaks observed in the spectral reflectance curves can be attributed to the presence of dissolved substances such as heavy metals (Putra et al., 2012; Seifi et al., 2019). However, the formation of heavy metal complexes with organic matter containing O-H bonds can indicate the presence of heavy metals (Nomngongo et al., 2017). The absorption properties of water, particularly the O-H overtones, can be altered due to the binding reaction with the heavy metal ion. According to Putra et al. (2012), the absorption features of heavy metals related to the stretching and bending of organic molecules, hydroxyl and carboxyl groups in water can be detected from the 780–2500 nm spectral region.

The absorption features between 715 and 718 nm for arsenic, cadmium and magnesium heavy metals, as seen in figure 5.25, can be attributed to those absorption features being close to the water band. According to Sakudo et al. (2006), the third overtone of the hydroxide-stretching mode of water is assigned to the absorption features close to 760 nm. Therefore, the absorption features for these heavy metals located between 715 and 718 nm may result from absorbed water (Sakudo et al., 2006). The absorption features located between 1134 and 1136 nm for pH, electrical conductivity and iron, as depicted in figure 5.25, can be attributed to hydroxide activity (Heiman and Licht, 1999). This is consistent with a study conducted by Seifi et al. (2019) that investigated the visible-infrared spectroscopy and chemical properties of water near a mining area. The absorption features were analysed, and it was also found that the absorption features related to pH and electrical conductivity were found in the wavelength regions close to 975 nm. Another study conducted by Estifanos (2006) that analysed the spectral indicators for assessing pollution in a gold mining area in Rodalquilar, Spain. Sediment samples were collected from the study area, and one portion of the study involved dissolving 10 g of each sample in water and analysing the heavy metal, pH and electrical conductivity levels as well as the spectral reflectance of the water samples using ICP-OES and ASD, respectively. The results indicated that the absorption features in the spectra related to pH and electrical conductivity occurred in the regions 825-1036 nm (Estifanos, 2006). According to Zabcic (2008) and Seifi et al. (2019), the causes of absorption features at 450 nm and between the regions 550-650 nm, 750-950 nm and 900-1100 nm are a result of crystal field electronic transitions in ferrous (Fe^{2+}) and ferric (Fe^{3+}) iron oxidation states. Ferrous iron crystal field transitions generally occur at longer wavelengths in comparison to ferric iron crystal field transitions (Estifanos, 2006). This accounts for the absorption feature located at 1135 nm for iron, indicating an electronic transition of ferrous iron. These results are also consistent with

the findings of Putra et al. (2012), where absorption features for heavy metals were found between the 780-2500 nm wavelength range.

6.2.7) Factors influencing the concentrations of heavy metals in the sediments of estuaries

The sediment samples of the uMgeni Estuary were analysed for ten heavy metals, including aluminium, arsenic, cadmium, chromium, copper, iron, lead, magnesium, nickel and zinc. However, cadmium levels in the sediment were found below the detection limit at all sampling sites; thus, cadmium was excluded from further analyses. A reason for no detection of cadmium in the sediment could be that cadmium is a highly mobile heavy metal compared to other transition metals (Smedley and Kinniburgh, 2001). Another reason could be an anthropogenic source of cadmium being discharged into the water instead of the source being in situ sediment (Srivastava, 2016). The arsenic, chromium, and lead levels fell within the permissible ERL and ERM limits of the SQGs set by NOAA (1999). However, the permissible ERL limits for copper, nickel and zinc were exceeded at sampling sites A and C, but still fell within the ERM limits. A reason for the higher levels of copper, nickel and zinc in the sediment could be the land-use practices taking place along the uMgeni Estuary (Zheng et al., 2016). In addition, according to Cui et al. (2019), a higher level of copper in the sediment of rivers could be associated with traffic emissions. Furthermore, the concentrations of aluminium, iron and magnesium in the sediment samples displayed significantly higher levels in comparison to the other heavy metals and a reason for this could be that these heavy metals are highly abundant in the earth's crust (Jain et al., 2005).

According to Gabrielyan et al. (2018), the spatial distribution of heavy metals in the water and sediments of rivers is very similar. As with the heavy metal concentrations in the water samples, it was also noticeable that site C showed higher heavy metal concentrations for all heavy metals in the sediment samples compared to sites A and B. A similar trend was observed in a previous study conducted by Dikole (2014) that assessed the heavy metal concentrations in the sediment of the uMgeni River at various sampling sites along the river from the Inanda dam to the estuary. In the study, lead, chromium, copper and zinc concentrations in the sediments ranged from 12.1-601.7 mg/kg, 28.6-135.1 mg/kg, 11.9-168.5 mg/kg and 29.5-602.1 mg/kg, respectively. The results indicated generally higher lead, chromium, copper and zinc concentrations in the sediment at sampling sites closer to the mouth of the river in comparison to other sampling sites (Dikole, 2014). These results are also consistent with the findings of a study conducted by Gabrielyan et al. (2018) that investigated the distribution of the sources of

heavy metals in the Voghji River Basin, Armenia. It was also found that the heavy metal concentrations measured in the sediments were significantly higher at sampling sites near the mouth of the river in comparison to sampling sites further upstream. A reason for this could be the industrial, residential and commercial land-use activities taking place along the uMgeni Estuary (Dikole, 2014; Zheng et al., 2016). This is consistent with the results obtained in a study carried out by Cui et al. (2019), where the heavy metals in the sediment of the urban and rural rivers in Harbin City, Northeast China, were investigated. It was found that the sediments located near urban areas consisting of industrial activities contained significantly higher levels of heavy metals than suburban and rural rivers.

6.2.8) Prediction of the concentrations of heavy metals in the sediment samples using visible and near-infrared spectroscopy

The calibration and cross-validation R^2 and RMSE values were evaluated to determine the predictive accuracies of the models produced to predict heavy metal concentrations from the VNIR reflectance spectra. The predictions obtained for the heavy metals in the sediments from the most accurate to the least accurate in terms of R^2 calibration were nickel, iron, chromium, lead, zinc, magnesium, arsenic, copper and aluminium. The prediction results from the most accurate to the least accurate predictions in terms of R^2 cross-validation were nickel, chromium, lead, zinc, copper, iron, magnesium, arsenic and aluminium. As previously mentioned, an accurate prediction model has a small difference between its R^2 calibration and R^2 cross-validation values (Bevilacqua and Bro, 2020). The differences between the R^2 calibration and R^2 cross-validation results obtained for the predictions of the heavy metals from the spectral reflectance readings of the sediment samples in this study were small for most heavy metals. The differences between the R^2 calibration and R^2 cross-validation were <0.3 for all heavy metals except aluminium which had a difference of 0.48. Therefore, the least accurate prediction overall was obtained for aluminium. A reason for the poor predictive accuracy obtained for aluminium could be greater variability in the data and the small sample size used in this study (Todorova et al., 2014). In order to account for this variability and possibly produce better prediction results for aluminium, a larger dataset is required. According to Delwiche and Reeves (2010), the higher number of samples used will result in a more accurate representation of the relationships between the laboratory-measured heavy metals and the spectral responses.

The high prediction accuracies obtained for lead and nickel in this study is consistent with the prediction results obtained for lead and nickel in a study conducted by Pawar and Deshmukh (2021). The study involved predicting the concentrations of lead and nickel in contaminated soil of agricultural fields in Aurangabad, Maharashtra, India, using an ASD FieldSpec 4 spectroradiometer. A PLS regression model was built, and the R^2 results obtained for the prediction of lead and nickel were 0.96 and 0.95, respectively. A reason for the high predictive accuracies obtained for heavy metals including arsenic, chromium, copper, lead, nickel and zinc, despite the small sample size, could be a smaller variability in the dataset for these heavy metals (Kuang and Mouazen, 2013). However, the sample size could affect the reliability of these results; therefore, it is also important to evaluate the RMSE values for the models (Estifanos, 2006; Delwiche and Reeves, 2010).

The RMSE values obtained for arsenic, chromium, copper, lead, nickel and zinc were relatively low, indicating that the prediction results obtained for these heavy metals were accurate and reliable. The low RMSE results obtained for the prediction of copper, nickel and zinc is consistent with the low RMSE values obtained for these heavy metals in a study conducted by Wang et al. (2017). The study involved the estimation of heavy metals in soils of a metal tailing pond in the Anhui Province of China using multispectral remote sensing imagery. The spectral reflectance was extracted from the imagery, and soil samples were collected and analysed for copper, nickel and zinc. Thereafter, a PLS regression was developed to predict the concentrations of these heavy metals, and the model resulted in good predictions for copper, nickel and zinc with low RMSE values (Wang et al., 2017). However, the RMSE values obtained for aluminium, iron and magnesium were high; therefore, these models are less accurate and reliable. A reason for this could be that there was greater variability in the data for aluminium, iron, and magnesium compared to the other heavy metals, and the sample size was too small to account for the greater variability (Delwiche and Reeves, 2010; Kuang and Mouazen, 2013). According to Xu et al. (2021), to accurately estimate heavy metals in soils using VNIR spectroscopy, it is crucial to ensure that the soil samples are representative and the sample size is sufficient. Therefore, to improve the accuracy and reliability of these results, a larger dataset would be required. The best model overall was achieved for the prediction of nickel levels as the calibration and cross-validation R^2 values achieved were high with low RMSE values.

6.2.9) Important wavelengths for the prediction of metals and water quality parameters in sediment

The spectral reflectance of soil is impacted by soil moisture content, iron oxides and organic matter content. Soils with high moisture content and high concentrations of iron oxides and organic molecules tend to cause the soil to become darker in colour, causing an increase in the absorption of light in the soil and a decrease in reflectance (Tekin et al., 2012). According to Tekin et al. (2012), the absorption of light in the near-infrared (NIR) spectral region by organic molecules is caused by overtones and combination bands of C-H, N-H and O-H groups that are associated with molecular stretching in the mid-infrared spectral region. The amount of energy absorbed is specific to the type of bond and is also influenced by the chemical matrix and factors, including the kind of functional group, adjacent molecules and hydrogen bonds (Armenta and de la Guardia, 2014). Heavy metals do not display absorption features in the NIR spectral region; however, heavy metal detection in the NIR region is possible due to covariation with other active spectral components such as organic matter, hydroxides, oxides and carbonates (Wu et al., 2007; Armenta and de la Guardia, 2014).

The significant wavelengths for the prediction of arsenic, chromium, copper, lead and zinc obtained from the regression coefficient plots of this study were similar to the results obtained by Estifanos (2006) and Xu et al. (2021). According to the results obtained in the study previously mentioned conducted by Estifanos (2006), where another portion of the study investigated the use of the VNIR spectral region in predicting heavy metals in sediment. The results of this study indicated the spectral indicator regions important for the prediction of arsenic included 876-973 nm, 1397-1474 nm, 1882-1992 nm and 2125-2160 nm, the spectral indicator regions for zinc included 413-513 nm, 573-765 nm, 873-1101 nm and 2041-2139 nm and the spectral indicator regions for lead included 452-572 nm and 1190-1243 nm. According to the results obtained by a study conducted by Xu et al. (2021), where the VNIR spectroscopy was used to estimate heavy metals in the agricultural soils of the Suzi River Basin of the Liaoning Province, Northeast China. It was found that the important wavelengths for the estimation of chromium were 547 nm, 714 nm, 866 nm, 955 nm, 1137 nm, 2342 nm and 2346 nm, and the important wavelengths for the estimation of copper were 667 nm, 923 nm, 980 nm, 1015 nm, 1129 nm and 1562 nm.

The absorption features occurring from 900-1100 nm can be attributed to the crystal field electronic transitions in ferrous (Fe^{2+}) and ferric (Fe^{3+}) iron oxidation states with ferrous iron crystal field transitions occurring at longer wavelengths (Estifanos, 2006; Zabcic, 2008; Zheng et al., 2019) Therefore, the absorption features observed near 1090 nm for the heavy metals can be attributed to the crystal field electronic transitions of ferrous iron. According to Todorova et al. (2014), the absorption features located close to 1500 nm are associated with the absorption of amine N-H vibrational processes in organic components. Absorption features occurring near 1550-1650 nm are associated with the N-H bending vibrations of primary amines (Reusch, 2013). Therefore, the absorption feature located between 1675 nm and 1678 nm for the heavy metals could be linked to the absorption of N-H bending vibrations of primary amines.

6.3) Limitations

A significant limitation to this study was the time constraints imposed by the ongoing Coronavirus Pandemic that caused devastating effects worldwide. As a result of the many lockdowns imposed in South Africa to try and slow down the spread of the virus, field data collection was difficult to conduct and could not be conducted in 2020. Field sampling could only be conducted in 2021, and due to the limited time remaining, field sampling was only done once. In addition to time constraints, another limitation of the study was cost constraints; thus, a small number of water and sediment samples were collected and analysed. Another limitation was the lockdown imposed in 2020 caused universities to be closed for many months of the year, and laboratory testing machines were not used for a prolonged period. This resulted in the unprecedented breakdown of many machines making it difficult to analyse the samples for heavy metals, which imposed further time constraints. It is for this reason that an independent laboratory had to be used to analyse the sediment samples.

6.4) Conclusion and recommendations

The rapid increase in industrialisation and urbanisation has put a severe strain on the quality of our aquatic ecosystems. The increased use of heavy metals in several human activities has led to increased concentrations of these heavy metals entering watercourses and eventually leading to estuaries. These heavy metals in excess can cause severe health complications in the organisms that inhabit aquatic ecosystems, thus making it imperative to ensure the frequent monitoring of the levels of heavy metals so that there can be intervention if need be. However, conventional methods of testing water and sediment for heavy metals are extremely costly

when required regularly; therefore, it is necessary to include alternate methods that are more cost-effective.

The aim of this study was to assess the use of visible and near-infrared reflectance spectroscopy in the detection of heavy metals in the water and sediment of the uMgeni Estuary. The results obtained for the water and sediment analyses indicated that the heavy metal concentrations were much higher in the sediment than in the water of the uMgeni Estuary. Furthermore, the heavy metals fell within the permissible limits of the target water quality range guidelines and sediment quality guidelines. However, the concentrations of copper, nickel and zinc exceeded the effects range low limit of the sediment quality guidelines, which indicate the levels below which toxic effects rarely occur. Therefore, copper, nickel and zinc could potentially cause toxic effects in aquatic organisms inhabiting the estuary. Thus, the concentrations of these heavy metals in the uMgeni Estuary should be regularly monitored so that there can be proper intervention should the concentrations of these heavy metals continue to increase.

Heavy metals are featureless in the visible and near-infrared region; however, their indirect detection is possible by association with other detectable constituents. The results of the calibration models indicated that the models performed much better in predicting the heavy metal concentrations in the sediment compared to the heavy metal concentrations in the water. Most of the heavy metals in the sediments were predicted with high accuracy compared to the low accuracy predictions obtained for most of the water quality parameters and heavy metals. The best model for the prediction of heavy metals in the sediment was obtained for nickel with high calibration and cross-validation R^2 values and low RMSE values. The best model for the prediction of water quality parameters was obtained for pH with moderate calibration and cross-validation R^2 values and low RMSE values. The best model for the prediction of heavy metals in the water was obtained for arsenic. Although the model for arsenic produced very low calibration and cross-validation R^2 values, the difference between the calibration and cross-validation R^2 values was the lowest compared to the other metals and it also had low calibration and cross-validation RMSE values. A reason for the lower prediction accuracies obtained for the heavy metals in the water could be that the calibration models are sensitive to analytes with very low concentrations, as observed for the metals in the water. In addition, greater variability in datasets also impacts the accuracies of calibration models. The results of previous studies indicated that using larger datasets could improve the prediction accuracies of the models as the larger sample size can account for the large variations in the data. The results of the

regression coefficients plots indicated that the important wavelengths for the detection of pH, electrical conductivity, arsenic, cadmium, iron and magnesium in the water were from 715-725 nm, at 929 nm, and from 1134-1137 nm, 1663-1667 nm and 1707-1731 nm. The regression coefficient plots also indicated that the important wavelengths for the detection of aluminium, arsenic, chromium, copper, iron, lead, magnesium, nickel and zinc in the sediment were from 1090-1091 nm, 1278-1284 nm, 1392-1398 nm, 1471-1479 nm and 1675-1678 nm.

The visible and near-infrared spectrum provides a time- and cost-effective way to predict heavy metals and their concentrations, especially from sediments, as it facilitates the analysis of a large number of samples and reduces the need for lengthy chemical processes and the need to purchase chemicals. However, a limitation to using the visible and near-infrared spectrum in predicting heavy metals is a reduced accuracy in the prediction of heavy metals with a greater variability in their concentrations. For this reason, visible and near-infrared reflectance spectroscopy should not be used to replace conventional methods of analysing heavy metals in water and sediment entirely but rather to complement them. Reflectance spectroscopy as a tool to analyse heavy metals in environmental samples is still relatively new, and more research needs to be conducted to improve the accuracy of predictions.

In terms of recommendations for future research on the use of the visible and near-infrared spectrum in predicting heavy metals in water and sediment, it is recommended that a larger dataset be used to minimise the effects of highly variable data on prediction results. It is also recommended to determine the effects of low analyte concentrations on the performance of the calibration models in predicting heavy metals. The effects of other soil constituents such as organic matter and soil organic carbon on the spectral reflectance of soil and how these constituents impact the detection of spectral indicator regions to predict heavy metals should also be explored further. In addition, it is recommended to determine the effects of the valency of ions in detecting spectral indicator regions for the prediction of heavy metals as valency may influence the interaction of ions with water and sediment.

References

Abbas, G., Murtaza, B., Bibi, I., Shahid, M., Niazi, N.K., Khan, M.I., Amjad, M. and Hussain, M., 2018. Arsenic uptake, toxicity, detoxification, and speciation in plants: physiological, biochemical, and molecular aspects. International Journal of Environmental Research and Public Health, 15(1), p.59.

Abed, R., 2009. An investigation into the suspended sediment flux and dynamics of the Mgeni estuary, Durban. MSc. University of KwaZulu-Natal.

Abdi, H., 2003. Partial least square regression (PLS regression). Encyclopaedia for Research Methods for the Social Sciences, 6(4), pp.792-795.

Adekunle, A.S. and Eniola, I.T.K., 2008. Impact of industrial effluents on quality of segment of Asa River within an industrial estate in Ilorin, Nigeria. New York Science Journal, 1(1), pp.17-21.

Adeogun, A.O., Babatunde, T.A. and Chukwuka, A.V., 2012. Spatial and temporal variations in water and sediment quality of Ona River, Ibadan, Southwest Nigeria. European Journal of Scientific Research, 74(2), pp.186-204.

Agency for Toxic Substances and Disease Registry (ATSDR)., 2012. Toxguide for cadmium. CAS# 7440-43-9. [Online]. Available at https://www.atsdr.cdc.gov/toxguides/toxguide-5.pdf [Accessed: 16 February 2022].

Aggarwal, S., 2004. Principles of remote sensing. In Satellite Remote Sensing and GIS Applications in Agricultural Meteorology, 23, pp.23-28.

Agrawal, R.V. and Deshmukh, R.R., 2018. Develop non-destructive database of seasonal fruits and reviews on spectral pre-processing techniques. International Journal of Emerging Trends and Technology in Computer Science, 7(2), pp.090-094.

Ahmad, M.S.A. and Ashraf, M., 2012. Essential roles and hazardous effects of nickel in plants. Reviews of Environmental Contamination and Toxicology, pp.125-167.

Akpor, O.B., Ohiobor, G.O. and Olaolu, D.T., 2014. Heavy metal pollutants in wastewater effluents: sources, effects and remediation. Advances in Bioscience and Bioengineering, 2(4), pp.37-43.

Akram, Z., Fatima, M., Shah, S.Z.H., Afzal, M., Hussain, S.M., Hussain, M., Khan, Z.I. and Akram, K., 2019. Dietary zinc requirement of Labeo rohita juveniles fed practical diets. Journal of Applied Animal Research, 47(1), pp.223-229.

Alam, J.B. (Md.), Islam, M.R., Muyen, Z., Mamun, M. and Islam, S., 2007. Water quality parameters along rivers. International Journal of Environmental Science and Technology, 4(1), pp.159-167.

Ali, H., Khan, E. and Ilahi, I., 2019. Environmental chemistry and ecotoxicology of hazardous heavy metals: environmental persistence, toxicity, and bioaccumulation. Journal of chemistry, 2019, pp.1-14.

Analytical Spectral Devices (ASD), Inc., 2000. FieldSpec Pro User's Guide (Boulder, Colorado: Analytical Spectral Devices, Inc.).

Anderson, D.M., Glibert, P.M. and Burkholder, J.M., 2002. Harmful algal blooms and eutrophication: nutrient sources, composition, and consequences. Estuaries, 25(4), pp.704-726.

Antelo, J., Avena, M., Fiol, S., López, R. and Arce, F., 2005. Effects of pH and ionic strength on the adsorption of phosphate and arsenate at the goethite–water interface. Journal of Colloid and Interface Science, 285(2), pp.476-486.

Appel, C. and Ma, L., 2002. Concentration, pH, and surface charge effects on cadmium and lead sorption in three tropical soils. Journal of Environmental Quality, 31(2), p.581.

Armenta, S. and de la Guardia, M., 2014. Vibrational spectroscopy in soil and sediment analysis. Trends in Environmental Analytical Chemistry, 2, pp.43-52.

Arnous, M.O. and Hassan, M.A., 2015. Heavy metals risk assessment in water and bottom sediments of the eastern part of Lake Manzala, Egypt, based on remote sensing and GIS. Arabian Journal of Geosciences, 8(10), pp.7899-7918.

Ashraf, M.A., Maah, M.J. and Yusoff, I., 2011. Introduction to remote sensing of biomass. In Biomass and Remote Sensing of Biomass, pp.129-170. IntechOpen.

Atkinson, C.A., Jolley, D.F. and Simpson, S.L., 2007. Effect of overlying water pH, dissolved oxygen, salinity and sediment disturbances on metal release and sequestration from metal contaminated marine sediments. Chemosphere, 69(9), pp.1428-1437.

Azevedo, J.W.D.J., Castro, A.C.L.D. and Santos, M.C.F.V.D., 2016. Siltation rate and main anthropic impacts on sedimentation of the São Luís tidal inlet-State of Maranhão, Brazil. Brazilian Journal of Oceanography, 64(1), pp.9-18.

Banda, T.D. and Kumarasamy, M., 2020. Development of a Universal Water Quality Index (UWQI) for South African River Catchments. Water, 12(6), p.1534.

Barbier, E.B., Hacker, S.D., Kennedy, C., Koch, E.W., Stier, A.C. and Silliman, B.R., 2011. The value of estuarine and coastal ecosystem services. Ecological Monographs, 81(2), pp.169-193.

Barker, S. and Ridgwell, A., 2012. Ocean acidification. [online]. Nature Education. Available at: https://www.nature.com/scitable/knowledge/library/ocean-acidification-25822734/ [Accessed: 03 September 2021].

Bartram, J. and Ballance, R. (eds.)., 2020. Water quality monitoring: a practical guide to the design and implementation of freshwater quality studies and monitoring programmes. CRC Press.

Beachwood Mangroves Nature Reserve., 2013. Beachwood Mangroves Nature Reserve: Protected Area Management Plan. Ezemvelo KZN Wildlife, Pietermaritzburg. [Online]. Available at: http://www.kznwildlife.com/Documents/ApprovedProtectedAreaManagementPlans/beachwood_mangroves_mp_a_072014.pdf [Accessed: 17 February 2022].

Begg, G. W., 1978. The estuaries of Natal. Natal Town and Regional Planning Report 41, Pietermaritzburg, South Africa.

Bell, R., Green, M., Hume, T. and Gorman, R., 2000. What regulates sedimentation in estuaries? Water and Atmosphere, 8(4), pp.13-16.

Bellhouse, D.R., 2005. Systematic sampling methods. Encyclopaedia of Biostatistics, 8.

Bevilacqua, M. and Bro, R., 2020. Can we trust score plots? Metabolites, 10(7), p.278.

Birkhofer, K., Diehl, E., Andersson, J., Ekroos, J., Früh-Müller, A., Machnikowski, F., Mader, V.L., Nilsson, L., Sasaki, K., Rundlöf, M. and Wolters, V., 2015. Ecosystem services—current challenges and opportunities for ecological research. Frontiers in Ecology and Evolution, 2 (87), pp.1-12.

Bisht, A.S., 2019. Bioavailability of Metals in Sediment. In Commercial Surfactants for Remediation, pp.9-11. Springer, Singapore.

Bogrekci, I. and Lee, W.S., 2004. The effects of soil moisture content on reflectance spectra of soils using UV-VIS-NIR spectroscopy. In Proceedings of 7th International Conference on Precision Agriculture.

Borengasser, M., Hungate, W.S. and Watkins, R., 2007. Imaging spectrometers: operational considerations. In Hyperspectral Remote Sensing: Principles and Applications. CRC Press, 21: London.

Boss, B.C. and Fredeen, K.J., 1997. Concepts, instrumentation and techniques in inductively coupled plasma optical emission spectrometry. Perkin Elmer Corporation 2nd edition.

Bot, A. and Benites, J., 2005. The importance of soil organic matter: Key to drought resistant soil and sustained food production. Food and Agricultural Organisation (FAO) of the United Nations, Rome.

Boyd, C.E., 2015. pH, carbon dioxide, and alkalinity. Water Quality, pp. 153-178. Springer, Cham.

Bradl, H.B., 2005. Sources and origins of heavy metals. Interface Science and Technology, 6, pp.1-27. Elsevier.

Brady, N.C. and Weil, R., 2007. Soil colloids: Seat of soil chemical and physical acidity. In Elements of the Nature and Properties of Soil, 15th edition, Pearson.

Brand, J.H., Spencer, K.L., O'shea, F.T. and Lindsay, J.E., 2018. Potential pollution risks of historic landfills on low-lying coasts and estuaries. Wiley Interdisciplinary Reviews: Water, 5(1), p.e1264.

Brando, V. E. and Dekker, A. G., 2003. Satellite hyperspectral remote sensing for estimating estuarine and coastal water quality. IEEE Transactions on Geoscience and Remote Sensing, 41(6), pp.1378-1387.

Brijlal, N., 2005. The environmental and health status of the Mgeni Estuary in KwaZulu-Natal, South Africa. MSc. University of KwaZulu-Natal.

Brini, E., Fennell, C.J., Fernandez-Serra, M., Hribar-Lee, B., Luksic, M. and Dill, K.A., 2017. How water's properties are encoded in its molecular structure and energies. Chemical Reviews, 117(19), pp.12385-12414.

Bromba, M.U. and Ziegler, H., 1981. Application hints for Savitzky-Golay digital smoothing filters. Analytical Chemistry, 53(11), pp.1583-1586.

Bruens, A.W., Kranenburg, C. and Winterwerp, J.C., 2002. Physical modelling of entrainment by a concentrated benthic suspension. In Proceedings in Marine Science, 5, pp.109-124. Elsevier.

Campbell, J.B. and Wynne, R.H., 2011. Introduction to remote sensing. The Guilford Press, New York, London.

Canuel, E.A. and Hardison, A.K., 2016. Sources, ages, and alteration of organic matter in estuaries. Annual Review of Marine Science, 8, pp.409-434.

Caporale, A.G. and Violante, A., 2016. Chemical processes affecting the mobility of heavy metals and metalloids in soil environments. Current Pollution Reports, 2(1), pp.15-27.

Chai, T. and Draxler, R.R., 2014. Root mean square error (RMSE) or mean absolute error (MAE) – Arguments against avoiding RMSE in the literature. Geoscientific Model Development, 7(3), pp.1247-1250.

Chapman, P.M. and Wang, F., 2001. Assessing sediment contamination in estuaries. Environmental Toxicology and Chemistry: An International Journal, 20(1), pp.3-22.

Chen, T.B., Zheng, Y.M., Lei, M., Huang, Z.C., Wu, H.T., Chen, H., Fan, K.K., Yu, K., Wu, X. and Tian, Q.Z., 2005. Assessment of heavy metal pollution in surface soils of urban parks in Beijing, China. Chemosphere, 60(4), pp.542-551.

Cheung, K. C., Poon, B. H. T. Lan, C. Y. and Wong, M. H., 2003. Assessment of metal and nutrient concentrations in river water and sediment collected from the cities in the Pearl River Delta, South China. Chemosphere, 52, pp.1431-1440.

Chili, N.S., 2008. A study of the environmental impacts (natural and anthropogenic) on the estuaries of KwaZulu-Natal, South Africa: implications for management. PhD. University of KwaZulu-Natal, South Africa.

Choe, E., van der Meer, F., van Ruitenbeek, F., van der Werff, H., de Smeth, B. and Kim, K.W., 2008. Mapping of heavy metal pollution in stream sediments using combined geochemistry, field spectroscopy, and hyperspectral remote sensing: A case study of the Rodalquilar mining area, SE Spain. Remote Sensing of Environment, 112(7), pp.3222-3233.

Cierniewski, J. and Kuśnierek, K., 2010. Influence of several size properties on soil surface reflectance. Quaestiones Geographicae, 29(1), pp.13-25.

Cisneros, K.O., 2013. Ecosystem functioning of selected estuaries on the east coast of South Africa. PhD. University of KwaZulu-Natal.

Clark, R. and O'Connor, K., 2019. A systematic survey of bar-built estuaries along the California coast. Estuarine, Coastal and Shelf Science, 226, p.106285.

Cloern, J.E., Abreu, P.C., Carstensen, J., Chauvaud, L., Elmgren, R., Grall, J., Greening, H., Johansson, J.O.R., Kahru, M., Sherwood, E.T. and Xu, J., 2016. Human activities and climate variability drive fast-paced change across the world's estuarine–coastal ecosystems. Global Change Biology, 22(2), pp.513-529.

Člupek, M., Matějka, P. and Volka, K., 2007. Noise reduction in Raman spectra: Finite impulse response filtration versus Savitzky–Golay smoothing. Journal of Raman Spectroscopy: An International Journal for Original Work in all Aspects of Raman Spectroscopy, Including Higher Order Processes, and also Brillouin and Rayleigh Scattering, 38(9), pp.1174-1179.

Cochran, J.K., Bokuniewicz, H.J. and Yager, P.L., 2019. Encyclopedia of Ocean Sciences. Academic Press.

Colby, B. R., 1963. Fluvial sediments - A summary of source, transportation, deposition and measurement of sediment discharge. In Contributions to General Geology, Geological Survey Bulletin 1181. United States Government Printing Office, Washington.

Colloty, B.M., Adams, J.B. and Bate, G.C., 2002. Classification of estuaries in the Ciskei and Transkei regions based on physical and botanical characteristics. South African Journal of Botany, 68(3), pp.312-321.

Cooper, J.A.G., 1990. Ephemeral stream-mouth bars at flood-breach river mouths on a wave-dominated coast: Comparison with ebb-tidal deltas at barrier inlets. Marine Geology, 95(1), pp.57-70.

Cooper, J.A.G., 1991. Sedimentary models and geomorphological classification of river-mouths on a subtropical, wave-dominated coast, Natal, South Africa. PhD. University of KwaZulu-Natal.

Cooper, J.A.G., 1993. Sedimentation in a river dominated estuary. Sedimentology, 40(5), pp.979-1017.

Crowley, J.K., Williams, D.E., Hammarstrom, J.M., Piatak, N., Chou, I.M. and Mars, J.C., 2003. Spectral reflectance properties (0.4–2.5 μm) of secondary Fe-oxide, Fe-hydroxide, and Fe-sulphate-hydrate minerals associated with sulphide-bearing mine wastes. Geochemistry: Exploration, Environment, Analysis, 3(3), pp.219-228.

Cui, S., Zhang, F., Hu, P., Hough, R., Fu, Q., Zhang, Z., An, L., Li, Y.F., Li, K., Liu, D. and Chen, P., 2019. Heavy metals in sediment from the urban and rural rivers in Harbin City, Northeast China. International journal of environmental research and public health, 16(22), p.4313.

Daborn G.R. and Redden A.M., 2016. Estuaries. In: Finlayson C., Milton G., Prentice R., Davidson N. (eds). The Wetland Book. Springer, Dordrecht.

Daily, G. C. (ed.)., 1997. Nature's services: Societal dependence on natural ecosystems. Island Press, Washington, DC.

Danner, M., Locherer, M., Hank, T., Richter, K., 2015. Spectral Sampling with the ASD FieldSpec 4 – Theory, Measurement, Problems, Interpretation. EnMAP Field Guides Technical Report, GFZ Data Services.

Davies, P.J., Wright, I.A., Jonasson, O.J. and Findlay, S.J., 2010. Impact of concrete and PVC pipes on urban water chemistry. Urban Water Journal, 7(4), pp.233-241.

Davies, G.E. and Calvin, W.M., 2016. Quantifying iron concentration in local and synthetic acid mine drainage: a new technique using handheld field spectrometers. Mine Water and the Environment, 36(2), pp.299-309.

Day, J.H., 1980. What is an estuary. South African Journal of Science, 76(5), p.198.

Day, J.W., Hall, C., Kemp, W.M. and Yáñez-Arancibia, A., 1990. Estuarine Ecology. Estuaries, 13(1).

Dean, A., 2018. Monitoring estuarine water quality: Teacher guide. Data in the classroom. Second edition. [Online]. https://dataintheclassroom.noaa.gov/sites/default/files/waterquality_teacherguide_2017.pdf [Accessed: 17 February 2022].

De Groot, R.S., Wilson, M.A. and Boumans, R.M., 2002. A typology for the classification, description and valuation of ecosystem functions, goods and services. Ecological economics, 41(3), pp.393-408.

Delwiche, S.R. and Reeves III, J.B., 2010. A graphical method to evaluate spectral pre-processing in multivariate regression calibrations: Example with Savitzky-Golay filters and partial least squares regression. Applied Spectroscopy, 64(1), pp.73-82.

de Matos, A.T., Fontes, M.P.F., Da Costa, L.M. and Martinez, M.A., 2001. Mobility of heavy metals as related to soil chemical and mineralogical characteristics of Brazilian soils. Environmental Pollution, 111(3), pp.429-435.

Department of Water Affairs and Forestry (DWAF)., 1996. South African Water Quality Guidelines - Volume 7 - Aquatic Ecosystems, First edition. Department of Water Affairs and Forestry, Pretoria, South Africa.

de Souza Machado, A.A., Spencer, K., Kloas, W., Toffolon, M. and Zarfl, C., 2016. Metal fate and effects in estuaries: a review and conceptual model for better understanding of toxicity. Science of the Total Environment, 541, pp.268-281.

Dierssen, H.M., Ackleson, S.G., Joyce, K.E., Hestir, E.L., Castagna, A., Lavender, S. and McManus, M.A., 2021. Living up to the hype of hyperspectral aquatic remote sensing: science, resources and outlook. Frontiers in Environmental Science, 9.

Dikole, M., 2014. Seasonal analysis of water and sediment along the uMgeni River, South Africa. MSc. University of KwaZulu-Natal.

do Nascimento, R.J.A.D., Macedo, G.R.D., Santos, E.S.D. and Oliveira, J.A.D., 2017. Real time and in situ near-infrared spectroscopy (NIRS) for quantitative monitoring of biomass, glucose, ethanol and glycerine concentrations in an alcoholic fermentation. Brazilian Journal of Chemical Engineering, 34, pp.459-468.

Drexler, J., Fisher, N., Henningsen, G., Lanno, R., McGeer, J., Sappington, K. and Beringer, M., 2003. Issue paper on the bioavailability and bioaccumulation of metals. In US Environmental Protection Agency Risk Assessment Forum: Washington, DC, USA.

Du Laing, G., De Vos, R., Vandecasteele, B., Lesage, E., Tack, F.M. and Verloo, M.G., 2008. Effect of salinity on heavy metal mobility and availability in intertidal sediments of the Scheldt estuary. Estuarine, Coastal and Shelf Science, 77(4), pp.589-602.

Du Preez, M. and Hosking, S.G., 2010. Estimating the recreational value of freshwater inflows into the Klein and Kwelera Estuaries: An application of the zonal travel cost method. Water SA, 36(5).

Dunn, R.J., Waltham, N.J., Huang, J., Teasdale, P.R. and King, B.A., 2019. Protecting water quality in urban estuaries: Australian case studies. In Coasts and Estuaries, pp.69-86. Elsevier.

Dunn, K.G., 2021. Process improvement using data, version 3ce778. [online]. Learning Chemical Engineering. Available at: https://learnche.org/pid/latent-variable-modelling/principal-component-analysis/interpreting-score-plots-and-loading-plots [Accessed: 18 August 2021].

Ebenstein, A., 2012. The consequences of industrialization: evidence from water pollution and digestive cancers in China. Review of Economics and Statistics, 94(1), pp.186-201.

Edgar, G.J., Barrett, N.S., Graddon, D.J. and Last, P.R., 2000. The conservation significance of estuaries: a classification of Tasmanian estuaries using ecological, physical and demographic attributes as a case study. Biological Conservation, 92(3), pp.383-397.

Edmunds, W.M., Ahmed, K.M. and Whitehead, P.G., 2015. A review of arsenic and its impacts in groundwater of the Ganges–Brahmaputra–Meghna delta, Bangladesh. Environmental Science: Processes and Impacts, 17(6), pp.1032-1046.

Eitelwein, M.T., Demattê, J.A.M., Trevisan, R.G., Anselmi, A.A. and Molin, J.P., 2015. Performance of spectrometers to estimate soil properties.

Elkhorn Slough Reserve., 2017. Elkhorn Slough Reserve water quality information: Salinity and conductivity background. [online]. Available at: https://www.elkhornslough.org [Accessed: 6 September 2021].

Estifanos, S., 2006. Spectral indicators for assessing pollution in the epithermal gold mining area of Rodalquilar, SE Spain. MSc, International Institute for Geo-information Science and Earth Observation, Enschede, Netherlands.

Evans, R.H., 1996. An analysis of criterion variable reliability in conjoint analysis. Perceptual and Motor Skills, 82(3), pp.988-990.

Fang, Q., Hong, H., Zhao, L., Kukolich, S., Yin, K. and Wang, C., 2018. Visible and near-infrared reflectance spectroscopy for investigating soil mineralogy: A review. Journal of Spectroscopy, 2018. https://doi.org/10.1155/2018/3168974.

Fashae, O.A., Ayorinde, H.A., Olusola, A.O. and Obateru, R.O., 2019. Landuse and surface water quality in an emerging urban city. Applied Water Science, 9(25), pp.1-12.

Fatima, M. and Usmani, N., 2013. Histopathology and bioaccumulation of heavy metals (Cr, Ni and Pb) in fish (Channa striatus and Heteropneustes fossilis) tissue: A study for toxicity and ecological impacts. Pakistan Journal of Biological Sciences, 16(9), pp.412-420.

Ferreira, A.J., Soares, D., Serrano, L.M., Walsh, R.P., Dias-Ferreira, C. and Ferreira, C.S., 2016. Roads as sources of heavy metals in urban areas. The Covões catchment experiment, Coimbra, Portugal. Journal of Soils and Sediments, 16(11), pp.2622-2639.

Finlayson, C.M., Milton, G.R., Prentice, R.C. and Davidson, N.C. (eds.)., 2018. The Wetland Book: II: Distribution, Description, and Conservation. Springer Netherlands.

Finnegan, P. and Chen, W., 2012. Arsenic toxicity: the effects on plant metabolism. Frontiers in Physiology, 3, p.182.

Flemming, B.W., 2011. Geology, morphology and sedimentology of estuaries and coasts. In Treatise on Estuarine and Coastal Science, Estuarine and Coastal Geology and Morphology, 3, pp.7–38. Elsevier, Amsterdam.

Fondriest Environmental, Inc., 2014. Sediment transport and deposition. [online]. Available at: https://www.fondriest.com/environmental-measurements/parameters/hydrology/sediment-transport-deposition/ [Accessed: 09 February 2021].

Forbes, A.T. and Demetriades, N.T., 2008. Estuaries of Durban. eThekwini Municipality Environmental Management Department: Durban. [Online]. Available at:

https://www.researchgate.net/publication/311740507_Durban's_Estuaries [Accessed: 17 February 2022].

Forbes, N.T. and Forbes, A.T., 2012. Estuaries of the Kwadukuza Municipality. Preliminary Assessment for the Biodiversity and Open Space Management Plan. Institute of Natural Resources. [Online]. Available at: https://carbonn.org/uploads/tx_carbonndata/Kwadukuza%20Estuaries%20report.pdf [Accessed: 17 February 2022].

Gabrielyan, A.V., Shahnazaryan, G.A. and Minasyan, S.H., 2018. Distribution and identification of sources of heavy metals in the Voghji River basin impacted by mining activities (Armenia). Journal of Chemistry, 2018. https://doi.org/10.1155/2018/7172426.

Galvao, L.S. and Vitorello, I., 1998. Role of organic matter in obliterating the effects of iron on spectral reflectance and colour of Brazilian tropical soils. International Journal of Remote Sensing, 19(10), pp.1969-1979.

Gao, Y., Kan, A.T. and Tomson, M.B., 2003. Critical evaluation of desorption phenomena of heavy metals from natural sediments. Environmental Science and Technology, 37(24), pp.5566-5573.

Geyer, W. R., 2004. Where the Rivers Meet the Sea. Oceanus Magazine, 43(1).

Gholizadeh, M.H., Melesse, A.M. and Reddi, L., 2016. A comprehensive review on water quality parameters estimation using remote sensing techniques. Sensors, 16(8), p.1298.

Ghosh, S., Prasanna, V.L., Sowjanya, B., Srivani, P., Alagaraja, M. and Banji, D., 2013. Inductively coupled plasma–optical emission spectroscopy: a review. Asian Journal of Pharmaceutical Analysis, 3(1), pp.24-33.

Gibson, P.J., 2000. Introductory remote sensing: Principles and concepts. Routledge, London and New York.

Glamore, W. C., Rayner, D. S. and Rahman, P. F., 2016: Estuaries and climate change. Technical monograph prepared for the National Climate Change Adaptation Research Facility. Water Research Laboratory of the School of Civil and Environmental Engineering, UNSW.

Glennie, L., 2001. An environmental history of the Mgeni River estuary: A study of human and natural impacts over time. MSc. University of KwaZulu-Natal.

Goetz, A.F., 2009. Three decades of hyperspectral remote sensing of the earth: A personal view. Remote Sensing of Environment, 113, pp.S5-S16.

Gómez, R.A., 2014. Spectral reflectance analysis of the Caribbean Sea. Geofísica Internacional, 53(4), pp.385-398.

González-Fernández, A.B., Sanz-Ablanedo, E., Gabella, V.M., García-Fernández, M. and Rodríguez-Pérez, J.R., 2019. Field spectroscopy: A non-destructive technique for estimating water status in vineyards. Agronomy, 9(8), pp.427.

Gordon, A.K. and Muller, W.J., 2010. Developing sediment quality guidelines for South Africa. PHASE 1: Identification of international best practice and applications for South Africa to develop a research and implementation framework. Water Research Commission (WRC) Report Number KV 242/10. [Online]. Available at: http://www.wrc.org.za/wp-content/uploads/mdocs/KV%20242-10%20Conservation%20of%20Water%20Ecosystems.pdf [Accessed: 17 February 2022].

Govender, M., Chetty, K. and Bulcock, H., 2007. A review of hyperspectral remote sensing and its application in vegetation and water resource studies. Water SA, 33(2), pp.145-151.

Gregersen, E. and Hanusa, T.P., 2012. Magnesium. [online]. Britannica. Available at: https://www.britannica.com/science/magnesium [Accessed: 25 June 2021].

Griffin, N.J., Palmer, C.G. and Scherman, P.A., 2014. Critical analysis of environmental water quality in South Africa: Historic and current trends (No. 2184/1, pp. 14). WRC report. [Online]. Available at: http://www.wrc.org.za/wp-content/uploads/mdocs/2184-1-14.pdf [Accessed: 17 February 2022].

Grzywna, A. and Bronowicka-Mielniczuk, U., 2020. Spatial and temporal variability of water quality in the Bystrzyca River Basin, Poland. Water, 12(1), p.190.

Guéguen, C. and Dominik, J., 2003. Partitioning of trace metals between particulate, colloidal and truly dissolved fractions in a polluted river: The Upper Vistula River (Poland). Applied Geochemistry, 18(3), pp.457-470.

Gupta, N., Gaurav, S.S. and Kumar, A., 2013. Molecular basis of aluminium toxicity in plants: A review. American Journal of Plant Sciences, 4, pp.21–37.

Güven, D. and Akinci, G., 2011. Comparison of acid digestion techniques to determine heavy metals in sediment and soil samples. Gazi University Journal of Science, 24(1), pp.29-34.

Hacısalihoğlu, S. and Karaer, F., 2016. Relationships of Heavy Metals in Water and Surface Sediment with Different Chemical Fractions in Lake Uluabat, Turkey. Polish Journal of Environmental Studies, 25(5).

Haile, B.G., Czarniecka, U., Xi, K., Smyrak-Sikora, A., Jahren, J., Braathen, A. and Hellevang, H., 2019. Hydrothermally induced diagenesis: Evidence from shallow marine-deltaic sediments, Wilhelmøya, Svalbard. Geoscience Frontiers, 10(2), pp.629-649.

Harris, P., Muelbert, J., Muniz, P., Yin, K., Ahmed, K., Folorunsho, R. and Bernal, P., 2016. Estuaries and Deltas. In United Nations World Ocean Assessment. Cambridge University Press.

Harrison, T.D., Cooper, J.A.G. & Ramm, A.E.L. 2000. State of South African estuaries: Geomorphology, ichthyofauna, water quality and aesthetics. State of the Environment Series, Report No. 2. Department of Environmental Affairs and Tourism. [Online]. Available at: https://www.researchgate.net/publication/277096369_State_of_South_African_estuaries-geomorphology_ichthyofauna_water_quality_and_aesthetics [Accessed: 17 February 2022].

Harrison, T.D., 2004. Physico-chemical characteristics of South African estuaries in relation to the zoogeography of the region. Estuarine, Coastal and Shelf Science, 61(1), pp.73-87.

Hartwell, S.I., Apeti, D.A., Pait, A.S., Bricker, S. and Warner, R., 2018. NOAA National Status & Trends Bioeffects Program: A Summary of the Magnitude and Effects of Contaminants in the Nation's Coastal Waters. NOAA Technical Memorandum NOAA/NCCOS 236. Silver Spring, MD. [Online]. Available at: https://nccospublicstor.blob.core.windows.net/projects-attachments/238/Bioieffects%20February%20Interactive%20for%20Ian_IH_2.pdf [Accessed: 17 February 2022].

Hatchell, D.C. (ed.)., 1999. ASD technical guide. 3rd edition, section 0-1. Analytical Spectral Devices, Inc. (ASD). [Online]. Available at: https://docplayer.net/9161600-Asd-technical-guide-3rd-ed-section-0-1.html [Accessed: 17 February 2022].

Hay, D., 2017. Our water our future: Securing the water resources of the uMgeni River Basin. uMgeni Handbook. [Online]. Available at: http://www.watersecuritynetwork.org/wp-

content/uploads/2017/02/uMngeni-Handbook-February-2017.pdf [Accessed: 17 February 2022].

He, T., Wang, J., Lin, Z. and Cheng, Y., 2009. Spectral features of soil organic matter. Geo-spatial Information Science, 12(1), pp.33-40.

He, Z., Li, F., Dominech, S., Wen, X. and Yang, S., 2019. Heavy metals of surface sediments in the Changjiang (Yangtze River) Estuary: Distribution, speciation and environmental risks. Journal of Geochemical Exploration, 198, pp.18-28.

Heckbert, S., Costanza, R., Poloczanska, E.S. and Richardson, A.J., 2011. 12.10–Climate regulation as a service from estuarine and coastal ecosystems. Treatise on Estuarine and Coastal Science, pp.199-216.

Heiman, A. and Licht, S., 1999. Fundamental baseline variations in aqueous near-infrared analysis. Analytica Chimica Acta, 394(2-3), pp.135-147.

Henseler, J., Ringle, C.M. and Sinkovics, R.R., 2009. The use of partial least squares path modeling in international marketing. In New Challenges to International Marketing. Emerald Group Publishing Limited.

Hicks, N., 2009. A combined sedimentological-mineralogical study of sediment-hosted gold and uranium mineralization at Denny Dalton, Pongola Supergroup, South Africa. MSc. University of KwaZulu-Natal.

Hively, W.D., McCarty, G.W., Reeves, J.B., Lang, M.W., Oesterling, R.A. and Delwiche, S.R., 2011. Use of airborne hyperspectral imagery to map soil properties in tilled agricultural fields. Applied and Environmental Soil Science, 2011. doi:10.1155/2011/358193.

Hsu, L.C., Huang, C.Y., Chuang, Y.H., Chen, H.W., Chan, Y.T., Teah, H.Y., Chen, T.Y., Chang, C.F., Liu, Y.T. and Tzou, Y.M., 2016. Accumulation of heavy metals and trace elements in fluvial sediments received effluents from traditional and semiconductor industries. Scientific Reports, 6(1), pp.1-12.

Hu, C., Chen, Z., Clayton, T. D., Swarzenski, P., Brock, J. C. and Muller–Karger, F. E., 2004. Assessment of estuarine water-quality indicators using MODIS medium-resolution bands: Initial results from Tampa Bay, FL. Remote Sensing of Environment, 93(3), pp.423-441.

Huang, Y., Zhang, D., Xu, Z., Yuan, S., Li, Y. and Wang, L., 2017. Effect of overlying water pH, dissolved oxygen and temperature on heavy metal release from river sediments under laboratory conditions. Archives of Environmental Protection, 43(2), pp.28-36.

Huang, L., Rad, S., Xu, L., Gui, L., Song, X., Li, Y., Wu, Z. and Chen, Z., 2020. Heavy metals distribution, sources, and ecological risk assessment in Huixian wetland, South China. Water, 12(2), p.431.

Hubbard, R.K., Newton, G.L. and Hill, G.M., 2004. Water quality and the grazing animal. Journal of Animal Science, 82(13), pp.E255-E263.

Hübner, R., Astin, K.B. and Herbert, R.J., 2009. Comparison of sediment quality guidelines (SQGs) for the assessment of metal contamination in marine and estuarine environments. Journal of Environmental Monitoring, 11(4), pp.713-722.

Hughes, B.B., Levey, M.D., Brown, J.A., Fountain, M.C., Carlisle, A.B., Litvin, S.Y., Greene, C.M., Heady, W.N. and Gleason, M.G., 2014. Nursery functions of US West Coast estuaries: The state of knowledge for juveniles of focal invertebrate and fish species. Arlington, Virginia: Nature Conservancy.

Hui, C., 2008. The possibility of assessing heavy metal concentrations in reed along Le An River (China) using hyperspectral data. MSc. University of Wuhan, China.

Hutcheson, W., Hoagland, P. and Jin, D., 2018. Valuing environmental education as a cultural ecosystem service at Hudson River Park. Ecosystem Services, 31, pp.387-394.

Igiri, B.E., Okoduwa, S.I., Idoko, G.O., Akabuogu, E.P., Adeyi, A.O. and Ejiogu, I.K., 2018. Toxicity and bioremediation of heavy metals contaminated ecosystem from tannery wastewater: a review. Journal of Toxicology, 2018. https://doi.org/10.1155/2018/2568038.

Ingerman, L., Jones, D.G., Keith, S. and Rosemond, Z.A., 2008. Toxicological profile for aluminium. [Online]. Available at: https://www.atsdr.cdc.gov/toxprofiles/tp22.pdf [Accessed: 17 February 2022].

Jain, C.K., Singhal, D.C. and Sharma, M.K., 2005. Metal pollution assessment of sediment and water in the river Hindon, India. Environmental Monitoring and Assessment, 105(1), pp.193-207.

Jaishankar, M., Tseten, T., Anbalagan, N., Mathew, B.B. and Beeregowda, K.N., 2014. Toxicity, mechanism and health effects of some heavy metals. Interdisciplinary toxicology, 7(2), pp.60-72.

Janse, P.V., Kayte, J.N., Agrawal, R.V. and Deshmukh, R.R., 2018. Standard Spectral Reflectance Measurements for ASD FieldSpec Spectroradiometer. In 2018 Fifth International Conference on Parallel, Distributed and Grid Computing (PDGC), pp.729-733. IEEE.

Javed, M. and Usmani, N., 2017. An overview of the adverse effects of heavy metal contamination on fish health. Proceedings of the National Academy of Sciences, India Section B: Biological Sciences, 89(2), pp.389-403.

Jensen, J.R., 2015. Introductory digital image processing: A remote sensing perspective (4th ed.). Prentice Hall Press, Upper Saddle River, NJ, USA.

Jeppesen, E., Brucet, S., Naselli-Flores, L., Papastergiadou, E., Stefanidis, K., Noges, T., Peeter Noges, P., Attayde, J.L., Zohary, T., Coppens, J., Bucak, T., Menezes, R.F., Freitas, F.R.S., Kernan, M., Søndergaard, M. and Beklioglu, M., 2015. Ecological impacts of global warming and water abstraction on lakes and reservoirs due to changes in water level and related changes in salinity. Hydrobiologia, 750, pp.201-227.

Jewitt, D., Goodman, P.S., Erasmus, B.F., O'Connor, T.G. and Witkowski, E.T., 2015. Systematic land-cover change in KwaZulu-Natal, South Africa: Implications for biodiversity. South African Journal of Science, 111(9-10), pp.01-09.

Jezek, M., Geilfus, C.M., Bayer, A. and Mühling, K.H., 2015. Photosynthetic capacity, nutrient status, and growth of maize (Zea mays L.) upon MgSO4 leaf-application. Frontiers in Plant Science, 5, p.781.

Johansson, L., 2014. Salinity effects on cadmium concentrations in blue mussels in the Baltic Sea. Bachelors Essay, Swedish University of Agricultural Sciences.

Jolliffe, I.T. and Cadima, J., 2016. Principal component analysis: A review and recent developments. Philosophical Transactions of the Royal Society A: Mathematical, Physical and Engineering Sciences, 374(2065), p.20150202.

Kaflé, B.P., 2019. Chemical analysis and material characterization by spectrophotometry. Elsevier.

Kaleita, A.L., Tian, L.F. and Hirschi, M.C., 2005. Relationship between soil moisture content and soil surface reflectance. Transactions of the ASAE, 48(5), pp.1979-1986.

Kang, M., Tian, Y., Peng, S. and Wang, M., 2019. Effect of dissolved oxygen and nutrient levels on heavy metal contents and fractions in river surface sediments. Science of the Total Environment, 648, pp.861-870.

Karabulut, M. and Ceylan, N., 2005. The spectral reflectance responses of water with different levels of suspended sediment in the presence of algae. Turkish Journal of Engineering and Environmental Sciences, 29(6), pp.351-360.

Karaca, A., 2004. Effect of organic wastes on the extractability of cadmium, copper, nickel, and zinc in soil. Geoderma, 122(2-4), pp.297-303.

Karakus, C.B., Cerit, O. and Kavak, K.S., 2015. Determination of land use/cover changes and land use potentials of Sivas city and its surroundings using Geographical Information Systems (GIS) and Remote Sensing (RS). Procedia Earth and Planetary Science, 15, pp.454-461.

Kaushal, S.S., Likens, G.E., Utz, R.M., Pace, M.L., Grese, M. and Yepsen, M., 2013. Increased river alkalinization in the Eastern US. Environmental science & technology, 47(18), pp.10302-10311.

Keen, T. and Furukawa, Y., 2007. A modular entrainment model for cohesive sediment. In Proceedings in Marine Science, 8, pp.189-207. Elsevier.

Kemper, T. and Sommer, S., 2002. Estimate of heavy metal contamination in soils after a mining accident using reflectance spectroscopy. Environmental Science and Technology, 36(12), pp.2742-2747.

Keniston, C., 2015. Increasing salinity effects on heavy metal concentration. Cary Institute of Ecosystem Studies. [Online]. Available at: https://www.caryinstitute.org/sites/default/files/public/reprints/keniston_2015_REU.pdf [Accessed: 17 February 2022].

Kercival, N., 2015. Assessing changes in land use and land cover using remote sensing: A case study of the Umhlanga Ridge sub – place. MSc. University of KwaZulu-Natal.

Kianpoor Kalkhajeh, Y., Jabbarian Amiri, B., Huang, B., Henareh Khalyani, A., Hu, W., Gao, H. and Thompson, M.L., 2019. Methods for Sample Collection, Storage, and Analysis of Freshwater Phosphorus. Water, 11(9), p.1889.

Kinuthia, G.K., Ngure, V., Beti, D., Lugalia, R., Wangila, A. and Kamau, L., 2020. Levels of heavy metals in wastewater and soil samples from open drainage channels in Nairobi, Kenya: Community health implication. Scientific reports, 10(1), pp.1-13.

Kiran, B.S.S. and Raja, S., 2017. A Review on Inductively Coupled Plasma Optical Emission Spectrometry (ICP-OES) with a Special Emphasis on its Applications. Der Pharmacia Lettre, 9(10), pp.44-54.

Krishnan, S.R. and Seelamantula, C.S., 2012. On the selection of optimum Savitzky-Golay filters. IEEE Transactions on Signal Processing, 61(2), pp.380-391.

Kuang, B. and Mouazen, A.M., 2013. Effect of spiking strategy and ratio on calibration of on-line visible and near infrared soil sensor for measurement in European farms. Soil and Tillage Research, 128, pp.125-136.

Kumar, V., Sinha, A.K., Rodrigues, P.P., Mubiana, V.K., Blust, R. and De Boeck, G., 2015. Linking environmental heavy metal concentrations and salinity gradients with metal accumulation and their effects: a case study in 3 mussel species of Vitória estuary and Espírito Santo Bay, Southeast Brazil. Science of the Total Environment, 523, pp.1-15.

Kumar, A., MMS, C.P., Chaturvedi, A.K., Shabnam, A.A., Subrahmanyam, G., Mondal, R., Gupta, D.K., Malyan, S.K., S Kumar, S., A Khan, S. and Yadav, K.K., 2020. Lead toxicity: health hazards, influence on food chain, and sustainable remediation approaches. International Journal of Environmental Research and Public Health, 17(7), p.2179.

Lane, D.M., Scott, D., Hebl, M., Guerra, R., Osherson, D. and Zimmer, H., 2013. Introduction to statistics: An interactive e-book. University of Houston.

Lee, J.W., Choi, H., Hwang, U.K., Kang, J.C., Kang, Y.J., Kim, K.I. and Kim, J.H., 2019. Toxic effects of lead exposure on bioaccumulation, oxidative stress, neurotoxicity, and immune responses in fish: A review. Environmental Toxicology and Pharmacology, 68, pp.101-108.

Lerberg, S.B., Holland, A.F. and Sanger, D.M., 2000. Responses of tidal creek macrobenthic communities to the effects of watershed development. Estuaries, 23(6), pp.838-853.

Lerda, D.E. and Prosperi, C.H., 1996. Water mutagenicity and toxicology in Rio Tercero (Cordoba, Argentina). Water Research, 30(4), pp.819-824.

Levit, S.M., 2010. A literature review of effects of cadmium on fish. The Nature Conservancy, pp.1-15.

Li, H., Shi, A., Li, M. and Zhang, X., 2013. Effect of pH, temperature, dissolved oxygen, and flow rate of overlying water on heavy metals release from storm sewer sediments. Journal of Chemistry, 2013.

Liang, S., Xiaowen, L. and Wang, J. (eds.)., 2012. Advanced remote sensing: Terrestrial information extraction and applications. Academic Press.

Lillesand, T., Kiefer, R.W. and Chipman, J., 2015. Remote sensing and image interpretation. John Wiley and Sons.

Lin, J.G. and Chen, S.Y., 1998. The relationship between adsorption of heavy metal and organic matter in river sediments. Environment International, 24(3), pp.345-352.

Loaiza, E. and Findlay, S.E.G., 2008. Effects of different vegetation cover types on sediment deposition in the Tivoli North Bay tidal freshwater marsh, Hudson River, New York. Cary Institute of Ecosystem Studies, pp.1-7.

Lodhi, M.A., Rundquist, D.C., Han, L. and Kuzila, M.S., 1998. Estimation of suspended sediment concentration in water using integrated surface reflectance. Geocarto International, 13(2), pp.11-15.

Long, E.R. and L.G. Morgan 1990. The potential for biological effects of sediment-sorbed contaminants tested in the national status and trends program. NOAA Technical Memorandum NOS OMA 52. Seattle, WA. [Online]. Available at: file:///C:/Users/suvas/Downloads/C&EE122.pdf [Accessed: 17 February 2022].

Long, E.R., MacDonald, D.D., Smith, S.L. and Calder, F.D., 1995. Incidence of adverse biological effects within ranges of chemical concentrations in marine and estuarine sediments. Environmental Management, 19(1), pp.81-97.

Luo, S., Wu, B., Xiong, X. and Wang, J., 2016. Effects of total hardness and calcium: magnesium ratio of water during early stages of rare minnows (Gobiocypris rarus). Comparative medicine, 66(3), pp.181-187.

Mac Arthur, A., MacLellan, C.J. and Malthus, T., 2012. The fields of view and directional response functions of two field spectroradiometers. IEEE Transactions on Geoscience and Remote Sensing, 50(10), pp.3892-3907.

Mack, P., 2003. Dissolved oxygen and the three s's sources, sinks and solubility. Sierra Club River Monitoring Program. [Online]. Available at: https://www.sierraclub.org/sites/www.sierraclub.org/files/sce/river-prairie-group/WaterProject/InternalDocumentation/do1.pdf [Accessed: 17 February 2022].

Mackenzie, J., 2015. Riparian vegetation and wetland assessment for the proposed new Malelane safari lodge within KNP along the crocodile and Timfenheni rivers. [Online]. Available at: https://www.sanparks.org/assets/docs/groups_eia_notices/malelane_safari_lodge/d2.pdf [Accessed: 17 February 2022].

Magdof, F. and Van Es, H., 2021. Building soils for better crops ecological management for healthy soils, 4th edition. Handbook series 10. Sustainable Agriculture Research and Education (SARE).

Mann, R.M., Vijver, M.G. and Peijnenburg, W.J.G.M., 2011. Metals and metalloids in terrestrial systems: Bioaccumulation, biomagnification and subsequent adverse effects. Ecological Impacts of Toxic Chemicals. Bentham Science Publishers, pp.43-62.

Mark, H. and Workman Jr, J., 2010. Chemometrics in Spectroscopy. Elsevier.

Mark, H. and Workman Jr, J., 2018. Choosing the best regression model. In Chemometrics in Spectroscopy. Elsevier.

Marshak, S., 2008. Earth: Portrait of a planet, 3rd edition. WW Norton and Company, Inc. United States of America.

Marshall, C.G.A. and von Brunn, V., 1999. The stratigraphy and origin of the Natal Group. South African Journal of Geology, 102(1), pp.15-25.

Masindi, V. and Muedi, K.L., 2018. Environmental contamination by heavy metals. Heavy Metals, 10, pp.115-132.

Maslennikova, S., Larina, N. and Larin, S., 2012. The effect of sediment grain size on heavy metal content. Lakes, Reservoirs and Ponds, 6(1), pp.43-54.

McGrane, S.J., 2016. Impacts of urbanisation on hydrological and water quality dynamics, and urban water management: a review. Hydrological Sciences Journal, 61(13), pp.2295-2311.

McLean, J.E. and Bledsoe, B.E., 1992. Ground water issue. Behavior of metals in soils. United States Environmental Protection Agency: Ground Water Issue, pp.5-92.

McNally, W. H. and Mehta, A. J., 2004. Coastal zones and estuaries - Sediment transport in estuaries. Encyclopaedia of life Support Systems (EOLSS).

Meetei, T.T., Devi, Y.B. and Chanu, T.T., 2020. Ion exchange: The most important chemical reaction on earth after photosynthesis. International Research Journal of Pure and Applied Chemistry, pp.31-42.

Melesse, A., Weng, Q., Thenkabail, P. and Senay, G., 2007. Remote sensing sensors and applications in environmental resources mapping and modelling. Sensors, 7(12), pp.3209-3241.

Mesner, N. and Geiger, J., 2010. Understanding your watershed fact sheet: Dissolved oxygen. [online]. Extension Utah State University. Available at: https://extension.usu.edu/waterquality/files-ou/whats-in-your-water/do/NR_WQ_2005-16dissolvedoxygen.pdf [Accessed: 18 June 2021].

Mevik, B.H. and Wehrens, R., 2020. Introduction to the pls package. Help Section of the "Pls" Package of R Studio Software, pp.1-23.

Milton, E.J., Schaepman, M.E., Anderson, K., Kneubühler, M. and Fox, N., 2009. Progress in field spectroscopy. Remote Sensing of Environment, 113, pp.S92-S109.

Miththapala, S., 2013. Lagoons and estuaries. Coastal Ecosystems Series, Volume 4. IUCN Sri Lanka Country Office, Colombo. [Online]. Available at: https://portals.iucn.org/library/sites/library/files/documents/CES-004.pdf [Accessed: 16 February 2022].

Monaledi, M.O., 2019. Remote sensing of water quality indicators associated with mining activities – the case study of Mooi River in Carletonville, South Africa. MSc. University of Johannesburg.

Moodley, K., Pillay, S., Pather, K. and Ballabh, H., 2014. Heavy Metal Contamination of the Palmiet River: KwaZulu Natal South Africa. International Journal of Scientific Research in Environmental Sciences, 2(11), pp.0397-0409.

Moroşanu, G.A., Zaharia, L., Belleudy, P. and Toroimac, G.I., 2017. Methodology to identify the leading factors of rivers' electrical conductivity. Case study: Jiu Catchment (Romania). Aerul si Apa. Componente ale Mediului, pp.26-33.

Mouazen, A.M., Nyarko, F., Qaswar, M., Tóth, G., Gobin, A. and Moshou, D., 2021. Spatiotemporal Prediction and Mapping of Heavy Metals at Regional Scale Using Regression Methods and Landsat 7. Remote Sensing, 13(22), p.4615.

Moyle, P.B., 2020. Estuaries and fishes in southern Africa: A legacy of knowledge. South African Journal of Science, 116(3/4).

Munjal, S. and Singh, A., 2020. The Arrhenius Acid and Base Theory. In Corrosion. IntechOpen.

Nadal, M., Schuhmacher, M. and Domingo, J.L., 2004. Metal pollution of soils and vegetation in an area with petrochemical industry. Science of the Total Environment, 321(1-3), pp.59-69.

Naidoo, K., 2005. The anthropogenic impacts of urbanization and industrialisation on the water quality, ecology and health status of the Palmiet River Catchment in Durban, KwaZulu-Natal. MA. University of KwaZulu-Natal, South Africa.

Namieśnik, J. and Rabajczyk, A., 2010. The speciation and physico-chemical forms of metals in surface waters and sediments. Chemical Speciation and Bioavailability, 22(1), pp.1-24.

Namugize, J.N., 2017. Effects of land use and land cover changes on water quality of the upper Umngeni River, KwaZulu-Natal province, South Africa. PhD, University of KwaZulu-Natal.

Narwal, R.P. and Singh, B.R., 1998. Effect of organic materials on partitioning, extractability and plant uptake of metals in an alum shale soil. Water, Air, and Soil Pollution, 103(1), pp.405-421.

Nas, F.S. and Ali, M., 2018. The effect of lead on plants in terms of growing and biochemical parameters: A review. MOJ Ecology and Environmental Science, 3(4), pp.265-268.

Nathanson, J.A., 2010. Pollution. Encyclopaedia Britannica. [Online]. Available at: https://www.britannica.com/science/pollution-environment [Accessed: 10 April 2020].

National Aeronautics and Space Administration, Science Mission Directorate (NASA)., 2010. The Earth's Radiation Budget. [Online]. Available at: http://science.nasa.gov/ems/13_radiationbudget [Accessed: 11 February 2021].

National Oceanic and Atmospheric Administration (NOAA)., 1999. Screening quick reference tables (SquiRTs). [Online]. Available at: http://response.restoration.noaa.gov/cpr/sediment/squirt/squirt.html [Accessed: 26 June 2021].

National Oceanic and Atmospheric Administration (NOAA)., 2018. What is an estuary? [Online]. Available at: https://oceanservice.noaa.gov/facts/estuary.html. [Accessed: 22 April 2020].

National Oceanic and Atmospheric Administration (NOAA)., 2019. Life in an estuary. [online]. Available at: https://www.noaa.gov/education/resource-collections/marine-life/life-in-estuary [Accessed: 13 January 2021].

National Oceanic and Atmospheric Administration (NOAA)., 2020. Classifying estuaries: By Geology. [Online]. Available at: https://oceanservice.noaa.gov/education/tutorial_estuaries/est04_geology.html#:~:text=The%20mixture%20of%20seawater%20and,example%20of%20a%20tectonic%20estuary [Accessed: 09 June 2020].

National Oceanic and Atmospheric Administration (NOAA)., 2020. Classifying estuaries: by Water circulation. [Online]. Available at: https://oceanservice.noaa.gov/education/tutorial_estuaries/est05_circulation.html#:~:text=In%20slightly%20stratified%20or%20partially,decreases%20as%20one%20moves%20upstream [Accessed: 07 January 2021].

National Oceanic and Atmospheric Administration (NOAA)., 2020. Estuary habitat. [Online]. Available at: https://www.fisheries.noaa.gov/national/habitat-conservation/estuary-habitat#:~:text=feeding%2C%20and%20growing.-,Estuaries%3A%20Nurseries%20of%20the%20Sea,a%20wide%20range%20of%20habitats [Accessed: 13 January 2021].

National Oceanic and Atmospheric Administration (NOAA)., 2020. Estuaries. Human disturbances to estuaries. [Online]. Available at:

https://oceanservice.noaa.gov/education/kits/estuaries/estuaries09_humandisturb.html. [Accessed: 01 June 2020].

National Oceanic and Atmospheric Administration (NOAA)., 2020. What is dredging? [Online]. Available at: https://oceanservice.noaa.gov/facts/dredging.html [Accessed: 8 February 2021].

National Oceanic and Atmospheric Administration (NOAA)., 2021. Monitoring estuaries. [Online]. Available at: https://oceanservice.noaa.gov/education/tutorial_estuaries/est10_monitor.html [Accessed: 13 July 2021].

Navalgund, R.R., 2001. Remote sensing. Resonance, 6(12), pp.51-60.

Nellemann, C., Corcoran, E., Duarte, C.M., Valdés, L., DeYoung, C., Fonseca, L. and Grimsditch, G., 2009. Blue carbon. A rapid response assessment. United Nations Environment Programme, GRID-Arendal. [Online]. Available at: https://gridarendal-website-live.s3.amazonaws.com/production/documents/:s_document/83/original/BlueCarbon_screen.pdf?1483646492 [Accessed: 17 February 2022].

Nelson, S.A., 2012. Magmatic Differentiation. [Online]. Archive Tulane University. Available at: https://www.tulane.edu/~sanelson/eens212/magmadiff.htm [Accessed: 17 June 2021].

Nelson, S.A., 2015. Streams and drainage systems. [Online]. Archive Tulane University. Available at: https://www.tulane.edu/~sanelson/eens1110/streams.htm [Accessed: 05 March 2021].

Nelson, J.L. and Zavaleta, E.S., 2012. Salt marsh as a coastal filter for the oceans: Changes in function with experimental increases in nitrogen loading and sea-level rise. Public Library of Science One, 7(8), p.e38558.

Njoya, N. S., 2002. Post-dam sediment dynamics below the Inanda dam at the Mgeni Estuary, KwaZulu-Natal, South Africa. MSc. University of KwaZulu-Natal, South Africa.

Noegrohati, S., 2005. Sorption-desorption characteristics of heavy metals and their availability from the sediment of Segara anakan estuary. Indonesian Journal of Chemistry, 5(3), pp.236-244.

Nomngongo, P.N., Munonde, T.S., Mpupa, A. and Biata, N.R., 2017. Near-Infrared Spectroscopy Combined with Multivariate Tools for Analysis of Trace Metals in Environmental Matrices. In Developments in Near-Infrared Spectroscopy. IntechOpen.

Nthunya, L.N., Maifadi, S., Mamba, B.B., Verliefde, A.R. and Mhlanga, S.D., 2018. Spectroscopic determination of water salinity in brackish surface water in Nandoni Dam, at Vhembe District, Limpopo Province, South Africa. Water, 10(8), p.990.

Nunkumar, S., 2002. Monitoring the health of the rivers of the Durban Metropolitan area using fresh water invertebrates: A pilot study. MSc. University of KwaZulu-Natal.

O'Boyle, S., McDermott, G. and Wilkes, R., 2009. Dissolved oxygen levels in estuarine and coastal waters around Ireland. Marine pollution bulletin, 58(11), pp.1657-1663.

Olaniran, A.O., Naicker, K. and Pillay, B., 2014. Assessment of physico-chemical qualities and heavy metal concentrations of Umgeni and Umdloti Rivers in Durban, South Africa. Environmental monitoring and assessment, 186(4), pp.2629-2639.

Ouillon, S., 2018. Why and how do we study sediment transport? Focus on coastal zones and ongoing methods. Water, 10(4), p.390.

Owen, A.J., 1995. Uses of Derivative Spectroscopy: Application note. Agilent Technologies, publication number 5963-3940E. [Online]. Available at: https://www.whoi.edu/cms/files/derivative_spectroscopy_59633940_175744.pdf [Accessed: 17 February 2022].

Pal, M., Samal, N.R., Roy, P.K. and Roy, M.B., 2015. Electrical conductivity of lake water as environmental monitoring–A case study of Rudrasagar Lake. IOSR Journal of Environmental Science, Toxicology and Food Technology, 9(3), pp.66-71.

Parker, J.G., 1983. A comparison of methods used for the measurement of organic matter in marine sediment. Chemistry in Ecology, 1(3), pp.201-209.

Pather, K., 2014. Spatio-temporal Variations of the Sedimentology and Geochemistry of Six Estuaries Within the eThekwini Municipality, KwaZulu-Natal, South Africa. MSc. University of KwaZulu-Natal.

Pati, P., Patra, P.K. and Goswami, S., 2013. Heavy Metal Distribution in Major Estuaries of Northern Odisha along the East Coast of India: An Indexing Approach. International Journal of Earth Sciences and Engineering, 6, pp.1094-1102.

Pawar, B. and Deshmukh, R., 2021. Predicting lead and nickel contamination in soil using spectroradiometer. International Journal of Recent Technology and Engineering, 10, pp.121-125.

Pearce, M.W. and Schumann, E.H., 2003. Dissolved oxygen characteristics of the Gamtoos estuary, South Africa. African Journal of Marine Science, 25, pp.99-109.

Pedersen, O., Colmer, T.D. and Sand-Jensen, K., 2013. Underwater photosynthesis of submerged plants – recent advances and methods. Frontiers in Plant Science, 4(140), pp.1-19.

Pereira, G.E., Sequinatto, L., de Almeida, J.A., ten Caten, A. and Mota, J.M., 2019. VIS-NIR spectral reflectance for discretization of soils with high sand content. Semina: Ciências Agrárias, Londrina, 40(1), pp.99-112.

Perera, K.A.R.S. and Amarasinghe, M.D., 2019. Carbon sequestration capacity of mangrove soils in micro tidal estuaries and lagoons: A case study from Sri Lanka. Geoderma, 347, pp.80-89.

Perveen, I., Raza, M.A., Sehar, S., Naz, I., Young, B. and Ahmed, S., 2017. Heavy metal contamination in water, soil, and milk of the industrial area adjacent to Swan River, Islamabad, Pakistan. Human and Ecological Risk Assessment: An International Journal, 23(7), pp.1564-1572.

Pillay, V., 2002. An investigation into the spatial and temporal variations in water quality of selected rivers in the Durban Metropolitan Area. MSc. University of KwaZulu-Natal.

Pinto, R., Patrício, J., Neto, J.M., Salas, F. and Marques, J.C., 2010. Assessing estuarine quality under the ecosystem services scope: ecological and socioeconomic aspects. Ecological Complexity, 7(3), pp.389-402.

Pires, N., Muniz, D., Kisaka, T., Simplicio, N., Bortoluzzi, L., Lima, J. and Oliveira-Filho, E., 2015. Impacts of the urbanization process on water quality of Brazilian Savannah Rivers: the case of Preto River in Formosa, Goias State, Brazil. International Journal of Environmental Research and Public Health, 12(9), pp.10671-10686.

Pirouz, D.M., 2006. An overview of partial least squares. Unpublished PhD dissertation. University of California, Irvin.

Potasznik, A. and Szymczyk, S., 2015. Magnesium and calcium concentrations in the surface water and bottom deposits of a river-lake system. Journal of Elementology, 20(3).

Press, W.H. and Teukolsky, S.A., 1990. Savitzky-Golay smoothing filters. Computers in Physics, 4(6), pp.669-672.

Putra, A., Meilina, H. and Tsenkova, R., 2012. Use of near-infrared spectroscopy for determining the characterization metal ion in aqueous solution. In Proceedings of The Annual International Conference, Syiah Kuala University - Life Sciences and Engineering Chapter, 2(2), pp.154-158.

Ramzai, J., 2020. Clearly explained: Pearson vs Spearman correlation coefficient. [online]. Towards data science. Available from: https://towardsdatascience.com/clearly-explained-pearson-v-s-spearman-correlation-coefficient-ada2f473b8 [Accessed: 31 August 2021].

Ratnayake, A.S., Dushyantha, N., De Silva, N., Somasiri, H.P., Jayasekara, N.N., Weththasinghe, S.M., Samaradivakara, G.V.I., Vijitha, A.V.P. and Ratnayake, N.P., 2017. Sediment and physicochemical characteristics in Madu-Ganga Estuary, southwest Sri Lanka. Journal of Geological Society of Sri Lanka, 18, pp.43-52.

Raymond, P.A., Oh, N.H., Turner, R.E. and Broussard, W., 2008. Anthropogenically enhanced fluxes of water and carbon from the Mississippi River. Nature, 451(7177), pp.449-452.

Remeikaitė-Nikienė, N., Lujanienė, G., Malejevas, V., Barisevičiūtė, R., Žilius, M., Garnaga-Budrė, G. and Stankevičius, A., 2016. Distribution and sources of organic matter in sediments of the south-eastern Baltic Sea. Journal of Marine Systems, 157, pp.75-81.

Renaud, O. and Victoria-Feser, M.P., 2010. A robust coefficient of determination for regression. Journal of Statistical Planning and Inference, 140(7), pp.1852-1862.

Reusch, W., 2013. Infrared Spectroscopy. [online]. Department of Chemistry – Michigan State University. Available at: https://www2.chemistry.msu.edu/faculty/reusch/virttxtjml/spectrpy/infrared/infrared.htm [Accessed: 19 October 2021].

Riba, I., Garcia-Luque, E., Blasco, J. and DelValls, T.A., 2003. Bioavailability of heavy metals bound to estuarine sediments as a function of pH and salinity values. Chemical Speciation and Bioavailability, 15(4), pp.101-114.

Richards, J.A. and Jia, X., 2006. Remote Sensing Digital Image Analysis: An Introduction. Springer.

Rieuwerts, J.S., Thornton, I., Farago, M.E. and Ashmore, M.R., 1998. Factors influencing metal bioavailability in soils: preliminary investigations for the development of a critical loads approach for metals. Chemical Speciation & Bioavailability, 10(2), pp.61-75.

Riley, M.K., 2008. The Effects of Urbanization on Water Quality: A Biological Assessment of Three Bay Area Watersheds using Benthic Macroinvertebrates as Biological Indicators. Water Quality and Urbanization, pp.1-20.

Rosipal, R. and Trejo, L.J., 2001. Kernel partial least squares regression in reproducing Kernel Hilbert space. Journal of Machine Learning Research, 2(Dec), pp.97-123.

Rostom, N.G., Shalaby, A.A., Issa, Y.M. and Afifi, A.A., 2017. Evaluation of Mariut Lake water quality using Hyperspectral Remote Sensing and laboratory works. The Egyptian Journal of Remote Sensing and Space Science, 20, pp.S39-S48.

Rout, G.R. and Das, P., 2009. Effect of metal toxicity on plant growth and metabolism: I. Zinc. Sustainable Agriculture, pp.873-884.

Rout, G.R. and Sahoo, S., 2015. Role of iron in plant growth and metabolism. Reviews in Agricultural Science, 3, pp.1-24.

Rudani, L., Vishal, P. and Kalavati, P., 2018. The importance of zinc in plant growth - A review. International Research Journal of Natural and Applied Sciences, 5(2), pp.38-48.

Sahwan, W., Lucke, B., Sprafke, T., Vanselow, K.A. and Bäumler, R., 2020. Relationships between spectral features, iron oxides and colours of surface soils in northern Jordan. European Journal of Soil Science, 72(1), pp.80-97.

Sakudo, A., Tsenkova, R., Tei, K., Onozuka, T., Ikuta, K., Yoshimura, E. and Onodera, T., 2006. Comparison of the vibration mode of metals in HNO3 by a partial least-squares regression analysis of near-infrared spectra. Bioscience, biotechnology, and biochemistry, 70(7), pp.1578-1583.

Salisbury, J.W., 1998. Spectral measurements field guide. Earth Satellite Corporation. Defense Technology Information Center, Report Number: ADA362372. [Online]. Available at: http://www.dpinstruments.com/papers/spectral_guide.pdf [Accessed: 17 February 2022].

Salles, T., 2020. Fluvial sediment transport. [online]. Available at: https://earthsurface.readthedocs.io/en/latest/sedtransport.html. [Accessed: 05 March 2021].

Savitzky, A. and Golay, M.J., 1964. Smoothing and differentiation of data by simplified least squares procedures. Analytical Chemistry, 36(8), pp.1627-1639.

SA-Venues., 2021. KwaZulu-Natal climate and weather. [Online]. Available at: https://www.sa-venues.com/weather/kwazulunatal.php [Accessed: 04 November 2021].

Schafer, R.W., 2011. What is a Savitzky-Golay filter? [lecture notes]. IEEE Signal Processing Magazine, 28(4), pp.111-117.

Schlüter, T., 2008. Geological atlas of Africa. Springer-Verlag, Berlin.

Schmidt, M.W., Torn, M.S., Abiven, S., Dittmar, T., Guggenberger, G., Janssens, I.A., Kleber, M., Kögel-Knabner, I., Lehmann, J., Manning, D.A. and Nannipieri, P., 2011. Persistence of soil organic matter as an ecosystem property. Nature, 478(7367), pp.49-56.

Schober, P., Boer, C. and Schwarte, L.A., 2018. Correlation coefficients: appropriate use and interpretation. Anesthesia and Analgesia, 126(5), pp.1763-1768.

Scott, E., 2019. Re: What are the values of R2 and Q2 for the model to be acceptable in PLS regression? [Online]. Research Gate. Available at: https://www.researchgate.net/post/What_are_the_values_of_R2_and_Q2_for_the_model_to_be_acceptable_in_PLS_regression/5c631eddb93ecda39963e95a/citation/download [Accessed 15 September 2021].

Seifi, A., Hosseinjanizadeh, M., Ranjbar, H. and Honarmand, M., 2019. Visible-infrared spectroscopy and chemical properties of water in mining area. Water Science and Technology, 80(9), pp.1612-1622.

Sharma, R. and Srivastava, P.K., 2014. Hydrothermal fluids of magmatic origin. In Modelling of Magmatic and Allied Processes, pp.181-208. Springer.

Sherwood, J.E., Stagnitti, F., Kokkinn, M.J. and Williams, W.D., 1991. Dissolved oxygen concentrations in hypersaline waters. Limnology and Oceanography, 36(2), pp.235-250.

Showalter, P.S., Silberbauer, M., Moolman, J. and Howman, A., 2000. Revisiting Rietspruit: Land Cover Change and Water Quality in South Africa. Proceedings of the ICRSE 28th International symposium on Remote Sensing of environment and the Third AARSE Symposium, Cape Town, South Africa.

Siebielec, G., McCarty, G.W., Stuczynski, T.I. and Reeves III, J.B., 2004. Near-and mid-infrared diffuse reflectance spectroscopy for measuring soil metal content. Journal of Environmental Quality, 33(6), pp.2056-2069.

Singh, A., 2013. Surveillance of microbial pathogens in the uMgeni River, Durban South Africa. MSc. University of KwaZulu-Natal.

Singh, N.U., Roy, A., Tripathi, A.K., 2013. Non-parametric tests: Hands on SPSS. ICAR Research Complex for NEH Region, Umiam, Meghalaya.

Sisitka, L., 2008. Taking Care of Our Estuaries. [Online] Available at: https://www.iwrm.co.za/resource%20doc/od_diverse_docs/october_2008_updates/wua_eco_capacity_building%20Booklets_08/wr_1estuaries.pdf [Accessed 29 April 2020].

Smedley, P.L. and Kinniburgh, D.G., 2001. Source and behaviour of arsenic in natural waters. United Nations synthesis report on arsenic in drinking water. World Health Organization, Geneva, Switzerland, pp.1-61.

Smith, W.S., Silva, F.L.D. and Biagioni, R.C., 2019. River dredging: When the public power ignores the causes, biodiversity and science. Ambiente and Sociedade, 22, p.e00571.

Sojka, M., Jaskuła, J. and Siepak, M., 2019. Heavy metals in bottom sediments of reservoirs in the lowland area of western Poland: Concentrations, distribution, sources and ecological risk. Water, 11(1), p.56.

Srivastava, P., 2016. Re: Is it possible that cadmium can be detected in water and not detected in sediment of the same station and why? [Online]. Available at: https://www.researchgate.net/post/Is_it_possible_that_cadmium_can_be_detected_in_water_and_not_detected_in_sediment_of_the_same_station_and_why/57d1a0eeed99e11fc30dd754/citation/download [Accessed: 18 October 2021].

Srivastava, N., 2021. Spectral reflectance curves. [Online]. Online Study Material, Faculty of Engineering, University of Lucknow, India. Available at:

https://www.lkouniv.ac.in/en/article/e-content-faculty-of-engineering [Accessed: 11 October 2021].

Strawn, D., Bohn, H. L. and O'Connor, G. A., 2015. Soil Chemistry. Wiley-Blackwell, Chichester, West Sussex.

Sukdeo, P., 2010. A Study of the Natural and Anthropogenic Impacts on the Sediment and Water Quality of the Middle and Lower Mvoti River System, KwaZulu-Natal, South Africa. MSc. University of KwaZulu-Natal.

Superville, P.J., Prygiel, E., Magnier, A., Lesven, L., Gao, Y., Baeyens, W., Ouddane, B., Dumoulin, D. and Billon, G., 2014. Daily variations of Zn and Pb concentrations in the Deûle River in relation to the resuspension of heavily polluted sediments. Science of the Total Environment, 470, pp.600-607.

Tariq, S.R., Shafiq, M. and Chotana, G.A., 2016. Distribution of heavy metals in the soils associated with the commonly used pesticides in cotton fields. Scientifica, 2016. http://dx.doi.org/10.1155/2016/7575239.

Tchounwou, P.B., Yedjou, C.G., Patlolla, A.K. and Sutton, D.J., 2012. Heavy metal toxicity and the environment. Molecular, Clinical and Environmental Toxicology, pp.133-164.

Tekin, Y., Tumsavas, Z. and Mouazen, A.M., 2012. Effect of moisture content on prediction of organic carbon and pH using visible and near-infrared spectroscopy. Soil Science Society of America Journal, 76(1), pp.188-198.

Thrush, S.F., Townsend, M., Hewitt, J.E., Davies, K., Lohrer, A.M., Lundquist, C., Cartner, K. and Dymond, J., 2013. The many uses and values of estuarine ecosystems. Ecosystem services in New Zealand–conditions and trends. Manaaki Whenua Press, Lincoln, New Zealand.

Tinmouth, N., 2010. The Mgeni estuary pre- and post Inanda Dam estuarine dynamics. MSc. University of KwaZulu-Natal.

Todorova, M., Mouazen, A.M., Lange, H. and Atanassova, S., 2014. Potential of near-infrared spectroscopy for measurement of heavy metals in soil as affected by calibration set size. Water, Air, and Soil Pollution, 225(8), pp.1-19.

Trettin, C.C., Jurgensen, M.F. and Dai, Z., 2019. Effects of climate change on forested wetland soils. In Developments in Soil Science, 36, pp. 171-188. Elsevier.

Trujillo, A. P. and Thurman H. V., 2011. Essentials of oceanography. Prentice Hall Recommended Reading Walker, New Jersey, USA.

Turpie, J.K., Adams, J.B., Joubert, A., Harrison, T.D., Colloty, B.M., Maree, R.C., Whitfield, A.K., Wooldridge, T.H., Lamberth, S.J., Taljaard, S. and Van Niekerk, L., 2002. Assessment of the conservation priority status of South African estuaries for use in management and water allocation. Water SA, 28(2), pp.191-206.

Turpie, J.K., 2004. South African national spatial biodiversity assessment 2004: Technical report. Volume 3: Estuary component. South African National Biodiversity Institute: Pretoria. [Online]. Available at: https://saeis.saeon.ac.za/Document/1963 [Accessed: 16 February 2022].

Turpie, J., Letley, G., Schmidt, K., Weiss, J., O'Farrell, P. and Jewitt, D., 2020. Towards a method for accounting for ecosystem services and asset value: Pilot accounts for KwaZulu-Natal, South Africa, 2005-2011. Natural Capital Accounting and Valuation of Ecosystem Services (NCAVES) project.

Umgeni Ecological Infrastructure Partnership (UEIP)., 2016. The uMgeni Ecological Infrastructure Partnership: A strategy, July 2016. [Online]. Available at: http://biodiversityadvisor.sanbi.org/wp-content/uploads/2017/05/UEIP-Strategy-July2016.pdf [Accessed: 16 February 2022].

Umgeni Water., 2013. Infrastructure Master Plan 2013: 2013/2014–2043/2044, volume 1. Planning Services, Engineering and Scientific Services Division, Umgeni Water, Pietermaritzburg, KwaZulu-Natal, South Africa. [Online]. Available at: https://www.umgeni.co.za/projects/infra-structuremasterplans/docs/2013/IMP_2013_Vol_1_5Sep13.pdf [Accessed: 16 February 2022].

Umgeni Water., 2017. Infrastructure Master Plan 2017/2018 – 2047/2048, volume 1. Planning Services, Engineering and Scientific Services Division, Umgeni Water, Pietermaritzburg, South Africa. [Online]. Available at: https://www.umgeni.co.za/projects/infra-structuremasterplans/docs/2017/UW%20IMP%202017%20Vol1.pdf [Accessed: 16 February 2022].

United States Environmental Protection Agency (USEPA)., 2006. Volunteer estuary manual: A methods manual. EPA-842-B-06-003. 2nd edition. [Online]. Available at: https://www.epa.gov/sites/default/files/2015-09/documents/2007_04_09_estuaries_monitoruments_manual.pdf [Accessed: 16 February 2022].

United States Environmental Protection Agency (USEPA)., 2012. Conductivity: What is conductivity and why is it so important? [online]. United States Environmental Protection Agency Web Archive. Available at: https://archive.epa.gov/water/archive/web/html/vms59.html [Accessed: 6 September 2021].

United States Environmental Protection Agency (USEPA)., 2021. Indicators: Conductivity. [online]. USEPA National Aquatic Resource Survey. Available at: https://www.epa.gov/national-aquatic-resource-surveys/indicators-conductivity [Accessed: 9 September 2021].

Ural, N., 2018. The importance of clay in geotechnical engineering. In Zoveidavianpoor, M (ed.). Current topics in the utilization of clay in industrial and medical applications. IntechOpen, London.

Usman, A.R., 2015. Influence of NaCl-induced salinity and Cd toxicity on respiration activity and Cd availability to barley plants in farmyard manure-amended soil. Applied and Environmental Soil Science, 2015. http://dx.doi.org/10.1155/2015/483836.

Valentine, P.C., 2019. Sediment classification and the characterization, identification, and mapping of geologic substrates for the glaciated Gulf of Maine seabed and other terrains, providing a physical framework for ecological research and seabed management. Scientific Investigations Report 2019-5073, United States Geological Survey.

Van Dam, R.A., Hogan, A.C., McCullough, C.D., Houston, M.A., Humphrey, C.L. and Harford, A.J., 2010. Aquatic toxicity of magnesium sulfate, and the influence of calcium, in very low ionic concentration water. Environmental Toxicology and Chemistry, 29(2), pp.410-421.

Van Niekerk, L. and Turpie, J.K. (eds.)., 2012. South African National Biodiversity Assessment 2011: Technical Report. Volume 3: Estuary Component. CSIR Report Number CSIR/NRE/ECOS/ER/2011/0045/B. Council for Scientific and Industrial Research,

Stellenbosch. [Online]. Available at: http://mpaforum.org.za/wp-content/uploads/2016/08/Nat-Biodiversity-AssTechRepEstuary.pdf [Accessed: 18 February 2022].

Van Niekerk, L., Adams, J.B., Bate, G.C., Forbes, A.T., Forbes, N.T., Huizinga, P., Lamberth, S.J., MacKay, C.F., Petersen, C., Taljaard, S., Weerts, S.P., Whitfield, A.K. and Wooldridge, T.H., 2013. Country-wide assessment of estuary health: An approach for integrating pressures and ecosystem response in a data limited environment. Estuarine, Coastal and Shelf Science 130, pp.239-251.

Van Niekerk, L., Adams, J.B., Lamberth, S.J., MacKay, C.F., Taljaard, S., Turpie, J.K., Weerts S.P. and Raimondo, D.C. (eds.)., 2019. South African National Biodiversity Assessment 2018: Technical Report. Volume 3: Estuarine Realm. CSIR report number CSIR/SPLA/EM/EXP/2019/0062/A. South African National Biodiversity Institute, Pretoria. Report Number: SANBI/NAT/NBA2018/2019/Vol3/A. [Online]. Available at: http://hdl.handle.net/20.500.12143/6373 [Accessed: 18 February 2022].

Veerasamy, R., Rajak, H., Jain, A., Sivadasan, S., Varghese, C.P. and Agrawal, R.K., 2011. Validation of QSAR models-strategies and importance. International Journal of Drug Design and Discovery, 3, pp.511-519.

Verma, R. and Dwivedi, P., 2013. Heavy metal water pollution - A case study. Recent Research in Science and Technology, 5(5), pp.98-99.

Villars, M. T. and Delvigne, G. A. L., 2001. Estuarine processes. Literature review. Final draft prepared for the European Chemistry Industry Council (CEFIC), Z2725.10. WL, Delft Hydraulics.

Vuori, K.M., 1995. Direct and indirect effects of iron on river ecosystems. Annales Zoologici Fennici, pp.317-329. Finnish Zoological and Botanical Publishing Board.

Walling, D.E. and Webb, B.W., 1975. Spatial variation of river water quality: a survey of the River Exe. Transactions of the institute of British Geographers, pp.155-171.

Wang, Y.P., Voulgaris, G., Li, Y., Yang, Y., Gao, J., Chen, J. and Gao, S., 2013. Sediment resuspension, flocculation, and settling in a macrotidal estuary. Journal of Geophysical Research: Oceans, 118(10), pp.5591-5608.

Wang, R., Wu, S., Wu, K., Huang, S., Wu, R., Liu, B., Lin, M., Li, L., Zhou, D. and Diao, X., 2017. Estimation and spatial analysis of heavy metals in metal tailing pond based on improved pls with multiple factors. IEEE Access, XX, 2017.

Warburton, M.L., Schulze, R.E. and Jewitt, G.P., 2012. Hydrological impacts of land use change in three diverse South African catchments. Journal of Hydrology, 414, pp.118-135.

Water Research Commission (WRC)., 2002. State of rivers report: Mngeni River and neighbouring rivers and streams. WRC Report no. TT 200/02, Water Research Commission, Pretoria, SA.

Webb, P., 2019. Introduction to oceanography. Press Books. Roger Williams University, USA.

Wenner, E., Sanger, D., Arendt, M., Holland, A.F. and Chen, Y., 2004. Variability in dissolved oxygen and other water-quality variables within the national estuarine research reserve system. Journal of Coastal Research, (10045), pp.17-38.

Wentworth, C.K., 1922. A scale of grade and class terms for clastic sediments. Journal of Geology, 30, pp.377-392.

Whitfield, A.K., 1992. A Characterization of South African Estuarine Systems. South African Journal of Aquatic Science, 18(1-2), pp.89-103.

Whitfield, A. and Bate, G., 2007. A review of information on temporarily open/closed estuaries in the warm and cool temperate biogeographic regions of South Africa, with particular emphasis on the influence of river flow on these systems. Water Research Commission, Report, 1581(1), p.07.

Whitfield, A.K., Bate, G.C., Adams, J.B., Cowley, P.D., Froneman, P.W., Gama, P.T., Strydom, N.A., Taljaard, S., Theron, A.K., Turpie, J.K. and Van Niekerk, L., 2012. A review of the ecology and management of temporarily open/closed estuaries in South Africa, with particular emphasis on river flow and mouth state as primary drivers of these systems. African Journal of Marine Science, 34(2), pp.163-180.

Wilde, F.D. and Radtke, D.B. (eds.)., 1998. Handbooks for Water-resources Investigations: National field manual for the collection of water-quality data. Field measurements. US Department of the Interior, US Geological Survey.

Woody, C.A. and O'Neal, S., 2012. Effects of copper on fish and aquatic resources. The Nature Conservancy. [Online]. Available at: https://www.conservationgateway.org/ConservationByGeography/NorthAmerica/UnitedStates/alaska/sw/cpa/Documents/W2013ECopperF062012.pdf [Accessed: 15 February 2022].

Wu, Y., Chen, J., Ji, J., Gong, P., Liao, Q., Tian, Q. and Ma, H., 2007. A mechanism study of reflectance spectroscopy for investigating heavy metals in soils. Soil Science Society of America Journal, 71(3), pp.918-926.

Wuana, R.A. and Okieimen, F.E., 2011. Heavy metals in contaminated soils: a review of sources, chemistry, risks and best available strategies for remediation. International Scholarly Research Notices, 2011. doi:10.5402/2011/402647.

Xing, W. and Liu, G., 2011. Iron biogeochemistry and its environmental impacts in freshwater lakes. Fresenius Environmental Bulletin, 20(6), pp.1339-1345.

Xu, L., Zhou, Y.P., Tang, L.J., Wu, H.L., Jiang, J.H., Shen, G.L. and Yu, R.Q., 2008. Ensemble preprocessing of near-infrared (NIR) spectra for multivariate calibration. Analytica Chimica Acta, 616(2), pp.138-143.

Xu, X., Chen, S., Ren, L., Han, C., Lv, D., Zhang, Y. and Ai, F., 2021. Estimation of heavy metals in agricultural soils using VIS-NIR spectroscopy with fractional-order derivative and generalized regression neural network. Remote Sensing, 13(14), p.2718.

Yang, Z., Lu, W., Long, Y., Bao, X. and Yang, Q., 2011. Assessment of heavy metals contamination in urban topsoil from Changchun City, China. Journal of Geochemical Exploration, 108(1), pp.27-38.

Yang, Y., Cui, Q., Jia, P., Liu, J. and Bai, H., 2021. Estimating the heavy metal concentrations in topsoil in the Daxigou mining area, China, using multispectral satellite imagery. Scientific Reports, 11(1), pp.1-9.

Zabcic, N., 2008. Derivation of Surface pH-Values Based on Mineral Abundances Over Pyrite Mining Areas with Airborne Hyperspectral Data (Hymap) of Sotiel-Migollas Mine Complex, Spain. MSc. University of Alberta, Edmonton.

Zeitoun, M.M. and Mehana, E.E., 2014. Impact of water pollution with heavy metals on fish health: overview and updates. Global Veterinaria, 12(2), pp.219-231.

Zhang, C., Yu, Z.G., Zeng, G.M., Jiang, M., Yang, Z.Z., Cui, F., Zhu, M.Y., Shen, L.Q. and Hu, L., 2014. Effects of sediment geochemical properties on heavy metal bioavailability. Environment International, 73, pp.270-281.

Zhang, Y., Zhang, H., Zhang, Z., Liu, C., Sun, C., Zhang, W. and Marhaba, T., 2018. pH effect on heavy metal release from a polluted sediment. Journal of Chemistry, 2018. https://doi.org/10.1155/2018/7597640.

Zheng, R., Zhao, J., Zhou, X., Ma, C., Wang, L. and Gao, X., 2016. Land use effects on the distribution and speciation of heavy metals and arsenic in coastal soils on Chongming Island in the Yangtze River Estuary, China. Pedosphere, 26(1), pp.74-84.

Zheng, G., Ryu, D., Jiao, C., Xie, X., Cui, X. and Shang, G., 2019. Visible and near-infrared reflectance spectroscopy analysis of a coastal soil chronosequence. Remote Sensing, 11(20), p.2336.

Appendix

Table 1: Raw pH, electrical conductivity and dissolved oxygen concentration data of the water samples.

Sample	pH	Electrical Conductivity	Dissolved oxygen
AW1	7.79	532.2	6.34
	7.89	488.5	7.06
	7.9	573.4	7.19
AW2	7.75	572	6.94
	7.82	586.5	7.11
	7.84	553.2	7.28
AW3	7.81	611.2	6.41
	7.86	614.4	6.61
	7.85	620.8	6.74
AW4	7.73	684.6	6.78
	7.69	686	6.9
	7.71	685	7.06
AW5	7.64	612.1	6.81
	7.67	611.5	6.87
	7.68	615	6.96
BW1	7.42	606.8	7.32
	7.44	606.1	7.67
	7.43	607	7.58
BW2	7.42	677.4	6.29
	7.44	666.4	6.43
	7.45	674.4	6.52
BW3	7.49	698.5	6.85
	7.5	708.7	6.93
	7.49	708.2	7.02

BW4	7.45	702.7	6.85
	7.46	701.2	6.87
	7.49	706	7.21
BW5	7.46	683.3	6.48
	7.56	679.2	6.66
	7.51	684.2	6.73
CW1	7.46	1040	6.3
	7.44	1032	6.38
	7.47	1044	6.47
CW2	7.5	744.2	6.8
	7.43	747.1	7.01
	7.42	749.6	6.97
CW3	7.38	1751	5.08
	7.34	1740	5.24
	7.34	1742	5.34
CW4	7.55	4.209	7.03
	7.56	4.193	7.11
	7.55	4.185	7.12
CW5	7.5	4.427	5.95
	7.46	4.424	6.08
	7.46	4.428	6.16

Table 2: Mean pH, electrical conductivity, and dissolved oxygen concentrations of the water samples.

Sample	pH	Electrical Conductivity	Dissolved oxygen
AW1	7.86	531.37	6.87
AW2	7.81	570.57	7.11
AW3	7.84	615.47	6.59
AW4	7.71	685.2	6.92
AW5	7.67	612.87	6.88
BW1	7.43	606.64	7.53
BW2	7.44	672.74	6.42
BW3	7.5	705.14	6.94
BW4	7.47	703.3	6.98
BW5	7.51	682.24	6.63
CW1	7.46	1038.67	6.39
CW2	7.45	746.97	6.93
CW3	7.36	1744.34	5.22
CW4	7.56	4.196	7.09
CW5	7.48	4.427	6.07

Table 3: Results of the Spearman correlation analyses between each metal and the water quality parameters.

		pH	EC	DO
As	Spearman's rho Correlation Coefficient	.100	.129	-.179
	Sig. (2-tailed)	.723	.648	.524
	N	15	15	15
Cd	Spearman's rho Correlation Coefficient	-.117	-.584*	.318
	Sig. (2-tailed)	.678	.022	.248
	N	15	15	15
Fe	Spearman's rho Correlation Coefficient	.061	.339	.197
	Sig. (2-tailed)	.829	.216	.480
	N	15	15	15
Mg	Spearman's rho Correlation Coefficient	-.446	.254	-.339
	Sig. (2-tailed)	.095	.362	.216
	N	15	15	15

* Correlation is significant at the 0.05 level (2-tailed).

Table 4: Raw data of sediment samples.

Samples	Al (%)	As (mg/kg)	Cd (mg/kg)	Cr (mg/kg)	Cu (mg/kg)	Fe (%)	Pb (mg/kg)	Mg (%)	Ni (mg/kg)	Zn (mg/kg)
AS1	0.17	1.7	<1	42	42	2.47	28	0.24	20	182
AS2	0.24	2.3	<1	54	48	2.19	31	0.27	27	199
AS3	0.07	<1	<1	17	13	0.90	10	0.11	7.7	69
AS4	0.15	1.8	<1	45	38	2.11	26	0.23	24	162
AS5	0.21	2.4	3.2	58	49	2.68	32	0.28	31	189
BS1	0.20	<1	<1	6.5	2.1	0.16	2.2	0.04	1.8	29
BS2	0.02	<1	<1	7.0	3.4	0.22	2.6	0.04	2.2	31
BS3	0.23	2.3	<1	52	46	2.11	29	0.28	24	190
BS4	0.08	1.1	<1	26	20	0.95	14	0.14	11	100
BS5	0.17	2.1	<1	46	42	2.27	26	0.24	22	171
CS1	0.24	2.9	<1	63	53	2.86	35	0.34	32	204

CS2	0.14	2.3	<1	38	31	1.39	21	0.25	18	133
CS3	0.21	3.0	<1	54	50	2.07	33	0.34	28	202
CS4	0.21	2.8	<1	57	48	1.98	32	0.33	26	202
CS5	0.27	3.4	<1	65	28	2.42	40	0.33	30	232

* Values of <1 indicate the metal concentrations found below the detection limit that was set.

Table 5: Showing the concentrations of aluminium, iron and magnesium in mg/kg.

Samples	Al (mg/kg)	Fe (mg/kg)	Mg (mg/kg)
AS1	1700	24700	2400
AS2	2400	21900	2700
AS3	700	9000	1100
AS4	1500	21100	2300
AS5	2100	26800	2800
BS1	2000	1600	400
BS2	200	2200	400
BS3	2300	21100	2800
BS4	800	9500	1400
BS5	1700	22700	2400
CS1	2400	28600	3400
CS2	1400	13900	2500
CS3	2100	20700	3400
CS4	2100	19800	3300
CS5	2700	24200	3300

* 1% by mass or weight is equivalent to 10000 mg/kg; therefore, the % concentrations of each metal were converted into a mg/kg concentration by multiplying each % concentration by 10000.